Defining the mechanism of *Yersinia entomophaga* MH96 exoprotein release

---

A thesis

submitted in partial fulfillment

of the requirements for the Degree of

Ph.D. of Microbiology

at

Lincoln University

by

Marion Schoof

Lincoln University

2020

Abstract
of a thesis submitted in partial fulfilment of the
requirements for the Degree of PhD Microbiology.

Defining the mechanism of *Yersinia entomophaga* MH96 exoprotein release

by
Marion Schoof

There is an increasing need in New Zealand for the development of new solutions and improvement of currently available biological control agents of pasture pests. In the last two decades, the entomopathogen *Yersinia entomophaga* was isolated, characterised, and defined as an economically viable agent for use in biopesticides against pasture pests, such as the New Zealand grass grub *Costelytra giveni*, the black beetle *Hetreronychus arator,* and other insects from the orders Coleoptera and Lepidoptera. *Y. entomophaga* produces an ABC toxin complex, called the Yen-TC, which is its main orally active virulence factor. Although previous studies have revealed how the toxin is affecting the host, the mechanism for Yen-TC production and cellular release have yet to be fully elucidated. Furthermore, the roles of other virulence factors of *Y. entomophaga* and their effects and mechanisms of cellular release are yet to be determined. *In silico* analysis of the draft genome sequence revealed several gene clusters encoding for virulence factors such as Rhs with predicted function in the type 6 secretion system, YenT as a possible heat-stable enterotoxin, and PirAB, a haemocoelic-active toxin. This study aimed to identify regulators of exoproteome release in *Y. entomophaga* MH96. The *Yersinia entomophaga* region of exoproteome release (YeRER) was identified by an exoproteome screening assay developed in this study. The YeRER is comprised of the transcriptional regulator RoeA, a regulatory ncRNA, and the *Yersinia* lysis cassette (YLC). Transcriptomics, mutagenesis, and *tran*s complementation experiments were used to elucidates the importance of YeRER in *Y. entomophaga* protein release and changes in cell morphology. The global regulator, RoeA, strictly down-regulates the YLC expression which is involved in protein release and vesicle formation. Expression levels of the encoded secretion systems in MH96, T1SS, T3SS, T3SS2, and T6SS are not under the control of YeRER or quorum sensing (QS), which are involved in protein secretion. The T2SS expression is increased in *roeA* and QS mutants, which in turn showed reduced global exoproteome concentration. It is unlikely that the MH96 secretion systems are involved in MH96 exoproteome production *in vitro.* While underlying mechanisms have yet to be investigated, this study strongly suggests that exoproteins such as the Yen-TC are secreted by membrane vesicles which are induced by activation of a holin-endolysin complex.

Acknowledgments

I would like to thank my supervisory team: Mark Hurst, Travis Glare, Maureen O'Callaghan, and Campbell Sheen for their guidance, support, and constructive criticism. I am very grateful to have had a supervisory team that was always accessible and which provided very good feedback.

I want to acknowledge Callaghan Innovation, the Bioprotection Research Centre, and AgResearch for financial support, which allowed me to undertake this Ph.D.

I am thankful for the help of Charles Hefer of the Bioinformatics Team at AgResearch, for RNAseq analysis. Thank you to Prof. Martin Pilhofer and Miki Feldmüller from the ETH Zurich, for inviting me as a guest in their laboratory and providing me with training in Cryo-ET methodology and analysis and successful collaboration.

Thanks also to my co-workers of the Soil Biology team at AgResearch especially Amy Beattie, Sandra Jones, and Mitchel Weston for technical support and tools as well as my Ph.D. colleagues especially Amber Paulson and Lesley Sitter for tools and critical thinking during my thesis. Thank you to Campbell Sheen and the Callaghan Innovation team, who have provided me with a workspace, equipment, and training for protein extractions.

A big thank you to the AgResearch statistics and bioinformatics team, especially to Chikako van Koten for training me in statistical analysis and Aurelie Laugraud for introduction and training in the use of the Geneious software.

At last, I want to thank my emotional and financial support group, especially my parents Anke and Peter Schoof, who always supported and believed in me, as well as my loving partner Deborah Porter and her family.

Table of Contents

List of Tables

List of Figures

List of Abbreviations

Abbreviation	Definition
AHL	N-acyl homoserine lactone
ALA	Aminolevulinic acid
Amp	Ampicillin
asRNA	Anti-sense ribonucleic acid
ATP	Adenosine triphosphate
β gal	β galactosidase
BLAST	Basic Local Alignment Search Tool
BLASTn	Nucleotide BLAST against other nucleotide sequences
BLASTp	Protein BLAST search against a protein sequence
BLASTx	Translated nucleotide BLAST search against a protein sequence
Bt	*Bacillus thuringiensis*
CFU	Colony-forming units
Cm	Chloramphenicol
COG	Clusters of Orthologous Groups
CP	Cell pellet
CS	Cell supernatant
Cryo-ET	Cryo-freeze Energy-filtered Transmission electron microscopy
DDT	Dichlorodiphenyltrichloroethane
DE	Differentially expressed
DNA	Deoxyribonucleic acid
DRS	Direct repeat sequence
EDTA	Ethylenediaminetetraacetate
EM	Electron Microscopy
EMSA	Electrophoretic Mobility Shift Assay
EPEC	Enteropathogenic *Escherichia coli*
Fe-S	Iron-sulfur cluster
G6PD	Glucose-6-phosphate dehydrogenase
GFP	Green fluorescent protein
GH	Glycosyl hydrolase
GI	Genomic island
GlcNAc	N-acetyl glucosamine
GMP	Guanosine monophosphate
GOI	Gene of interest
h	Hour
Hcp	Hemolysin co-regulated protein
HESA	High-throughput Exoproteome Screening Assay
Hf	High-fidelity
hpi	Hours post-inoculation

Abbreviation	Definition
HTH	Helix-turn-helix
IM	Inner membrane
INT	Intergenic region
LB	Luria Bertani bacteria growth medium
LC-ESI-MS/MS	Liquid chromatography-electrospray ionization ion trap-tandem mass spectrometry
LD_{50}	Lethal dose 50
LPS	Lipopolysaccharide
MCS	Multiple cloning site
min	Minute
mRNA	Messenger ribonucleic acid
MW	Molecular weight
NADPH	Nicotinamide adenine dinucleotide phosphate oxidase
NCBI	National Centre for Biotechnology Information
ncRNA	Non-coding ribonucleic acid
NEB	New England Biolabs
OD	Optical density
OM	Outer membrane
OMP	Outer membrane protein
OMV	Outer membrane vesicles
ORF	Open reading frame
PAGE	Polyacrylamide gel electrophoresis
PAI	Pathogenicity island
PBS	Phosphate-buffered saline
PCA	Principle component analysis
PCR	Polymerase chain reaction
PG	Peptidoglycan
POI	Protein of interest
PP	Periplasm
PPP	Pentose phosphate pathway
PPT	Phosphopantetheinyl transferase
PTS	Phosphotransferase system
QS	Quorum sensing
RBS	Ribosomal binding site
Rhs	Rearrangement hotspot
RNA	Ribonucleic acid
RNA-seq	Whole transcriptome shotgun sequencing
rpm	Rotations per minute
RR	Response regulator
rRNA	Ribosomal ribonucleic acid
RTX	Repeats-in-toxin
SD	Standard deviation
SDS-PAGE	Sodium dodecyl sulphate polyacrylamide gel electrophoresis

Abbreviation	Definition
Spec	Spectinomycin
T1SS	Type 1 secretion system
T2SS	Type 2 secretion system
T3SS	Type 3 secretion system 1
T3SSY2	Type 3 secretion system 2
T4SS	Type 4 secretion system
T5SS	Type 5 secretion system
T6SS	Type 6 secretion system
T7SS	Type 7 secretion system
T8SS	Type 8 secretion system
T9SS	Type 9 secretion system
TC	Toxin complex
TCA	Tricarboxylic acid cycle
TCS	Two-component system
Tet	Tetracycline
Tm	Annealing temperature
tRNA	Transfer ribonucleic acid
U.K.	United Kingdom
UTR	Untranslated region
VF	Virulence factor
VFDB	Virulence factor database
X-gal	5-bromo-4-chloro-3-indolyl-β-D-galacto-pyranoside
Yen-TC	*Yersinia entomophaga* insecticidal toxin complex
YeRER	*Yersinia entomophaga* Region of Exoproteome release
YLC	*Yersinia* Lysis Cassette

Chapter 1

Introduction

1.1 Overview

To meet the demand for global food production, it is important to fight pests sustainably. Global crop loss caused by insects alone is estimated to be 5 -20% of production but is predicted to increase by 10 -25% for every degree Celsius of warming, due to global warming (Deutsch *et al.*, 2018). Insecticidal products can be natural occurring plant products, such as extracts from tobacco, which have been used against aphids, and minerals such inorganic sulphur and calcium, which have been used for centuries for control of fleas, beetles, and aphids (Dahlawi and Siddiqui, 2017; Andreazza *et al.*, 2018). Synthesised chemicals, including Dichlorodiphenyltrichloroethane (DDT), have been used as highly effective insecticides for several decades since the 1940s. However, DDT, alongside other chemical insecticides, has been shown to affect non-target organisms, such as honeybees, mammals, birds, and even reptiles (Choudhary and Sharma, 2008; Pignati *et al.*, 2018; Bouwman *et al.*, 2019; Motohira *et al.*, 2019; Jayakumar *et al.*, 2020). In addition, DDT does not readily degrade in the environment, can be found at significant distances from the site of application, and can accumulate in the human body due to being lipophilic (Jan *et al.*, 2009).

The consumer drive for low residue produce and environmentally acceptable cropping practices has led to increased demand for biopesticides. The first biological pesticide, based on the bacterium *Bacillus thuringiensis,* then known as *B. sotto,* was isolated in the early 19th century from a diseased silkworm by Ishiwata and later isolated from a Mediterranean flour moth by Berliner when it was termed *B. thuringiensis* (Roh *et al.*, 2007; Kumar *et al.*, 2008). Further studies showed the insecticidal potential of *B. thuringiensis* and in the late 1920s, the bacterium was first used as a biological control agent against insect pests and was commercialised in the late 1930s in France (Roh *et al.*, 2007). Since the launch of that first biopesticide, several biological control agents have been identified from fungi, bacteria, and nematodes worldwide and 279 products have been developed, of which 151 are bioinsecticides originating from 62 microorganism species, including *B. thuringiensis* (Glare *et al.*, 2016). In 2019, there were twelve biopesticides registered for use in New Zealand; these were based on three bacterial species, *B. thuringiensis, B. firmus* and *Serratia entomophila,* the fungi *Beauveria bassiana* and *Lecanicillum lecanii,* and *Cydia pomonella* granulosis virus (Glare and O'Callaghan, 2019).

A promising candidate as a biopesticide is the Gram-negative bacterium, *Y. entomophaga* (Yersiniaceae) which was isolated from a diseased New Zealand grass grub, *Costelytra giveni*. Oral

infection studies of the wild type strain *Y. entomophaga* MH96 demonstrated its pathogenicity to various host species in the orders Coleoptera and Lepidoptera, including internationally important pests such as the diamondback moth, *Plutella xylostella,* and the cotton bollworm, *Helicoverpa armigera* (Hurst *et al.*, 2011b). Further studies identified the main virulence factor of *Y. entomophaga* as a multiprotein toxin complex, termed the Yen- TC. Through genome sequencing and bioinformatic analysis, a range of primary virulence factors such as toxins, secretion systems and secondary virulence factors (such as degrading proteins, invasion, and adhesion proteins) were identified (Hurst *et al.*, 2016).

1.2 The genus *Yersinia*

Yersinia spp. are Gram-negative, rod-shaped Gamma-proteobacteria of the family Yersiniaceae. The genus was named after Alexandre Émile Jean Yersin, who first isolated *Y. pestis* from human bodies (Hawgood, 2008). Through evolution, members of the *Yersinia* genus have diverged over the millennia. The genus currently comprises 18 recognised species: *Y. pestis, Y. enterocolitica*, *Y. pseudotuberculosis*, *Y. aldovae, Y. bercovieri, Y. frederiksenii, Y. intermedia, Y. kritsensenii, Y. mollaretii, Y. rohdei, Y. ruckeri*, *Y. aleksiciale* (Sprague and Neubauer, 2005)*, Y. massiliensis, Y. similis, Y. entomophaga*, *Y. nurmii, Y. pekkanenii* and *Y. wautersii* (Savin *et al.*, 2014). The species *Y. pestis*, *Y. enterocolitica* and *Y. pseudotuberculosis* are human pathogens and therefore the most studied species within the genus. While *Y. pestis* is the causative agent of bubonic plague*, Y. enterocolitica* and *Y. pseudotuberculosis* are enteropathogenic bacteria causing enteric yersiniosis in humans, especially in children younger than 10 years (Le Guern *et al.*, 2016). Another pathogenic species is *Y. ruckeri,* which was first isolated in 1966 from kidney tissue of rainbow trout (*Oncorhynchus mykiss)* in Idaho (USA) and is described as an enterocolitica-like species of *Yersinia* which also has high DNA homology to *Serratia marcescens* (Ewing *et al.*, 1978). Further studies proved that *Y. ruckeri* is the causative agent of enteric redmouth disease in rainbow trout and causes disease in other fish such as carp (Berc *et al.*, 1999; Kumar *et al.*, 2015).

The bacterium *Y. entomophaga* was isolated from a dead larva of the New Zealand grass grub, *C. giveni*, and defined as an insect pathogen with a broad host range (Hurst *et al.*, 2011b). The genome of *Y. entomophaga* MH96 shows 93.8% nucleotide sequence identity to *Y. nurmii* APN3a-c, isolated from packages of broiler meat cut in Finland (Murros-Kontiainen *et al.*, 2011a, Hurst *et al*., 2014). These two species, together with *Y. ruckeri,* form a discrete clade within the genus *Yersinia* (Murros-Kontiainen *et al.*, 2011a; Hurst *et al.*, 2014; Hurst *et al.*, 2016). Although only three species are

described as human pathogens, previous studies using PCR validation revealed that several *Yersinia* species were found in 7% of 470 human ileum samples examined, including strains *Y. enterocolitica*, *Y. pseudotuberculosis*, *Y. aldovae, Y. intermedia,* and *Y. molareii* (Le Baut *et al.*, 2018). Furthermore, *Y. enterocolitica, Y. rohdei*, *Y. intermedia, Y. pseudotuberculosis, Y. ruckeri, Y. mollaretii*, *Y. bercovieri*, and atypical undescribed *Yersinia* spp. were detected in food samples including milk and meat products (Ozdemir and Arslan, 2015). Recently, the *Yersinia* strain IP36721, which was isolated from human catheter urine (France), was classified as *Y. entomophaga* due to its genomic homology to *Y. entomophaga* MH96 (Le Guern *et al.*, 2018). The species *Y. pekkanii,* which is phenotypically similar to *Y. pseudotuberculosis*, has been isolated from water, soil, and lettuce samples (Murros-Kontiainen *et al.*, 2011b). In summary, species of the genus *Yersinia* are highly adaptable to their environment and able to persist in very diverse habitats including soil, water, mammals, fish, and invertebrates such as insects.

1.3 Pathogenicity of *Yersinia* spp.

Bacteria from the genus *Yersinia* can survive in a range of hosts. While *Y. pestis* uses fleas as vectors and infects the mammalian host, other species persist in and infect fish, birds, or insects (Pierson, 1994; Cork *et al.*, 1999; Hinnebusch and Erickson, 2008; Hurst *et al.*, 2011a; Davis, 2018; Guijarro *et al.*, 2018). To enable this, the *Yersinia* genome encodes for a variety of virulence factors. Virulence factors of the three human pathogenic species are located both on the chromosome and on the virulence plasmid pYV (Chen *et al.*, 2010). The pYV-plasmid encodes proteins to adhere, invade, and cause virulence in the host cell. For adherence, the pYV and pYV-like plasmids carry the *Yersinia* adhesin A (YadA) (El Tahir and Skurnik, 2001). Additionally, in *Y. pseudotuberculosis* IP 31758 (serotype O:1b) genes on the plasmid encode a type IV pili, which is involved in adherence and is crucial for virulence (Collyn *et al.*, 2002). The majority of *Yersinia* human pathogenic strains encode anti-phagocytosis proteins, the surface protease Pla (an aspartate protease), and *Yersinia* murein toxin (Ymt) on the virulence plasmid (Lahteenmaki *et al.*, 2001; Atkinson and Williams, 2016). The main virulence factor in human pathogenic strains is the Yop virulon and the associated Ysc type 3 secretion system (T3SS) located on the plasmid (Cornelis, 1998; Rohde *et al.*, 1999).

The pathogenic *Yersinia* strains *Y. entomophaga* and *Y. ruckeri* lack the pYV virulence plasmid and require proteins of the same function to enter and persist in the host cell (Chen *et al.*, 2010). The human and non-human pathogens share several virulence factors encoded in the genome. While only *Y. pseudotuberculosis* IP 31758 (serotype O:1b) carries the type IV pilus on its plasmid, the pilus is

encoded in the genome of most *Yersinia* strains and allows adherence to the host cell together with the Myf/pH6 antigen (Mikula *et al.*, 2012). Once *Yersinia* cells adhere to the host cell, the invasion occurs due to the genome encoded invasins (InvABCD) and the outer membrane protein and attachment protein Ail. Furthermore, the type 2 secretion system (T2SS), the type 3 secretion system (T3SS), and the flagellar apparatus are genome encoded virulence factors in *Yersinia* spp. Additionally, the toxin cytotoxic necrotizing factor (CNF) and iron sequestration systems (Yersiniabactin) are necessary for bacterial virulence. O-Antigens common in all *Yersinia* species have been linked to virulence in a temperature-dependent manner (Bengoechea *et al.*, 2004).

1.4 Secretion systems

Bacterial protein secretion is crucial for the maintenance of viability and pathogenicity. Secretion can be triggered by contact with host organisms and/or environmental factors, such as changes in temperature and pH, or stress factors such as excessive oxygen levels or nutrient deprivation (Zheng *et al.*, 2011; Gonzales *et al.*, 2013). Tight regulation of gene expression in response to these stimuli allows the cell to adapt and react to environmental changes. Transport of protein complexes across cell walls is essential to bacterial survival, with protein secretion involved in a variety of functions, including nutrient acquisition, antimicrobial resistance, and the delivery of toxins or other virulence factors by pathogens, enabling the bacteria to attach to and/or invade host tissues (Christensen *et al.*, 2009; Haurat *et al.*, 2011; Maffei *et al.*, 2017). The protective lipid bilayer of the Gram-negative bacterial cell wall, composed of peptidoglycan and lipopolysaccharides (LPS), presents a barrier through which exoproteins must pass. Several secretion pathways have evolved to enable the movement of proteolytic enzymes and other virulence factors across the lipid bilayer. These pathways range from simple protein channels and pores that span the cell wall to more complex multicomponent secretion systems, including the type 1–9 secretion systems (T1-9SS) of Gram-negative bacteria (Green and Mecsas, 2016; Li *et al.*, 2017). In addition to cell wall-based secretion systems, indirect mechanisms such as cell lysis via phage-like lysis cassettes (Turnbull *et al.*, 2016; Toyofuku *et al.*, 2017) or the release of outer membrane vesicles (OMVs), have been recognized as alternative mechanisms for protein release and/or transport (Beveridge, 1999; Kulp and Kuehn, 2010; Roier *et al.*, 2016).

1.4.1 Classification of secretion systems

The secretions systems from type 1-9 (T1SS-T9SS) can be classified into twin-arginine translocation (Tat) and secretory (Sec) pathway-dependent and independent systems.

In Gram-negative bacteria, exoproteins must pass through the bacterial inner membrane (IM), the periplasm (PP), and the outer membrane (OM). Some proteins can be directly transported into the extracellular matrix or directly into the host cell by the T3SS, T4SS, and T6SS (Green *et al.*, 2016). Other proteins need to pass the IM before further secretion. Translocation of these proteins can occur by the Sec or the Tat pathway but also through an autotransporter and two-component systems such as described for T5SS (Leo *et al.*, 2012). The Sec- and Tat-dependent, two-step, secretion systems are T2SS, T5SS, T7SS, T8SS, and T9SS. One-step secretion systems are cell wall spanning systems and independent from the Sec- or Tat pathway including T1SS, T3SS, T4SS, and T6SS as well as resistance-nodulation-division (RND) pumps. In the following Chapter, these translocation systems and T1-6SSs and are further described, but not T7-9SS as these are less frequently found in Gram-negative bacteria, and are not encoded in the *Y. entomophaga* genome.

1.4.2 Sec and Tat translocon

The secretory pathway (Sec) is composed of the integral membrane protein complex SecYEG which forms a protein-conducting channel (Sachelaru *et al.*, 2017). The ATPase SecA acts as a motor protein to generate the translocation of secretory proteins through the channel. In Gram-negative bacteria, exoproteins are often recruited post-transcription by a protein chaperon SecB, which maintains the unfolded stage after release from the ribosome and is targeted to SecYEG (Denks *et al.*, 2014). Proteins with a Sec signal sequence, often integral membrane proteins (IMP), are bound by the signal recognition particle (SRP), a complex of Ffh and 4.5S RNA. The SRP is bound to the ribosome and targets the SRP-receptor FtsY, which is bound to SecYEG (Denks *et al.*, 2014). The FtsY-SRP dissociates from the SecYEG complex, in a GTPase-dependent manner, allowing translocation of the IMP from the cytosol into the periplasm (Shan *et al.*, 2009). The outer membrane (OM) spanning secretions systems further transport the protein outside of the cell. Such OM-spanning secretion systems in Gram-negative bacteria are the T5SS, the chaperone-usher pathway, and the curli biogenesis system (Costa *et al.*, 2015). While the Sec-translocon transports unfolded proteins, the Tat pathway translocates fully folded proteins carrying a Tat signal sequence (Natale *et al.*, 2008; Crane and Randall, 2017). Tat-dependent secretion systems in Gram-negative bacteria are comprised of TatAC or TatABC and form a conducting translocation pore and a protein receptor (Blummel *et al.*, 2017). Tat-dependent proteins

contain a signal sequence. The pre-protein is often bound by chaperones such as DnaK and SlyD, which are proposed to fold and protect the protein from premature binding to the Tat system and from degradation (Perez-Rodriguez *et al.*, 2007; Robinson *et al.*, 2011). The precursor protein is targeted to TatABC where the proton motor force (PMF) provides energy for translocation. The Tat system translocate fully folded proteins across biological membranes and is required for biological processes such as the redox pathway, anaerobic respiration but also nitrogen regulation (Ochsner *et al.*, 2002; Rose *et al.*, 2002; Lee *et al.*, 2006). In contrast, the Sec pathway translocates unfolded proteins which either accumulate in the periplasm or are further secreted into the extracellular milieu. Sec-dependent proteins are often associated with the secretion systems and therefore play a part in virulence.

1.4.3 Type 1 secretion system

In the type 1 secretion system (T1SS), a variety of proteins are exported in a single step from the cytoplasm into the extracellular milieu (Linhartova *et al.*, 2010; Kanonenberg *et al.*, 2013). While various T1SS have been described, as an example the Hly/Tol system will be described in more detail below as an example. All T1SSs comprise at least three proteins: an outer membrane pore-forming protein (TolC), a membrane fusion protein (HlyD), and the ABC transporter protein (HlyB), which is anchored in the inner membrane (Wandersman and Delepelaire, 1990; Pimenta *et al.*, 1999; Thomas *et al.*, 2014). Substrates of the T1SS are heme-binding proteins, repeat-toxins (RTX) such as the hemolysin HlyA, lipases, adhesins, and/or S-layer proteins (Kanonenberg *et al.*, 2013). These substrates are located in the cytoplasm as unfolded proteins. A secretion signal sequence on the C-terminus, or N-terminus for bacteriocins, of the T1SS substrates, direct the preprotein to the ABC transporter, from where translocation is initiated (Jarchau *et al.*, 1994; Lenders *et al.*, 2015; Smith *et al.*, 2018)Currently, T1SS ABC transporter are classified as: i) Bacteriocin Cva/TolC transporter; ii) RTX toxin Hly-TolC transporter; and iii) BTLCP (bacterial transglutaminase-like cysteine proteinase)-linked RTX Adhesin LapA that is translocated by the Lap transporter found in *Pseudomonas fluorescens* (Smith *et al.*, 2018b).

The *Y. entomophaga* MH96 T1SS putatively comprises the T1SS ATPase (PL78_03985), the HlyD-like membrane fusion protein (PL78_03990), and the TolC-like outer membrane protein (PL78_03995) which genes are co-located with the genes of the serralysin cluster of the loci PL78_03960, PL78_03965, PL78_03970, and PL78_03976 (Hurst *et al.*, 2016).

1.4.4 Type 2 secretion system

The type 2 secretion system (T2SS) is a conserved protein secretion system confined to Gram-negative bacteria specifically among the Gamma-proteobacteria, which have adapted to exploit a wide range of habitats including soil and water (Sandkvist, 2001a). Gram-negative bacteria may also be symbionts and pathogens in plants and insects or mammals including humans. To survive in different habitats, these bacteria need to adapt to their environment, typically regulating cell metabolism in response to the surrounding conditions. In particular, the expression of secretory proteins (including degradative enzymes such as chitinases and protease), outer membrane lipoproteins (such as SsIE from *E. coli*), proteins necessary for biofilm formation, and toxins such as heat-labile toxin from *E. coli*, are important in adapting to the environment (Baldi *et al.*, 2012; von Tils *et al.*, 2012). The transfer of many of these proteins occurs by the outer membrane-spanning secretion system, termed the general secretion pathway (Gsp) (Pugsley, 1993). The T2SS substrates such as pseudolysin, pullulanase, a cell-wall degrading enzyme, or toxins are translocated into the inner membrane by the SecYEG or Tat system (Pugsley, 1993; Voulhoux *et al.*, 2001; Natale *et al.*, 2008). The SecYEG proteins form a heterotrimeric protein channel complex. Through the Sec system, cytosolic proteins can be inserted into the plasma membrane and further translocated along the membrane or be secreted into the extracellular matrix. Whether a protein is located along the membrane or is secreted depends on its signal-anchor sequence. The SecYEG translocon mainly inserts unfolded proteins while the Tat system transports fully folded proteins along the cytosolic membrane (Pugsley, 1993).

The Gsp is composed of 12-15 components which form the secretome (Fig. 1A) of the T2SS (Sandkvist, 2001b). The secretome is formed by an outer membrane (OM) complex (GspD,S), linked over a periplasmic pseudopilus (GspGHIJK) with the inner membrane (IM) platform (GspCFLM). The transport of exoproteins via the T2SS is actively driven by cytoplasmic ATPase activity (GspE) (Costa *et al.*, 2015). The secretory proteins, translocated into the cytosol via Tat or Sec system, are inserted into the secretin by the interaction of GspD and GspC units (Korotkov *et al.*, 2012). The extension of the pseudopilus (GspGHIJK), driven by ATPase activity, then pushes out the exoprotein through the secretin, a 55-70 Å dodecameric channel of GspD proteins, into the extracellular (Korotkov *et al.*, 2012; Yan *et al.*, 2017). In *Y. entomophaga* MH96*,* the T2SS is encoded by genes in the locus PL78_08970 - PL78_08930, with GspCF forming the IM platform, the ATPase GspE, the pseudopilus GspGIJK, and the OM pore GspD (Hurst *et al.*, 2016). The adjacent gene, PL78_08975, encodes for a (putatively the T2SS) transcriptional regulator (Fig. 1B).

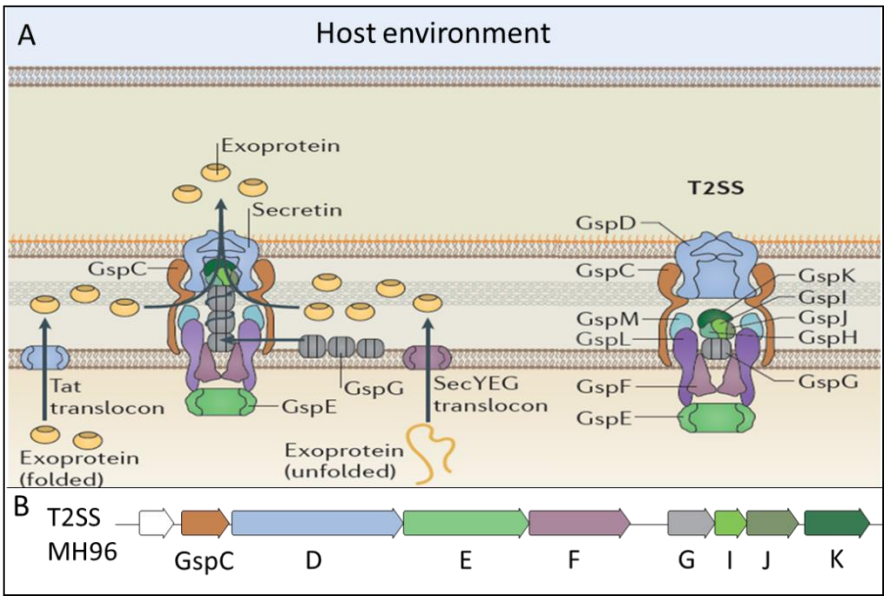

Figure 1. Type 2 secretion system (T2SS). A) Model of the general T2SS. Modified figure sourced from Costa *et al.* with permission (Costa *et al.*, 2015). B) Genetic locus (GspC-K) of the *Y. entomophaga* MH96 T2SS with arrow coloured according to the T2SS model by Costa *et al.* (Costa *et al.*, 2015) . White arrow denotes predicted T2SS transcriptional regulator (PL78_08975).

1.4.5 Type 3 secretion system

The type 3 secretion system (T3SS) of pathogenic Gram-negative bacteria is a flagella-like system that injects effector proteins into eukaryotic cells, such as plant or mammalian cells, with a needle-like structure (Buttner and He, 2009; Block and Alfano, 2011). Such effector proteins have various functions, including cell adhesion and invasion, persistence within the host cells, or host toxicity (Dean, 2011). The core machinery of the T3SS is highly conserved within enteropathogenic bacteria (Notti and Stebbins, 2016). In 1998 Hueck proposed a general nomenclature of the T3SS termed as Sct proteins, for secretion and cellular translocation, cluster (*sctA-sctW*). Since then, different terminology of the T3SS in different strains has evolved: e.g. Ysc in *Yersinia* sp., Psc in *Pseudomonas aeruginosa,* and Esc in *Escherichia coli* (Notti *et al.*, 2016). For simplification, the general structure of the T3SS will be explained below based on the Sct cluster.

The core of the T3SS is comprised of the basal body, formed by an OM-anchored protein (SctC), similar to that of T2SS secretin, which is connected with the IM-anchored proteins SctDJ, spanning the periplasm. SctC and SctDJ form the outer and inner ring of the T3SS basal body, respectively (Hueck,

1998; Marlovits *et al.*, 2004). The T3SS spans through the cell wall and therefore is Sec/Tat independent. The T3SS is comprised of cytoplasmic proteins (SctLKOQ), export apparatus (SctRSTUV), base and needle components (SctCDFIJP) including a needle tip, and translocator proteins, the translocon (Diepold and Wagner, 2014). A variety of T3SS effector proteins exist within Gram-negative bacteria, which are secreted as unfolded proteins, by an ATPase (SctN) and chaperon complex (SctV) driven by the proton-motive force (Terashima and Imada, 2018; Wagner *et al.*, 2018). While it is commonly understood that T3SS effectors are targeted toward eukaryotic host cells, a recent study by Qaidi *et al.* (2020) suggests that the T3SS effector NleB in *Citrobacter rodentium* can be targeted towards bacteria from a different species.

The Ysc T3SS formed by *ysc-yop* operon and the flagellar T3SS is associated with the virulence plasmid, pYV, in all human-pathogenic *Yersinia* strains (Cornelis, 2002). In *Y. pseudotuberculosis*, T3SS expression is low in anaerobic, iron-rich conditions, which mimic the host's intestinal lumen (Hooker-Romero *et al.*, 2019). The same study showed iron-dependent regulation by LscR, a transcriptional regulator of the master regulator LcrF (Hooker-Romero *et al.*, 2019). The master regulator LcrF regulated transcription of effector genes *yopE, yopH, yadA* and *ylpA* of the T3SS in the human pathogenic *Yersinia* strains (Schwiesow *et al.*, 2015). Additionally, gene expression of the *ysc-yop* operon is repressed by the LysR-like transcriptional regulator YtxR, shown in *Y. enterocolitica* to lead to the absence of Yop proteins in the supernatant (Axler-DiPerte *et al.*, 2009). The T3SS effector proteins of human-pathogenic *Yersinia* cause suppression of the tumour necrotic factor alpha (TNF-α) in macrophages and therefore block immune mechanisms, such as cytokines and chemokines, and can induce apoptosis of the host cell (Hartland *et al.*, 1994; Palmer *et al.*, 1998; Chung and Bliska, 2016; Dave *et al.*, 2016). The T3SS in the human pathogenic strains of *Yersinia* is highly expressed *in vivo* at 37°C, but in *Y. enterocolitica* biovar 1B, a hyper-pathogenic isolate causing severe illness in humans, the T3SS was found to be expressed *in vitro* at 26°C in a nutrient-rich medium (Bent *et al.*, 2013).

In *Y. entomophaga* MH96, two T3SSs encoded by PL78_18075-18225 (T3SSYE1) and PL78_14485-14620 (T3SSYE2), have been identified and described by Hurst *et al.* (2016). Additionally, T3SS associated effector proteins, WapA_1 (PL78_12130) and LopT (PL78_18760) are encoded in the MH96 genome (Hurst *et al.*, 2016).

1.4.6 Type 4 secretion system

The type 4 secretion system (T4SS), found in a range of Gram-positive, Gram-negative bacteria and Archaea, can have diverse functions, even within one bacterial species. In Gram-negative bacteria, the general functions of the T4SS are described as cell adhesion and colonisation, motility, biofilm formation, and auto-aggregation (Kirn *et al.*, 2003; Morris *et al.*, 2003; Coil and Anne, 2009; Heiniger *et al.*, 2010). The *Bortdetella pertussis* T4SS complex, called Ptl, secretes the Pertussis Toxin (PT) which acts as the main virulence factor (Christie *et al.*, 2014). In contrast to most Gram-negative T4SS, the *B. pertussis* T4SS secretes the toxin into the extracellular milieu rather than injecting it into a host cell (Weiss *et al.*, 1993). In *Agrobacterium tumefaciens,* the T4SS has been described as secretion machinery for T-DNA into bacterial or plant host membranes. *Y. enterocolitica* subsp. e*nterocolitica* 8081 (biotype 1B) and *Y. pseudotuberculosis* IP31758 (Serotype O:1B) encode chromosomally for a PilD-W Type 4 pili. The latter additionally encodes T4 pili on two plasmids. *Y. entomophaga* and most other pathogenic *Yersinia* strains do not use the T4SS system, so this will not be discussed further.

1.4.7 Type 5 secretion system

The type 5 secretion system (T5SS) is a two-step secretion mechanism that secretes proteins that have been translocated into the periplasm by either Tat or Sec pathway, into the extracellular matrix. T5SS secreted virulence factors are important for cell-to-cell adhesion and biofilm formation (Depluverez *et al.*, 2016). The outer membrane channels of the T5SS can differ and are either formed by autotransporters (type Va) such as the Bam transporter, or are pores of a two-partner secretion system (type Vb) such as Tps, or a third system type Vc a trimeric autotransporter (Desvaux *et al.*, 2005). Further systems are type Vd, a novel T5SS system in *P. aeruginosa* which is a fusion between Va and Vb, and type Ve, a structurally reverse Va system (Salacha *et al.*, 2010; Leo *et al.*, 2012; Meuskens *et al.*, 2019). Protein translocation via the autotransporter systems occurs by a single protein, which are adhesins, proteases, or esterases (Guerin *et al.*, 2017). The protein comprises a signal sequence for either the Tat- or the Sec-pathway, allowing the translocation of the pro-protein into the periplasm, by cleaving the C-domain. The pro-protein harbours a translocation unit, which folds into a beta-barrel with 12-12 transmembrane strand and forms a pore, which enables the translocation of the pro-protein through the OM, and release of the autotransporter into the extracellular milieu (Loveless and Saier, 1997; Henderson *et al.*, 2000; Desvaux *et al.*, 2005). The type Vb secretion system is a two-partner secretion system (TPS) comprised of a secretory passenger protein (TspA) and the transporter protein (TspB). TpsA proteins have varying functions such as hemolysins as seen in *Serratia marcescens* (ShlA) and *Photorhabdus luminescens* (PhlA); proteases in

Pseudomonas aeruginosa (LepA); adhesion in *E. coli* (EtpA) and *P. aeruginosa* (CdrA); and iron acquisition in *Heamophilus influenza* (HxuA) (Cope *et al.*, 1995; Konninger *et al.*, 1999; Brillard *et al.*, 2002; Roy *et al.*, 2009; Borlee *et al.*, 2010; Kida *et al.*, 2011). The proteins of the type Vc are called autotransports-2 (AT-2) or trimeric autotransporters. AT-2 is involved in adhesion and colonisation as described for *Yersinia* YadA, *H. influenza* Hia and Hap (Laarmann *et al.*, 2002; Fink *et al.*, 2003; Roggenkamp *et al.*, 2003).

The *Y. pestis* and *Y. pseudotuberculosis* autotransporter YadA is crucial for cell adhesion (El Tahir *et al.*, 2001; Bancerz-Kisiel *et al.*, 2018). Genome annotation of *Y. entomophaga* MH96 by Hurst *et al.* (2016) did not identify T5SS associated proteins and will therefore not be further discussed in detail.

1.4.8 Type 6 secretion system

The Type 6 Secretion System (T6SS) is a highly conserved system within pathogenic bacteria. Roughly 25% of Gram-negative bacteria exploit a 1.7 MDa T6SS contractile nanomachine which is comprised of 13 or 14 core TssA-M or PAAR components as well as the Val-Gly Repeats (Vgr) tip and Haemolysin-Coregulated Protein (Hcp) tube component (Boyer *et al.*, 2009a; Drebes Dorr and Blokesch, 2018; Coulthurst, 2019). These elements are often encoded on a ~20 kb operon (Silverman *et al.*, 2012). The system consists of a TssL bound element that traverses the IM and reaches the PP. From here TssM interacts with lytic transglycosylase (LTG) to degrade the PP before TssJ can connect the TssL and TssM and breach the OM. Once the TssLJM construct is assembled, TssAEFG and TssK are employed to construct the baseplate structure. This structure is used to build up the inner tube in a head-to-head or head-to-tail fashion from the Vgr point with PAAR tip, using Hcp (Cascales and Cambillau, 2012; Silverman *et al.*, 2012) with help of the TssBC complex. The contraction of TssBC complex results in rapid extrusion of the Vgr/Hcp tube. This rapid extrusion occurs in the presence of target cells and injects the Vgr/Hcp tube through the target's membrane, transporting proteins to the target's cytoplasm. TssH (ClpV) is used to deconstruct the remaining T6SS components, such as TssA, post-injection (Gallique *et al.*, 2017). The T6SS is regulated through numerous pathways including transcriptional activation through the bacterial enhancer-binding protein (bEBP), threonine phosphorylation pathways (TPP), Two-Component Signal Transduction systems (TCSTs) including the Gac/Rsm pathway, through quorum sensing (QS) or transcriptional repression by the iron uptake regulator Fur (Silverman, 2012). T6SSs can target eukaryotic cells, bacterial cells or both, and are used to externalize proteins including QS elements and pathogen effectors, directly into the target cell (Gallique *et al.*, 2017). Some T6SSs secrete effectors directly into the extracellular milieu as shown in the T6SS-4 found in *Y. pseudotuberculosis*, which translocates Zn^{2+} ions through the zinc binding effector YezP (Want *et al.*, 2015).

1.4.9 Alternative secretion pathways

In addition to the classical secretion systems, other mechanisms have been described as crucial for protein secretion in prokaryotes. These systems include OMVs, pore/channel-forming proteins such as holins, large-conductance mechanosensitive ion channels (MscL), ABC exporters, fimbrial usher, and the flagellar export system. In the following Chapter, the flagellar apparatus system as a secretion pathway, holins which are part of a phage-like lysis system and two-partner system (TPS) systems, will be further described.

Flagella

Flagella of many Gram-negative bacteria form the motor for cell motility. Swimming and swarming motility exist in many enteric bacteria which need to be able to adapt to a fast-changing environment upon uptake by the host (Kuhn *et al.*, 2018). The flagellum plays a crucial role in bacterial virulence, as has been shown in species of the genera *Salmonella, Yersinia,* and *Helicobacter pylori* (Kim *et al.*, 2008; Lertsethtakarn *et al.*, 2011; Yang *et al.*, 2012). The general model of the flagellar apparatus was studied in detail in *Salmonella enterica*. The apparatus forming the flagellum can be classified into three major components: the flagellar base; the flagella hook/rod, and the flagella filament (Das *et al.*, 2018). Located in the cytoplasm and the inner membrane are the motor proteins and the basal body proteins encoded by the Fli operon and the motor proteins MotAB in *S. enterica*, which are similar to the basal body of the T3SS. This structure acts as the export apparatus of flagella proteins for the assembly of the flagella (Minamino, 2014). The proton motive force across the bacteria cell membrane delivers energy for the flagellar motor (Nirody *et al.*, 2016). The flagellar motor is comprised of a rotor and stator units forming a transmembrane ion-channel for translocation of protons or sodium ions, which causes rotation of the flagellum (Morimoto and Minamino, 2014). The rotation of the flagellum, clockwise or anti-clockwise, depends on the CheA/CheY chemotaxis system, by which -upon sensing of environmental stimuli - the auto-phosphorylated sensor kinase CheA, transfers the phosphoryl group to the response regulator CheY allowing binding to the basal body and triggering the rotation (Briegel *et al.*, 2012). The flagellum is important for cell invasion and cell adhesion but has also been shown to secrete the virulence factor MakA (motility associated killing factor A) in *V. cholerae* (Dongre *et al.*, 2018).

In *Y. entomophaga* MH96, the flagellum is encoded by the locus PL78_17520-17820 and was studied by Hurst *et al.* (2011), who identified the formation of up to three flagella in culture when grown at 25°C.

Outer membrane vesicles (OMVs)

The secretion of virulence factors in Gram-negative bacteria is complex since the protecting bilayer of the bacterial cell wall is a barrier for the secretion of proteins into the extracellular milieu. Therefore, many secretion mechanisms have evolved in Gram-negative bacteria enabling the extracellular release of proteins. Whereas the T1SS, T3SS, and T4SS use a mechanism for direct translocation into the extracellular milieu, T2SS and T5SS use a two-step mechanism (Korotkov *et al.*, 2012; Leo *et al.*, 2012; Costa *et al.*, 2015). Aside from these dedicated secretion systems, there are other mechanisms for the release of proteins such as release by OMVs.

Outer membrane vesicles have been documented in a wide range of Gram-negative bacteria (Beveridge, 1999; McBroom and Kuehn, 2007). They are secretory vehicles that transport proteins, lipids, and DNA that interact with prokaryotic or eukaryotic cells in their environment (Schwechheimer and Kuehn, 2015). Both pathogenic and non-pathogenic bacteria release OMVs during their growth. Native OMVs of 20 – 400 nm in diameter are composed of at least an outer membrane and cytoplasmic components (Kuehn and Kesty, 2005; Deatherage and Cookson, 2012). OMVs can be distinct in composition and structure depending on the route of formation (Toyofuku *et al.*, 2019). OMVs are responsible for transport along the outer membrane of proteins and lipids that are used for communication and host cell intoxication (Toyofuku, 2019). OMVs have important roles in nutrient degradation, and virulence by the elimination of competing organisms and toxin delivery towards eukaryotic cells (Fiocca *et al.*, 1999; Kadurugamuwa and Beveridge, 1999; Kuehn *et al.*, 2005). Not only do OMVs act as virulence factors, they also serve a protective function by removing potentially toxic, misfolded, or unwanted proteins from the cell. In *E. coli* it was shown that OMV production is decreased under low-stress conditions and increased when an accumulation of overexpressed, misfolded proteins occurred. Furthermore, in *E. coli*, increased vesicle production has been shown to lead to increased survival of bacteria exposed to chemical stress (McBroom *et al.*, 2007).

Scanning electron microscopy (Fig. 2) of *Y. entomophaga* showed OMV formation alongside the cell wall (Hurst *et al.*, 2011b). Furthermore, the LC-MS/MS analysis of MH96 cells showed Yen-TCs co-purified with membrane proteins OmpA and OmpC (Fig. 2B) and the chaperonin GroEL. GroEL is a heat-shock protein that participates in the folding of polypeptides in a temperature-dependent manner (Melkani *et al.*, 2005). GroEL and GroES are chaperonins, which are required for protein folding and play an essential role in proteostasis in cells (Lin *et al.*, 2013; Mizobata and Kawata, 2018). The co-purification of OmpA, OmpC, and GroEL with Yen-TC, which is also temperature-dependent, possibly indicates the secretion of Yen-TC via OMVs but this has yet to be elucidated.

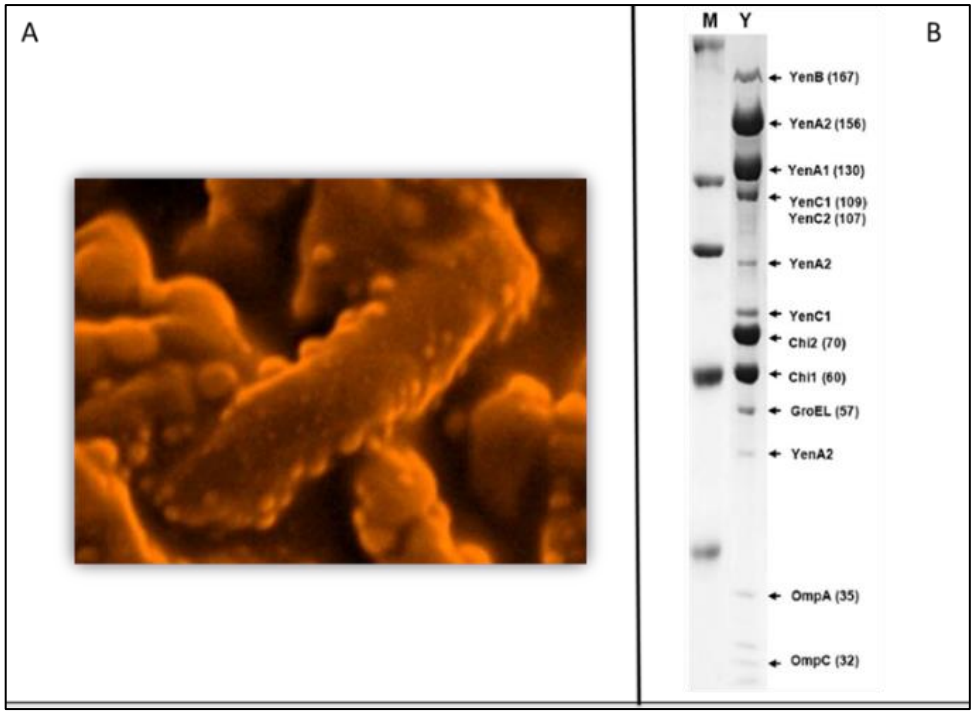

Figure 2: Secretion-phenotype associated cell morphology of *Y. entomophaga* MH96 and exoproteome profile. At 25°C in LB broth. *A)* Outer membrane vesicle (OMV) formation on the cell wall of Y. e*ntomophaga* MH96 (Hurst *et al.*, 2011b). *B)* SDS-PAGE of exoproteome with bands analysed by LC-MS/MS comprising OMV associated proteins including GroEL, OmpA, and OmpC (Hurst *et al.*, 2011b).

1.5 Secondary virulence factors

Secretion systems, toxins, degradative proteins, and invasion/adhesion systems are classified as the main virulence factors in *Yersinia* species. However, other systems with a function that is not primarily for virulence can affect the pathogenicity or toxicity of a bacterial cell. In this thesis, those mechanisms are classified as secondary virulence factors. Secondary virulence factors can contribute significantly to pathogenicity by allowing the cell to adapt to environmental factors and respond to host/ pathogen interactions. Secondary virulence factors include quorum sensing, LPS, and transcriptional regulators of primary virulence factors, including two-components systems, and RNA-interference. These systems are further described in the following Chapters.

1.5.1 Quorum sensing

Quorum sensing (QS), once known as autoinduction and first described in *Vibrio fischeri*, is understood as communication between cells of the same and different species (Turovskiy *et al.*, 2007). Cells require mechanisms to sense and react to changing environmental conditions. Bacteria cells release chemical signal molecules, called autoinducers, to communicate with each other (Miller and Bassler, 2001). With changes in cell density, the accumulated autoinducers in the cell environment activate a signal kinase protein that detects QS molecules (Xavier and Bassler, 2005). In return, the same kinase acts as the transcriptional regulator of the signal molecules synthetase, hence the term autoinduction (Tsai and Winans, 2010). Quorum sensing has been shown to play a role in motility, conjugation, competence, biofilm formation, and virulence (Abisado *et al.*, 2018).

In Gram-negative bacteria, there are two autoinducer molecules: Acetyl-homoserine lactones (AHL) and a molecule termed Autoinducer-2 (AI-2), which was first identified in *Vibrio harvey* (Waters and Bassler, 2005). For a functional QS system, AHL molecules need to be produced, secreted and sensed. Translation and sensing of AHL molecules occur by the two-component system of LuxI and LuxR. LuxI is the AHL synthetase and LuxR is a DNA-binding protein containing the AHL sensor domain (Winans and Bassler, 2002). Most AHLs are very small molecules that are transported by influx/efflux pumps across the cell membrane as shown in *Vibrio parahaemolyticus, E. coli,* and *P. aeruginosa* (Kaplan and Greenberg, 1985; Morita *et al.*, 1998; Pearson *et al.*, 1999; Rahmati *et al.*, 2002). When the AHL molecules accumulate in the micro-environment and a threshold (~1-10 µM in *Photobacterium fischeri* – now known as *Aliivirbrio fischeri*) is reached, LuxR regulates the transcription process of QS-dependent target genes (Eberhard *et al.*, 1981). Chip-seq of LasR (LuxR-like) in *P. aeruginosa* revealed that most of the target genes encode secretion apparatus, secretion factors and genes involved in the biosynthesis of cofactors and carriers (Gilbert *et al.*, 2009). In many bacteria, LuxR also binds to the LuxI promoter causing a negative feedback-loop which leads to quorum-sensing in the cell population. Interestingly, the sensory domains of LuxR proteins are very specific to the respective homoserine lactone. Acetyl-homoserine lactones are composed of a homoserine lactone ring (HSL) and a specific acetyl-chain. Acetyl-chain length can range from C4 to C18 and can be modified with a 3- oxo or 3 – hydroxy substituent or by different stages of saturation (Pearson *et al.*, 1999; Wagner-Dobler *et al.*, 2005; Turovskiy *et al.*, 2007). The specificity is beneficial for populations of multiple species, where it is suggested that each LuxR of a certain species can mainly detect AHL molecules from its species, but some can detect interspecies AHL molecules (Wellington and Greenberg, 2019).

In *Yersinia* spp., the number of QS systems can vary from one to three, and up to sixteen different AHL molecules can be synthesized (Ng *et al.*, 2018). *Y. enterocolitica* encodes YenI/R proteins and an

orphan LuxR-like protein termed YcoR. *Y. pseudotuberculosis* encodes two QS systems: the YpsI/R system that senses the AHL N-(3-oxohexanoyl)-HSL, and the two-component system YtbI/R that senses the AHL termed the N-octanosyl-HSL. *Y. pestis* encodes three QS systems, including Lux systems (YpeIR and YspIR) and an AI-2/LuxS system (LaRock *et al.*, 2013). In *Y. entomophaga,* the QS system has yet to be characterised. Genome annotations reveal the existence of one potential LuxR-like protein (PL78_03845; ANI28431.1) and one LuxI-like protein (PL78_03850; ANI28972.1) (Hurst *et al.*, 2016)

1.5.2 Lipopolysaccharides (LPS)

LPS are surface proteins of the outer membrane and are crucial for the interaction with and reaction to environmental factors. LPS are composed of four structures: the O-polysaccharide chain (O-antigen), the outer core, the inner core, and lipid A (Zgurskaya *et al.*, 2015). While LPS within different bacteria species contain the same basic architecture, modifications in each of these structures lead to a specific endotoxicity (Raetz and Whitfield, 2002). The lipid A, which is anchored within the OM bilayer, comprises two glucosamine molecules, and acyl chains. While the glucosamine backbone is highly conserved, lipid A structures can vary within different bacterial species. Differences can be observed in the number, position, and length of acyl chains, as well as additional groups such as phosphate groups bound to the acyl chain (Raetz *et al.*, 2006). The *Salmonella minnesota* R595 lipid A compound 506 shows less serological specificity than the compound 516, which had a substitution at the C-2 molecule from 3-hydroxytetradecanoyl group to an acyloxyacyl residue (Kasai *et al.*, 1986). The inner and outer core of LPS are conserved and are usually comprised of the sugars keto-deoxyoctulosonate, and heptose (inner core), and hexoses or hexosamines (outer core). The composition of these sugars differs within different types of LPS (Erridge *et al.*, 2002). The most outer structure of LPS is the O-polysaccharides also called O-antigen. The structure is a glycan polymer and consists of up to eight sugar units (Raetz *et al.*, 2002). The O-antigen structure is very diverse within bacterial species but also each bacterial cell produces O-antigens of variable lengths. Because of the physical arrangement outside the cell, O-antigens are one of the first bacterial signals recognised by host cells and are therefore a great target for antimicrobials. LPS not only contributes to cell wall integrity and acts as a barrier against antimicrobials, but it has also been implicated to play an active role in virulence (Gunn, 2001; Pier, 2007). The modification of the O-antigen in *Salmonella typhimurium* strain NCTC 12023 decreased replication rates and the deletion of the O-antigen resulted in non-virulence in the caterpillar *Galleria mellonella* (Bender *et al.*, 2013).

LPS also plays a role in adhesion and motility (Bradfield *et al.*, 2008; Lindhout *et al.*, 2009; Li *et al.*, 2014). They can also elicit an immune response as they have pathogen-associated molecular patterns recognisable by host cells. In *Y. pestis,* restructuring of the LPS molecules occurs upon exposure to different temperatures, altering resistance to polymixin B (representing cationic antimicrobial peptides secreted by immune and epithelial cells upon bacterial infection), and immune response was decreased (Anisimov *et al.*, 2005). In *Y. entomophaga* MH96, LPS genes are encoded on loci PL78_ 00680 – 00765 and PL78_07545 - 07480 forming a tyvelose- containing O-polysaccharide, similar to *Y. pseudotuberculosis* as described by Sizova *et al.* (2017).

1.5.3 Transcriptional and post-transcriptional regulation of exoproteome release

Crucial for bacterial virulence is the activation of secretion systems and other virulence factors, but only when this is beneficial for the cell. Synthesising toxins and other virulence factors exert a high metabolic burden on cells, which can reduce the growth of the cell population. Therefore, protein synthesis needs to be tightly regulated in response to environmental factors (Sturm *et al.*, 2011). For this reason, a cascade of regulatory systems is often in place. In *Yersinia* and *Salmonella,* early stages of host colonisation are under the regulation of several proteins in response to environmental factors such as temperature, osmolarity, pH, and nutrient availability (Erhardt and Dersch, 2015; Chen *et al.*, 2016). Many of these conditions are sensed by two-component systems such as EnvZ/OmpR, BarA/UvrY, or CpxA/CpxR and affect further regulators e.g. the carbon storage circuit (CsrABC), or the AraC-like transcriptional regulator LcrF and the LysR-like transcriptional regulator RovM (Erhardt *et al.*, 2015). In *Y. pseudotuberculosis*, OmpR acts as a transcriptional regulator of the invasion *inv* and the T6SS in response to pH homeostasis and acid tolerance (Brzostkowska *et al.*, 2012; Zhang *et al.*, 2013). OmpR is part of a two-component regulatory system (TCS) with its counterpart EnvZ, which acts as the signal sensor (Hoch, 2000). Two-component regulatory systems (TCS) are ubiquitous, well-characterised systems that sense and respond to environmental changes. Generally, a two-component regulatory system consists of a membrane-bound histidine kinase, that responds to a specific environmental stimulus such as phosphate, pH, osmotic stress, nutrient availability, and a corresponding receiver protein, which acts as a transcriptional regulator upon phosphorylation by the histidine kinase (Groisman, 2016; Lubin *et al.*, 2016; Chakraborty and Kenney, 2018; Bontemps-Gallo *et al.*, 2019). In *Y. pestis* the TCSs, PhoP/PhoQ and OmpR/EnvZ are required to cause the bubonic plague (Reboul *et al.*, 2014).

Another mechanism of regulation of protein secretion is the transcription regulation of exoproteins or secretion systems by secondary structures of DNA and RNA. The formation of DNA loops is initiated by the binding of a single protein or protein complex simultaneously to two different sites of the DNA (Cournac and Plumbridge, 2013). DNA-loops can be formed by binding DNA from different loci, a mechanism often imitated by the histone-like nucleoid-structuring protein H-NS (Dame *et al.*, 2006). H-NS binds AT-rich region and predominantly binds within intergenic regions (Dillon and Dorman, 2010). H-NS has been shown to play an important role in virulence by silencing transcription of the invasin Inv in *Y. enterocolitica*, or silencing the gene expression of *rovA*, encoding the transcriptional regulator of *inv* in *Y. pseudotuberculosis* (Heroven *et al.*, 2004; Ellison and Miller, 2006).

Post-transcriptional regulation occurs when transcribed mRNA is modified, stabilised, or degraded to modulate the balance between transcription and mRNA translation rate in response to environmental growth conditions. Upon DNA transcription, mRNAs can be modified in several ways. Faulty mRNAs, or too high concentrations of mRNA, are degraded by endonucleases such as RNaseE (Picard *et al.*, 2009). As protection against unwanted degradation by an endonucleases mRNA, stability in prokaryotes is achieved by triphosphorylation of mRNA 5' region, or by RNA-binding proteins, which protects mRNA cleavage by binding to poly(A) tail (Folichon *et al.*, 2003). Furthermore, secondary structures in the 5' UTR of the transcribed genes, which are part of the mRNA, such as forming hairpin-structures, protect mRNA from cleavage by RNaseE (Picard *et al.*, 2009). Some RNAs form thermo-switches or riboswitches. Riboswitches are cis-acting elements, that are predominantly found in 5' UTRs of mRNAs, controlling transcription of the adjacent gene (Garst *et al.*, 2011). Riboswitches commonly bind small molecules (ligands), causing a change in conformation which results in either transcription attenuation or translation initiation (Smith *et al.*, 2011). Such ligands are often small metabolites or ions such as Mg2+, nucleic acid precursors, enzyme co-factors, and amino-acid residues (Hammann and Westhof, 2007). RNA thermometers, thermo-switches, are also commonly located in the 5' UTR of mRNAs and change their conformation in response to temperature changes. The RNA thermometer forms a loop, which sequesters the ribosomal binding site, which is available after conformational changes of the RNA with increasing temperature (Rossmanith and Narberhaus, 2016). Such an RNA thermometer was previously shown to regulate gene expression of the cytotoxic necrotizing factor (CNFY), which is released by membrane vesicles in *Y. pseudotuberculosis* (Twittenhoff *et al.*, 2020).

Another RNA-based translational regulation occurs by binding of non-coding RNA (ncRNA) or small RNA (sRNA) to the complementary sequence of the mRNA. Binding of mRNA by an sRNA in close proximity (c*is*-sRNA) often does not require a co-factor (Liu and Camilli, 2010). In contrast, *trans*-sRNA located on a distinct locus, requires a co-factor, such as Hfq, to bind to the mRNA (Liu and Camili, 2010). In most cases, sRNAs act as negative post-transcriptional regulators, causing the degradation of the target mRNA, but a few sRNAs have been identified as a transcriptional activator by removing 5'UTR stem-loop structures enabling transcription or inhibiting mRNA degradation (Frohlich and Vogel, 2009; Lee and Gottesman, 2016; Durand *et al.*, 2017).

1.6 Bacteriophages

Bacteriophages are viruses that infect Bacteria or Archaea. They have been studied in detail and over many decades. Several forms have been identified and the classification of bacteriophages has been adapted in response to new findings. Bacteriophage can differ in the morphology of capsid and envelope, type of nucleic acid (RNA or DNA), and double or single-stranded nucleic acid. The bacteriophage genome can vary from 3.5 kb ssRNA to 500 kb dsDNA (Salmond and Fineran, 2015). Bacteriophages are divided into orders: *Caudovirales, Ligamenvirales, Herpesvirales, Ortevirales,* or referred to as "unclassified". Most common phages belong to the order *Caudovirales* which can be classified into families of *Myoviridae, Siphoviridae, Podovirdidae, Ackermannviridae,* and *Herelleviridae* (International Committee on taxonomy of Viruses, ICTV, 2019).

Phages from the order *Caudovirales* are typically dsDNA, tailed bacteriophages. The genome encodes for structural components of the head, tail, and tail fibres, but also regulatory, metabolic, and replication genes. The tail fibres of bacteriophages attach to the host cell. With a needle-like complex, the contractile tail, the bacteriophage transfers phage DNA into the host cell. In the host cell, the phage enters one of two known cycles: the lytic or lysogenic cycle. In the lytic cycle, phage DNA is rapidly replicated for assembly of the phage within the host. Upon assembly, a holin-endolysin lysis cassette leads to disruption of the cell membrane allowing multiple phages to exit the cell and to enter new host cells. Temperate phages, such as the λ phage, replicate by the lysogenic cycle, where phage DNA is either integrated into the host chromosome or persists in a plasmid-like state (Hertwig *et al.*, 2003). Replication of the host DNA for cell duplication automatically leads to the multiplication of the phage DNA. At this stage, the phage can persist in the host cell until a trigger causes the phage to enter the lytic state, ultimately causing cell lysis (Laganenka *et al.*, 2019). These triggers are often environmental changes such as nutrient deficiency or DNA-damaging stress. A recent study also

showed that cell density and the metabolic state of the cell, indicated by cAMP levels, can trigger the induction of the lytic cycle (Laganenka *et al.*, 2019). The late expression genes of the lytic cycle include a lysis cassette comprised of a holin, endolysin of muralytic function and, in some phages, a spanin-complex. The activation of the lysis cassette leads to disruption of the host cell membrane, causing cells to burst and allowing re-assembled bacteriophages to then infect new host cells.

1.6.1 Lysis-cassettes

Once the bacteriophage genome has integrated into the host chromosome during the lysogenic cycle, the term prophage is used. Prophage-derived lysis cassettes are virulence factors in Gram-negative bacteria and comprise at least an inner membrane pore-forming protein called holin and cell wall degrading enzymes (endolysins), such as glycosidases, amidases, muramidase, and carboxy/endo-peptidase (Schmelcher *et al.*, 2012; Fernandez-Ruiz *et al.*, 2018). Gene arrangements and numbers of genes within the phage lysis cassette can differ and are dependent on the host (Fig. 3A) (Kongari *et al.*, 2018). The classical phage λ consists of a holin-antiholin complex, an endolysin and spanin complex Rz/Rz1 (Berry *et al.*, 2012). Some phages, such as P2 phage, encode for a second endolysin or an additional esterase (To *et al.*, 2013). Phages, especially from Gram-positive bacteria, such as *Listeria* phage A118 and *Bacillus* phage SPP1 do not encode for spanins and the lysis cluster is only comprised of a holin and one or more endolysins (Catalao *et al.*, 2013; Gigante *et al.*, 2017). Mycobacteria phages such as Ms6, on the other hand, often encode for a holin, an endopeptidase, and a LysB-like IM-spanin (Catalao *et al.*, 2013). Holins encoded within the lysis cassette can be classified as Holin I, Holin II, and Holin III (To *et al.*, 2013). The classification is according to the arrangement of the holin transmembrane domains anchored within the inner membrane. Holins can be further classified into canonical or pinholins (Fig. 3B). Canonical holins integrate as homodimers in the IM (Grundling *et al.*, 2000). Upon a certain trigger, redistribution of the holin homodimers occurs, forming a raft of hundreds of holin molecules, with an average pore size of up to 1 µm in diameter (White *et al.*, 2011; Savva *et al.*, 2014; Young, 2014). In contrast, pinholin only forms heptameric channels with a pore of ~2 nm in diameter (Pang *et al.*, 2009; White *et al.*, 2011). These pores do not allow endolysin translocation, but rather the assembly of 1000 of these channels causes the pmf to collapse, which causes the release of signal-anchor release (SAR) endolysins from the IM (Cahill and Young, 2019). SAR endolysins can be translocated independently of holins. SAR endolysins have a signal anchor release (SAR) domain, and upon translocation into the IM by the Sec-pathway, cleavage of the inactive endolysin at the SAR domain occurs, releasing protein and activating proteolytic function (Xu *et al.*, 2004; Cahill *et al.*, 2019).

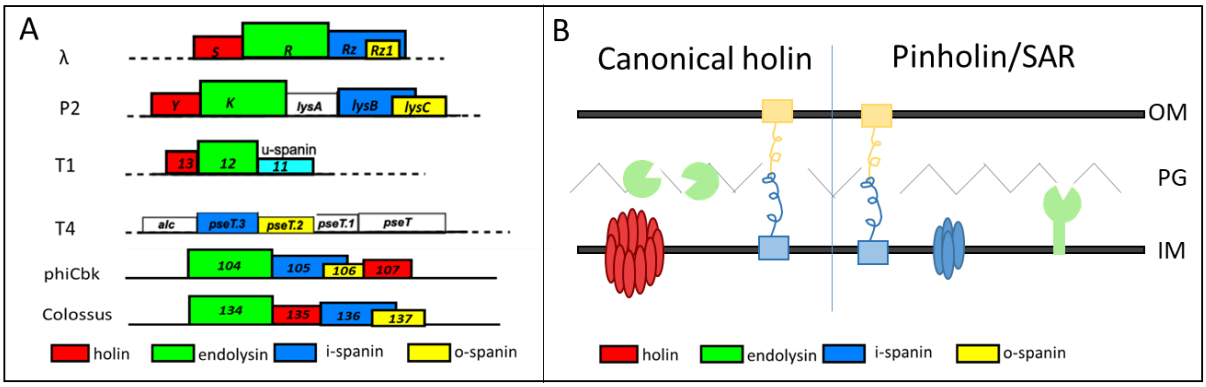

Figure 3: Schematic of lysis cassettes. *A)* Arrangement and integration of bacteriophage lysis cassettes - modified (Gill *et al.*, 2012; Kongari *et al.*, 2018)). *B)* Model of the function of the lysis cassette components and integration in the outer membrane (OM), inner membrane (IM), and peptidoglycan (PG).

Bacteriophages of the virus orders *Tectivirales, Corticovirales,* and the majority of *Caudovirales*, which are commonly found in Gram-negative bacteria, encode a λ phage-like two-component spanin complex (Gill *et al.*, 2012; Cahill *et al.*, 2017; Cahill *et al.*, 2019). The complex comprises an i-spanin, with N-terminal integration into the inner membrane (IM), and an o-spanin, with N- terminal integration into the outer membrane (OM) (Berry *et al.*, 2008). The free C-terminal sites can interact and form a complex which spans the periplasm and, upon degradation of the peptidoglycan (PG) by the endolysin, the spanin complex undergoes a hairpin-like conformational change, resulting in the fusion of IM and OM, and subsequent OM disruption and cell lysis (Berry *et al.*, 2008; Rajaure *et al.*, 2015). The second form of spanins are found in phages JK06, Stx2-II, *Rosebacter phage* SI01 and others, and consist of a single unimolecular spanin (u-spanin) (Kongari *et al.*, 2018; Cahill *et al.*, 2019). The gene is often associated with genes encoding a canonical-holin, an endolysin and a hypothetical gene, and a rho-independent transcriptional terminator. U-spanin is formed by a protein with an integral membrane C-terminus and an N-terminus which is linked with the outer membrane (Summer *et al.*, 2007). The spanin-complex in Gram-negative bacteria is essential for bacterial lysis (Berry *et al.*, 2012). The formation of the holin-endolysin complex and the resulting cell lysis is a rapid process once the pore formation by holins is induced. Based on this, holins are often classified as the gatekeeper of bacteriophage induced cell lysis (Krupovic and Bamford, 2008).

1.7 *Yersinia entomophaga*

The entomopathogen *Y. entomophaga* carries several genes associated with virulence factors and a toxin associated gene cluster. Some of these genes are encoded in rearrangement-hotspot-associated regions (Rhs1–Rhs5), whereas others encode virulence factors such as a haemocoel-active toxin (PirAB) and repeats in toxin (RTX) (Hurst *et al.*, 2016). Similar to *Y. enterocolitica, Y. entomophaga* encodes two T3SSs designated T3SSYE1 and T3SSYE2. In addition, cell surface adhesion proteins, a T2SS, a T6SS, and iron acquisition and transport systems, such as OMVs, identified in *Y. entomophaga,* likely contribute to its pathogenesis (Hurst *et al.*, 2016). The genome of *Y. entomophaga* encodes several proteins that may cause virulence. Some of these genes are involved in iron transport and iron homeostases, such as those encoding iron siderophores, including enterobactin and ferrichrysobactin, and the ferric uptake regulator (Fur). Proteolytic enzymes encoded in the *Y. entomophaga* genome, including proteases, chitinases, haemolysin and lipase, are often co-located with these iron-associated gene clusters (Hurst *et al.*, 2016) suggesting that regulation of virulence factors is iron-dependent. The regulation and mechanisms of protein release in *Y. entomophaga* have not yet been determined, but temperature and media components affect protein secretion (Hurst *et al.*, 2011b). Yen-TC is regulated in a temperature-dependent manner, with secretion into the culture supernatant at <25°C but not at 37°C. At 25°C, up to 0.5 mg of Yen-TC was released into the supernatant per 100 ml of Luria Bertani (LB) broth, at 8 h post-inoculation (Hurst *et al.*, 2011b). Growth of *Y. entomophaga* in LB broth has shown that the release of Yen-TC occurs at the mid-log stage in the fermentation process by a yet-to-be-determined mechanism.

1.8 Hypothesis and aims

This study is based on the assumption that protein secretion is a highly complex process that imposes a significant burden on the cell. The secretome is the accumulation of proteins actively secreted by several secretory systems and through passive protein release such as cell lysis, processes which can be regulated under conditions beneficial for expression of these pathways. Integration of secretion systems often requires restructuring of cell membranes, a process of high metabolic burden and activation of secretion requires ATP and proton motive force, resulting in high energetic burden for the cell. Processes such as cell lysis cause cell death of a single cell which can be beneficial for the bacterial population e.g. biofilm formation.

Y. entomophaga MH96 releases a high amount of Yen-TC (5 g/L), a member of the toxin complex family of insecticidal proteins. Hurst *et al.* (2011) showed that only at low temperature is the Yen-TC expressed and secreted into the supernatant.

Through the development of *Y. entomophaga* as a biopesticide, in-house studies undertaken by AgResearch have found, similar to many Gram-negative bacteria, that limited shelf life stability is a barrier to its commercial development. In the instance of *Y. entomophaga* MH96 this limited shelf life is thought to be influenced by the metabolic burden of producing exoproteins. In addition to limited *Y. entomophaga* MH96 shelf stability, previous studies by S. Jones, of the Hurst laboratory, showed that the exoproteome release occurs with increasing cell numbers. Under fermentation conditions, oxygen and temperature are constant so that any changes in the secretion profile are the direct effects of population growth and nutrient depletion. During the fermentation process, a temporary drop in pH was observed which could be correlated with the onset of protein secretion.

Hypothesis: A more stable, robust product can be developed by decreasing the metabolic burden of the cell, caused by the production of large toxins and the associated secretion system.

Aim 1: To decrease the metabolic burden caused by exoproteome release over secretion systems, it is of importance to identify the secretion mechanism and regulation in *Y. entomophaga* MH96.

Approach 1: In Chapter 3, a consistent sampling protocol was developed, which allowed the analysis of the exoproteome to determine at which growth phase the exoproteome

is detectable in the supernatant and the correlation of this with cell counts and cell density.

Approach 2: To identify genes that are involved in the regulation of protein release, a high-throughput exoproteome screening assay of transposon mutants for altered production and release of exoproteins was developed in Chapter 4. Using the developed screening, assay the exoproteome release was investigated in an up-scaled production experiment.

Aim 2: To understand the underlying regulation the identified genes involved in the exoproteome release were characterised, with the overall goal to identify possible triggers that initiate the release of exoproteins.

Approach 1: The *Y. entomophaga* quorum sensing system was analysed to determine the effect on exoproteome release (Chapter 5).

Approach 2: An identified unique cluster, YeRER, was identified as a potential regulatory region for exoproteome production and release. The genetic elements of this region were assessed by microscopy, mutation, *trans* complementation, and transcriptomics to investigate their respective function in exoproteome release (Chapter 6).

Aim 3: To understand exoproteome release during fermentation, it was of interest to investigate if a changing pH in the culture could trigger the release of exoproteins.

Approach: During the fermentation process, with unadjusted pH, samples were collected prior, during, and after a temporary pH drop and assessed by proteomics and transcriptomics, to understand gene regulation of release mechanisms upon the change in pH (Chapter 7).

Chapter 2

Materials and Methods

2.1 Media, bacterial strains, plasmids and culture conditions

Bacterial strains and plasmids used in this study are listed in Table 1. Bacteria were cultured in the lysogenic broth (LB) (Miller) or on LB agar plates according to the manufacturer's instructions (Merck, Darmstadt, Germany). *E. coli* strains were incubated under standard laboratory condition in LB broth at 37°C, 200 rpm, shaking in an orbital shaker. Unless stated otherwise, *Y. entomophaga* MH96 and its derivates for standard growth were grown in LB broth at 25°C with shaking at 200 rpm in a Ratek model OM11 orbital incubator. Agar plates were incubated at 37°C for *E. coli,* and at 30°C for *Y. entomophaga* and *Chromobacterium violaceum*, respectively.

Table 1: Bacteria strains and plasmids used in this study

Strains	Description	Reference
E. coli strains		
ST18	*Escherichia coli* S17 λpir Δ*hemA*	(Thoma and Schobert, 2009)
DH10β	F- *mcrA* Δ(*mrr-hsdRMS-mcrBC*) Φ80d*lacZ*ΔM15 Δ*lacX*74 *endA1 recA1 deoR* Δ(*ara,leu*)7697 *araD*139 *galU galK nupG rpsL* λ-	(Lorow and Jessee, 1990)
EC100D pir^{+}	F− *mcrA* Δ(*mrr-hsdRMS-mcrBC*) φ80d*lacZ*ΔM15 Δ*lacX*74 *recA1 endA1 araD139*Δ(*ara, leu*)7697 *galU galK* λ− *rpsL nupG* pir+ (DHFR)	(Metcalf *et al.*, 1994)
CM2929	Cm^{R}, *dam*13::Tn*9*, *dam*-6	(Marinus *et al.*, 1983)
Y. entomophaga strains		
MH96	Wild-type strain, isolated from diseased *Costelytra giveni* larva	(Hurst *et al.*, 2011a)
K18	Spontaneous MH96 non-secreting derivative, isolated at 4 weeks post field trial application.	AgResearch culture collection
KTMS04-53	Transposon mutants of MH96 generated by random Tn5 insertion in this study, Kan^{R}	This study
MH96ΔYLC	Δ*holA-pepB-rz* by replacement with kanamycin cassette, Kan^{R}	This study
MH96Δ*gspD*	Δ*gspD* by replacement with kanamycin cassette, Kan^{R}	This study
MH96Δ*roeA*	*roeA:spc* interruption *reoA* with Spc^{R} cassette	This study
Chromobacterium violaceum		
CV026	AHL biosensor	(McClean *et al.*, 1997)
Plasmid	Description	Source or reference
pKD4	Kan^{R}, cloning vector	(Datsenko and Wanner, 2000)
pGEM T-Easy	Amp^{R}, cloning vector, LacZ multi-cloning site	Promega Ltd.
pJP5608	Tet^{R}, suicide vector,	(Penfold and Pemberton, 1992)

pARA	Amp^R, arabinose induction vector	(Shaw *et al.*, 2003)
pACYC184	Cm^R, Tet^R, cloning vector	(Chang and Cohen, 1978)
pHP45	Spc^R, cloning vector	(Moore 1995)
pKRPCN	mini-Tn5-based transposon Tn-DS1028uidAKm, uidA β-glucuronidase (GUS) reporter, tetracycline (Tc) resistance cassette and R6Kγ origin	(Mesarich *et al.*, 2017)

The culture medium for growing *E. coli* strain ST18 was supplemented with 50 µg/ml 5-aminolevulinic acid (Table 2).

All media and broth were autoclaved at 121 °C for 20 minutes. Antibiotics and supplements/substrates specific to the bacteria strain were added at the concentrations listed in (Table 2).

Table 2: Antibiotics and substrates used in this study

Antibiotic	*E. coli* (µg.ml^{-1})	*Y. entomophaga* (µg.ml^{-1})
Ampicillin (Amp)	100	400
Chloramphenicol (Cm)	30	30
Kanamycin (Kan)	50	100
Tetracyclin (Tet)	30	30
Spectomycin (Spec)	100	100
Substrate	***E. coli* (µg.ml^{-1})**	***Y. entomophaga* (µg.ml^{-1})**
(X-gal)	100	100
(ALA)*	50	N.A.

* only for *E. coli* strain ST18, N.A, not applicable

2.2 General culture conditions of *Y. entomophaga* for exoproteome and cell growth assessment

Pre-cultures of *Y. entomophaga* MH96 cells and its derivates were grown in 3 ml of LB broth for 7 h at 25°C and 200 rpm shaking. MH96 mutant strains were supplemented with the respective antibiotics. LB broth (50 ml) was added to a 250-ml Erlenmeyer flask, which was then inoculated with 1% of 7 h culture and then cultured for 16 h at 25°C and 200 rpm shaking. Samples were then taken at 16 hpi to assess CFUs, OD (Chapter 2.2), and exoproteome via Sodium dodecyl sulphate polyacrylamide gel electrophoresis (SDS-PAGE) (Chapter 2.5.1) and Bradford assay (Chapter 2.5.2). Where applicable, alternative culture conditions are defined in the method Chapter of the appropriate chapter.

2.3 Assessment of cell growth

Cell growth was determined by measurement of optical density at 600 nm (OD_{600}) and defining colony forming units (CFUs) through serial dilution on LB agar plates.

For optical density, 1 ml of cell culture was transferred into cuvettes and measured at 600 nm. ODs over 1 were diluted in 1:10 in water and measured again. Each cuvette was measured twice, and experimental triplicates were used, the values were then averaged.

To measure CFUs, a dilution series of the culture broth was undertaken. One hundred µl of cell culture was independently mixed with 900 µl of sterile 0.01M phosphate-buffered saline (PBS) (0.138M NaCl, 0.0027M KCl, pH 7.4) provided by Sigma-Aldrich (Merck, Darmstadt, Germany) in a 1.5 ml microcentrifuge tube, and gently vortexed. The initial dilution was considered 10^{-2} dilution, and from the 10^{-2} dilution 100 µl was removed and diluted in 900 µl PBS and vortexed, resulting in the second dilution of 10^{-3}. This process was followed until the dilution 10^{-9} was reached. Based on OD_{600}, 50 µl or 100 µl of the appropriate dilution was plated on LB agar plates. For plasmid stability tests, the appropriate antibiotics were added to LB agar plates and the serial dilutions independently plated in parallel on LB and LB with antibiotic plates. The resultant colony number was then multiplied by factor 20 (50 µl) or 10 (100 µl) and by a factor of the plated dilution, e.g. when 10^{-3} dilution it was multiplied by factor 1000.

2.4 Molecular DNA techniques

2.4.1 Isolation of genomic DNA and plasmid DNA

For isolation of genomic and plasmid DNA, a 3-ml culture of the appropriate strain was grown overnight under standard conditions. One millilitre of the overnight culture was then used to isolate genomic or plasmid DNA using the extraction kits: ISOLATE II Genomic DNA kit (BioLine) and High Pure Plasmid Isolation Kit (Roche), respectively, according to manufacturer's protocols. For DNA cloning plasmid isolation was performed following the method of Birnbolm and Doly (1979). For plasmid DNA extraction, alkaline lysis was undertaken (Birnbolm and Doly, 1979). One millilitre of an overnight culture was pelleted by centrifugation and supernatant aspirated. The resultant cell pellet was then resuspended in 150 µl Solution 1 (5 mM Tris-HCl (pH8), 10 mM EDTA and 0.9% glucose). Then, 200 µl of Solution 2 (200 mM NaOH, 1% SDS in water) was added, inverted and incubated at 37°C for 5 min. Then 150 µl of 3M sodium acetate (pH 5.2) was added, vigorously mixed, and placed in ice for 10 min. Afterwards, the reaction was spun down at 16,100 × *g* for 10 min and the supernatant was transferred

into a new 1.5 ml microcentrifuge tube containing 1 ml 100% ethanol. The microcentrifuge tube was inverted several times and centrifuged at 16,100 × *g* for 5 min. The supernatant was aspirated and the pellet air dried, for evaporation of residual ethanol, at 37°C for 25 min. The cell pellet was then resuspended in 25 µl sterile dH_20.

2.4.2 Polymerase chain reaction (PCR)

To amplify genetic regions of interest a PCR with platinum Taq DNA Polymerase (Invitrogen) was conducted according to the manufacturer's instruction. A standard PCR of a 50 µl reaction was set up using the following reaction conditions (Table 3):

Table 3: Mastermix of PCR for 50 µl reaction

Reagent	Volume (µl)
Nuclease-free water	38.8
10 x PCR- Buffer, – Mg	5
MgCl2 (50mM)	2
dNTP Mix (10 mM)	1
Primer I (10 µM)	1
Primer II (10 µM)	1
Template DNA (undiluted)	1
Platinum Taq Polymerase	0.2

Primer used in this study are listed in Table 4:

Table 4: Primers used in this study*

ID	Description	Sequence 5'-3'	Template	Restriction site
MS01	primer FRT-Kan-FRT fw	GTGTAGGCTGGAGCTGCTTC	pKD4	FRT-site1
MS02	primer FRT-Kan-FRT rev	CATATGAATATCCTCCTTAGTTCC	pKD4	FRT-site2
MS03	Δ*gspD* UP (500bp flanking region) fw	aaaGAGCTCGGATTCACGCCTGACAGGAAC	MH96	SacI
MS04	mutagenesis *gspD* UP (500bp flanking region) rev	**GAAGCAGCTCCAGCCTACAC**GACAGACAAGCACAGTTTG	MH96	FRT-site1
MS05	mutagenesis *gspD* DOWN (500bp flanking region) fw	**ACTAAGGAGGATATTCATA**TGGTCGCTGTCGACAACCAT	MH96	FRT-site2
MS06	mutagenesis gspD DOWN (flanking region) rev	aaaGAGCTCCTTGCTTCACTGCTTCAGAC	MH96	SacI
MS11	Validation primer insight *kan*-cassette - rev towards 5'	GCAGTTCATTCAGGGCACCG	pKD4 - Kan-cassette	
MS12	Validation primer insight *kan*-cassette -fw towards 3'	GGCTGGGTGTGGCGGACCGC	pKD4 - Kan-cassette	
MS13	Validation primer *gspD* fw	CTCACCGTGGTTAGATGGTAAAG	MH96	
MS14	Validation primer *gspD* rev	CGAAACTCATGCCAACAATGACG	MH96	
MS23	KO *holA* 1kb up fw	aaaGAGCTCCTACCCTTGGTTATTGTTTG	MH96	SacI

MS24	KO *hoA* 1kb up rev	**GAAGCAGCTCCAGCCTACAC**CTCCCCATCCTGTTCTTCAC	MH96	FRT-site1
MS25	KO *holA*_operon 1kb Down fw	**ACTAAGGAGGATATTCATA**TGCTATCCCGGTTATGTGGAAG	MH96	FRT-site2
MS26	KO *holA*_operon 1kb Down rev	aaaGAGCTCGGAATCCCTATCATTTAGGG	MH96	SacI
MS29	Val. MH96ΔYLC fw	CCCTATCTATTAGCTGACCG	MH96	
MS30	Val. MH96ΔYLC rev	CACGAACATGTAGAGCCAGC	MH96	
MS40	YeRER for	aaaCCCGGGCGCGATTGTCTCCTCTTTTTG	MH96	SmaI
MS41	YeRER rev	AAACCCGGGCCCGATTAAGGAAACTTAG	MH96	SmaI
MS42	INT rev	aaaCCCGGGCCCTCCCCATCCTGTTCTTC	MH96	SmaI
MS43	INT fw	AAACCCGGGAACTACTCCTCCTTAAAATTAG	MH96	SmaI
MS44	INT_YLC PCRIII rev	aaaCCCGGGTCATGGGGCAATAGCAGCGC	MH96	SmaI
MS45	Holin-hypoPrI- PCRV rev	aaaCCCGGGATGATGTATTTTGTAGTGGCAG	MH96	SmaI
MS46	holin_noncodingregion2_ down PCRVI for	aaaCCCGGGCCCCCGTTATTTAACGTCAC	MH96	SmaI
MS71	*roeA*_ R deletion by interruption	CAATTACAACGTGGACCTCTGCCG	MH96	
MS72	*roeA*_ F2 deletion by interruption	TAAGCGTCGTCCAGTCACCGCCC	MH96	PmaCI
MS82	2kb_lysis_casette for UP	GCGGCGGAGCTCCGGTAGTGGCATAGGGTTAG	MH96	SacI
MS83	2kb_lysis_casette rev UP	GAAGCAGCTCCAGCCTACACCCCTCCCCATCCTGTTCTTC	MH96	
MS84	2kb_lysis_casette for DOWN	ACTAAGGAGGATATTCATATGCCCCCGTTATTTAACGTCAC	MH96	
MS85	2kb_lysis_casette rev DOWN	GCGGCGGAGCTCCCGATTAAGGAAACTTAGTCG	MH96	SacI
MS99	Cm-cassette SalI fw	aaaGTCGACGAAGCACTTCACTGACAC	pACYC184	SalI
MS100	Cm-cassette SalI rev	aaaGTCGACGGCGTAGCACCAGGCGTT	pACYC184	SalI
MS101	fw HML-pARA	aaaCATATGACGTTAAAGATTCCGACTG	MH96	NdeI
MS104	rev HML_pARA	aaaCTCGAGGGATAATGCCGACACACTTTAA	MH96	XhoI
MS105	val. *reoA* deletions	GATTGGTTCGGATCGGATTG	MH96	
MS111	validation EcoRI_Cm rev	CCGTTCAGCTGGATATTACG	pACYC148	
MS112	validation *Eco*RI_Cm fw	CGTCGTGGTATTCACTCCAG	pACYC148	
MS113	validation Spec out primer 5'	CGTTACCACCGCTGCGTTCG	pHP45	
MS114	validation Spec out primer 3'	GCGCGCAGATCAGTTGGAAG	pHP45	
MS115	val. Tet rev	GCACCTGTCCTACGAGTTGC	pACYC148	
MS116	val. Tet fw	CATCACCGATGGGGAAGATC	pACYC148	
MS118	184_msc_fw	CAACCCTTGGCAGAACATATC	pACYC148	
MS119	184_msc_rev	CCTCACCATCTATAAGCAAC	pACYC148	
MS120	184_pvu fw	GACTAAATCCAATAGACGCAG	pACYC148	

MS121	184_pvu rev	GTGCCAACATAGTAAGCCAG	pACYC 148	
MS127	o-spanin fw + RBS	AAAGGGCTCGCCATAACTCAGCGTCAGGC	MH96	XhoI
MS128	o-spanin fw2 + RBS	GGGCTCGAGGCCATAACTCAGCGTCAGGC	MH96	
MS130	i-spanin for	aaaCATATGAGTCTGCTCAGTGTTTTGA	MH96	NdeI
MS134	ncRNA YLC fw	CTAATTGTTCAATAATATGAAC	MH96	
MS135	ncRNA YLC rev	GTTAACGTCAGAATGACGCAG	MH96	
MS136	ncRNA YLC fw2	CATAGCGATATTGAGCTTATC	MH96	
MS137	ncRNA YLC rev2	CTTTATAATCAGCTTGAATAGC	MH96	
MS138	ncRNA YLC_repeat fw	GAGTTTCTCTGTCATTTCGAAG	MH96	
MS139	ncRNA YLC_repeat rev	CGTGATAAATAGATCTTGGATG	MH96	
M13F	Sequencing primer pGEM fw	GTAAAACGACGGCCAGT	pGEM	
M13R	Sequencing primer pGEM rev	GCGGATAACAATTTCACACAGG	pGEM	
ARAF	Sequencing primer pARA fw	TCCATAAGATTAGCGGATCCTAC	pARA	
ARAR	Sequencing primer pARA rev	CATGGGGTCAGGTGGCAC	pARA	
SpecF	Amplification Spc-cassette fw	ACCCTCACTGATCCGCATGCC	pHP45	
SpecR	Amplification Spc cassette rev	GTGCTTAGTGCATCTAACGCT	pHP45	

*Underscore denote restriction enzyme site. lowercase letters aaa/ttt-tail, Bold letters FRT-overlapping sites. Fw indicates forward primer, Rev indicates reverse primer.

PCR amplicons were purified using the High Pure PCR Product Purification Kit (Roche, Mannheim, Germany) following the manufacturer's instructions and visualised by agarose gel electrophoresis.

2.4.3 Colony-based PCR

To screen for potential cloned regions in both vector and *Y. entomophaga* genome recombinants, colony-based PCR was carried out using the DreamTaq (Thermoscience, USA) kit following the manufacturer's instructions. The reaction mix was directly loaded (10 µl) onto an agarose gel for electrophoresis.

To screen multiple colonies, a pooled sample of eight colonies, suspended in 1 ml of water, were screened. Of the fresh colonies, a toothpick was used to transfer a single colony from a plate to a fresh agar plate and subsequently into a microcentrifuge tube with 1 ml sterile MilliQ water. The pooled samples were vortexed and 1 µl was used as template DNA in the colony PCR using the following reaction conditions in Table 5:

Table 5: PCR program for amplification of DNA of length < 1.5 kb

Step	Temperature [°C]	Time
Initial Denaturation	98	3 min
Denaturation	98	30 s
Annealing	58	30 s
Extension	72	30 s/kb
Final extension	72	5 min

2.4.4 Agarose gel electrophoresis

Isolated or PCR amplified DNA was visualised by agarose gel electrophoresis. Depending on the DNA length, 0.5 – 2% (w/v) agarose was dissolved in TAE-buffer (40 mM tris-acetate, 1 mM EDTA pH 8.3) by microwaving. To the warm agarose, 0.1% (v/v) Sybre Safe (Invitrogen) was added to the molten agarose and mixed before pouring into a casting mould. The set agarose gel was placed into an electrophoresis apparatus, which was filled with TAE. For the electrophoresis, samples were mixed with 6 × Loading Dye (Thermofisher) and loaded on the gel. As a standard marker the Gene Ruler 1 kb (Thermofisher) was used. The electrophoresis was conducted at 100 V for 45 min and the gel visualised under UV using the Gel Doc UV transillumination system (BioRad).

2.4.5 Restriction enzyme digestion of DNA and precipitation

DNA fragments and plasmids were digested following the manufacturer's instructions. Restriction digests were carried out in either 100 µl (cloning) or 10 µl (diagnostic) reaction and at 25°C or 37°C, depending on the restriction enzyme used, for 1.5 h. For DNA cloning post digestion, ethanol precipitation with 200 µl ethanol (100%) was carried out (Chapter 2.4.1), a second restriction digest followed with a second enzyme. The final digested DNA was resuspended in 7 µl of MilliQ water, 2 µl of which was assessed by agarose gel electrophoresis before ligation.

2.4.6 Ligations

Ligations of plasmid DNA and amplified DNA after restriction digestion were carried out in 10 µl volumes. Based on DNA band intensities on the agarose gel, a ratio of 3:1 insert to plasmid was used for the ligations. Ligations were incubated overnight at ambient temperature (~22°C). For the following electroporation, the ligations were ethanol precipitated and, if required, enriched by enzymatic digestion using an enzyme specific to a region internal to the vector cloning polylinker in which the DNA was ligated.

2.4.7 Preparation of chemically competent cells and transformation

For chemical competent cells, a 50-ml LB broth flask was inoculated with 500 µl of an overnight culture. Cells were grown to an OD at 600 nm of 0.5-0.8 and then placed on ice for 20 min. The culture was spun down for 10 min at 2,264 × *g* at 4°C. The pellet was washed in transformation buffer (0.1M $CaCl_2$) and spun down at 2,264 × *g* for 10 min. The supernatant was discarded, and the final cell pellet was resuspended in 1 ml of transformation buffer and chilled on ice for 1 h before being aliquoted into 100 µl volumes in microcentrifuge tubes. To transform, 1 µl of plasmid DNA or 3 µl of ligation were added to 100 µl of cells and placed on ice. The microcentrifuge tube was then heat shocked by placing them into a 42°C water bath for 30 s after which the microcentrifuge tube was placed immediately back on ice. One mL of LB broth was then added and elaborated for 60 min at 37°C. For *E. coli* ST18 cells, 5-aminolevulinic acid (ALA) was added to the culture. After 1 h incubation, the cells were plated out on LB agar containing the appropriate antibiotics and supplements.

2.4.8 Preparation of electrocompetent cells and electro-transformation

A 50-ml broth was inoculated with 500 µl of overnight culture and the bacteria were grown at 37°C for *E. coli* or 25°C for *Y. entomophaga* strains until an OD600 nm of 0.5-0.8. The bacterial culture was chilled on ice for 20 min and then centrifuged at 2,264 × *g* for 10 min, at 4°C. The cells were washed twice with sterile water through pelleting at 2,100 × *g* for 4°C for 10 min, after which the cells were resuspended in 10% glycerol before a final centrifuging at 2,900 × *g* at 4°C for 10 min. The final cell pellet was resuspended in 10% glycerol at 4°C and aliquots of 50 µl were used for electroporation or were stored at - 80°C.

For electroporation, a microcentrifuge tube containing 100 µl of electrocompetent cells was placed on ice, 1 µl of chilled DNA was added and the cells transferred into electroporation cuvettes. The electroporation was carried out at 2.5 kV with a resistance of 200 Ω. Immediately after electroporation, the cells were resuspended in 1 ml LB broth and incubated at either 25°C (*Y. entomophaga)* or 37°C (*E. coli*) for 1 h. For *E. coli* ST18 cells, the culture was supplemented with ALA. Finally, the cell cultures were plated on LB agar containing the appropriate antibiotics, and the plates incubated at the appropriate temperature.

2.4.9 Plasmid transfer by conjugation

For conjugation, donor *E. coli* strains ST18 or S17 carrying derivatives of the suicide vector (Table 1) with the appropriate insert for homologous recombination were grown overnight at 37°C. The recipient *Y. entomophaga* strain was grown overnight at 25°C. For both recipient and donor strains, 1 ml cell culture was pelleted at 5,000 × *g* for 3 min and the cell pellet resuspended in 500 µl PBS. The final cell pellet was resuspended in 500 µl PBS. Each recipient strain (100 µl) and donor strain (100 µl) were pipetted onto the same area of a LB plate and mixed by gently swirling the plate on the bench. When the *E. coli* ST18 donor strain was used, ALA was added to the agar plate. The conjugation was incubated for 7 h at 25°C. To resuspend the cells, 1 ml of PBS was used to wash the cells from the agar and transfer them into a reaction tube. Cells were then washed in PBS and a dilution row was prepared and plated out on LB agar plates containing the appropriate antibiotics.

2.4.10 Construction of deletion mutants by three-step PCR

Deletion mutagenesis was performed by replacing the gene of interest (GOI) with an antibiotic resistance cassette flanked by flippase sites (FRT) using a three-step PCR approach modified from Datsenko and Wanner (2000) (Figure 4).

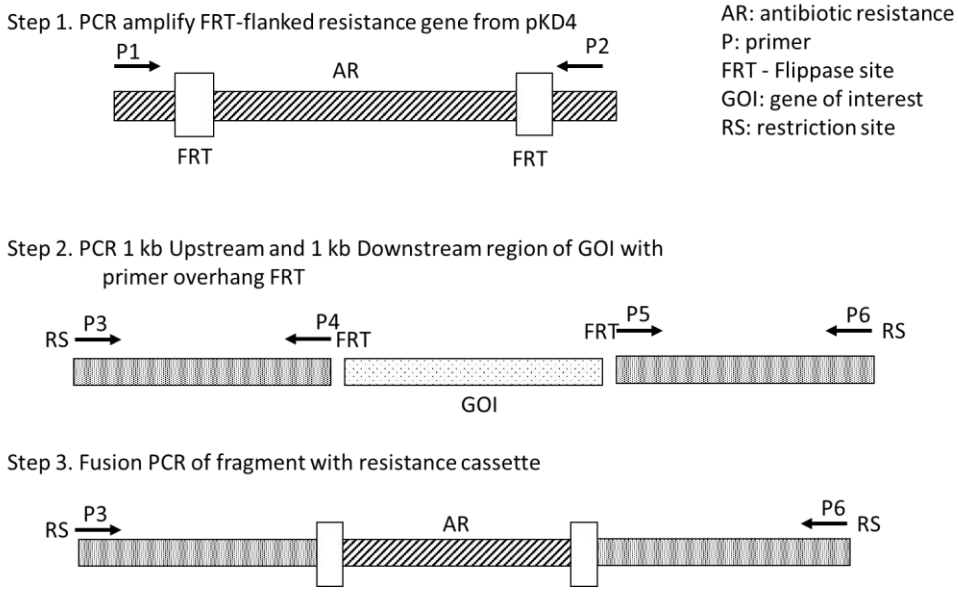

Figure 4: Three-step PCR for targeted mutagenesis. Step 1: Primer pairs P1 and P2 bind outside of flippase sites (FRT) to amplify the antibiotic resistance cassette (AR) flanked with FRT sites. Step 2: 1 kb flanking regions of the gene of interest (GOI) is amplified using the primer sets P3/P4 and P5/P6, with restriction sites (RS) on P3 and P6 and complementary sequence to flippase site in step 1 overhang on P4 and P5. Step 3: Fusion PCR of flanking regions from Step 2 and antibiotic resistance cassette containing FRT- sites from Step 1 using only outside primer P3 and P6 (Figure modified from Datsenko and Wanner, 2000).

In the first round of PCRs, 1-kb regions upstream and downstream region of the GOI were amplified (Fig. 4). These amplicons have FRT-sites adjacent to the GOI and a SacI restriction site (RS) on the outermost peripheral end. In the second PCR, a cassette with either kanamycin (kan) resistance (using pKD4 as a template) or chloramphenicol (cm) resistance (using pKD3 as a template) (Datsenko *et al.*, 2000), containing FRT-sites on both ends, was amplified. In the third PCR, all amplicons were fused using only the outside primers. The final 3.5 kb amplicon comprised a 1 kb upstream fragment, the antibiotic resistance cassette (kan or cm) and a 1 kb downstream fragment. The amplicon was then purified and ligated into pGEM T-Easy (Promega, Madison, WI) and a 3 µl aliquot of the ligation was transformed into chemically competent DH10β cells. After 1 h of incubation, the cells were plated on LB agar containing kanamycin (50 µg/ml), ampicillin (100 µg/ml) and X-gal (100 µg/ml) (ampicillin resistance and beta-galactosidase genes derived from pGEM T-Easy). White colonies were then assessed by plasmid extraction, followed by restriction digest with SacI and sequencing. The validated construct was designated pGEM- Δ*goi.* The plasmid pGEM-Δ*goi* was then digested with SacI and

ligated into the analogous site of the suicide vector pJP5608. The resultant ligation was ethanol precipitated and electroporated into electro-competent EC100D cells. Colonies containing pJP5608-Δ*goi* were selected on LB agar plates containing tetracycline (resistance derived from pJP5608) and kanamycin. To enable conjugation the final construct was then electroporated to either *E. coli* S17-1 λ *pir* or ST18.

2.5 Bioinformatic analysis

DNA sequencing was performed by Macrogen Sequencing Service (Seoul, South Korea), and DNA sequences were trimmed and aligned against the genome of strain MH96 (GenBank accession number NZ_CP010029.1) using the Map to Reference function of Geneious 10.0.9 (Kearse *et al.*, 2012).

Protein function prediction was performed using the Protein Fold Recognition Server PHYRE2 (http://www.sbg.bio.ic.ac.uk/phyre2/html/page.cgi?id=index). Amino acid sequences in fasta format were uploaded to the PHYRE2 webpage and run with default settings. For further functional protein predictions, the protein sequence was analyzed using BLASTP (https://blast.ncbi.nlm.nih.gov/Blast.cgi) with default settings.
Amino acid alignments were performed using Geneious 10.0.9 using ClustalW and BLOSUM Matrix with a Gap open cost of 10 and a Gap extension cost of 0.1. Amino acid alignments then visualized using GeneDoc 2.7.000 (Caffrey *et al.*, 2007).

Whole-genome sequencing of strain K18 was undertaken using the Illumina HiSeq 2500 System by Macrogen Sequencing Services. DNA sequences were trimmed using Trim_Galore (http://www.bioinformatics.babraham.ac.uk/projects/trim_galore/) and assembled using A5-miseq (Coil *et al.*, 2015). Nucleotide differences were identified by alignment of Illumina reads against the MH96 genome sequence using the conda package for breseq version 0.33.0 with default parameters http://barricklab.org/twiki/bin/view/Lab/ToolsBacterialGenomeResequencing (Deatherage and Barrick, 2014).

2.6 RNA procedures

2.6.1 Isolation of bacterial RNA

The RNA isolation was performed using the RNA Mini Kit (QIAGEN, Germany) and the corresponding RNAprotect Bacteria Reagent (QIAGEN) and RNase-Free DNase Set Kits (QIAGEN).

For each one litre fermentation in LB broth, 1 ml of sample culture was immediately transferred into 2 ml RNA protect bacteria (QIAGEN) and vortexed. After 5 min incubation time at 25°C, the samples were pelleted at 5,000 × *g* for 10 min. The supernatant was decanted, and pellets were left to air dry at 37°C before freezing at -20°C.

RNA was isolated using the RNA Mini Kit (QIAGEN) following the manufacturer's instruction. Following the on-column DNA digest with RNAse free DNAse, a second, off-column DNA digest was performed. To 40 µl RNA, RDD buffer (40 µl) and DNase stock I (2.5 µl) was added and the volume adjusted to 100 µl with DNA-free water. After 10 min of incubation time at 25°C, the RNA clean-up protocol (provided in the QIAGEN RNA mini Kit) was followed. The RNA was eluted in 40 µl RNAse-free water and isopropanol precipitated. The total volume was adjusted to 180 µl and 1% sodium acetate (3M) was added. Three times ice-cold 100% ethanol (600 µl) was added to the solution and vortexed. The microcentrifuge tube was then placed at – 20°C overnight, after which the suspension was centrifuged (10,000 g for 30 min at 4°C) and the supernatant discarded. The pellet was washed twice with ice-cold 75% ethanol (500 µl) and pelleted at 10,000 × *g* for 5 min at 4°C and the supernatant discarded. After the final wash step, the samples were pulse spun to remove residual ethanol by pipetting out residual supernatant. The pellets were airdried at 37°C for 30 min and then resuspended in RNase-free water. The resuspended sample was quantified by nanodrop. Of the sample RNA, 6 µg/ml were placed into a reaction tube, and the liquid was evaporated in a SpeedVac. RNAseq was quality controlled and performed by Macrogen.

2.6.2 RNAseq

RNAseq analyses were performed by Charles Hefer (AgResearch Ltd, Lincoln, New Zealand) using the following protocol:

The Illumina short reads were inspected for quality using FASTQC (https://www.bioinformatics.babraham.ac.uk/projects/fastqc/). Bases with low-quality PHRED scores (PHRED < 15 using a sliding window of 4 bases) were trimmed (using TRIMMOMATIC) from the short-read library, as well as any Illumina adapter sequences. Paired reads that were longer than 36 bp were kept for further analysis. The *Y. entomophaga* MH96 genome (Aug2018.NCBI.gb) was converted from GenBank format to fasta format using a custom BIOPYTHON script before indexing. Gene annotations were converted to gff format using the BIOPERL program bp_genbank2gff3.pl (https://manpages.debian.org/testing/bioperl/bp_genbank2gff3.1p.en.html). The genome fasta file was indexed and the short-read libraries aligned to the reference genome using HISAT2 with the default parameters. STRINGTIE was used for novel transcript assemblies, and BALLGOWN calculated the transcript count matrix for each sample.

The transcript count matrix was read into R and differential gene expression calculated using the DESeq2 package. Genes were considered differentially expressed when the adjusted p-value was less than 0.05. For analysis purposes differently expressed genes of a log2Fold change <-1 and >1 were considered of interest and further assessed.

2.7 Protein analysis

To investigate the exoproteome, unless otherwise stated, *Y. entomophaga* was grown in 50-ml cultures at 25°C and 200 rpm shaking. The bacterial cell culture was separated by centrifugation and both supernatant and cell pellets were used for further analysis by either Bradford assay or SDS -PAGE.

2.7.1 Preparation of protein samples

Of a 16-h bacterial culture, 1 ml was transferred into a 1.7 ml microcentrifuge tube and the sample pelleted at 5,000 × *g* for 15 min. The supernatant was removed from the pellet and filter-sterilised using a 0.22-µm polyvinylidene fluoride syringe filter (Merck, Darmstadt, Germany) removing any remaining bacteria cells. The cell pellet was resuspended in 1 ml of MilliQ water and diluted in 1:10 in water.

2.7.2 Sodium dodecyl sulfate polyacrylamide gel electrophoresis (SDS-PAGE)

To compare protein concentration between samples by SDS-PAGE, the crude exoproteome was used to avoid loss of proteins during precipitation or resuspension steps. Normalising SDS-PAGE samples by protein concentration, as it is often used in single protein analysis, helped to understand the composition of the exoproteome, but did not indicate changes in the amount of protein secretion in the population. Therefore, SDS-PAGE samples were prepared in the same manner and the same volume loaded on SDS-PAGE for normalisation and the wild type MH96 was used as the positive control. To visualise the exoproteome, 25 µl of supernatant and 25 µl of diluted (1:10) cell pellet were mixed with reducing buffer (4 ×), and 1 µl of the Broad-Range SDS-PAGE Standard (BioRad) were mixed with 25 µl of 1 × Reducing buffer (Table6) and heated at 95°C for 10 min in a water bath.

Table 6: Buffers and reagents for 10% SDS-PAGE

Solution	Reagents
1 × Reducing buffer	125 mM Tris/HCL (pH 6.8), 20% glycerol (v/v), 3.8% (w/v) SDS, 0.1% bromophenol blue, 10% (v/v) β-mercaptoethanol
4 × Reducing buffer	125 mM Tris/HCL (pH 6.8), 20% glycerol (v/v), 3.8% (w/v) SDS, 0.1% bromophenol blue, 10% (v/v) β-mercaptoethanol
Running Buffer	25 mM Tris/HCL, 200 mM glycine, 0.1% (w/v) SDS, pH 8.3
Separation Gel	10% (v/v) acrylamide, 375 mM Tris/HCL (pH 8.8), 0.1% (w/v) SDS, 0.05% (v/v) ammonium persulphate (APS), 0.2% (v/v) tetramethylethylenediamine (TEMED)
Stacking Gel	3.6% (v/v) acrylamide, 125 mM Tris/HCL (pH 6.8), 0.1% (w/v) SDS, 0.05% (v/v) ammonium persulphate (APS), 0.2% (v/v) tetramethylethylenediamine (TEMED)

After a 30 s spin at 10,000 × *g* the samples were loaded in equal amounts on a 10% SDS-Polyacrylamide gel (Table 6) as described by Laemmli (1970) and run for 55 min at 200 V. The SDS-PAGE was visualised using the silver stain method (Blum *et al.*, 1987) (Table 7)

Table 7: Solutions for the silver staining of SDS-PAGE

Solution	Reagents
Fixation	50% methanol, 12% (v/v) acetic acid, 50 µl formaldehyde (for 100 ml solution)
Pre-treat	0.1 M sodium thiosulfate
Staining	0.2% silver nitrate, 75 µl formaldehyde (100 ml for solution)
Developing	6% sodium carbonate, 16 µl of 0.1 M sodium thiosulfate, 50 µl formaldehyde (for 100 ml solution)
Stop	10% acetic acid

The silver stain solutions listed in Table 7 were used following the procedure listed in Table 8. Each SDS-PAGE gel was transferred into a plastic tray and covered with the respective solution and incubated at room temperature on an orbital shaker with a slow rotation, allowing even distribution of the solution.

Table 8: Silver stain protocol SDS-PAGE

Solution	Duration
Fixation	30 min
Wash (Methanol 50%)	5 min
Wash (Methanol 50%)	5 min
Wash (Methanol 50%)	5 min
Pre-treatment	1 min
Wash (MilliQ)	20 s
Wash (MilliQ)	20 s
Wash (MilliQ)	20 s
Staining	10 min
Wash (MilliQ)	20 s
Wash (MilliQ)	20 s
Developing	5- 7 min
Wash (MilliQ)	20 sec
Stop	n.a.

2.7.3 Bradford assay

The Bradford assay was used to determine the culture supernatant exoproteome concentration. To enable this, 500 µl of cell culture was centrifuged (5,000 × *g* for 10 min) and the supernatant filter-sterilised using a 0.22-µm polyvinylidene fluoride syringe filter (Merck, Germany). The supernatant (12 µl) was mixed with 220 µl of dye reagent from a Protein Assay Kit (BioRad) in a 96-well microtiter plate according to the method of Bradford (1976) and the manufacturer's instructions. Absorbance at 595 nm was measured in a FLUOstar OPTIMA plate reader (BMG LABTECH) and protein concentration was determined by comparing results against a standard curve generated using known concentrations of bovine serum albumin (BSA) (0–500 mg/ml) diluted in LB broth. SDS-PAGE was performed as described previously (Chapter 2.5.2). Proteins were visualized by silver staining according to the method of Blum *et al.* (1987).

2.7.4 LC-MSMS analysis

For LC-MSMS analysis, SDS-PAGE was run as described previously. The SDS-PAGE was visualised using Coomassie stain. Bands of interest were removed from the gel and analysed using LC-MS. LC-MS was performed by Evelyne Maess (AgResearch) using the following procedure.

Each gel band was analysed by mass spectrometry after de-staining, reduction with 0.1 M tris (2-carboxyethyl) phosphine (Fluka Chemie,GmbH, Buchs, Germany), alkylation with 20 µl of 0.15 M iodoacetamide (Sigma, St. Louis, MO, USA) and digestion for 18 h with 1 µg of TPCK-trypsin (Promega, Madison, WI, USA) in presence of 10% acetonitrile (ACN). After digestion, the peptides were dried and resuspended in 50 µl of 0.1% FA prior to injection on the mass spectrometer.

LC-MSMS was performed on a nanoflow Ultimate 3000 UPLC (Dionex) coupled to maXis impact HD mass spectrometer equipped with a CaptiveSpray source (Bruker Daltonik, Bremen, Germany). For each sample, 1 µl of the sample was loaded on a C18 PepMap100 nano-Trap column (300 µm ID x 5 mm, 5- micron 100Å) at a flow rate of 3000 nl/min. The trap column was then switched in line with the analytical column ProntoSIL C18AQ (100 µm ID x 150 mm 3-micron 200Å). The reverse-phase elution gradient was from 2% to 20% to 45% over 60 min, a total of 84 min at a flow rate of 600 nl/min. Solvent A was LCMS-grade water with 0.1% formic acid (FA); solvent B was LCMS-grade ACN with 0.1% FA.

The Q-TOF Impact HD (Bruker Daltonics) mass spectrometer was set up in a data-dependent automatic MS/MS mode where a full scan spectrum (50-2000 m/z, 2Hz) followed by 10 MS/MS (350 to 1500 m/z, 1-20Hz) of the most intense ions with charge states 2-3 selected.

2.8 Microscopy

2.8.1 Light and Fluorescent microscopy

For microscopical analysis of MH96 cells, samples of 16 h cultures, incubated at 25°C and 200 rpm shaking, were collected. For light microscopy (LM) 3 µl of cell culture were pipetted on a slide. Cells were observed under phase contrast. For LIVE/DEAD staining, cells were incubated with Syto9/PI stain (LIVE/DEAD *BacLight* kit; Invitrogen, Carlsbad, CA, USA) at a 1:1 ratio for 5 min in a UV-safe tube before pipetted onto a slide. Cells were observed under an Olympus BX50 light microscope at × 400 magnification for both, light and fluorescence microscopy. The SYTO9 stain was visualised using FITC filter with excision of 460/515 nm, and the PI stain using Texas red 545/610 nm. For overlapping fluorescence, the red-orange filter 520/588 nm was used.

To measure cell size of TEM and LM images, as well as counting cell numbers, the imaging software ImageJ 1.47v was used (Schneider *et al.*, 2012). For cell counts, the following method was used.

All .tif images were imported into ImageJ and then changed to 8-bit format in ImageJ/Image/Type. At this stage images of fluorescence microscopy were inverted ImageJ/Edit/Invert. For phase-contrast images, the background was subtracted with rolling ball radius of 3 pixel (ImageJ/Process/Subtract background). In the next step, a threshold had to be defined, which was set between 0 – 220 (ImageJ/Image/Adjust/Threshold). To analyse the number of particles, the size was set between 3-350 pixel^2, based on the minimum cell size of 0.7 µm derived from Hurst *et al.* (2011), and adjusted on pixel size from the scale bar (20 µm = 84 pixel). The upper threshold was adjusted by measuring elongated cells of MH96 images, resulting in a maximum area of 332 pixel^2. For measurement of KTMS4 and MH96ΔYLC cells. The upper limit was increased to 1,200 pixel^2, due to elongated cell phenotype.

With these parameters, cell numbers were measured using the ImageJ function Analyse particles (ImageJ/Analyze/Analyse particles) and data summarised with the in-build function ImageJ/Analyse/Summarize, with an output of Mean Area, standard division (SD) min and maximum area. With the function, ImageJ/Analyze/Distribution cells of a specific size were sorted and used to compare between treatments.

2.8.2 Transmission electron microscopy

Transmission electron microscopy (TEM) was performed on live-cell cultures to observe cell shapes and structures including flagella and OMVs. For cell shape and flagella overnight cultures grown in LB at 25°C were harvested after 16 h and spun down at 3,000 × *g*. For negative staining, 3 µl of the crude cell culture and 3 µl of the diluted (1:5 in water) cell culture were used. The crude sample enabled observation of any extracellular proteins and OMVs in the culture medium. To avoid strong background staining of the secreted proteins and potential cell debris, and in the second set of samples, the culture was diluted by 3-fold in water. Both sample sets were negative-stained with uranyl acetate.

Copper grids (Proscitech, Thuringowa, Australia) with 200-mesh were coated with a carbon layer of 3 nm and negatively charged by glow discharge treatment. Three µl of the sample was pipetted on a grid and incubated at room temperature for 60 s. Residual liquid was removed with Whatman filter paper. For the negative stain, 3 µl of 0.7% uracil acetate were added to the grid and incubated for 45 s. Residual liquid was removed with Whatman paper. The grids were dried for at least 30 min and then examined in a Morgagni 268D transmission electron microscope (FEI, USA). Images were taken by an Olympus Megapixel III digital camera imaging system.

2.8.3 Cryo-electron tomography (Cryo-ET)

All Cryo-ET experiments were done in the Pilhofer Laboratory of the ETH Zurich (Switzerland) in collaboration with Miki Feldmüller.

For Cryo-ET, 7-h cultures of MH96 cells were grown in 3 ml LB broth at 25°C and 200 rpm shaking and used for inoculation of 50-ml culture at the same conditions for 16 h. The 16-h samples were then fixed for Cryo-electron microscopy, as described below.

The plunge freezing method was used to fix the samples. Plunge freezing was performed using a FEI Vitrobot (Thermo Fisher Scientific). For cryo-TM sample preparation of *Yersinia* cells, 10 nm colloidal gold (Sigma-Aldrich) was added to the sample as fiducial markers in a ratio of 1:5 (v/v) to allow tilt image alignments. For Vitrobot setup, a filter paper (Whatman, 47 mm diameter) and a Teflon sheet replacing the filter paper on the sample-facing blotting-pad were installed for single-sided blotting and the chamber was pre-cooled down to 4 °C with 100% humidity. Then the EM grids (R2/2, Cu 200 mesh; Quantifoil Micro Tools GmbH) were glow-discharged for 45 s at 25 mA by PELCO easiGlow discharger. The plunging container was placed in a styrofoam holder and cooled down by liquid nitrogen until

liquid nitrogen evaporated twice. The container was filled with a liquid ethane/propane mixture (37% v/v ethane/ 63% v/v propane). The glow discharged grid was put with its carbon side onto the carbon layer. Additional water was blotted away carefully with a filter paper. Three microlitres of the sample were applied to the EM grid with a waiting time of 15 s and a blotting time of 6.5 s and plunge-frozen into the ethane-propane mixture. Plunge frozen grids were afterwards transferred and stored in boxes in liquid nitrogen. Before loading the samples into the Cryo-electron microscope, the grids were clipped.

All tilt series were collected in a Titan Krios 300 kV transmission electron microscope (Thermo Fisher Scientific) equipped with a field emission gun (FEG), an energy filter (slit width 20 eV; Gatan Inc.) and K3 camera at ScopeM Zürich. Tilt series were collected from -60° to +60°degree with an increment step of 2° and -9 µm defocus and with a cumulative dose of 119.7 e / Å. Tilt series and 2D images were automatically acquired using SerialEM. Three-dimensional reconstructions were then calculated using IMOD software package. Visualization and two-dimensional slices through a three-dimensional volume were acquired using 3dMOD.

Chapter 3

Characterisation of the *Y. entomophaga* MH96 growth and secretion phenotype

3.1 Introduction

In liquid culture, *Y. entomophaga* produces heteromorph cells, with some smaller cells 0.7 µm wide and 1.7 µm long, and elongated rod-shaped cells with a width of one µm and up to 60 µm length. These larger cells can have up to three flagella with motility observed up to 37°C (Hurst *et al.*, 2011a). The *Y. entomophaga* MH96 harbours a 32-kb pathogenicity island (PAI^{Ye96}), encoding 11 ORFs of which the translated products combine to form an insecticidal toxin complex, termed Yen-TC, which is the main virulence factor (Hurst *et al.*, 2011b). The Yen-TC is a member of the toxin complex family comprised of three different proteins, termed TcA, TcB and TcC, which along with two chitinases, Chi1 and Chi2, combine to form a large insect active complex. Studies by Hurst *et al.* (2011b) identified the thermoregulation of Yen-TC release into the supernatant. At temperatures of 30°C and 37°C Yen-TC secretion was absent, while up to 5 mg/l Yen-TC was measured in the MH96 secretome at 25°C. Furthermore, MH96 protein secretion alters in different growth media (S. Jones, pers. comm.). During the growth of *Y. entomophaga* in LB, Yen-TC and other exoproteins are released at the mid-log stage and increased over time, by an unknown mechanism (S. Jones, pers. comm.). Given the initiation of protein secretion at the mid-log phase, it is plausible that *Y. entomophaga* protein secretion is a cell density-dependent process. In a previous study investigating the total exoproteome, *Staphylococcus aureus* protein secretion occurred throughout exponential growth until the early stationary growth phase (Abbas-Ali and Coleman, 1977). In *Y. pseudotuberculosis* and *Y. pestis* KIM the presence of a T6SS is growth phase-dependent, where T6SS expression started in the exponential phase and reached a maximum in the stationary phase (Pieper *et al.*, 2009; Zhang *et al.*, 2011). The T6SS in *Y. pseudotuberculosis* was also found to be optimally expressed at 26°C and was under the control of quorum sensing (QS) (Zhang *et al.*, 2011). The T3SS expression in *Pseudomonas syringae* is also cell-density dependent (Stauber *et al.*, 2012).

In Gram-positive and Gram-negative bacteria, toxins can also be released by OMVs as an alternative secretion mechanism (Lindmark *et al.*, 2009; Yu *et al.*, 2018). In the early stages of OMV research, it was identified that OMV formation occurs during all growth stages but reaches maximal levels in the late exponential phase (Hoekstra *et al.*, 1976; Orench-Rivera and Kuehn, 2016). Taking these studies into account, it is likely that such a cell density-dependent protein secretion also occurs in *Y.*

entomophaga. For this study, in which the goal was to identify genes underlying the regulation of exoproteome production, it was necessary to define the growth phase at which exoproteome release could be detected using the Bradford assay and SDS-PAGE from where a transposon-based screening assay for changes in exoproteome concentration could then be developed (Chapter 4). In this chapter, exoproteome release over time from cultures of *Y. entomophaga* MH96 was investigated and correlated to cell density.

3.2 Methods

3.2.1 Correlation of bacterial growth and exoproteome concentration in *Y. entomophaga* MH96

Aliquots (500 µl) from 3 ml cultures of *Y. entomophaga* MH96 cells were grown in LB broth for 12 h (OD_{600} ~ 6) at 25°C and were used to independently inoculate 50 ml LB broth cultures in triplicate. The cultures were returned to the 25°C incubators at 250 rpm and 1 ml aliquots were removed each hour for the first 12 h and every second hour from 12–24 h, and the CFU, OD_{600}, and exoproteome concentrations were measured. To determine CFUs, a dilution series was plated on LB agar plates and incubated at 25°C for 24 h (Chapter 2.2). The mean and standard error of the CFU values were plotted using Prism 7.04 software (GraphPad, USA). The OD_{600} of the cultures at each time point was measured using a SmartSpec Plus Spectrometer (BioRad, USA). Culture supernatant exoproteome concentration was determined by centrifuging 500 µl of culture (3,214 × *g* for 10 min) and filter-sterilizing the resulting supernatant using a 0.22 µm polyvinylidene fluoride syringe filter (Merck, Germany). The supernatant (12 µl) was mixed with 220 µl of dye reagent from a Protein Assay Kit (BioRad) in a 96-well microtiter plate according to the method of Bradford (1976) and the manufacturer's instructions. Absorbance at 595 nm was measured in a FLUOstar OPTIMA plate reader (BMG LABTECH, Germany) and protein concentration was determined by comparing results against a standard curve generated using known concentrations of bovine serum albumin (BSA) (0–500 mg/ml) diluted in LB broth. SDS-PAGE was performed as described previously in Chapter 2.4.2. Proteins were visualized by silver staining according to the method of Blum *et al.* (1987).

3.2.2 Microscopy of *Y. entomophaga* MH96 cells

For microscopic analysis of MH96 cells, fluorescence microscopy was used for samples of 16 h cultures, incubated at 25°C and shaking at 200 rpm, to measure cell viability using LIVE/DEAD stain, as outlined in Chapter 2.6.2. The same samples were investigated using light microscopy (Chapter 2.8.1.) for observations of cell morphology. Furthermore, TEM and Cryo-ET, as outlined in Chapter 2.8.2, were used for cells with the same culture conditions as mentioned above, to investigate cell morphology with higher magnification.

3.3 Results

3.3.1 Correlation of cell growth and exoproteome production

To understand exoproteome production in MH96, protein concentration by Bradford assay was determined, by establishing a regression line generated using a standard prepared by suspending BSA in LB broth (Fig. 5D). The supernatant protein concentration and bacterial growth in 50 ml LB broth shake-flask cultures were monitored over 24 h. Cell density peaked at 5.7×10^9 CFU/ml and an OD_{600} of 6, which occurred at 14 h post-inoculation (hpi) (Fig. 5A). The absorbance at 595 nm (Abs_{595}) of the supernatant protein concentration was measured, using the Bradford assay and normalized to LB broth (Fig. 5C). Based on the calculated protein concentrations, the MH96 exoproteome increases from 42.9 ± 9 µg/ml (11 hpi) to 364.9 ± 17 µg/ml (24 hpi) from late exponential (3×10^9 CFU/ml) to stationary phase (5.4×10^9 CFU/ml). The increase in exoproteome concentration corresponded with visible colour changes in the 96-well plates and increased band intensity in SDS-PAGE (Fig. 5B, C).

Through the use of the growth curve and exoproteome concentration assays, the optimal timeframe for collection and analysis of exoproteome content in MH96 broth cultures was between 14 hpi (OD_{600} = 6) and 16 hpi (OD_{600} = 5.5). Based on an established growth curve, samples at 16 hpi were assessed for LIVE/DEAD stain, TEM and Cryo-ET to validate if the exoproteome at 16 hpi is based on protein secretion or if the high exoproteome release is caused by cell lysis. These results formed the basis for assessments of the exoproteome at 16 hpi, when sufficient protein concentration in the supernatant could be detected in the wild type strain MH96 by Bradford assay. This approach was used as the basis for the high-throughput exoproteome screening assay (HESA) in Chapter 4.

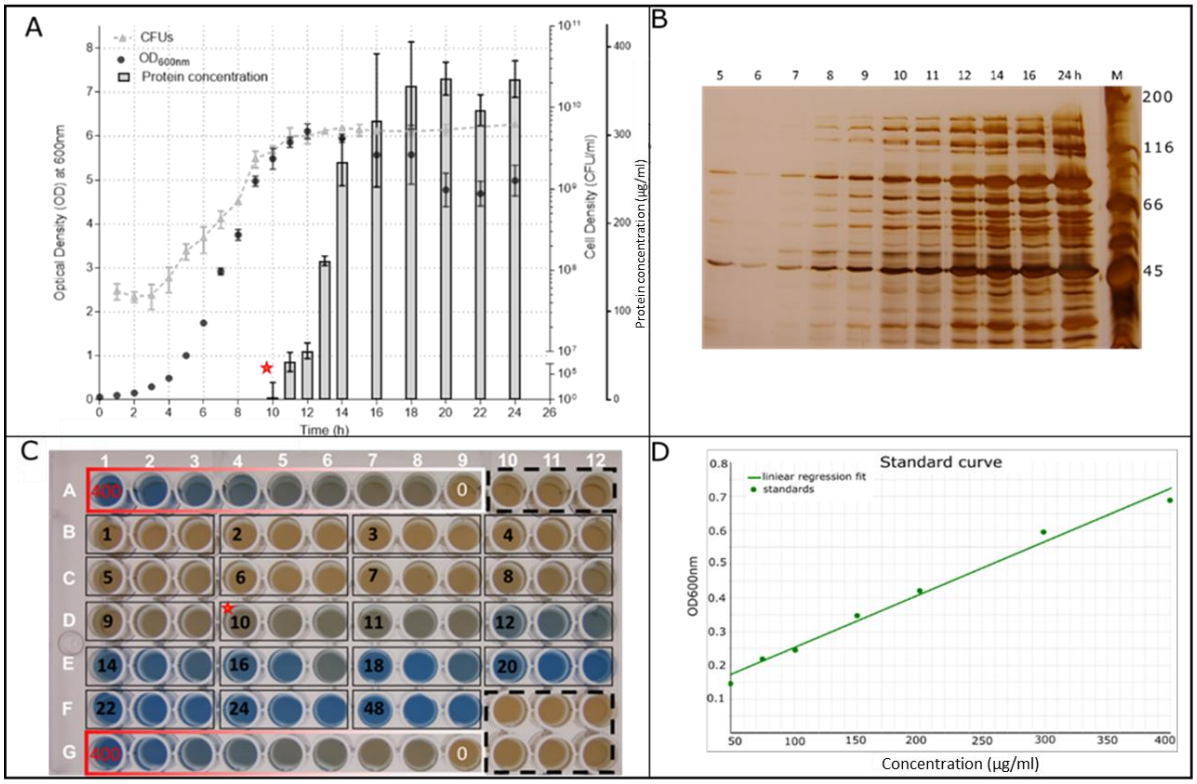

Figure 5: Assessment of exoproteome concentration in a 50 ml culture of *Y. entomophaga* MH96. *A)* Growth curve and protein secretion of *Y. entomophaga* MH96 cultured at 25°C and 200 rpm over 24 h. Data are presented as the mean ± SD of biological triplicates. The red star denotes the time point at which exoproteome was detectable by Bradford assay. *B)* SDS-PAGE of MH96 culture supernatant with increasing band intensity from 5- 24 hpi. *C)* Photograph of a modified Bradford assay conducted in a 96-well microtitre plate. Wells contained 12 µl of culture supernatant collected at 1–24 hpi and 48 hpi. The dashed black box indicates uninoculated LB broth blanks. The red-to-white gradient box indicates BSA concentrations (400, 300, 200, 150, 100, 75, 50, 25, and 0 µg/ml). Black solid boxes denote triplicates of culture supernatant collected at the hpi indicated by black numbers that were and measured in the Bradford assay. Red star denotes the time point at which exoproteome was detectable (0.2 µg/ml) by Bradford assay. *D)* Standard curve obtained from the BSA protein standards used in A and C.

3.3.2 Microscopy of *Y. entomophaga* MH96 cells

To understand if the increasing exoproteome over time, as observed in Chapter 3.3.1, is a result of cell lysis, cell viability was tested by LIVE/DEAD stain in conjunction with fluorescence microscopy. Cell cultures grown under the same condition as in Chapter 3.3.1 were sampled at 16 hpi, a time by which an amount of exoproteome was detectable (Chapter 3.3.1).

Light microscopy of the *Y. entomophaga* MH96 cell cultures at 16 hpi showed motile and rod-shaped cells (Fig. 6A). LIVE/DEAD staining of MH96 cells in 16 h cultures showed that 45% of the total cells fluoresced green (Fig. 6BD) and 4% of the total cells fluoresced red (Fig. 6CD), indicating low numbers of non-viable cells. No large-scale cell lysis was observed.

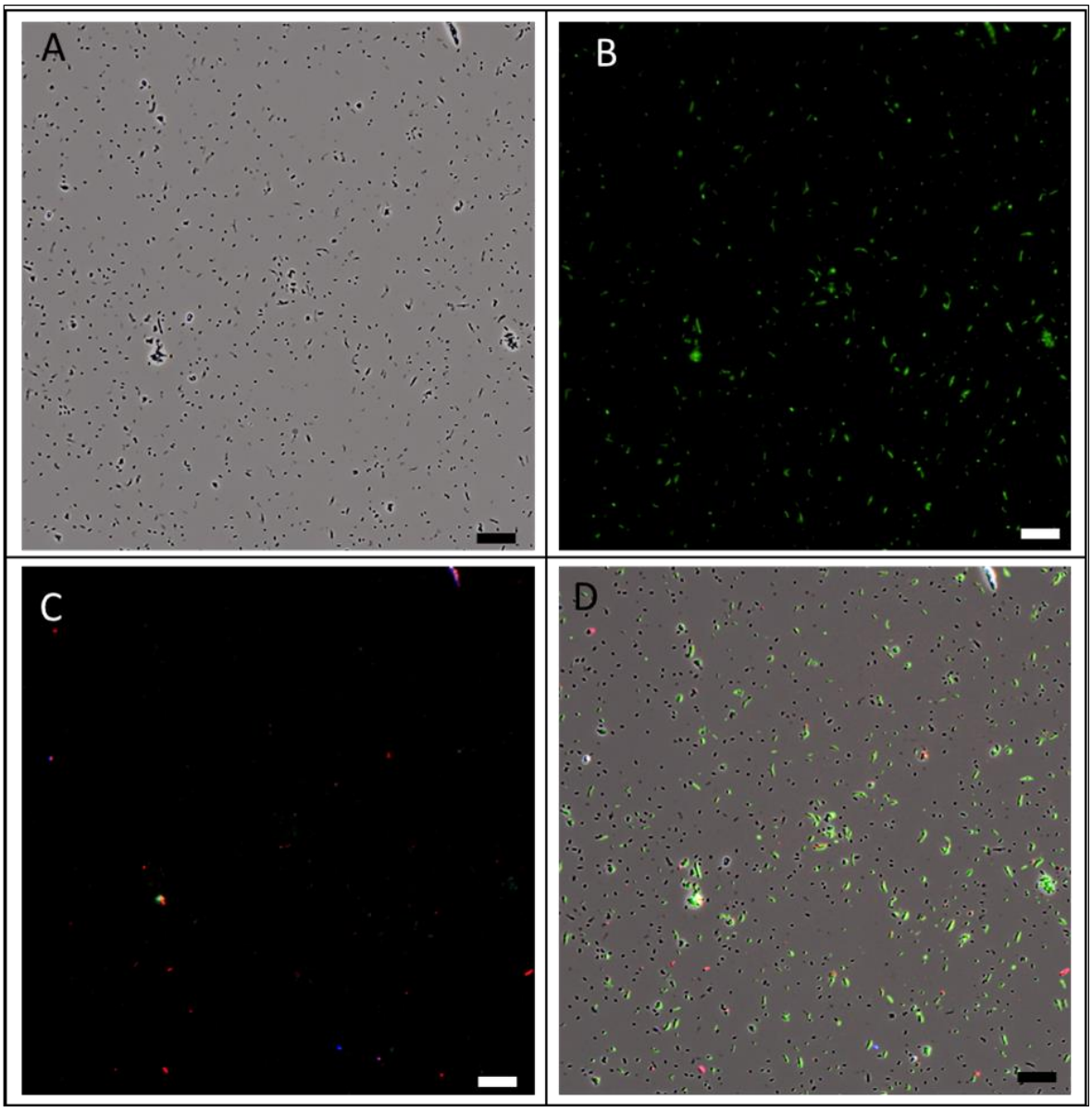

Figure 6: Representative images of Light and Fluorescence microscopy of *Y. entomophaga* MH96 culture at 16 hpi. *A)* Light microscopy of *Y. entomophaga* MH96 cells, seen as single rod-shaped bacteria. *B)* LIVE/DEAD stained *Y. entomophaga* MH96 bacteria under GFP-UV filter. *C)* Live-dead stained cells under Phyco-red filter. D) Overlay of light and fluorescence microscopy in ABC. Black bar denotes scale of 20 µm.

To investigate the cell morphology of *Y. entomophaga* MH96, when exoproteome release occurs, 16-h cultures were grown at the same parameters as outlined in Chapter 3.2.2 and were used in TEM and Cryo-ET analysis.

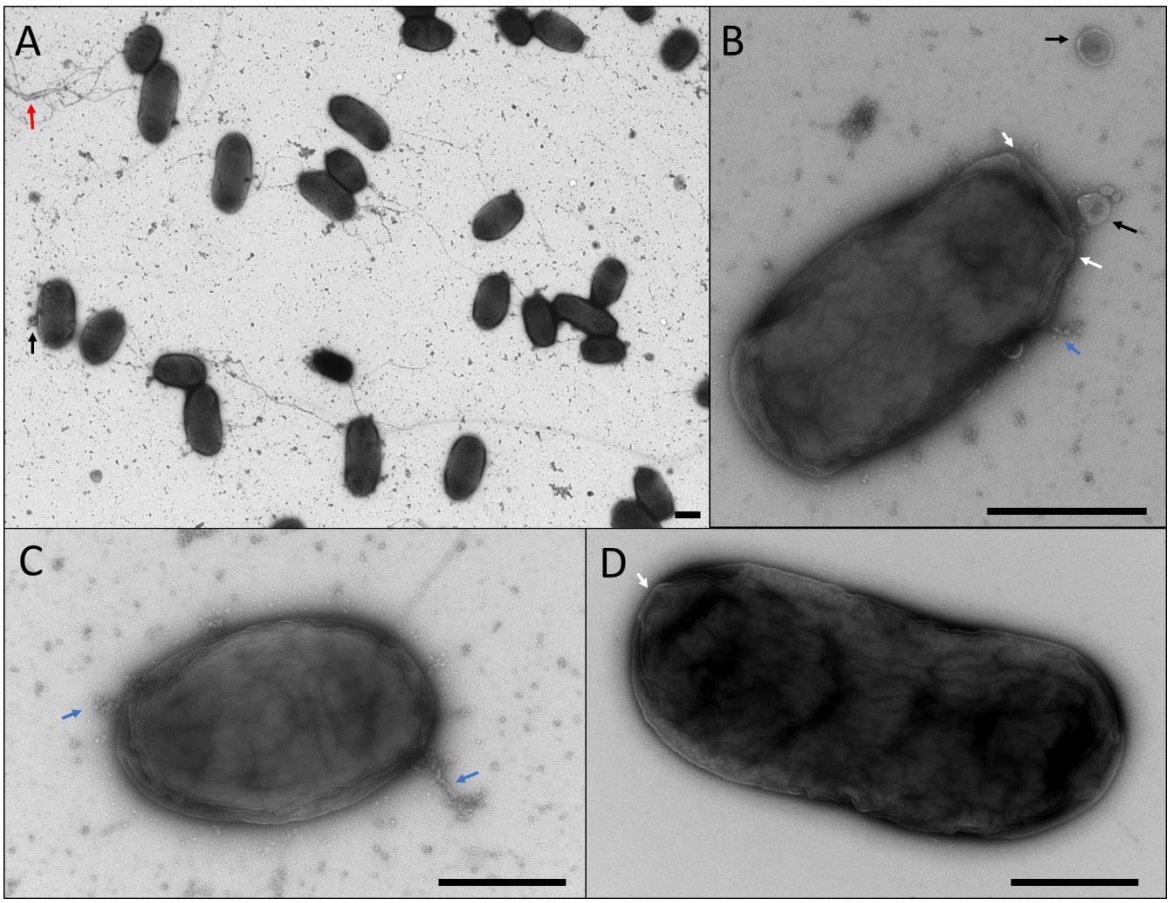

Figure 7: Transmission electron micrographs of *Y. entomophaga* MH96 cells grown in LB media for 16 h at 25°C. *A)* Overview image of *Y. entomophaga* MH96 cells. Red arrow denotes flagella-like structures. Black arrow denotes OMV. *B) Y. entomophaga* MH96 cell with OMV formation (black arrows) and membrane-bound undefined material (blue arrow). White arrows denote atypical cell membranes. *C) Y. entomophaga* MH96 cell with membrane-bound undefined material (blue arrows). A, B and C) show undiluted cell culture. *D) Y. entomophaga* MH96 cell diluted in water. White arrow denotes atypical cell membrane. Black scale bar: 500 nm.

TEM analysis confirmed that the rod-shaped *Y. entomophaga* MH96 cells were 1.5 -2 µm long and formed OMVs and flagella, as previously reported (Hurst *et al.*, 2011a; Hurst *et al.*, 2011b) (Fig. 7). Dissociated flagellar structures were frequently observed. The presence of dissociated flagella may have resulted from sample handling or vigorous shaking of the culture. In addition to OMVs and flagella, amorphous structures were observed along the outer cell membrane in the undiluted samples (Fig. 7BC). The tomograms also revealed an amorphous surface of MH96 cells (Fig 7BCD).

In the final stage of this research, Cryo-ET analysis (Chapter 2.8.3), was conducted in collaboration with Miki Feldmüller under the guidance of Associate Prof Martin Pilhofer at the ETH Zurich, Switzerland. The Cryo-ET images of MH96 revealed the presence of an amorphous outer membrane with the formation of abundant OMVs and deformation of the inner membrane (Fig. 8). The observed

Y. entomophaga MH96 cells showed outer membrane blebbing, over the length of the cell and differing widths between IM and OM (Fig. 8). In areas forming a void in the OM, connective-like structures, between IM and OM, were observed (Fig. 8). Cell shapes as shown in Figure 8 were observed in 90% of the cells harvested at 16 hpi (10^9 CFU/ml) (in collaboration with Feldmüller and Pilhofer, data not shown). The observed cell wall morphology and abundant OMV formation suggest that MH96 cells undergo a form of membrane blebbing.

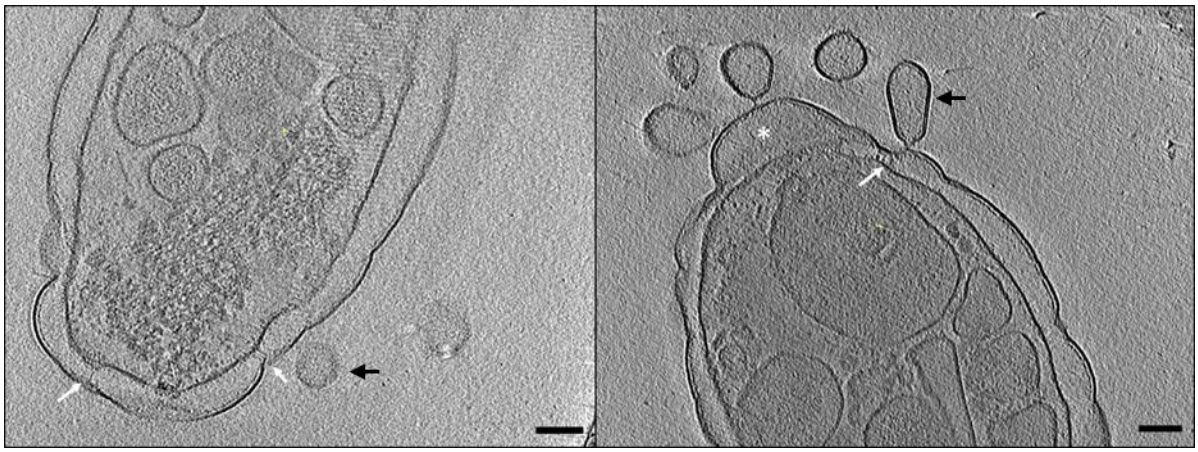

Figure 8: Cryo-ET image of *Y. entomophaga* MH96 cells. White asterisk denotes membrane bulging, black arrows denote OMVs and white arrows denote IM-OM connecting structure. Black bar denotes a scale of 10 nm.

In summary, *Y. entomophaga* MH96 is a rod-shaped flagellated bacterium. When grown in LB broth, *Y. entomophaga* MH96 cells had a varying cell morphology with apparent blebbing of abundant OMVs, as observed in TEM and Cryo-ET.

3.4 Discussion

The *Y. entomophaga* exoproteome increases with increasing cell density. The exoproteome is the concentration and content of proteins released via active transport using secretion systems like T1-9SS and OMVs, or proteins passively released by cell lysis (Armengaud *et al.*, 2012). In many Gram-negative bacteria, cell density-dependent mechanisms are often under the control of QS. QS has been implicated in the activation of secretion systems such as T1SS, T2SS, T3SS, and T6SS as shown in *P. aeruginosa* (Michel *et al.*, 2007; Lesic *et al.*, 2009; Schuster *et al.*, 2013; Liang *et al.*, 2014) which contribute to the exoproteome. Based on the literature, it is assumed that *Y. entomophaga* MH96 exoproteome release also occurs in a QS-dependent manner, by activation of secretion systems. The secreted proteins then accumulate in the supernatant over time and can be visualised in SDS-PAGE.

An alternative hypothesis of cell density-dependent increase in the exoproteome release is that the heteromorph and bulging cell morphology of *Y. entomophaga* MH96 (at 16 hpi) is indicative of disrupted cell wall integrity. The altered cell state causes cell proteins to enter the cell culture via some form of lysis or blebbing. This has been reported in *E. coli* upon phage lysis gene E induction, where the IM retracts from the cell wall causing lesion sites in the OM and release of cytoplasm (Fu *et al.*, 2014). Cell lysis of a single cell can be beneficial for the cell population, for example, by supporting the formation of biofilms using externalized DNA, or by the elimination of damaged cells and cell competence to acquire extracellular DNA (Rice and Bayles, 2008). Decreased cell wall integrity, maintained by cell wall hydrolases, hinders the integration of secretion system membrane-bound proteins such as T2-4SS (Koraimann, 2003; Vermassen *et al.*, 2019). In *P. aeruginosa*, OMVs have been found to transport QS molecules and vesicle formation increases with cell density (Mashburn and Whiteley, 2005). In *Vibrio vulnificus* OMVs are released from the intact OM and membrane blebbing was occasionally observed in late-log phase cell cultures (Hampton *et al.*, 2017). In *Y. entomophaga* MH96 cells, frequent membrane blebbing over the entire bacterium occurs, which causes atypical cell morphology. This outer membrane blebbing likely leads to OMV formation, as has been proposed for *P. aeruginosa* by Schertzer and Whiteley (2012).

An alternate mechanism of exoproteome release is cell lysis which often occurs in the stationary phase, when a balance between cell death and replication occurs, and new cells acquire nutrients from lysed cells (Bayles, 2007). If cell lysis was a major contributor to the exoproteome, an increased accumulation of exoproteins would be expected at this phase. However, it was not observed in *Y. entomophaga* MH96 as exoproteome production, relative to CFUs and OD, did not increase at the stationary phase. Based on this observation, combined with results of LIVE/DEAD staining, it is likely that cell lysis does not significantly contribute to the measured exoproteome, which indicates an inhibition of the, yet to be defined, exoproteome release mechanisms in the stationary growth phase.

TEM images of MH96 during the stationary phase identified structures connecting the IM and OM within the cell wall, forming voids in the OM. Similar connective structures were observed and identified as T2SS in *E. coli* (Ghosal *et al.*, 2019) and T6SS in *Legionella pneumophila* (Rapisarda *et al.*, 2019). Secretion systems like the T2SS are often integrated at the polar ends of the cell as demonstrated in *P. aeruginosa* (Senf *et al.*, 2008). While the Cryo-ET analysis of *Y. entomophaga* showed connecting structures near the cell poles, further investigation is needed to characterize these structures. The collaboration with the team in Zurich was only established at the end of this research and ongoing work by Miki Feldmüller is investigating the properties of these structures using Cryo-ET.

Type 1, 2, 3, and 6 secretion systems are encoded in the *Y. entomophaga* genome but have not been further analysed. The secretome is, by definition, the collection of proteins that are actively secreted by secretion systems, such as T1-6SS (Tjalsma *et al.*, 2000). It is therefore likely that an MH96 encoded secretion system plays a role in exoproteome. For further assessment of secretion systems in MH96, exoproteome analysis of mutations in the MH96 secretion systems should be performed. During this study, preliminary data of a T2SS mutant (MH96Δ*gspD*) did not show a reduced exoproteome when analysed by SDS-PAGE (Method S1, Fig. S1). In contrast, a study in *Burkholderia peudomallei* showed a strong decrease in secretion profiles upon GspD deletion when analysed by SDS-PAGE (Burtnick *et al.*, 2014). Therefore, further investigation on the relevance of the MH96 secretion systems including T2SS in the release of exoproteins are needed.

In conclusion, a secretory mechanism - either a secretion system or OMV formation - is activated in *Y. entomophaga* MH96 in the early stationary phase, contributing to high levels of exoproteome. LIVE/DEAD staining of MH96 at 16 hpi revealed a low abundance of dead cells suggesting that membrane blebbing is not a lytic event. Also, growth curve assessment did not show large decreases in cell counts or OD during the stationary phase, so programmed cell death is likely induced in only a subpopulation of the culture.

Chapter 4

Development of a high-throughput exoproteome screening assay (HESA) to identify regulators of *Y. entomophaga* exoproteome production

4.1 Introduction

The bacterial exoproteome consists of proteins that are either actively secreted or passively released in the extracellular milieu (Tjalsma *et al.*, 2000). Surface proteins such as adhesins, flagella, or pili which are located on the cell surface can also be classified as part of the exoproteome (Gagic *et al.*, 2016). In the literature, the exoproteome is often referred to as the secretome, which was defined by Tjalmsa *et al.* (2000) as native secreted proteins and their respective secretion systems, such as T1–6SS. Secretion systems are often specific for particular proteins and are triggered under certain conditions. While many secretion systems are well characterized, studies examining the mechanisms underpinning global protein secretion are limited to bioinformatic (Indrelid *et al.*, 2014; Abby *et al.*, 2016; Vivek-Ananth *et al.*, 2018) or transcriptomic (Garg and Ranganathan, 2011) assessments. Secretion assays are typically tailored to a specific protein of interest and involve the use of reporter systems such as an enzyme-linked immunosorbent assay (ELISA) (Engvall and Perlmann, 1971; Weber *et al.*, 2017) or western blotting using immuno- or fluorescently labelled target proteins (Faden *et al.*, 2016). Alternative strategies include indirect methods, such as assessment of bacterial mutants for alterations in the secretion of a range of degradative enzymes, including proteases, lipases, and chitinases, using agar plate-based halo assays (Agrawal and Kotasthane, 2012; Vijayaraghavan and Vincent, 2012; Ramnath *et al.*, 2017). Further methods are tailored to specific secretion pathways where, for example, TnPhoA reporters were used for detection of Type 1 secretion proteins (Das and Xie, 1998; Bailey and Manoil, 2002). Other methods, such as 2-D gel electrophoresis (O'Farrell, 1975; Pieper *et al.*, 2008) and mass spectrometry (Mariappan *et al.*, 2010), have been used to determine the entire exoproteome. However, there are currently no assays allowing the identification of genes involved in the global regulation of protein secretion. This chapter details the development of a rapid exoproteome screening system to examine the exoproteome of random mutants to identify genes involved in regulation of protein secretion.

4.2 Methods

4.2.1 Transposon mutagenesis

Escherichia coli strain ST18 transformed with pKRCPN2 (harbouring the miniTn*5*-derived transposon Tn-DS1028*uidA*Km) was used to conjugate pKRCPN5 into MH96, as outlined in Chapter 2.3.9, to generate a MH96 transposon mutant library (Thoma *et al.*, 2009; Mesarich *et al.*, 2014). Transconjugants of MH96 were plated on LB agar plates supplemented with 100 µg/ml kanamycin and incubated at 25°C for 24 h. Eighty mutants resulting from each conjugation were patched onto LB agar plates containing kanamycin and then used to inoculate 1-ml volumes of LB broth in the wells of 96-well deep-well plates.

4.2.2 Bacterial cultures in 96-well plates

A 96-well plate with 2 ml wells was filled with 1 ml LB broth per well (50% vol.). Each well of the 96-well plate was inoculated with a single colony using a sterile tip, then gently mixed into the broth, before incubation at 25°C for 16 h at 200 rpm shaking. Cell growth was assessed as outlined in Chapter 2.2.

	1	2	3	4	5	6	7	8	9	10	11	12
A	MH96	MH96	MH96	K18	K18	K18	BLANK	BLANK	BLANK			
B												
C												
D												
E					BLANK	BLANK	BLANK	BLANK				
F												
G												
H										BLANK	BLANK	BLANK

Figure 9: Schematic of the loading pattern of 96-deep well plate for High-throughput exoproteome screening assay. MH96 represents a positive secreting strain, and K18 represents a native non-secreting strain. BLANK represents LB broth only, white boxes represent wells inoculated with colonies of transposon mutants (n=80).

For the HESA, the same loading pattern was used to inoculate every 96-deep well plate (Fig. 9). MH96 was used as a positive strain for exoproteome production (wells A1–3). K18, a wild type non-secreting strain, was used as a negative exoproteome strain and inoculated in wells A4–6. Additionally, 10 LB broth blanks were used as controls, to exclude the possibility of cross-contamination of wells. When wells of the blank showed bacterial growth, identified by clouding of the broth, the experiment was

repeated until no contamination was seen. The 80 remaining wells (containing 100 µg/ml kanamycin in 1 ml LB) were used in the HESA by inoculating each with a transposon mutant colony.

After inoculation, the plates were sealed with semi-permeable seals (Thermofischer, USA) and incubated for 16 h at 25°C at 200 rpm.

4.2.1 Exoproteome analysis

To analyse the exoproteome of transconjugants, the deep-well plates were centrifuged at 2,200 ×× *g* (15 min) to retrieve the supernatant and cell pellets were observed by eye. Mutants with a similar-sized cell pellet but different exoproteome concentration relative to MH96 were further examined by SDS-PAGE and Bradford assay of the supernatant as outlined in Chapters 2.5.2 and 2.5.1.

A Bradford-based assay was used for protein quantification (Protein assay kit, BioRad, USA). A Bradford standard curve was generated as outlined in Chapter 3 using protein standards and was used to quantify protein secretion in the HESA. As described in Chapter 2.6.3, 12 µl of the supernatant was analysed in the Bradford assay.

4.2.2 Arbitrary PCR - Localisation of Tn*5* insertion

To identify the insertion sites of the Tn*5* transposon in the transconjugant strains, genomic DNA was isolated using PrepMan Ultra Sample Preparation Reagent. Genomic DNA was used as a template for arbitrary PCR using a nested primer and a random primer, as described by Mesarich *et al.* (2017). The resultant amplicons were purified using a High Pure PCR Product Purification Kit (Roche) and cloned into the pGEM-T Easy cloning vector (Promega). Plasmid DNA was isolated using a High Pure Plasmid Isolation Kit (Roche) and sequenced with M13F and M13R primers by Macrogen.
DNA sequences were trimmed and aligned against the genome of strain MH96 (GenBank accession number NZ_CP010029.1) using the Map to Reference function of Geneious 10.0.9 (Kearse *et al.*, 2012).

4.2.3 High-throughput exoproteome screening assay (HESA) to identify regulators of protein secretion

Y. entomophaga MH96 Tn*5* transposon mutants were screened for altered levels of exoproteome concentrations relative to wild-type strain MH96 and to a previously isolated spontaneous non-secreting MH96 derivative, strain K18 (Table 1) (Fig. 10, Step1).

As outlined in Fig. 10 (Steps 2 and 3), each mutant was assessed in a 96-well plate for exoproteome as outlined in Chapter 4.2.4. Mutant strains with altered protein secretion, identified by discolouration of the well from blue to brownish, were stored and further assessed. Based on the assumption that cultivation in 96-deep well plate limits oxygen availability and exposes the bacteria to greater shear forces during shaking, these mutants were grown in 50 ml LB broth cultures, allowing a more accurate determination of cell density and exoproteome concentration and composition, as outlined in Chapter 2.3.1. SDS-PAGE analysis of the resulting culture supernatants revealed the effects of transposon insertion on culture exoproteome in more detail (Fig. 10, Step 4). A parallel SDS-PAGE assessment of the cell pellet allowed visual detection of any proteins that were produced but not secreted. Strains with altered protein secretion and similar CFU, compared to the control MH96, were then used for arbitrary PCR, as outlined in the previous Chapter (4.2.2), to localize Tn5 insertion before storage at −80°C.

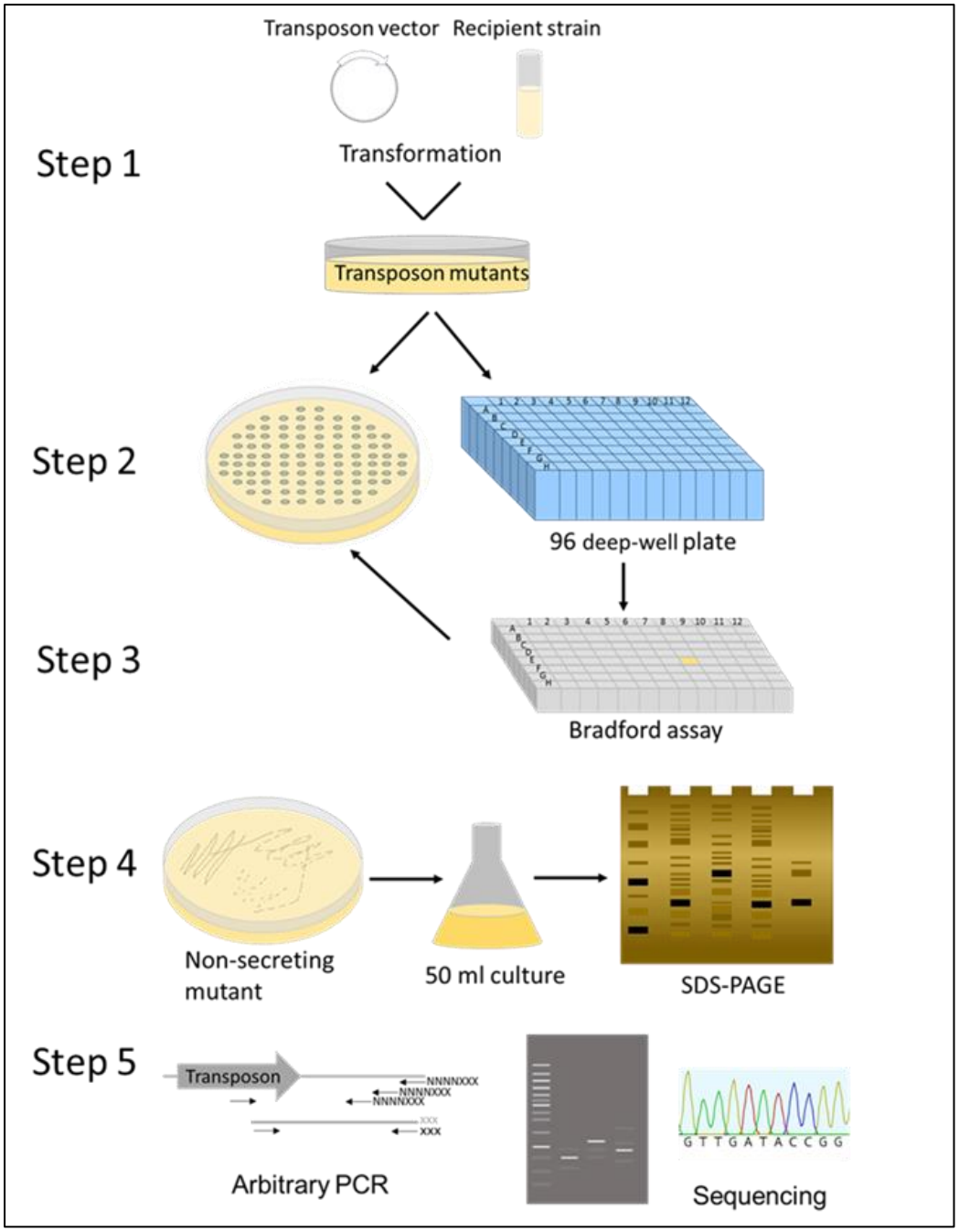

Figure 10: Steps involved in the high-throughput exoproteome screening assay of *Y. entomophaga*. Step 1: Construction of a transposon mutant library by the transformation of a Tn*5*-harboring plasmid into MH96. Step 2: Eighty random mutants per transformation event were patched onto a selective LB agar plate. The same tip was used to inoculate a single well of a 96-well plate, which was incubated at 25°C and 200 rpm for 24 h. Step 3: Following the centrifugation at 6000 *× g* for 15 min, 12 µl of the supernatant were transferred to a 96-well plate for quantification by Bradford assay. Non-secreting mutants, distinguishable by less blue colouration in the assay, could be traced back to the LB agar plate and stored. At this time, the relative size of the centrifuged cell pellet was visually compared with that of strain *Y. entomophaga* MH96, and strains showing impaired growth (smaller cell pellet) were omitted from subsequent screens. All putative secretion-altered mutants were re-assessed using the protein assay (Steps 2–3). Step 4: Mutants with an altered secretion profile were then validated through SDS-PAGE assessment of the exoproteome content derived from 50 ml LB broth cultures at 16 hpi. Step 5: Transposon insertion points within the genomes of non-secreting mutants were determined by arbitrary PCR and the resultant sequences aligned to the MH96 reference genome (GenBank accession number NZ_CP010029.1).

4.3 Results

4.3.1 Correlation of growth in 50 ml culture and 96-well deep plates

Before the initial HESA screening, the relative cell growths under these differing conditions were compared between 96-well plates versus 50 ml cultures, to eliminate any variables of cell growth, where the 96-deep well plates may have a low oxygen exchange and possibly higher shear force at 200 rpm than a 50 ml culture. Cultures incubated for 16 h in a 96-well plate reached a cell density of 2.4×10^9 CFU/ml, in comparison with 5.2×10^9 CFU/ml at 16 hpi of MH96 grown in 50 ml of LB broth. Chapter 3.1.1 reported that the exoproteome is detectable at 3×10^9 CFU/ml. The results show that cell growth and exoproteome production and release in 96-well plates are not severely inhibited and reach a similar OD to when the secretome was detected in 50 ml culture. Therefore, 96-deep well plates were used as culturing vessels for rapid screening of MH96 derivatives.

4.3.2 Identification of genes involved in exoproteome production using the HESA

In initial HESA screening, 4080 transposon mutants were screened in 96-well plates for cell pellet size and exoproteome concentration using the Bradford assay (Fig. 11). Out of 4080 mutants, 50 showed altered exoproteome release (an example in Fig. 11B) (Table S1), as visually determined by lighter or darker blue colouration compared to MH96 control, while still showing similar growth characteristics (similar pellet size -Fig. 11A).

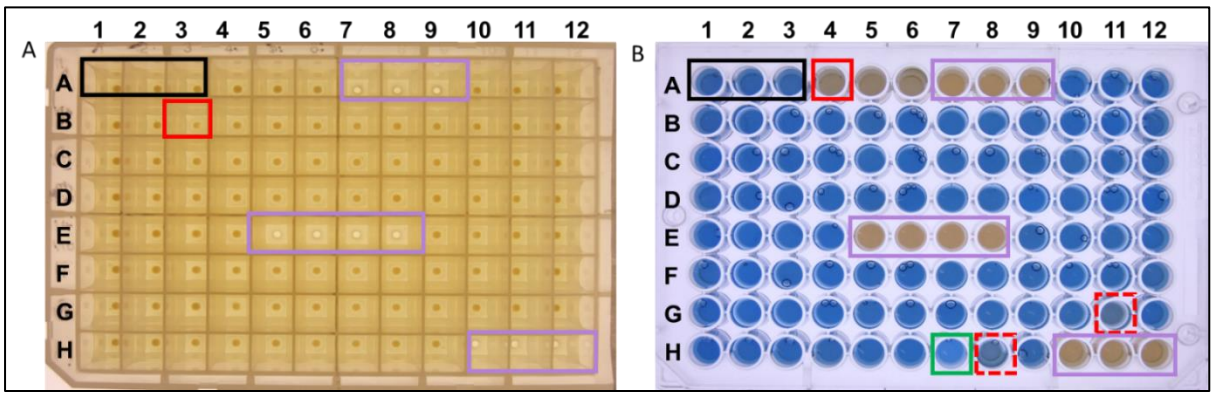

Figure 11: Assessment of exoproteome concentrations in a 96-well master plate. (*A*) Inoculation plate with wells containing A1–3, *Y. entomophaga* MH96 (wild-type); A4–6, *Y. entomophaga* K18 (non-secretion control); A7–9, E5–8, and H10–12 (purple boxes), LB broth blanks. The pellet sizes of the strains were compared with those of MH96 (black box) and the LB-only blank (purple box), and *Y. entomophaga* mutant strains with smaller cell pellets were identified (red box). (*B*) Bradford protein assay of supernatants from 96-well master plate shown in panel (*A*). No colour change was observed for strain K18 (non-secreting control, red box with solid lines). Transposon mutants with decreased (red boxes with dashed lines) and increased (green box) exoproteome concentrations are indicated.

To localize the transposon insertion points of the respective mutants, arbitrary PCR was used to amplify the genetic region of the transposon insertion and amplicons DNA sequenced and mapped to the *Y. entomophaga* MH96 genome (as outlined in Chapter 4.2.4). The results are presented in Table 6. The identified genes were then classified into Clusters of Orthologous Groups (COG) to assign a putative function. COG assignments (Fig. 12, Table 9) of 11 insertions were located in transcriptional regulators and intergenic regions. Another ten insertions were located in genes of LPS synthesis and 13 were located in genes for metabolic pathways (Fig. 12). Also, six insertions were in virulence-associated genes, three were in cell replication genes, and two were in QS genes. Six transposon mutants could not be assigned to a COG category.

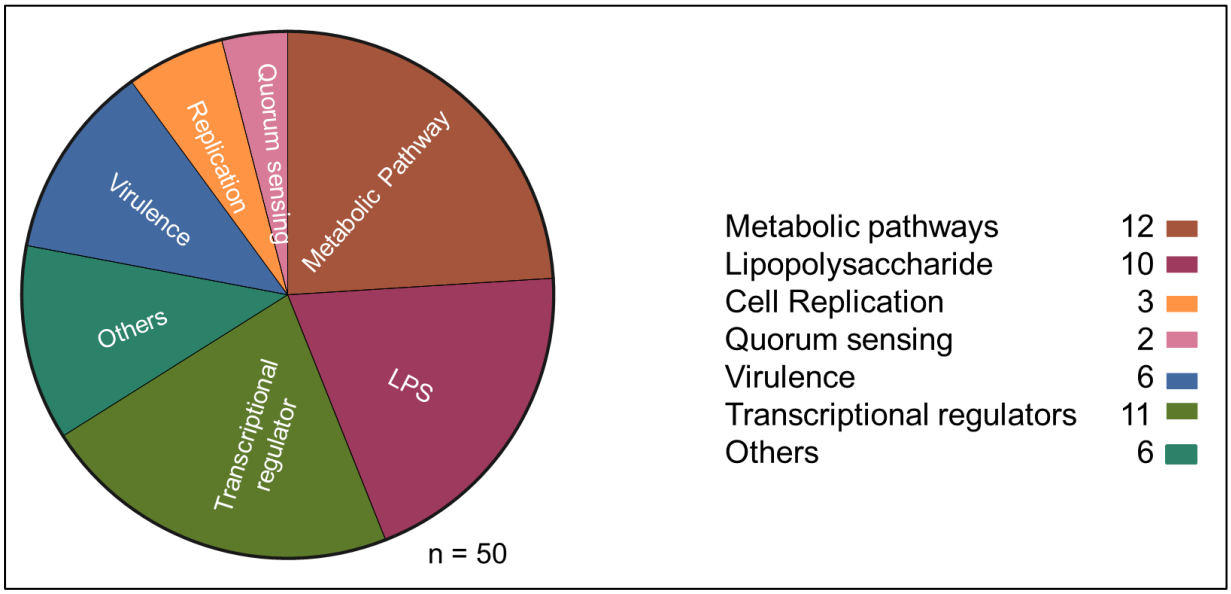

Figure 12: Clusters of Orthologous Groups assigned to secretion deficient *Y. entomophaga* transposon mutants identified using high-throughput exoproteome screening assay.

In line with the main objectives of this thesis, to define regulators of exoproteome production, 11 insertions identified through HESA resided within transcriptional regulators and intergenic regions. These intergenic regions included: the intergenic region of *yen*7 and *chi1* of the Yen-Tc operon; PL78_04800, encoding a histone-like nucleoid-structuring protein (H-NS); the intergenic region of PL78_14480 encoding for DNA mismatch repair protein MutS; the intergenic region of PL78_14485 encoding a hypothetical protein located in the T3SSY2 cluster (Fig. 13) and the intergenic region of PL78_17390, encoding for holin of a lysis cassette. Transcriptional regulators identified by the HESA were a GntR-like transcriptional regulator YhfX, with unknown function, and RbsR, a LacI -like transcriptional regulator of the ribose metabolism.

Table 9: *Y. entomophaga* MH96 transposon mutants generated in this study

Mutant	**Locus-Tag**	**Gene description**	**COG***	**COG_description**	**Gene length (bp)**	**Insertion in *gene/intergenic* (bp)**	**Exoproteome compared to MH96 BA†**	**CFU compared to MH96**
KTMS15	PL78_01430	Type II citrate synthase/*gltA*	C	Citrate synthase	1284	1242	-	- -
KTMS33	PL78_01430	Type II citrate synthase/*gltA*	C	Citrate synthase	1284	793	-	- -
KTMS55	PL78_09650	Dihydrolipoyl dehydrogenase/*lpdA*	C	Pyruvate/2-oxoglutarate dehydrogenase complex, dihydrolipoamide dehydrogenase (E3) component or related enzyme	1326	1250	-	0
KTMS11	PL78_12985	Malate dehydrogenase/*mdh*	C	Malate/lactate dehydrogenase	939	205	- - -	- - -
KTMS08	PL78_08330	Aspartate ammonia lyase/*aspA*	E	Aspartate ammonia-lyase	1437	149	- -	-
KTMS16	PL78_09380	Arginine decarboxylase	E	Arginine decarboxylase (spermidine biosynthesis)	1980	707	- -	0
KTMS42	PL78_07560	Guanosine polyphosphate pyrophosphohydrolase/*ppx*	F	Exopolyphosphatase/pppGpp phosphohydrolase	1494	877	-	0
KTMS48	PL78_00755	Phosphoglucosamine mutase/*glmM*	G	Phosphomannomutase	1371	145	-	0
KTMS24	PL78_03735-PL78_03740	N.A. §	K	Intergenic (Yen7 regulator - Chitinase)		193 5' *yen7*	+ +	- -
KTMS34	PL78_04800-PL78_04805	N.A.	K	Intergenic (DNA-binding protein H-NS - Thymidine kinase)		159 5' *hns*	-	0
KTMS56	PL78_04800-PL78_04805	N.A.	K	Intergenic (DNA-binding protein H-NS - Thymidine kinase)		357 5' *hns*	-	+ + +
KTMS19	PL78_11480-PL78_11485	N.A.	K	Intergenic (peroxiredoxin - global nitrogen regulator NtcA)		153 5' *ntcA*	- -	+ +
KTMS29	PL78_14480-PL78_14485	N.A.	K	Intergenic (DNA mismatch repair ATPase MutS - YscW T3SS lipoprotein chaperone)		160 3' *mutS*	-	0
KTMS25	PL78_15400	Hypothetical protein	K	DNA-binding transcriptional regulator, GntR family	900	581	-	+ +
KTMS30	PL78_15400	Hypothetical protein	K	DNA-binding transcriptional regulator, GntR family	900	767	-	+ + +
K18¶	PL78_17385-PL78_7390	N.A.	K	Intergenic (phoB-like regulator - holin)		131 5' *roeA*	- - -	+ + +
KTMS04	PL78_17385-PL78_7390	N.A.	K	Intergenic (phoB-like regulator - holin)		120 5' *holA*	- - -	- -

KTMS31	PL78_17385-PL78_7390	N.A.	K	Intergenic (phoB-like regulator - holin)		237 5′ *holA*	- - -	- -
KTMS46	PL78_17385-PL78_7390	N.A.	K	Intergenic (phoB-like regulator - holin)		70 5′ *holA*	- - -	0
KTMS12	PL78_17385	Hypothetical protein	K	PhoB- like regulator	419	139	- - -	+ + + +
KTMS02	PL78_07555	DNA helicase/*recQ*	L	Superfamily II DNA and RNA helicase	1290	1100	-	+ +
KTMS20	PL78_07980	LPS heptosyltransferase/*waaC*	M	ADP-heptose:LPS heptosyltransferase	966	791	- - -	- - -
KTMS05	PL78_00700	LPS paratose synthase	M	Nucleoside-diphosphate-sugar epimerase	867	256	- -	-
KTMS03	PL78_00710	LPS/*murJ*	M	Membrane protein involved in the export of O-antigen and teichoic acid	1425	554	- - -	0
KTMS07	PL78_00710	LPS/*murJ*	M	Membrane protein involved in the export of O-antigen and teichoic acid	1425	774	- - -	- - -
KTMS09	PL78_00710	LPS/*murJ*	M	Membrane protein involved in the export of O-antigen and teichoic acid	1425	252	- -	- - -
KTMS13	PL78_07500	LPS O-Antigen translocase	M	membrane protein involved in acid resistance	1266	114	- -	-
KTMS21	PL78_07505	LPS Aminotransferase/*wecE*	M	dTDP-4-amino-4,6- dideoxygalactose transaminase	1131	816	-	+
KTMS22	PL78_07505	LPS Aminotransferase/*wecE*	M	dTDP-4-amino-4,6- dideoxygalactose transaminase	1131	791	-	+ +
KTMS32	PL78_11175	Potassium transporter/*trkA*	P	Trk K^+ transport system, NAD- binding component	1377	469	- -	-
KTMS27	PL78_04165	non-ribosomal peptide synthetase	Q	Thioesterase domain of type I polyketide synthase or non-ribosomal peptide synthetase	5535	4419	-	+
KTMS53	PL78_04270	Hypothetical protein	T	Regulator of sirC expression, contains transglutaminase-like and TPR domains	810	795	- - -	+ + +
KTMS37	PL78_15570	Inosine-5′-monophosphate dehydrogenase/ *guaB*	T	CBS domain	1464	1319	-	- - - - -
KTMS23	PL78_03850	QS/N-acyl-L-homoserine lactone synthase	T	N-acyl-L-homoserine lactone synthetase	651	450	-	+ + +
KTMS45	PL78_03850	QS/N-acyl-L-homoserine lactone synthase	T	N-acyl-L-homoserine lactone synthetase	651	163	-	+ + +
KTMS41	PL78_11650	intracellular growth attenuator protein/*igaA*	S	intracellular growth attenuator protein	2151	2029	- - -	- -

* COG (Clusters of Orthologous Groups) classifications retrieved from Hurst *et al.* (2016):

C, energy production and conservation (11%); E, amino acid metabolism and transport (5.5%); F, nucleotide metabolism and transport (2.8%); G, carbohydrate metabolism and transport (2.8%); K, transcription (33.3%); L, replication and repair (2.8%); M, cell wall/membrane/envelope biogenesis (22.2%); P, inorganic ion transport and secretion (2.8%); Q, secondary structure (2.8%); T, signal transduction mechanisms (11%); S, unknown function (2.8%)

† BA, Bradford assay at 16 hpi were normalized to those of wild-type strain MH96 and classed as: reduced secretion mutants (- - -; - -; -) or enhanced secretion mutants (+; ++; +++; ++++) on the basis of a mutant to wild-type ratio of less than 25%, 50%, or 75% or higher than 125%, 150%, 175%, or 200%, respectively. Mutants classed as having secretion levels similar to those of the wild-type strain MH96 (0) had a ratio of 75–125%

‡ CFU, CFU counts at 16 hpi were normalized to those of wildtype strain and classed as; reduced secretion mutants (- - -; - -; -) or enhanced secretion mutants (+; ++; +++; ++++) on the basis of a mutant to wild-type ratio of less than 25%, 50%, or 75% or higher than 125%, 150%, 175%, or 200%, respectively. Mutants classed as having secretion levels similar to those of the wild-type strain MH96 (0) had a ratio of 75–125%

§ N.A., not applicable, insertion located in intergenic region

¶ indicates K18, a spontaneous MH96 non-secreting mutant with a 3-bp deletion within intergenic region PL78_17385–17390

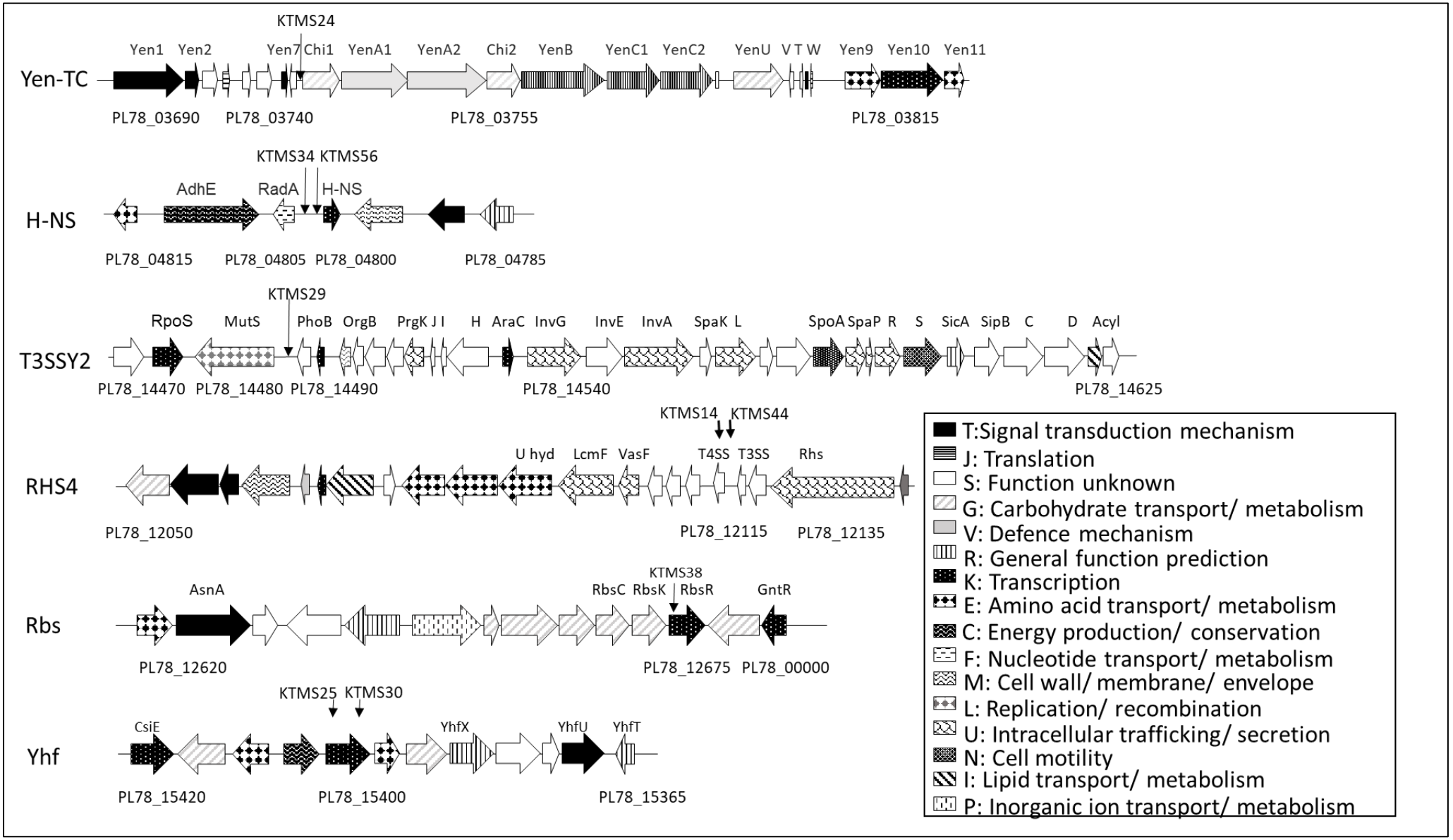

Figure 13: Schematic of the transposon insertions in transcriptional regulators. A) Transposon insertions in the intergenic regions of Yen-Tc, H-NS, T3SSY2, and Rhs4 clusters (1). B) Transposon insertion within the Rbs (ribose metabolism) and Yhf (pathway unknown) cluster in the RbsR (PL78_12675) and genes YfhX (PL78_15400) encoding putative transcriptional regulators of LacI- and GntR-family, respectively. Boxed inset: Fill pattern of the protein function according to COG classification.

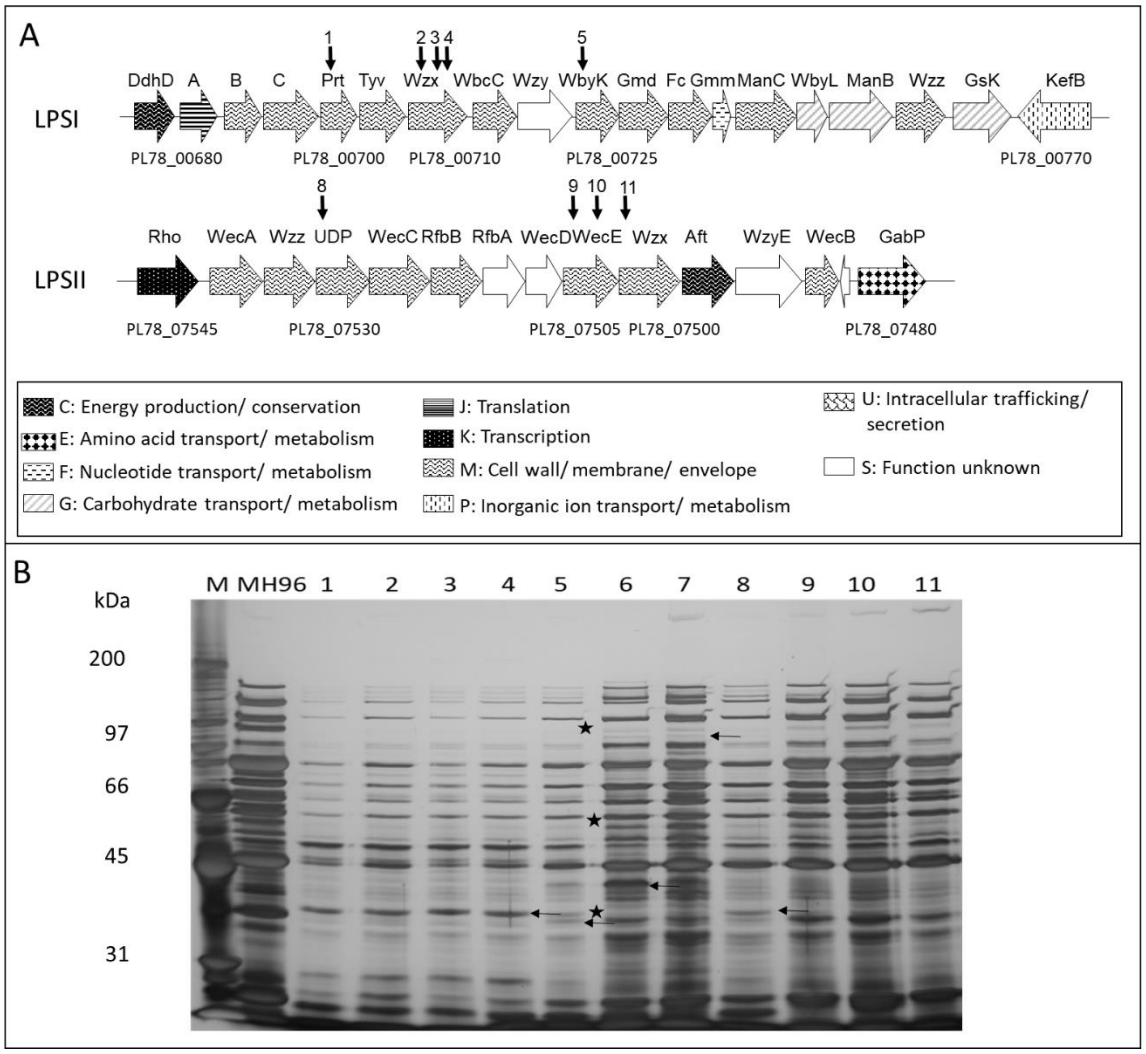

Figure 14: Transposon insertion sites (number 1-11) in the *Y. entomophaga* MH96 LPSI, LPSII, and Rhs4 gene clusters. (*A*) Schematic of selected operon structures. Arrows denote Tn*5* insertion sites in the LPSI cluster: 1, KTMS05; 2, KTMS03; 3, KTMS07; 4, KTMS09; 5, KTMS18; and in the LPSII cluster: 8, KTMS35; 9, KTMS21; 10, KTMS22; 11, KTMS13. Box insert indicates pattern fill according to COG-classification. (*B*) SDS-PAGE of culture supernatant from 16-h cultures of the strains listed in (*A*), as well as the QS mutants (KTMS23, lane 6; KTMS45, lane 7). Arrow (←) and asterisk (*) denotes bands that increased or decreased in intensity respectively relative to MH96. M, Bio-Rad broad-range marker.

Five transposon insertions were co-located in the LPSI cluster (Fig. 14A, LPSI, Table 9), required for O-antigen synthesis (Skurnik *et al.*, 2000) and significantly decreased exoproteome release (Fig. 14B). Of these, three independent insertions were in genes encoding an inner membrane protein involved in murein biosynthesis (Wzx), with the remaining two insertions in paratose synthase (*prt*) and mannosyltransferase (*wbyK*) genes. Four additional transposon insertions were identified in the LPSII cluster, which catalyses the biosynthesis of an enterobacterial common antigen (Muszyński *et al.*, 2013). These insertions were in genes encoding a uridine-5'-diphosphate (UDP) epimerase, an aminotransferase (WecE), and the O-antigen translocase (Wzx) (Fig. 14A, LPSII, Table 9).

Two mutants, KTMS23 and KTMS45, had insertions in PL87_03850, encoding for the AHL synthetase of the QS system. Compared to the LPS mutants, the QS mutant showed only a slightly reduced

exoproteome (Fig. 15). Due to the importance of QS in cell communities and the initially low exoproteome result observed in the HESA, the effect of QS in *Y. entomophaga* exoproteome production was further assessed in Chapter 5.

To further validate the role of these mutants in exoproteome production, cultures were scaled up to 50 ml and CFUs were determined (Table S1). A Bradford assay and SDS-PAGE of the supernatant were also performed (Fig. 15). Through these approaches, 35 of the original 50 mutants were validated as having altered exoproteome profiles at this scale, compared with MH96. Of these, 27 showed reduced and eight mutants showed elevated exoproteome concentrations, respectively (Table 9).

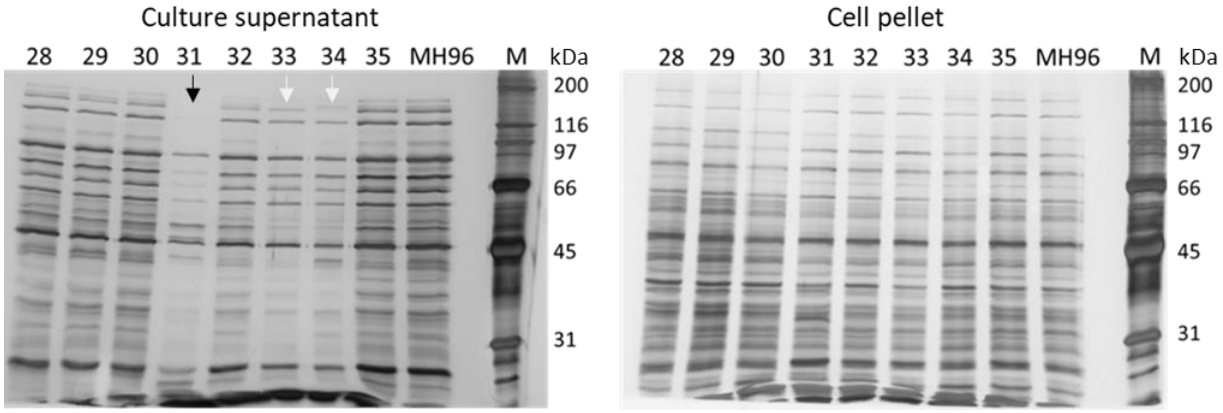

Figure 15: SDS-PAGE (10%) of culture supernatant and the cell pellet of representative HESA-derived Tn5 mutants KTMS28–35 (Table 9), cultured for 16 h. The protein samples of the mutants KTMS28–35 with the wild type control MH96 are presented. Location of transposon insertion: 28 (*hrpB*), 29 (*mutS-YscW*), 30 (hypothetical, locus PL78_15400), 31 (intergenic *roeA-holA*), 32 (*trk*), 33 (*gltA*), 34 (intergenic *hns*-hypothetical), 35 (*galE*). SDS-PAGE was normalized by using supernatant from cultures of similar CFU compared to MH96 (Table S1). White and black arrows denote altered exoproteome profiles in transposon mutants relative to MH96, respectively. M, Bio-Rad broad-range marker

Of the 35 transposon mutants with altered exoproteome profiles relative to strain MH96, SDS-PAGE analysis revealed that mutants with transposon insertions within locus PL78_17385, or in the intergenic region between PL78_17385 and PL78_17390 (Table 6 and Fig. 16A) had similar exoproteome profiles to the non-secreting MH96 derivative K18, with only a few prominent protein bands visible (Fig. 16B). Based on this finding, HiSeq genome sequencing of strain K18 was performed and the resulting whole-genome sequence was compared with that of strain MH96 (GenBank accession number NZ_CP010029.1), as outlined in Chapter 2.5. DNA alignments revealed a single 3-bp deletion located 132 bp 5′ of PL78_17385 (Fig. 16).

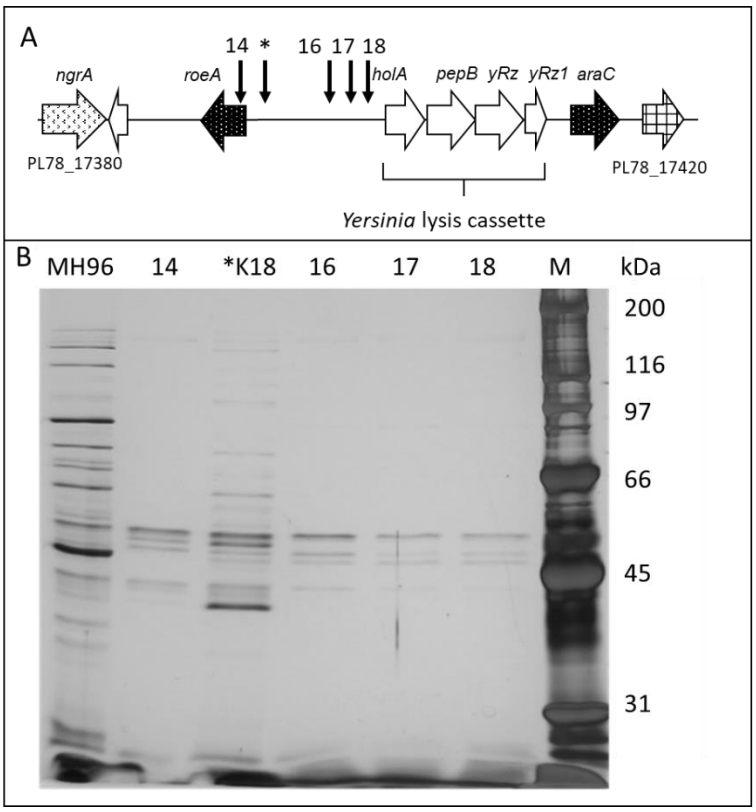

Figure 16: Assessment of the YeRER and its associated mutants. (A) Schematic of the *Y. entomophaga* MH96 YeRER. Black vertical arrows indicate positions of the transposon insertions in mutants: KTMS12 (14); KTMS31 (16); KTMS04 (17) and KTMS46 (18). Predicted lysis cassette and associated ORFs are indicated. * denotes the location of the 3-bp deletion in strain K18. White arrows denote genes adjacent to the Roe cluster, *ngrA* (encoding phosphopantetheinyl transferase) and *araC* (encoding a transcriptional regulator) are indicated (B) SDS-PAGE profiles of the 16-h culture supernatants of wild-type strain MH96, YeRER mutants KTMS12 (14), KTMS04 (16), KTMS31 (17), and KTMS46 (18), and reduced secretion strain K18 (*). M, Bio-Rad broad-range marker.

A BLASTP search of the PL78_17385–PL78_17400 region (Fig 16A and Table S2) predicted that PL78_17385, a putative 139-amino acid residue protein, contained a helix-turn-helix (HTH) motif. Helix-turn-helix motifs are commonly found in DNA binding domains of PhoB-like regulators. Based on protein homology (59% similarity) of the HTH-motif, and the decreased exoproteome release phenotype of a mutant with a transposon insertion in this gene, PL78_17385 was classified as a regulator of exoproteome and named RoeA.

In addition to RoeA, the PL78_17385–PL78_17390 region encodes a holin, endopeptidase, and hypothetical protein, as found in phage derived lysis cassettes (PL78_17390–PL78_17400) positioned in the opposite orientation, 1,038–2,125 bp 5’ of *roeA*. The predicted lysis cluster (PL78-17390-17400) is designated the *Yersinia* lysis cassette (YLC), which shares gene synteny with a lysis cassette of *Y. enterocolitica* strain W22703 (Table S2) and comprises genes encoding a holin (*holA*), peptidase M15 (*pepB*), and a third ORF (PL78_17400) sharing 53% homology with i-spanin (yRz) of W22703 (Table S2) (Springer *et al.*, 2018). Based on the gene synteny and amino acid similarity to the lysis cassette of

W22703, the MH96 loci PL78_17400 was designated as an o-spanin (*Rz).* Due to the altered exoproteome of mutants with transposon insertions in the lysis cassette and RoeA 5′ region, the cluster was named YeRER for "*Y. entomophaga* region of exoproteome release" and was further characterized in Chapter 6.

One hyper-secreting strain was identified in the HESA (KTMS24) (Fig. 17A). The transposon insertion of KTMS24 was located in the intergenic region between *yen7* and *chi1* of the Yen-TC cluster. Yen7 is a hypothetical transcriptional regulator consisting of a DNA-binding HTH-motif. Furthermore, BLASTP of the Yen7 amino acid sequence revealed 59% identity and 77% similarity to RoeA (Fig. 17C, Table S2). The increased exoproteome release, visualised by SDS-PAGE, by similar CFU in KTMS24 compared to MH96 (Fig. 17AB), indicates the RoeA paralog Yen7 might also be involved in exoproteome release and should be investigated further.

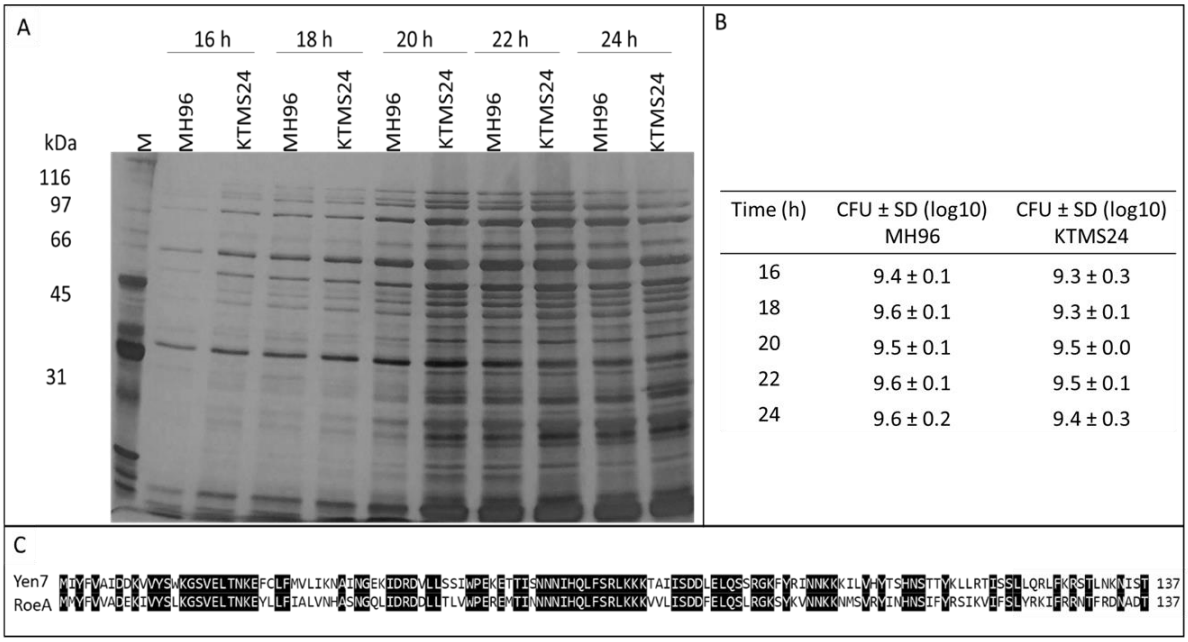

Figure 17: Phenotypic effects of KTMS24 with transposon insertion 5′ of Yen7. *A)* Exoproteome assessment by SDS-PAGE comparing KTMS24 and MH96 at stationary phase (16–24 h). Standardized CFUs (log10) per timepoint: 16 (9.6), 18 (9.5), 20 (9.5), 22 (9.7), 24(9.5) were loaded on SDS-PAGE. *B)* Comparison of MH96 and KTMS24 CFUs at stationary phase at time points when the exoproteome in A was sampled. *C)* Protein alignment of putative transcriptional regulators Yen7 and RoeA. Black boxes indicate identical residues.

4.4 Discussion

This chapter describes the development of an exoproteome screening assay to identify genes involved in the production and release of the exoproteome. By definition, the exoproteome consists of all secreted (secretome) and non-secreted (passively exported) proteins (Armengaud *et al.*, 2012). The supernatant, separated from the cell pellet by centrifugation, also contains surface proteins (surface proteome) such as flagellar or fimbrial proteins, which are components of the exoproteome in this study.

To identify genes involved in *Y. entomophaga* MH96 exoproteome production, the HESA was developed and used to screen transposon mutants for alterations in exoproteome profile. Using the HESA, 35 mutants with altered exoproteome concentrations relative to wild-type strain MH96 were identified. Several transposon insertions were located in LPS clusters and the YeRER cluster, indicating these clusters are essential to MH96 exoproteome production. In line with the goal to define regulators involved in exoproteome production, transposon insertions were identified in AHL synthase, as well as four insertions in transcriptional regulators and eight further insertions located in intergenic regions adjacent to transcriptional regulators, including H-NS and RoeA. The remaining mutations that resulted in altered exoproteome production were in genes of metabolic function, energy production, and signal transduction.

A limitation of the HESA method is the level of detection of the exoproteome. Only strains with clear alterations in secretion can be identified with the initial screening. The exoproteome is composed of actively secreted proteins and those that can passively pass the membrane barrier. Of note, no mutant with a reduced exoproteome identified using the HESA had a transposon insertion in genes encoding any of the six common secretion systems (T1–6SS). It is plausible that the absence or inactivation of a single secretion system does not lower the protein concentration in the supernatant sufficiently to be detected by the HESA. Furthermore, secretion systems such as T3SS or T6SS are not expected to be active under standard laboratory conditions and, therefore, contribute to the exoproteome. Another limitation of the HESA is the already high concentration of exoproteome of *Y. entomophaga* MH96. With reference to the standard curve of cell culture and visual assessment by the Bradford assay, the protein concentration of the crude MH96 supernatant is close to the maximum visual threshold and therefore the assay would be unlikely to detect hyper-secreting strains. However, the HESA method could be modified to detect hyper-secreting strains through adjustment of the threshold by appropriate dilution of the supernatant.

In *Y. entomophaga* MH96*,* transposon insertions in the LPSI and LPSII operons resulted in reduced concentrations of exoproteome. Interestingly, LPSII mutants KTSM10 and KTMS22 with insertions in

wecE, encoding dTDP-4-amino-4,6-dideoxygalactose transaminase, showed reduced exoproteome release but higher cell densities relative to *Y. entomophaga* MH96. In *E. coli,* the enterobacterial common antigen pathway regulates OMV formation, with a mutation of *wecE* resulting in increased OMV formation (Kulp *et al.*, 2015). A similar scenario was observed in a *P. aeruginosa galU*-mutant (UTP-glucose-1-phosphate uridylyltransferase), which also showed elevated OMV production (Crhanova *et al.*, 2011; Ruhal *et al.*, 2015). In *Salmonella enterica* serovar the mutation of the LPS synthesis gene *rfaC* (LPS heptosyltransferase) Typhimurium strain LT2 abolished protein secretion (Crhanova *et al.*, 2011). The authors suggested that structural changes in the LPS core interfered with the assembly of membrane-bound machinery such as the T3SS and the flagellum. It is plausible that LPS and OMV formation are linked in *Y. entomophaga* MH96 and are crucial for exoproteome release. However, this scenario requires further studies.

Of note was the identification of four independent insertions in the 2366-bp long YeRER, resulting in significantly decreased exoproteome release. Within this region, the translated product of PL78_17385, identified by a transposon insertion that abolished exoproteome production, contains a putative HTH-motif and shares amino acid identity with the DNA binding region of PhoB-like proteins. Based on this, the translated product of PL78_17385 was termed Regulator of Exoproteome, RoeA. The RoeA N-terminal region lacks a phosphorylation site which changes protein confirmation to enable DNA binding when phosphorylated in PhoB-like proteins. This suggests RoeA is activated or functions by an alternate, yet to be determined mechanism (Zschedrich *et al.*, 2016). RoeA shares 77% amino acid similarity with Yen7, located 5' of the Yen-TC encoding cluster. In this context, the KTMS24 intergenic insertion between *yen*7 and *chi1* resulted in elevated exoproteome production (Fig. 17). These regions share 40% nucleotide identity over 758 nucleotides (Table S2) suggesting that MH96 exoproteome and/or Yen-TC production is regulated by these RoeA/Yen7 orthologues.

Three insertions located within a region 70–120 bp 5' of *hol*A (PL78_17390), a homolog to holin of *Y. enterocolitica* lysis cassette, had abolished exoproteome production. While the MH96 lysis cassette is not in close proximity to the Yen-TC encoding cluster, an orthologue of the MH96 lysis cassette resides in the in *Y. enterocolitica* insecticidal pathogenicity island, Tc-PAI$_{Ye}$, encoding a toxin complex (Hurst *et al.*, 2011a; Hurst *et al.*, 2011b). Springer *et al.* (2018) demonstrated the functionality of the *Y. enterocolitica* lysis cassette through its overexpression, but the authors did not define its role in the bacterium. Lysis systems in *Pseudomonas aeruginosa* and *Bacillus subtilis* have been linked to the induction of OMV formation and biofilm production (Turnbull *et al.*, 2016; Toyofuku *et al.*, 2017). Combined with the finding that transposon insertions 70–120 bp 5' of *hol*A (PL78_17390) abolished exoproteome production, this supports the hypothesis that RoeA regulates cell lysis mediated by the

YeRER-encoded MH96 lysis cassette. The finding of a 3-bp deletion 132 bp 5' of *roe*A in the spontaneous non-secreting MH96-derivative K18 further supports the importance of this region in exoproteome production. The YeRER was further characterised for its effect on exoproteome release (Chapter 6). In addition to RoeA, the transcriptional regulators YhfX and RbsR were identified as regulators involved in exoproteome release by HESA.

Using the HESA, transposon insertions in PL78_03850, encoding the enzyme that synthesizes the QS signaling molecule AHL, showed decreased exoproteome concentrations. QS has been implicated in competence, microbial defence, biofilm formation, and virulence in many bacterial species (Rutherford and Bassler, 2012) via the regulation of gene expression (Papenfort and Bassler, 2016; Abisado *et al.*, 2018). It has been linked to regulation of dedicated secretion systems, such as the T3SS of enterohemorrhagic *E. coli* O157:H7, enteropathogenic *E. coli* E2348/69 (Sperandio *et al.*, 1999) and the T6SS of *V. cholerae* strains 2740-80, V52, and C6706 (Shao and Bassler, 2014). QS has been linked with protein secretion in a model where an increased metabolic burden of protein secretion is tolerated at high cell densities to support the acquisition of nutrients from the environment (Cezairliyan and Ausubel, 2017). The finding that the *Y. entomophaga* AHL synthase (PL78_03850) mutant had abolished exoproteome release in the post-exponential phase (16 hpi) and achieved a higher cell density relative to MH96 indicates that QS is integral to the continued production of exoproteins in the post-exponential phase (Table 9). Likewise, the non-secreting strain K18 also exhibited a higher cell density (1.6×10^{10} CFU/ml) than MH96 (5.4×10^{9} CFU/ml) at 16 hpi (Table 9). These findings suggest that the cell directs its energy to increased cell growth in the absence of exoproteome production, achieving a higher cell density. As described in Chapter 3, cell density is likely to play a role in protein secretion and cell density-dependent pathways are commonly regulated by QS. The decreased secretome in the QS mutant KTMS23 identified in the HESA indicates a direct link between QS and protein secretion and is investigated further in the next chapter.

In conclusion, the HESA method is applicable to any exoprotein-producing bacterial species that is conducive to transposon mutagenesis. To enable this, a growth medium in which a high level of exoproteome production is achieved should be defined by analysing the exoproteome profile by SDS-PAGE. In this format, 0.2 mg of BSA/ml is detectable by plate reader and a concentration of ≥1 mg/ml is discernible by eye. The identification and characterization of genes involved in exoproteome production in different microorganisms will further advance our understanding of the underlying mechanism and cues of exoproteome production in bacteria.

Chapter 5

Quorum sensing controls protein secretion in *Y. entomophaga*

5.1 Introduction

Bacterial cell communication, referred to as QS, regulates protein expression in a cell density-dependent manner (Schuster *et al.*, 2013). Autoinducers, such as acyl-homoserine lactone (AHL) are signalling molecules that are secreted and sensed by cells of either the same population or by other populations, as examples of interspecies and interkingdom communications (Simon *et al.*, 2015). In some cases, cross-regulation by QS molecules can occur between different bacterial species (Xavier *et al.*, 2005). QS can alter global patterns of gene expression of entire populations or subpopulations of bacteria, affecting biofilm formation, secretion of virulence factors, bioluminescence, and production of "public goods" such as antimicrobials, surfactants, and siderophores (Kummerli and Brown, 2010; Grote *et al.*, 2015; Papenfort *et al.*, 2016; Paulander *et al.*, 2018; Xavier, 2018). Using the HESA (Chapter 4), two independent insertion points were localised to the gene encoding the enzyme that synthesises AHL, the QS molecule in *Y. entomophaga*. While other QS molecules like S-adenosylmethionine derivatives exist, AHL is a common QS molecule throughout the genus *Yersinia* and Gram-negative bacteria (Winans, 2011; Papenfort *et al.*, 2016). Originally it was proposed that QS molecules only passively migrate into the extracellular space by diffusion, a term which is still commonly used, where AHL molecules affect bacterial processes (Boyer and Wisniewski-Dye, 2009b; West *et al.*, 2012; Trovato *et al.*, 2014). Since then, it has been shown that QS molecules can be actively transported through cell membranes (Yang *et al.*, 2006). In Gram-positive bacteria, peptides can act as autoinducers for QS (Verbeke *et al.*, 2017). In Gram-negative bacteria, including *Yersinia* species, the main QS autoinducer is AHL. AHL is a small lipophilic molecule, which allows diffusion through the Gram-negative cell wall (Kaplan *et al.*, 1985; Li and Nair, 2012). Once a threshold of AHL in the environment is reached, molecules can diffuse to the cell wall and bind to LuxR (YenR) or LuxR-like proteins, activating DNA binding and regulation of target genes (Gray and Garey, 2001). In *Y. pseudotuberculosis*, QS modulates T3SS and the Yop effector, which is encoded on the pYV plasmid specific to the human pathogens *Y. enterocolitica*, *Y. pestis,* and *Y. pseudotuberculosis* (Atkinson *et al.*, 2011). Furthermore, QS can modulate motility in *Y. enterocolitica* (Ng *et al.*, 2018). In *P. aeruginosa*, QS controls types 2, 3, and 6 secretion systems, showing the importance of QS in protein secretion (Wagner *et al.*, 2003; Lesic *et al.*, 2009; Liang *et al.*, 2014). Those secretion systems are typically expressed in the presence of a host cell or other bacteria and are used for host invasion, adherence, or defence against host and other bacteria cells.

Quorum sensing is essential for bacteria to react to changing environments. *Y. entomophaga* is pathogenic to insect larvae where it reaches high cell numbers in the hind- and mid-gut (Hurst *et al.*, 2014; Hurst *et al.*, 2015). Therefore, the role that QS plays in virulence towards the insect host is of interest. Larvae of the greater waxworm (*Galleria mellonella*) are commonly used as a model organism to study bacteria and insect/host interaction. In this chapter, the growth and protein secretion profiles, transcriptome, and host colonisation ability of the *Y. entomophaga* QS mutants (KTMS23 and KTMS45) and wild-type, MH96 strains were studied to determine the effect of QS-regulated protein secretion on bacterial virulence.

5.2 Methods

5.2.1 Relationship of growth and exoproteome production and release

To assess exoproteome production and release during the exponential and stationary growth phase of KTMS23, a 50 ml culture was inoculated and grown as outlined in Chapter 3.2.1. Differing from Chapter 3.2.1, sampling time points were from 4 – 24 hpi. Therefore, a 1 ml sample was taken every hour from 4– 12 hpi, and then 750 µl every second hour from 12 – 20 hpi and again 24 hpi and assessed for CFU, OD, and exoproteome as outlined in Chapter 3.2.1.

5.2.2 QS indicator plate assay

To investigate the QS activity of the *Y. entomophaga* strains, a QS indicator strain of *Chromobacterium violaceum* (CV026) was streaked onto a LB agar plate. KTMS23, KTMS45, and MH96 strains were then streaked near to CV026. CV026 does not produce the AHL molecule but produces the purple pigment violacein when it senses AHL produced by other bacteria.

5.2.3 *In vivo* analysis of QS in KTMS23 and MH96 using a green fluorescent protein reporter

A plasmid-based quorum-sensing green fluorescent protein (GFP) reporter, pJBA132 (Andersen *et al.*, 2001) was used to further investigate QS in *Y. entomophaga*. This plasmid contains a GFP reporter under the control of a LuxR-regulated promoter, which causes green fluorescence in the presence of AHL. The vector pJBA132 was transformed into *Y. entomophaga* MH96 electrocompetent (Chapter 2.4.8) cells, the wild-type strain MH96, and the QS mutant KTMS23. The transformed derivatives were

validated for the presence of pJBA132 by miniprep and restriction enzyme digestion (Chapter 2.4.1). As an insect model, *G. mellonella* larvae (Biosuppliers, New Zealand) were used. The larvae were maintained on honey, glycerol, plain baby rice cereal, and granular yeast for up to 7 days. For bacterial injection into *G. mellonella* larvae, bacteria cultures were grown overnight for 16 h in LB with the appropriate antibiotics, to reach similar CFU/ml. Third instar *G. mellonella* larvae were then injected, behind the third leg, with 10 µl of diluted (1/100000) bacterial culture to deliver an inoculum of 10–100 cells per larvae. A drop (3 - 5 µl) of haemocoel was collected by inserting a 20-gauge needle through the dorsal cuticle of the larvae which causes the haemocoel to exit the body as described by Hurst *et al.* (2015). Samples were collected at 24 h, 36 h, and 48 h post-injection. The haemocoel was then assessed under light and fluorescent microscopy using a GFP/UV filter.

5.2.4 Transcriptomics of *Y. entomophaga* KTM23 and MH96

To define QS-dependent regulation in *Y. entomophaga* MH96 and KTMS23, RNAseq and transcriptomic analysis were performed as outlined in Chapter 2.3.2. *Y. entomophaga* MH96 and KTMS23 were grown to 4.35×10^9 and 4.26×10^9 CFU/ml, respectively, and RNA was extracted from two biological replicates. RNA was isolated and purified as outlined in Chapter 2.5.1. The transcriptome data of *Y. entomophaga* KTMS23 was compared to that of the wild-type strain MH96.

5.3 Results

5.3.1 Characterisation of the quorum-sensing mutant

In Chapter 4, mutants KTMS23 and KTMS45 containing transposon insertions within the gene encoding N-acyl-homoserine lactone (AHL) synthase were identified. The loss of QS signalling in these strains was validated by their inability to cause AHL-dependent violacein production in the QS indicator strain *C. violaceum* (CV026) (Fig. 18D). Because QS plays a pivotal role in cell density-dependent signalling, the growth and exoproteome production rates of mutant KTMS23 were assessed (Fig. 18). Optical density (OD) measurements at 600 nm showed no difference of growth rate until the stationary phase, when MH96 reached an OD of 6, compared to the maximum OD of 5 in KTMS23 (Fig. 18A). Measurement of OD, especially of cells in stationary phase, can be prone to errors where the presence of cell debris from dying and dead cells can cause aberrant readings. In addition, CFUs were also assessed to measure cell density. In contrast to the OD measurements, the QS mutant strain KTMS23 reached a higher cell density ($2.8 \times 10^8 \pm 9.4 \times 10^7$ CFU/ml) than the wild-type strain MH96 ($1.7 \times 10^8 \pm 3.8 \times 10^7$ CFU/ml) at 5 hpi (Fig. 18BE). In both strains, exoproteome production started in late

exponential phase from $2.9 \times 10^9 \pm 4.8 \times 10^8$ CFU/ml (MH96) and $6.6 \times 10^9 \pm 1.6 \times 10^9$ CFU/ml (KTMS23) onwards (Fig. 18 CF). Through plotting of CFUs from *Y. entomophaga* MH96 and KTMS23 during exponential phase and using the linear regression model, the replication rates in mid- to late-log phase of MH96 (1.8 cells/h) and KTMS23 (1.73 cells/h) were not significantly different (Fig S4D). Although KTMS23 had similar cell density to MH96, the exoproteome concentration was significantly lower ($p <$ 0.0001, using 2-tailed, paired t-test) than that of MH96, as measured by a Bradford-assay (Fig. 18B/C).

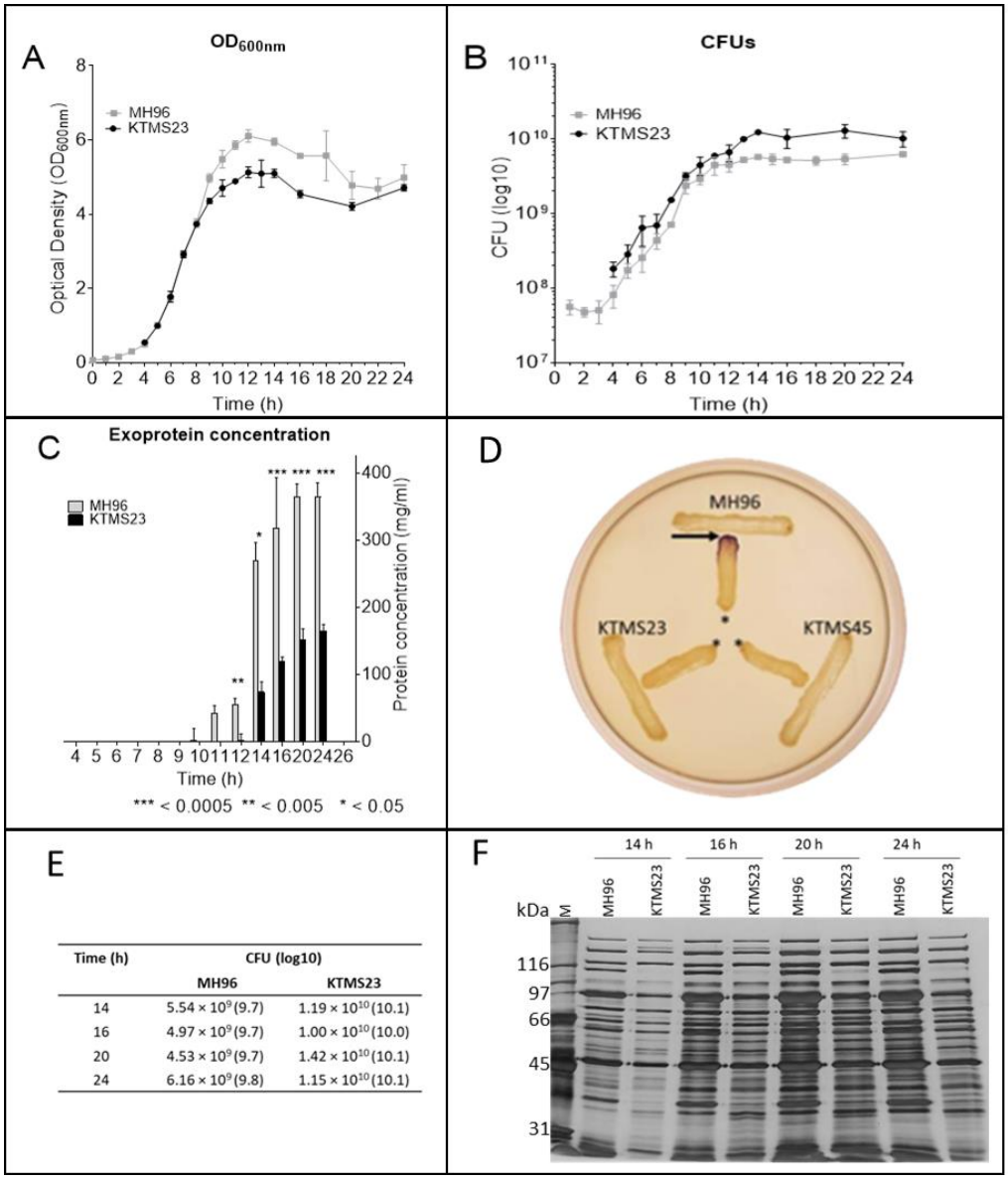

Time (h)	CFU (log10)	
	MH96	KTMS23
14	5.54×10^9 (9.7)	1.19×10^{10} (10.1)
16	4.97×10^9 (9.7)	1.00×10^{10} (10.0)
20	4.53×10^9 (9.7)	1.42×10^{10} (10.1)
24	6.16×10^9 (9.8)	1.15×10^{10} (10.1)

Figure 18: Comparison between *Y. entomophaga* MH96 and QS mutant strain KTMS23. *A)* Data points indicate mean OD_{600} of MH96 (●) and of KTMS23 (●) measured over 24 h. *B)* Cell growth measured in CFU/ml over 24 h of MH96 and KTMS23 culture. *C)* Protein concentration in supernatant of MH96 (□) and KTMS23(■) at the indicated sampling points. In *A, B, C* samples were taken in triplicate and points indicate the mean ± SD, and significance, analysed by paired t-test, is indicated by an asterisk (*). (D) Cross-streak analysis of *C. violaceum* strain CV026 (*) with wild-type strain MH96 and QS mutants KTMS23 and KTMS45. Cross-streaking with *Y. entomophaga* MH96 initiates purple violacein production in strain CV026 (arrow), which is not activated by the KTMS23 and KTMS45 AHL-deficient strains. *E)* Comparison of log10 CFU values from growth curve in B at timepoints 14, 16, 20 and 24 hpi. *F)* SDS-PAGE with silver staining of the culture supernatant of MH96 and KTMS23 culture at timepoints in *E,* when CFU was in similar range.

5.3.2 Pathogenicity of *Y. entomophaga* QS-mutant in *G. mellonella*

To determine of QS is required for virulence of *Y. entomophaga* in *G. mellonella*, *Y. entomophaga* MH96, and QS mutant KTMS23 carrying the indicator plasmid pJBA132 were injected into *G. mellonella*. The pJBA132 is a GFP-fluorescing QS indicator plasmid, which allows rapid visual assessment by microscopy of quorum sensing and was shown to be a functional indicator for *in vivo* quorum sensing (Andersen *et al.*, 2001). As an insect host model, *G. mellonella* larvae were used, due to the wide range of temperature that can be used with *G. mellonella*. Furthermore, in contrast to grass grub larvae, which are seasonal, *G. mellonella* are mass-produced and available throughout the year. Control *G. mellonella,* injected with PBS only, remained healthy throughout the experiment. Larvae injected with MH96 showed melanisation after 24 h, while the QS mutant caused little to no melanisation. After 36 h, *G. mellonella* larvae injected with MH96 pJBA132 and KTMS23 pJBA132, showed complete melanisation and decreased body turgor. Light microscopy of the haemolymph from control larvae detected intact haemocytes and no bacteria at all time points (Fig. S2). After 24 h, haemolymph of MH96- and KTMS23-injected larvae was brown, compared with transparent haemolymph in control larvae. The brown colouration indicated melanisation. Furthermore, both bacterial strains could be observed in the haemolymph of the respective samples (Fig. 19). Bacteria cells of KTMS23 and MH96 *in vivo* at 24 h showed cell elongation (Fig. 19).

At 24 h post-injection, only MH96 cells, which carried pJBA132, could be seen under fluorescent light, indicating that QS occurs in the larvae gut upon injection. As expected, the QS mutant strain KTMS23 pJBA132, which lacks the QS synthetase, did not result in pJBA132 mediated fluorescence. After 36 h post-injection, the larval gut had disintegrated, with lipid vesicles readily observed in the haemolymph samples in both strains (Fig. 19 36 hpi). Due to the high lipid and organic content in the samples, autofluorescence was increased but MH96 cells were still clearly observed, while KTMS23 cells are not visible under fluorescent light.

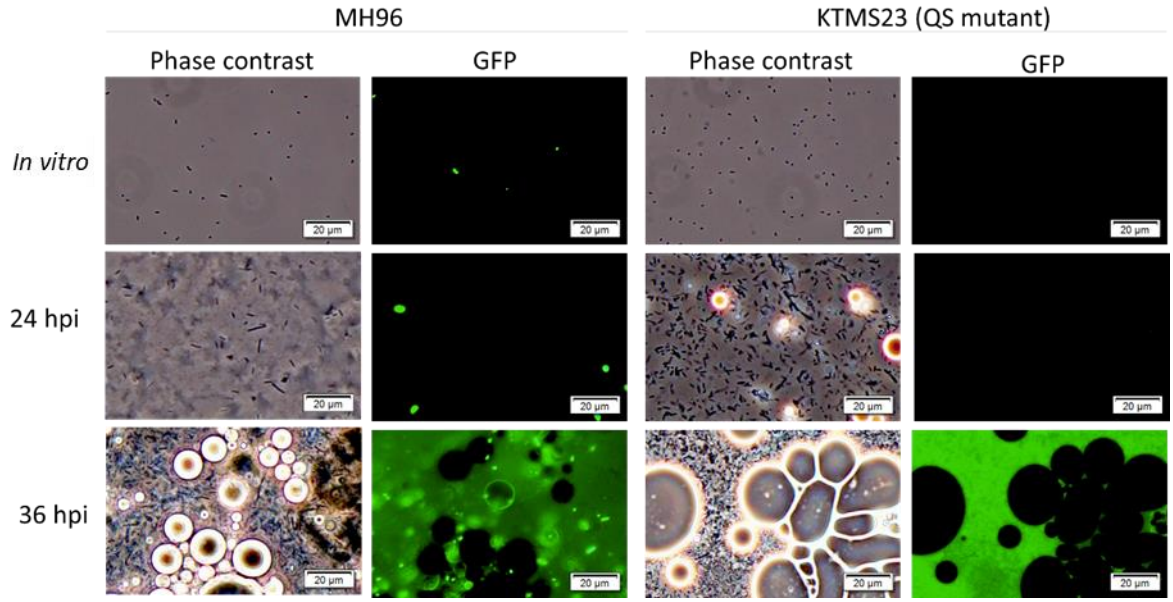

Figure 19: Assessment of *G. mellonella* larval haemocoelic fluid injected with either MH96 (pJBA132) or KTMS23 (pJBA132). Bacterial strains MH96 (pJBA132) and the quorum-sensing mutant KTMS23 (pJBA132) were grown in LB (Miller) for 16 h (*in vitro*). Bacterial dilutions in PBS were used for *G. mellonella* injections. Haemolymph samples of larvae injected with MH96 and KTMS23 were collected at 24 (morbid larvae) and 36 hpi (post-mortem) when degradation of intestinal tissue occurs. Light microscopy (left panel) and fluorescent microscopy using GFP filter (right panel) of each strain at each time point. Scale bar (20 µm) indicated. Exposure time was 200 ms.

Through microscopy of *Y. entomophaga* MH96 and its QS mutants, it was evident that the reduced protein secretion of the QS mutant did not affect its virulence in the insect model *G. mellonella* when injected with 10-100 cells the QS mutant caused the same phenotype as *Y. entomophaga* MH96 resulting in the death of the larvae. Even though QS of KTMS23 pJBA132 did not occur within 36 h, identified by the absence of green fluorescence from the indicator plasmid, bacterial replication within the host haemocoel was observed microscopically. Based on comparative observations of MH96 and its QS mutants, it appears that QS plays no role in colonisation and haemocoelic-based virulence towards *G. mellonella*. *Y. entomophaga* MH96 is a highly virulent strain, with as few as three cells causing death four days after injection into *G. mellonella* (Hurst *et al.*, 2015). While the QS mutant reduced the overall amount of exoproteome release, the content of the exoproteome did not differ, especially the release Yen-TC proteins, as determined by SDS-PAGE. Considering the already high exoproteome concentration of MH96, the lowered amount of exoproteins in the QS mutant was still sufficient to induce virulence.

5.3.3 Transcriptomics of the QS mutant KTMS23

Based on the predicted role of QS in exoproteome production, *Y. entomophaga* wild type strain MH96 and its QS-negative derivative (KTMS23) were subjected to RNAseq (Chapter 2.6.2) assessing the gene expression levels within the stationary growth phase of a cell density of 4.35 x 10^9 CFU-ml in *Y. entomophaga* MH96 and 4.26 X 10^9 CFU/ml in KTMS23. Principle component analysis (PCA) of the KTSM23 transcriptome data compared to *Y. entomophaga* MH96, confirmed the clustering of the duplicate sample of KTMS23 and the wild type strain MH96 (Fig. 20A).

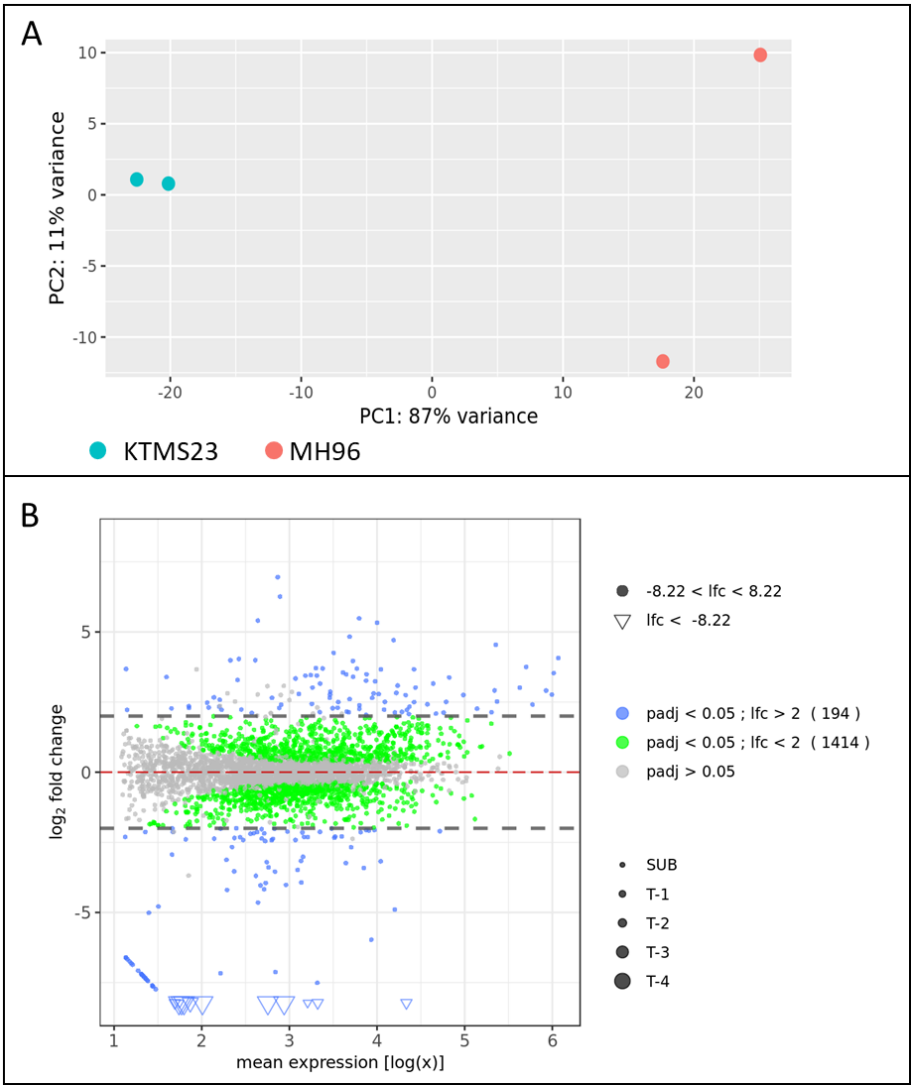

Figure 20: Analysis of transcriptome data from *Y. entomophaga* MH96 with KTMS32. *A)* Principle component and analysis of KTMS23 and MH96 library of normalized count data. *B)* Analysis of transcriptome data between MH96 and KTMS12. Differential gene expression analysis of transcripts expressed in KTMS23 compared to MH96. Blue dots denote significantly differently expressed genes with adjusted p-value cutoff point (padj) log2fold change (lfc)>2 (threshold = grey dashed line), green dots denote significantly differently expressed genes with log2fold change <2, grey dots are non-significantly expressed genes. Up-regulated genes are depicted above the red dashed line as log2 (0). Numbers in brackets denote the number of genes expressed according to these conditions. Triangles denote outliers, which are genes outside the viewing area of the graph. Dots size (Sub, T1-4) denotes the magnitude of lfc values of the outliers.

The transcriptome analysis identified 787 out of 4068 genes were differentially expressed by at least log2fold >|1| (2 fold change) in the QS mutant KTMS23 (Table S3) compared to wild type MH96, of which 657 are significantly $p < 0.005$ differentially expressed (Fig. 20B).

The transcriptome data, comparing the gene expression in *Y. entomophaga* and KTMS23, defined 98 genes that were significantly up-regulated (log2fold >|2|and $P<0.05$) and 116 genes that were significantly down-regulated in the QS mutant compared to MH96 genes (Table S3, Fig. 20B). COG functions could be assigned to 65 of the 98 up-regulated genes, with a majority in cell motility (32%), mobilome, prophage (17%), amino acid metabolism and transport (12%), cell wall/membrane biogenesis (8%), and carbohydrate metabolism and transport (8%) (Fig. 21). COG functions were also assigned to 70 of the 116 down-regulated genes, including amino acid metabolism and transport (22%), lipid metabolism (15%), energy production and conversion (11%), inorganic ion transport and metabolism (8%), and carbohydrate metabolism and transport (8%), with a large proportion of general (11%) or unknown (8%) function (Fig. 21). To note is that differentially expressed genes of the functions nucleotide (F), coenzyme (H), and lipid (I) transport and metabolism, as well as posttranscriptional modification and secondary metabolite biosynthesis, are all only down-regulated. This was also seen in COG classification R and S, which are of general and unknown function respectively. In contrast, some COG function only had up-regulated genes in KTMS23 compared to MH96 gene expression: replication, recombination, and repair (L); and mobile elements (X); such as prophage genes, and the majority of genes encoding for proteins with function in cell wall biogenesis (M); cell motility (N) are up-regulated (Fig. 21).

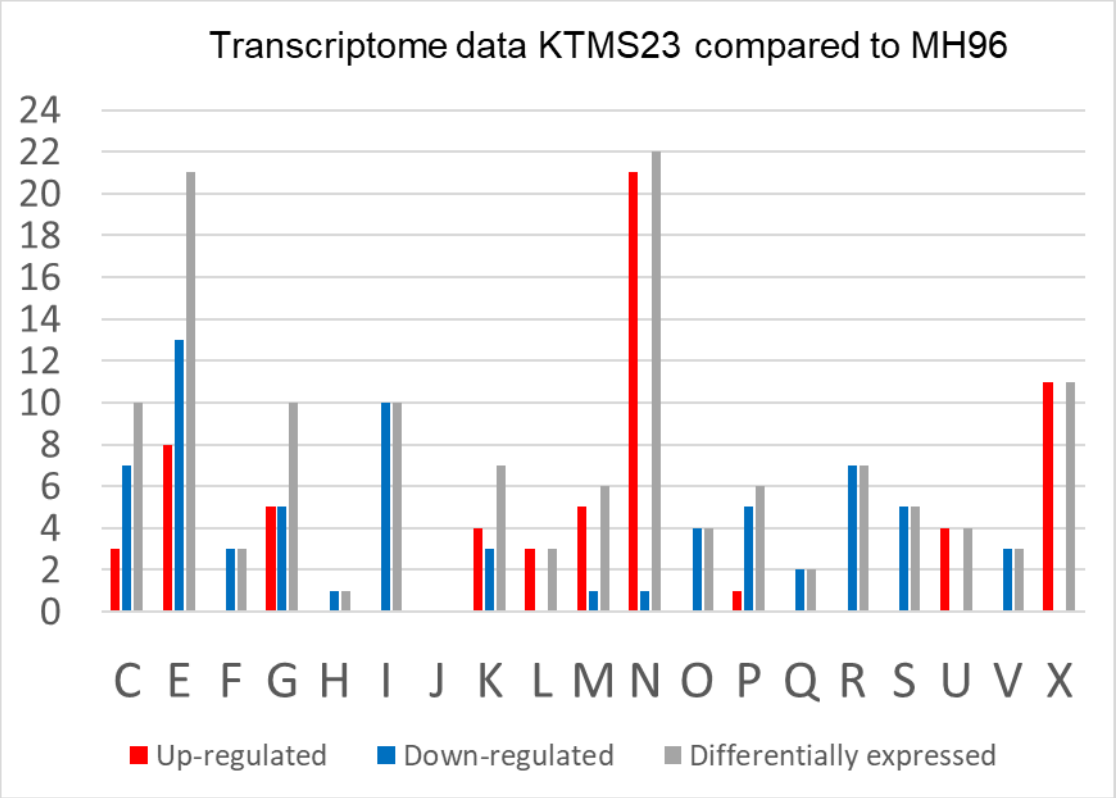

Figure 21: COG classification of significant transcribed genes of KTMS23 in comparison to the *Y. entomophaga* MH96 gene expression. Red indicates genes that are up-regulated in KTMS23 compared to MH96. Blue indicates the number of genes that are down-regulated in KTMS23 compared to MH96. Grey indicates the number of differentially expressed genes in the respective COG of KTMS23 compared to MH96. Indicated are: C, Energy production and conversion; E, Amino acid metabolites and transport; F Nucleotide metabolism and transport; G, Carbohydrate metabolism and transport; H Coenzyme transport and metabolism; I, Lipid metabolism; K, Transcription; L, Replication and repair; M, Cell wall/membrane/envelop biogenesis; N, Cell motility; P, Inorganic ion transport and metabolism; Q, Secondary structure; U, Intracellular trafficking and secretion; V, Defense mechanisms, X, Mobilome: Prophages, Transposons; R, General functional prediction only; S, Function unknown.

Mutation of the AHL synthetase led to up-regulation of genes located in three major clusters: a) a prophage cluster; b) the flagellar apparatus; and c) the T3SS1 (Table 10). While the majority of all phage (PL78_09145–PL78_09335) and flagellar genes (PL78_17520–PL78_17795) were highly up-regulated, the majority of genes in the T3SS1 were slightly up-regulated (1–2 fold change) with the inner membrane bound-proteins SpaQRS (PL78_18155–PL78_18165), YscJL and OrgA (PL78_18220–PL78_18235) highly up-regulated (>2 fold change). Apart from the T3SS1, none of the other secretion systems encoded by *Y. entomophaga* were differentially expressed in KTMS23 compared to MH96 (Fig. S3).

Table 10: Genes with predicted functions displaying significantly differential expression between *Y. entomophaga* QS mutant KTMS12 and wild-type strain MH96

Up-regulated genes in KTMS12					Down-regulated genes in KTMS12				
ID	**log2FC**	**Description #**	**COG**	**Protein**	**ID**	**log2FC**	**Description #**	**COG**	**Protein**
PL78_09335	11.99	Xre, transcriptional regulator	K	ANI30021	PL78_09875	-6.95	NudF, 8-oxo-dGTP pyrophosphatase	V	ANI30128
PL78_09211	11.44	type VI secretion system protein	U	NA	PL78_00655	-6.26	YbaB, conserved DNA-binding protein	R	ANI28352
PL78_09340	9.58	XerD, integrase	L	ANI30022	PL78_04115	-5.48	AstA, arginine N-succinyltransferase beta a subunit	E	ANI29024
PL78_09150	9.51	late control protein D	X	ANI29984	PL78_01500	-5.40	YbgC, acyl-CoA thioesterase	I	ANI28514
PL78_01465	9.18	SucC, succinyl-CoA synthetase subunit beta	C	ANI28507	PL78_04110	-5.33	acetylornithine/succinyldiamopimelate /putrescine aminotransferase	E	ANI29023
PL78_09160	9.05	phage tail tape measure protein	X	ANI29986	PL78_04120	-4.83	AstD, aldehyde dehydrogenase family	C	ANI29025
PL78_09175	8.81	phage tail protein	X	ANI29989	PL78_01180	-4.71	amino acid transporter	E	ANI28456
PL78_09280	8.72	bacteriophage protein		ANI30010	PL78_11910	-4.54	glycosyl hydrolase family protein	G	ANI30527
PL78_09185	8.64	phage-related tail fibre protein	X	ANI29991	PL78_04125	-4.25	AstB, succinylarginine dihydrolase	E	ANI29026
PL78_09218	8.62	virion morphogenesis protein	X	NA	PL78_05495	-4.07	peptidase M66		ANI29294
PL78_09255	8.46	phage capsid protein		ANI30005	PL78_11440	-4.04	TauB, taurine transporter ATP-binding subunit	P	ANI30433
PL78_09265	7.74	Terminase, Terminase-like family	X	ANI30007	PL78_11445	-3.99	TauA, taurine transporter ATP-binding subunit	P	ANI30434
PL78_09290	7.64	Phage GPA, Bacteriophage replication gene A		ANI30012	PL78_05310	-3.75	chitin-binding protein	R	ANI29258
PL78_09231	7.61	Rz, spanin - lysis protein		NA	PL78_04130	-3.71	AstE, succinylglutamate desuccinylase	E	ANI29027
PL78_09220	7.44	tail fiber protein		ANI29998	PL78_11085	-3.69	AceB, malate synthase	C	ANI30369
PL78_09170	7.41	major tail tube protein	X	ANI29988	PL78_12010	-3.68	BcsF, cellulose biosynthesis protein		ANI30547
PL78_09145	7.35	phage transcriptional activator		ANI29983	PL78_11080	-3.55	AceA, isocitrate lyase	C	ANI30368
PL78_09155	7.35	tail assembly protein	X	ANI29985	PL78_15055	-3.49	Acyl dehydratase	I	ANI31132
PL78_09195	7.29	baseplate assembly protein	X	ANI29993	PL78_16540	-3.46	HisJ, histidine ABC transporter substrate-binding protein	E	ANI31420
PL78_09260	7.28	capsid scaffolding protein		ANI30006	PL78_15045	-3.44	Acyl carrier protein	I	ANI31130

Up-regulated genes in KTMS12					Down-regulated genes in KTMS12				
PL78_09330	7.20	phage regulatory protein		ANI30020	PL78_04670	-3.44	BudA, alpha-acetolactate decarboxylase	Q	ANI29133
PL78_09295	7.19	dam adenine methylase	L	ANI30013	PL78_15050	-3.40	Acyl dehydratase	I	ANI31131
PL78_09270	7.17	capsid portal protein	X	ANI30008	PL78_17655	-3.39	FlgJ	N	ANI31635
PL78_09300	6.86	dnaQ 3'-5' exonuclease	L	ANI30014	PL78_15070	-3.38	Rhs, type IV secretion protein Rhs	R	ANI31135
PL78_09230	6.67	lysozyme	M	ANI30000	PL78_01175	-3.34	EhuC, amino acid ABC transporter permease	E	ANI28455
PL78_13180	5.97	SspeF, ornithine decarboxylase	E	ANI30770	PL78_03780	-3.29	YenV	S	ANI28960
PL78_09205	5.01	baseplate assembly protein V	X	ANI29995	PL78_06675	-3.26	FadE, acyl-CoA dehydrogenase	I	ANI29524
PL78_17820	4.90	putative delta-1-pyrroline- 5-carboxylate dehydrogenase	E	ANI31668	PL78_18780	-3.24	YenC3, toxin complex protein	R	ANI31857
PL78_17790	4.65	FliA, flagellar biosynthesis protein	K	ANI31662	PL78_16360	-3.16	long-chain fatty acid transporter	I	ANI31384
PL78_17795	4.20	FliZ, flagellar biosynthesis protein		ANI31663	PL78_08445	-3.09	Acs, acetyl-CoA synthetase	I	ANI29851
PL78_17620	4.17	FlgC	N	ANI31628	PL78_07005	-3.02	FadB, multifunctional fatty acid oxidation complex subunit alpha	I	ANI29576
PL78_17625	4.02	FlgD	N	ANI31629	PL78_03760	-3.01	YenB, toxin complex component	R	ANI28956
PL78_17615	3.95	FlgB	N	ANI31627	PL78_02090	-3.01	MFS transporter	G	ANI28627
PL78_13175	3.93	PotE, putrescine transporter	E	ANI30769	PL78_03755	-2.91	Chi2, toxin complex component	G	ANI28955
PL78_17725	3.69	FliG	N	ANI31649	PL78_03750	-2.91	YenA2, toxin complex component	V	ANI28954
PL78_17710	3.55	FliJ	N	ANI31646	PL78_04675	-2.87	AlsS, acetolactate synthase	E	ANI29134
PL78_17635	3.48	FlgF	N	ANI31631	PL78_10260	-2.83	SStT, serine/threonine transporter	E	ANI30204
PL78_08375	3.41	AckA, propionate kinase	C	ANI29837	PL78_18435	-2.80	acid-resistance protein		ANI31788
PL78_17730	3.39	FliF	N	ANI31650	PL78_08450	-2.79	membrane protein	S	ANI29852
PL78_17630	3.24	FlgE	N	ANI31630	PL78_07010	-2.78	FadA, acetyl-CoA C- acyltransferase	I	ANI29577
PL78_08380	3.18	Stp, serine transporter	E	ANI29838	PL78_07900	-2.77	CpxP, periplasmic stress adaptor protein	O	ANI29744
PL78_17640	3.16	FlgG	N	ANI31632	PL78_03745	-2.77	YenA1, toxin complex component		ANI28953

Up-regulated genes in KTMS12					Down-regulated genes in KTMS12				
PL78_17705	3.02	FliK, flagellar hook-length control protein	N	ANI31645	PL78_03765	-2.75	YenC1, toxin complex component	R	ANI28957
PL78_01845	2.94	ABC-type phosphate/phosphonate transport system, permease component	P	ANI28579	PL78_00635	-2.75	tricarboxylic transport membrane protein	C	ANI28348
PL78_08385	2.67	IlvA, threonine dehydratase	E	ANI29839	PL78_15975	-2.67	CysT, sulfate ABC transporter, permease protein	P	ANI31315
PL78_17735	2.67	FliE	N	ANI31651	PL78_02085	-2.65	LysR family transcriptional regulator	K	ANI28626
PL78_17650	2.45	FlgI	N	ANI31634	PL78_05085	-2.65	CbbBc protein	C	ANI29214
PL78_17610	2.43	FlgA	N	ANI31626	PL78_00630	-2.65	TctB, membrane protein Tripartite tricarboxylate transporter		ANI28347
PL78_18225	2.42	OrgA, Bacterial type III secretion apparatus protein (OrgA MxiK)		ANI31745	PL78_17875	-2.60	GabP, amino acid permease	E	ANI31679
PL78_17645	2.42	flagellar basal body L-ring protein	N	ANI31633	PL78_18440	-2.58	CytA, cytolethal distending toxin A/C domain protein		ANI31789
PL78_10900	2.39	citrate lyase beta subunit	G	ANI30332	PL78_17740	-2.52	DNA/RNA non-specific endonuclease	F	ANI31652
PL78_11915	2.38	MetC, cystathionine beta-lyase	E	ANI30528	PL78_05010	-2.51	AcnA, aconitate hydratase	C	ANI29199
PL78_17585	2.37	FlhB, flagellar biosynthesis protein	N	ANI31621	PL78_04135	-2.51	Porin	M	ANI29028
PL78_11920	2.34	sodium:dicarboxylate symporter	C	ANI30529	PL78_15075	-2.50	NusG, transcription antitermination factor NusG	K	ANI31136
PL78_02115	2.34	XylG, sugar ABC transporter ATP-binding protein	G	ANI28632	PL78_00625	-2.50	TctA, tripartite tricarboxylate transporter	R	ANI28346
PL78_18230	2.31	YscL, type III secretion apparatus protein, HrpE/YscL family		ANI31746	PL78_11352	-2.48	NifU, bacterioferritin-associated ferredoxin	P	NA
PL78_16650	2.31	LrH, transcriptional regulator, LysR family	K	ANI31442	PL78_01165	-2.43	ArtP, arginine transporter ATP-binding subunit	E	ANI28453
PL78_00115	2.31	lysozyme	M	ANI28245	PL78_17385	-2.42	RoeA, PhoB-like regulator		ANI31584
PL78_02330	2.29	L-serine ammonia-lyase	E	ANI28675	PL78_03740	-2.41	Chi1, toxin complex component	G	ANI28952
PL78_13140	2.19	serine transporter	E	ANI30762	PL78_04535	-2.38	AMP binding enzyme	I	ANI29106
PL78_18160	2.18	SpaR	U	ANI31732	PL78_10885	-2.35	adenine/guanine phosphoribosyltransferase	F	ANI30329

Up-regulated genes in KTMS12					Down-regulated genes in KTMS12				
PL78_11925	2.15	DsdC, LysR family transcriptional regulator	K	ANI30530	PL78_16545	-2.33	EhuC, amino acid ABC transporter permease	E	ANI31421
PL78_17085	2.14	cell wall-associated hydrolase, NlpC family	M	ANI31526	PL78_10880	-2.29	carbamoyl-phosphate synthase large chain	H	ANI30328
PL78_17675	2.13	FliQ	N	ANI31639	PL78_07380	-2.29	PaaI, Acyl-coenzyme A thioesterase	Q	ANI29651
PL78_18165	2.13	SpaS	N	ANI31733	PL78_12070	-2.28	organic hydroperoxide resistance protein	V	ANI30558
PL78_02120	2.12	MglC, beta-methylgalactoside transporter permease	G	ANI28633	PL78_17395	-2.26	PepB, peptidase M15	S	ANI31586
PL78_17375	2.10	anion permease	G	ANI31582	PL78_17200	-2.23	iron ABC transporter substrate-binding protein	P	ANI31549
PL78_19055	2.08	Porin	M	ANI31912	PL78_12040	-2.23	NikA, peptide ABC transporter substrate-binding protein	E	ANI30553
PL78_08335	2.06	C4-dicarboxylate transporter	G	ANI29830	PL78_16250	-2.22	Phage cap_P2		ANI31363
PL78_16930	2.06	OmpC, porin	M	ANI31498	PL78_08455	-2.16	ActP, acetate permease	C	ANI29853
PL78_17700	2.03	FliL	N	ANI31644	PL78_06530	-2.15	membrane protein	S	ANI29495
PL78_17685	2.01	FliO	N	ANI31641	PL78_16125	-2.14	IpdC, indolepyruvate decarboxylase	G	ANI31338
PL78_17720	2.01	FliH	N	ANI31648	PL78_13720	-2.14	DnaK, molecular chaperone	O	ANI30874
PL78_18220	2.01	YscJ, type III secretion inner membrane ring protein	U	ANI31744	PL78_17400	-2.14	Rz, spanin		ANI31587
PL78_18155	2.00	SpaQ	U	ANI31731	PL78_00665	-2.12	heat shock protein 90	O	ANI28354
					PL78_14475	-2.09	RpoS, RNA polymerase sigma factor	K	ANI31025
					PL78_04010	-2.07	endonuclease		ANI29004

#: hypothetical genes were not included (can be found in Table S3)

5.4 Discussion

Quorum-sensing is essential for bacteria to communicate with each other and to organize population-dependent gene expression. QS is often associated with biofilm formation, conjugation, production of secondary metabolite, and virulence factors (Mukherjee and Bassler, 2019). Population density cell-mediated signalling is based on the production and sensing of homoserine lactones, such as AHL. Homoserine lactones consist of a lactone ring and acyl chains, and formation is catalysed by the AHL synthetase. The transcriptome data of KTMS23 reveals that in the absence of AHL, genes involved in fatty acid biosynthesis are down-regulated. By the acetyl-coenzyme A pathway, fatty acids are synthesized and elongated, forming the membrane lipids (Hoang *et al.*, 2002). Intermediates of fatty acid biosynthesis form the acyl chains of homoserine lactones (Papenfort *et al.*, 2016). The transcriptome data indicated that in these non-favourable conditions, transport of amino-acid and inorganic compounds, such as iron, was highly down-regulated, whereas motility genes, especially flagellar genes, were highly up-regulated. Interestingly, expression of genes for the Yen-TC complex (Chi1/2, YenA1/2, YenB, YenC1, and YenV) and YenC3, forming the primary virulence factor in MH96, were down-regulated, which confirms the lack of secretion of Yen-TC proteins observed by SDS-PAGE of the exoproteome. Pertinent to this study, the YeRER, comprising genes encoding for a DNA-binding protein PL78_17385 (RoeA) and a lysis cassette, identified in HESA screening (Chapter 4), were significantly down-regulated in the QS mutant, supporting its potential role in global protein secretion.

The importance of QS in bacterial virulence is the subject of many studies and has been reviewed in detail (Antunes *et al.*, 2010; Deep *et al.*, 2011; Rutherford *et al.*, 2012). In *Y. entomophaga*, QS regulates the expression of many genes, which leads to reduced exoproteome concentration. The exoproteome concentration is dependent on several factors: i) the production (transcription and translation) of exoproteins; ii) the release of these into the extracellular space, and iii) the rate of degradation or utilization by the cell. Pena *et al.* (2019) concluded that QS can regulate several secretion systems within one species, e.g. in *P. aeruginosa* T1–3SS and T6SS. Transcriptome data of *Y. entomophaga* showed that the T4SS-associated Rhs (PL78_15070) and the T6SS exoprotein (PL78_09211) were not significantly regulated by QS. This leads to the conclusion that either QS-dependent exoproteome secretion does not occur using a typical secretion system (T1–6SS), or QS regulates gene expression of exoproteins. The latter can be confirmed by the transcriptome data showing strong down-regulation of the Yen-TC genes in the KTMS23. Nevertheless, the Bradford assay identified that the QS mutant secreted ~170 µg/ml of exoproteins after 24 h *in vitro*, which is assumed to be sufficient for virulence in the *G. mellonella* insect model when bacteria are injected into the host. It is also important to note that yet to be determined host factors may override *in vitro* regulatory circuits to induce the production of virulence determinants. QS regulates other virulence genes involved in motility and

attachment (Wagner *et al.*, 2004). In the *Y. entomophaga* QS mutant, flagella proteins are strongly up-regulated. Flagella are often produced when the bacterium is in non-favourable conditions but can also be considered as virulence factors. In *Salmonella enterica* subspecies *enterica* serotype Dublin flagella are essential for bacterial adhesion and contribute to oral infection of mice (Olsen *et al.*, 2013). The absence of the QS signals in the QS mutant potentially mimics conditions initiating adherence, therefore upregulates expression of the flagella genes. In conclusion, QS in *Y. entomophaga* regulates protein secretion but does not influence *in vivo* virulence.

Chapter 6

Characterisation of the YeRER

6.1 Introduction

The *Y. entomophaga* MH96 genome encodes for a range of virulence factors such as the main virulence factor Yen-TC, putative toxins (Vip2, CdtB, LopT, PirAB), and degradative enzymes such as proteases, chitinases, esterases, and lipases (Hurst *et al.*, 2016). Using the high-throughput exoproteome screening assay (HESA) developed in this study, a genome cluster was identified which regulates not only Yen-TC but also global exoproteome release in *Y. entomophaga* (Chapter 3). Due to the altered exoproteome phenotype in mutants of this cluster, the gene cluster was termed YeRER. With reference to Figure 22, the YeRER is comprised of a predicted DNA binding protein (RoeA), a 1086 bp intergenic region, and a predicted phage-like cell wall lysis cassette comprising *holA, pepB, rz,* and *rz1,* designated YLC. Three transposon insertions and a natural mutation (in strain K18) that caused almost complete abolition of exoproteome production were located within the intergenic region. The three transposon insertions were located within the putative promoter region of *hol*A while the K18 mutation lies within the *roeA* promoter region (Fig. 22*).*

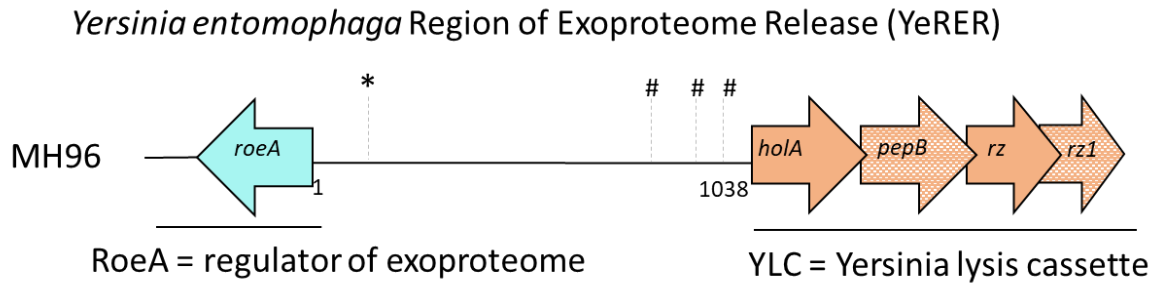

Figure 22: Schematic of the YeRER, consisting of the regulator of exoproteome (RoeA), an 1-1038 bp intergenic region (INT), and the YLC. * denotes 3 bp deletion in K18, and # denotes transposon insertion 5' of YLC.

The YLC encodes a holin (HolA), endopeptidase (PepB), and an IM-bound spanin (Rz). Holins are integral proteins, forming a relatively unspecific pore allowing for proteins such as endolysins (which are often muramidase or other endopeptidases) to translocate over the membrane (Wang *et al.*, 2003; Schmelcher *et al.*, 2012). Holins are categorised into three classes, dependent on the number of transmembrane domains (TMD) and length.

Endolysins can be differentiated into canonical and SAR endolysins. SAR endolysins, which were first described in the P1 phage, contain a Sec pathway signal sequence required for translocation into the

periplasm (Xu *et al.*, 2004). Canonical endolysins do not contain such a signal sequence and instead are translocated by the unspecific channel formed by the oligomerization of holin proteins (Catalao *et al.*, 2013). Endolysins can be functionally classified by their catalytic domain into amidases, carboxy- or endopeptidases, glycosidases, and cell wall binding proteins (Schmelcher *et al.*, 2012; Fernandez-Ruiz *et al.*, 2018). Generally, endolysins are released into the periplasm by either holins or SecA where they degrade the peptidoglycan. Depending on the enzymatic domain, endolysins cleave the peptidoglycan structure by different mechanisms; e.g., amidases hydrolyse amide bonds (CO-NH2), glycosidases hydrolyse glycosidic bonds (between sugars), and peptidases hydrolyse bonds in peptides in proteins either at the COOH ends (carboxy-) or within the molecule (endo-). Many holin/endolysin cassettes have been identified in phage and prophages of Gram-negative and Gram-positive bacteria. In Gram-negative bacteria, a third (*rz*) or third and fourth (*rz1)* gene can be found in some species (Kongari *et al.*, 2018). These encode for an inner membrane-bound and an outer membrane-bound protein, respectively, facing the periplasmic lumen. Summer *et al.* (2007) found that overlapping *rz* and *rz1* genes are commonly found in Gram-negative phages. These overlapping genes encode for the IM-bound i-spanin and the OM-bound o-spanin. In some phages, likeT1, the spanin complex is comprised of only one protein called the u-spanin (Young, 2014). Upon linkage of i-spanin and o-spanin within the periplasm, conformational changes lead to tension on the outer membrane resulting in cell disruption (Berry *et al.*, 2012).

This chapter further characterises YeRER using bioinformatic tools. An aim of this part of the study was characterise the YeRER elements and therefore to predict RoeA function by comparing RoeA to similar proteins, based on amino acid sequence and location within the genome of other Gram-negative bacteria. Also of interest was to determine if YeRER was present in other *Yersinia* spp. and other species within the Enterobacteriales, especially in virulent strains.

As previously outlined in Chapter 3, a MH96-like bacteriophage-like lysis cassette was described in pathogenic *Y. enterocolitica* W22043, located between TcB and TcC orthologues of the insecticidal toxin complex (Springer *et al.*, 2018), which is not observed in MH96. In the following Chapters, RoeA and the YLC are assessed for synteny and their role in exoproteome release determined by overexpression/ *trans* complementation and mutation experiments.

6.2 Methods

6.2.1 Bioinformatic analysis

Protein homology and synteny

Comparisons of the genomic arrangement of the YeRER components RoeA and YLC within the Gamma-proteobacteria, especially within the genus *Yersinia*, were performed using the online tool SyntTax (https://archaea.i2bc.paris-saclay.fr/synttax/Default.aspx) with default settings using the Absynth algorithm (Oberto, 2013). The amino acid sequences of RoeA and HolA were used as reference sequences. Listed in Table 11 are bacterial species, throughout Gram-negative bacterial species from the genera *Yersinia, Salmonella, Chania*, *Escherichia, Erwinia, Vibrio, Citrobacter, Serratia, Pseudomonas,* and *Legionella* that were selected for the comparison.

Table 11: Bacterial strains used for synteny of YeRER proteins RoeA and HolA.

Yersiniaceae		**Erwiniaceae**
Y. aldovae 670 83	*Y. pestis* FDAARGOS 601	*E. amylovora* ATCC 49946
Y. aleksiciae 159	*Y. pseudotuberculosis* IP32953	*E. pyrifoliae* Ep1 96
Y. enterocolitica 2516 87	*Y. pseudotuberculosis* NCTC3571	**Other Enterobacteriales**
Y. enterocolitica 8081	*Y. pseudotuberculosis* YPIII	*E. coli* ETEC 2264
Y. enterocolitica FORC 002	*Y. rohdei* YRA	*E. coli* K 12
Y. enterocolitica ssp palearctica	*Y. ruckeri* Big Creek 74	*S. bongori* N268 08
Y. enterocolitica type O5 YE53	*Y. similis* 228	*S. enterica* ATCC 8387
Y. enterocolitica WA	*Y.* sp CFS1934	*C. freundii* E2614
Y. enterocolitica YE1	*Y.* sp FDAARGOS 228	*C. amalonaticus* 13335
Y. entomophaga MH96	*C. multitudinisentens* RB 25	*C. freundii* CFNIH2
Y. frederiksenii FDAARGOS 417	*S. ficaria* NCTC12148	*P. aeruginosa* 12939
Y. intermedia FDAARGOS 358	*S. fonticola* DSM 4576	*P. aeruginosa* BA7823
Y. intermedia Y228	*S. grimesii* BXF	**Vibrionaceae**
Y. kristensenii ATCC 33639	*S. liquefaciens* ATCC 27592	*V. cholerae* A1552
Y. massiliensis GTA	*S. marcescens* 1274	*V. mediterranei* QT6D1
Y. pestis 1045	*S. odorifera* NCTC11214	*V. vulnificus* YJ016
Y. pestis Angola	*S. plymuthica* 3Re4	**Legionellaceae**
Y. pestis Antiqua	*S. proteamaculans* 568	*L. pneumophila* 2300 99 Alcoy
Y. pestis biovar Medievalis	*S. quinivorans* NCTC13188	
Y. pestis CO92	*S. rubidaea* 1122	

Repeats and motif search

The 1038 bp INT region is A/T rich with G/C content of 33.7. The INT region offers space in which transcription factors like inhibitors, activators, and enhancers can bind. To identify potential binding

sites of transcription factors, motifs from the CollecTF database (Kilic *et al.*, 2014) were selected and mapped to INT using the online tool FIMO (Grant *et al.*, 2011). All motifs from the Enterobacteriaceae annotated from the experimental analysis were included and assessed using FIMO.

Transmembrane domain analysis

To assess the holin classification of Y*. entomophaga* MH96 holin, HolA amino acid sequence in FASTA format was used for the webtool: Protter – visualize proteoforms (Omasits *et al.*, 2014).

6.2.2 Targeted mutagenesis of *roeA*

Attempts to construct a *roeA* deletion mutant using the three-step PCR protocol from Chapter 2.2.13 were not successful, possibly due to the AT-rich region. To mutate *roeA*, an alternate strategy was used. A 3 kb region, including *roeA,* was PCR amplified using the primer MS49/52 (Table 4). The purified amplicon was cloned into pGEM T-easy and the resultant sequence validated construct was designated pGEM-*roeA*. Using the template pHP45 Ω, a spectinomycin cassette was PCR amplified using the primers MS140/141. The purified amplicon was digested with MscI and ligated into the analogous site of pGEM-*roeA*. The plasmid was transferred into chemically competent *E. coli* DH10β and grown on LB agar plates containing ampicillin and spectinomycin for selection. The plasmid was termed pGEM-Δ*roeA*::Spec and digested with EcoRV for ligation into the analogous sites of the suicide vector JP5608 to form pJP-Δ*roeA*::Spec. The construct was electroporated into ST18, enabling its conjugation to *Y. entomophaga* MH96 for homologous recombination. For validation by PCR and final sequencing, the primer MS113/MS40 were used for the 5' region and MS114-MS42 to amplify the downstream region. The validated recombinant was designated MH96Δ*roeA*.

6.2.3 Targeted mutagenesis of YLC

To understand the role of the lysis cassette in protein secretion, YLC was mutated and the gene cluster *holA-pepB-rz* was replaced with a kanamycin cassette as outlined in Chapter 2.2.12. In summary, using fusion PCR of the YLC, 1000 bp 5' and 1000 bp 3' were PCR amplified using the primer MS23/MS24 and MS25/MS26, respectively. The primer MS24 and MS25 harbours an overlapping sequence to MS01 and MS02, which was used to PCR amplify the pKD4 kanamycin lysis cassette. Using an additional PCR step, the three amplicons were fused to 5'YLC-Kan-3'YLC and ligated into the pGEM T-Easy poly-T cloning site. The correct pGEM T-Easy insert was then digested with the restriction enzyme *Sac*I and the excised fragment ligated into the analogous site of the suicide vector pJP5608. The validated construct pJP-ΔYLC was electroporated to *E. coli* ST18 from where it was conjugated into MH96 as described in Chapter 2.2.12. The resultant sequence validated mutant strain was designated MH96ΔYLC.

6.2.4 Culture conditions

Cultures were grown in 50 ml LB broth for 16 h at 25°C and 200 rpm shaking, if not stated otherwise. To each flask, 10 µg/ml tetracycline or 30 µg/ml was added as appropriate for plasmids listed in Table 8. For the strains, KTMS4 and MH96ΔYLC, kanamycin at 50 µg/ml was added to the culture. Culture samples were assessed for exoproteome production, cell count, and cell morphology as described in Chapter 2 (Chapters 2.3 and 2.7).

6.2.5 Microscopy

Live-cell imaging

All cultures were grown in 100% LB broth (200 µg /ml ampicillin) until OD=1. For live-cell imaging, 10 µl of the culture were induced with 0.6% arabinose and immediately pipetted onto agarose covered glass slides and assessed by light-microscopy within the first minute post-induction. Agarose pads were used to eliminate cell movement during the imaging process. To compensate for agarose absorbing arabinose, a higher induction concentration (0.6%) of L-arabinose compared to commonly used 0.02% -0.2% arabinose inductions (Chapter 6.2.8) was used. Live-cell imaging was undertaken using the LSM710 microscope operated with Axiovision System (Carl Zeiss, Germany). All live-cell imaging was done in collaboration with Miki Feldmüller from the Pilhofer group at the ETH Zurich.

6.2.6 LC-MS analysis of K18 supernatant

For LC-MSMS analysis, a SDS-PAGE was run of K18 supernatant of a 16 h culture grown under conditions as outlined in Chapter 6.6.1. The SDS-PAGE was visualised using Coomassie stain. Bands of interest were excised from the gel and analysed using LC-MS. LC-MS was performed by Evelyne Maess (AgResearch, New Zealand) using the following protocol. The gel bands were analysed by mass spectrometry after de-staining, reduction with 0.1 M tris(2-carboxyethyl) phosphine (Fluka Chemie, GmbH, Buchs, Germany), alkylation with 20 µl of 0.15 M iodoacetamide (Sigma, St. Louis, MO, USA), and digestion for 18 hours with 1 µg of TPCK-trypsin (Promega, Madison, WI, USA) in presence of 10% acetonitrile (ACN). After digestion, the peptides were dried and resuspended in 50 µl of 0.1% formic acid (FA) before injection on the mass spectrometer.

LC-MS was performed on a nanoflow Ultimate 3000 UPLC (Dionex) coupled to maXis impact HD mass spectrometer equipped with a CaptiveSpray source (Bruker Daltonik, Bremen, Germany). For each sample, 1 µl of the sample was loaded on a C18 PepMap100 nano-Trap column (300 µm ID x 5 mm, 5-micron 100Å) at a flow rate of 3000 nl/min. The trap column was then switched in line with the analytical column ProntoSIL C18AQ (100 µm ID x 150 mm 3-micron 200Å). The reverse-phase elution gradient was from 2% to 20% to 45%B over 60 min, a total of 84 min at a flow rate of 600 nl/min. Solvent A was LCMS-grade water with 0.1% FA; solvent B was LCMS-grade ACN with 0.1% FA.

The Q-TOF Impact HD (Bruker Daltonics) mass spectrometer was set up in a data-dependent automatic MS/MS mode where a full scan spectrum (50-2000 m/z, 2Hz), followed by 10 MS/MS (350 to 1500 m/z, 1-20Hz) of the most intense ions with charge states 2-3 selected.

6.2.7 Complementation by overexpression in *roeA* and YLC mutant

Trans complementation *roeA* mutant

To enable *trans* complementation of *roeA* mutant and K18 the entire YeRER was PCR amplified using primer set MS40/MS41 (Table 4) and cloned into pGEM T Easy using the pGEM cloning kit. The sequence validated construct was designated as pGEM-YeRER. A second construct comprising only the intergenic region (INT) was amplified and cloned into pGEM and the validated construct termed pGEM-INT. Both constructs were independently transformed into MH96 and K18 cells. For selection, cells were grown on LB agar with 400 µg/ml ampicillin. For the complementation experiment, 50-ml cultures were incubated for 16 h and 24 h at 25°C and constant shaking at 200 rpm. Samples were taken at 16 h and 24 h to assess CFU, OD, and exoproteome.

Trans complementation in the YLC mutant

For *trans* complementation of the YLC mutant, the YLC including the entire intergenic region (5' of YLC) was cloned into pGEM T-Easy. The resulting vector was termed pGEM-INT_YLC. The vector pGEM T-Easy is a high copy vector which might have resulted in elevated expression of YLC leading to cell lysis. Based on this scenario the insert from pGEM-INT_YLC was digested with EcoRI and ligated into the analogous site of the mid-copy vector pACYC184 (positioned within the pACYC184 chloramphenicol cassette) and the resultant vector termed p184INT_YLC. The vector was then sequence validated with MSRF and MSR primers.

Trans complementation of YeRER constructs in *roeA* mutant, YLC mutant and MH96

To enable *trans* complementation of K18, MH96ΔYLC, KTMS4, and MH96, amplicons of the intergenic region with differing lengths were PCR amplified and cloned into expression vectors pGEM (high copy) and/or pACYC184 (mid copy) using the restriction enzyme EcoRI or EcoRV (Table 12). Initially, the intergenic region of K18 was amplified (INT(K18)). Then the wild type INT was divided into two parts comprising of 5' of *roeA* and *holA* and cloned into pACYC184 using the EcoRI restriction site to form the respective constructs p184-5'*roeA* and p184-5'*holA*. A fifth construct comprised of the ncRNA identified in INT, termed p184ncYLC220. The vector p184ncYLC220 harbours one of the two large degenerate repeats. A sixth construct was amplified from the start of ncYLC (*5' roeA*) to the second repeat (5' *holA*) and termed p184ncYLC673. Furthermore, constructs of INT with deletion of ncYLC220 (INTΔnvYLC220), INT without the predicted secondary loop structure (INTΔLoop), and ncYLC220 truncations ncYLC80 and ncYLC110, were synthesized by GeneScript with EcoRV restriction sites on 3' and 5', which was used to clone into the high copy vector pUC18. The inserts were then cloned into the EcoRV restriction site located within the tetracycline cassette of pACYC184 to form the plasmids p184 INTΔncYLC220, p184INTΔLoop, p184ncYLC80, and p184ncYLC110, respectively. The pACYC184 constructs were sequence validated with primer set MS/MS and transformed into MH96, K18, and MH96ΔYLC as well as KTMS4.

Table 12: Trans complementation constructs according to the plasmid, insert, restriction sites, antibiotic resistance and primers used to amplify the construct from MH96 (or K18).

Name	Origin	Insert	Insert length (bp)	Insertion cut sites	Antibiotics	Reference
pACYC184	pACYC184	NA	0	NA[#]	Tet, Cm	Change and Cohen, 2000
pGEM	pGEM	NA	0	NA[#]	Amp	(Mezei and Storts, 1994)
pGEM-YeRER	pGEM	YeRER	3145	MCS		This study
pGEM-INT	pGEM	INT	1038	MCS		This study
pGEM-INT(K18)	pGEM	INT(K18)	1035	MCS		This study
pGEM-INT_YLC	pGEM	INT_YLC	2157	MCS		This study
INT	pACYC184	Intergenic region *roeA-holA* from MH96	1038	EcoRI	Tet	This study
INT(K18)	pACYC184	Intergenic region *roeA-holA* from K18	1035	EcoRI	Tet	This study
5'*roeA*	pACYC184	5'UTR *roeA* (1-500bp)	467	EcoRI	Tet	This study
5'*holA*	pACYC184	5' UTR *holA* (1-500bp)	571	EcoRI	Tet	This study
INT_YLC	pACYC184	Intergenic region and *holA,pepB, rz*	2157	EcoRV	Cm	This study
ncYLC220	pACYC184	Intergenic region MH96 position 202-469, ncRNA	267	EcoRI	Tet	This study
ncYLC673	pACYC184	Intergenic region MH96 position 202-869, ncRNA and repeats	673	EcoRV	Tet	This study
INTΔncYLC220	pACYC184	Intergenic region MH96, without YLC220	818	EcoRV	Cm	This study
INTΔLoop	pACYC184	Intergenic region MH96 position, deleted loop structure	991	EcoRV	Cm	This study
ncYLC80	pACYC184	Truncation of ncYLC, first 80bp	80	EcoRV	Cm	This study
ncYLC110	pACYC184	Truncation of ncYLC, first 110 bp	110	EcoRV	Cm	This study

NA: not applicable when no insert was cloned into the plasmid

MCS: Multiple cloning site

6.2.8 Arabinose induced expression using pARA of the *Yersinia* lysis cassette

Native MH96 lysis cassette YLC

To test the functionality of the MH96 YLC, the genes *holA, pepB,* and *rz* were cloned into the arabinose inducible vector pARA using restriction sites NdeI and XhoI. Firstly, the native lysis cassette without the 5' untranslated region (UTR) of the three genes was PCR amplified using forward primer MS101 (NdeI) and reverse primer MS104 (XhoI) and the resultant amplicon was cloned into pGEM to form pGEM-HML. The sequence validated vector pGEM-HML was digested with NdeI and XhoI and the excised fragment was cloned into the respective restriction site in the arabinose inducible vector pARA. The induction vector was termed pARA-HML (Fig. 23) and sequence validated using primer ARAF and ARAR (Table2). The plasmids were transformed into *E. coli* DH10b and *Y. entomophaga* MH96.

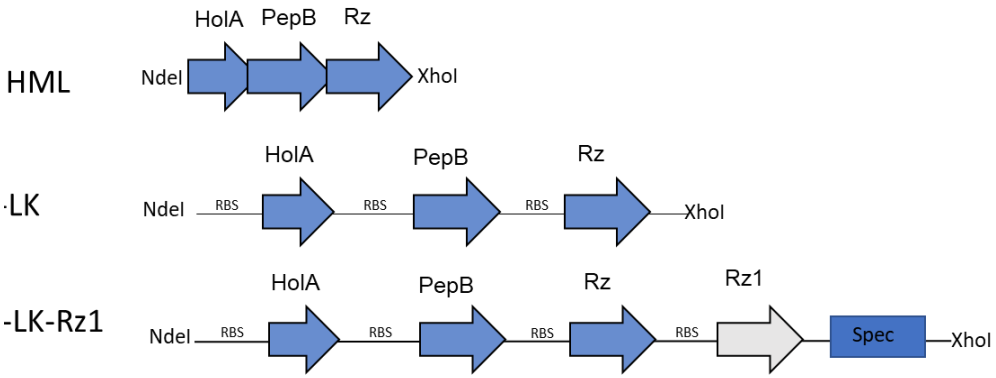

Figure 23: Schematic of lysis cassette genes for expression in pARA vector. RBS denotes ribosomal binding site 5' AGGAGG 3'. NdeI and XhoI denote restriction sites of the respective insert to clone into pARA.

E. coli cells harbouring pARA-HML were grown in LB (40%) broth at 200 rpm shaking and 37°C. To analyse the effect of induced pARA-HML, cells were grown until OD = 1 and then induced with 0.02 % arabinose. As the control, pARA-HML uninduced and pARA empty vector were used.

Optimised lysis cassette constructs

In the native lysis cassette, *holA, pepB,* and *rz* ORFs are overlapping (Fig. 23 "HML"). To address potential difficulties in the expression of overlapping ORFs, the YLC operon was synthesised so that all genes were separated, with each ORF having their ribosomal binding site (3' AGGAGG 5') of the genes as demonstrated in Figure 32 (LK). The translated amino acid sequence of these genes was unaffected (refer Fig. S4 for synthesised sequence). The optimised amplicon was synthesised by GeneArt (Thermofisher, USA) containing NdeI (5') and XhoI (3') restriction sites to clone into pARA. The amplicon was then cloned into the respective restriction sites in the arabinose inducible vector pARA and the resultant vector designated pARA-LK, which was sequence validated using primer ARAF and ARAR (Table 4). The plasmids were transformed into *E. coli* DH10b and *Y. entomophaga* MH96.

At the time of synthesis, the YLC 4th ORF encoding o-spanin had not been identified. To restore YLC including the o-spanin, a third construct was cloned by amplifying the fourth gene, *rz1,* including its ribosomal binding site of the lysis cassette with XhoI (Pimer MS128) 5'and a BglII/XhoI (MS126) 3' end. The amplicon was ligated into pGEM and termed pGEM-Rz1. Additionally, a spectinomycin cassette from pHP45Ω with BglII restriction site was amplified using the primers Spec_F_BglI and Spec_R_BglI and the resultant amplicon was digested with BglII and ligated into the analogous pGEM-Rz BglII restriction site to form pGEM-Rz1-Spec. To ligate Rz1-Spec to the existing pARA-LK, pGEM-Rz1-Spec

and pARA-LK were digested with XhoI. Ligations of Rz1-Spec and pARA-LK were plated onto LB plates with Amp100 and Spec100. The resulting colonies were screened by colony PCR using primer ARAF and ARAR and colonies, of which the expected amplicon size was received using PCR, were further validated by sequencing using M13F/R primer. The resulting plasmid was designated pARA-LK-Rz1 (Fig. 23). The plasmid was transformed into *Y. entomophaga* MH96 and *E. coli*.

Cells harbouring pARA-LK and pARA-LKRz1, respectively, were grown in LB (40%) broth at 25°C and 200 rpm shaking until OD 600 nm of 1 was reached. The culture was induced with arabinose (0.02% final concentration) or glucose (0.02%), to repress plasmid transcription, and placed at room temperature ~ 22^{o}C on a rotating platform at 40 rpm. The cell density was measured every 15 min until 3 h and at 24 h post-induction.

6.2.9 Transcriptomic assessment of *roeA* mutant

To define *roeA* regulation, transcriptome analysis of the *roeA* mutant KTMS12 was performed. The transcriptome data was compared to that of the wild type strain MH96. RNAseq and analysis were performed as outlined in Chapter 2.3.2. MH96 and KTMS12 were grown to 4.35 x 10^9 and 3.55 X 10^9 CFU/ml, respectively, from where RNA was extracted. RNA was isolated and purified, and RNAseq analysis was carried out as outlined in Chapter 2.3.

6.2.10 Motility plate assay

To determine the motility of MH96 and MH96 derivates, LB water agar plates (0.4% agar) were used. The strains MH96, KTM12, K18, KTMS4, and MH96ΔYLC were streaked for single colonies on LB agar plates and incubated overnight at 25°C. A single colony of each strain was transferred onto one individual LB water agar plate and incubated for 24 h at 25°C. To assess motility, the diameter of spread cells covering the plate was measured. These experiments were undertaken in triplicate.

6.3 Results

6.3.1 Bioinformatic analysis of the YeRER

Holins

The *Y. entomophaga* holin HolA (PL78_17390) is comprised of three TMD, which are typical to class I holins of the prototype λ-phage S105 holin (Fig. 24AB). Class I holins are typically 90 – 125 aa in length and the *Y. entomophaga* holin is 104 aa residues. S105 holins belong to the canonical holins which form a homo-oligomeric structure in the IM, with a pore size of 0.34 – 1 µm diameter within the IM (Fig. 24) (Rice *et al.*, 2008; Dewey *et al.*, 2010; Young, 2014). In contrast, pinholins are multimeric protein complexes forming 2 nm wide holes in the inner membrane. Therefore, endolysins of the pinholin/endolysin system are translocated by the Sec-pathway and are termed signal-anchor release (SAR) endolysins.

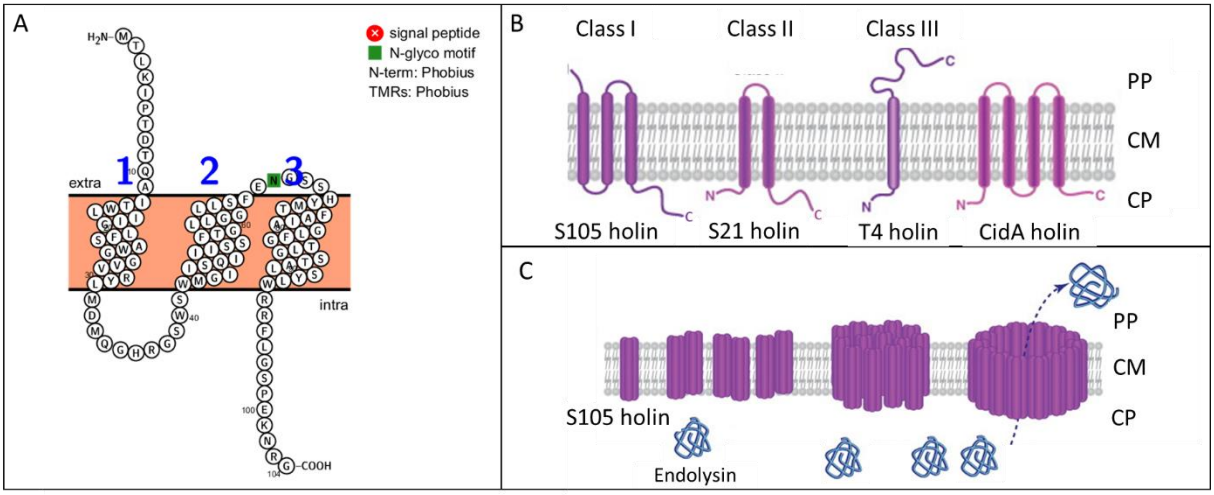

Figure 24: Schematic of holin anchored in the cell membrane. *A)* Visualization of protein features within the bacteria cell membrane of MH96 holin HolA, using Protter web tool. *B)* Holin classification according to transmembrane domains and length. *C)* Assembly of S105 canonical holin in the inner membrane. Modified from Desvaux *et al.* (2005).

Endolysins

The structure of YLC endolysin PepB, in *Y. entomophaga* MH96, was compared to known structures from the Protein Data Base (PDB) using the online tool Phyre2, which identified structural identity to the family of peptidase M15 of unknown function. Peptidases of the family M15 are zinc-metalloproteases and are involved in cell wall biosynthesis and metabolism.

Spanins

In the *Y. entomophaga* genome annotations, only three genes of the lysis cassette were annotated: *holA, pepB,* and *rz*. A detailed literature review suggested the possibility of a fourth gene, encoding for the o-spanin, which was not identified due to the overlapping genes and possible bias by annotation programs (Kongari *et al.*, 2018). The previous assessment of holin HolA and the endolysin PepB, and gene arrangement of the YLC (Fig. 25), indicate that the YLC is a λ phage-like lysis cassette, which encodes for i- and o-spanins.

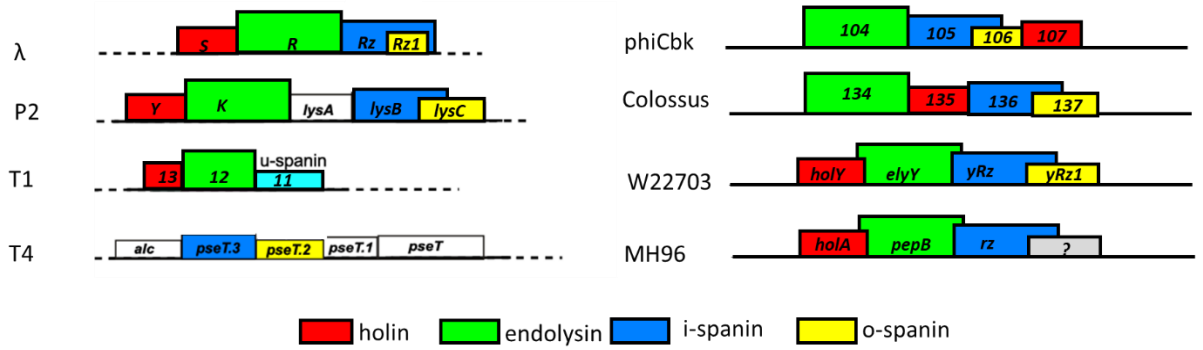

Figure 25: Genomic arrangement of common (λ, P2), specific phage lysis cassette (T1, T4, phiCbk, Colossus), *Y. enterocolitica* W22703, and *Y. entomophaga* MH96 genomically integrated lysis cassette YLC. Figure modified from Young (2014).

Manual assessment of the coding region in the PL78_17390 -17400 identified a possible start codon within *rz,* encoding for a 94 aa residue protein (Fig. 26B). A transmembrane (TMM) domain prediction tool (http://www.cbs.dtu.dk/services/TMHMM/) identified a single TMM-domain, which the o-spanin anchors in the OM (Fig. 26C). Furthermore, transcriptome data of *Y. entomophaga* MH96 and its derivate KTMS12 (Chapter 6.3) confirmed the expression of the lysis operon and its 3' region, which covers the hypothetical fourth gene (Fig. 26A).

BlastP analysis of the hypothetical protein Rz1 confirmed that this region may encode for an o-spanin (Table S2). These results suggest MH96 encodes for a lysis cassette as seen in *Y. enterocolitica* W22703 comprising of a holin, endopeptidase, and a spanin-complex formed by i- and o-spanin (Fig 26D).

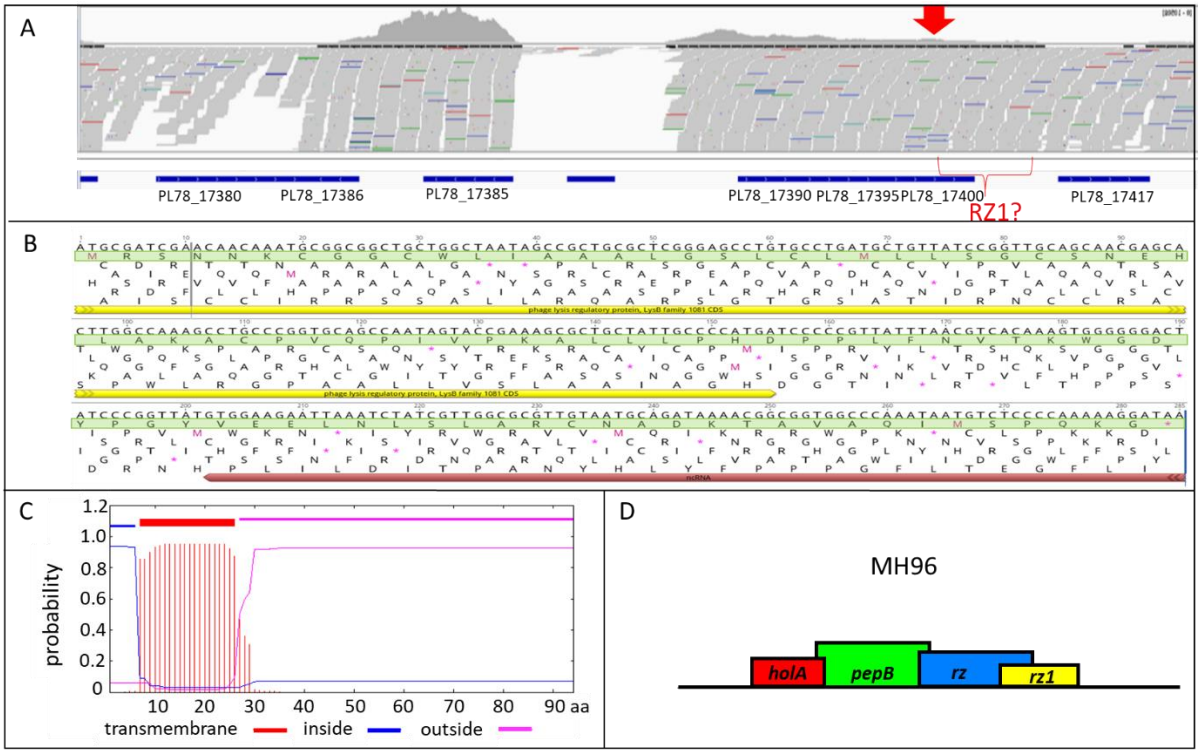

Figure 26: Identification of *rz1* gene encoding o-spanin. *A)* Transcriptome read of MH96 YLC. Reads over potential gene *rz1* (red bracket, arrow). *B)* Nucleotide sequence of *rz1* and amino acid sequence of 6 frames. The first frame indicates Rz1 amino acid (green highlight). Yellow arrow indicates *rz,* which overlaps with *rz1. C)* Rz1 amino acid analyzed by TMHMM Server, v.2.0 (http://www.cbs.dtu.dk/services/TMHMM/), showing the presence of one membrane-binding domain, which is common in o-spanin to anchor in OM. *D)* Resulting YLC gene arrangement in *Y. entomophaga* MH96.

The putative transcriptional regulator RoeA

The HESA method (Chapter 4) identified a non-secreting strain with a mutation in the PL78_17385 encoded gene *roeA.* A (protein-protein) BLASTP search of the PL78_17385–PL78_17390 region (Fig 6*A* and Table S2) revealed that PL78_17385, a 139-amino acid residue protein, contains a helix-turn-helix motif similar to DNA binding domains of PhoB-like regulators of *E. coli, Vibrio cholerae*, and *Pseudomonas aeruginosa* (Fig. 27A). Due to the homology of PL78_17385 to transcriptional regulators and the abolished exoproteome release phenotype of a transposon insertion in the strain KTMS12, PL78_17385 was designated as *roeA* for "regulator of exoproteome". RoeA shared closest (77%) amino acid similarity to *Y. entomophaga* MH96 Yen7 (PL78_03735), located 772 bp 5' of the Yen-TC encoding operon (Fig. 27B; Table S2). RoeA and Yen7 HTH-motifs showed homologous residues binding to DNA- of other transcriptional regulators from *E. coli* and *V. cholerae.* The regulation of RoeA and Yen7 and their mechanism of DNA binding has yet to be defined.

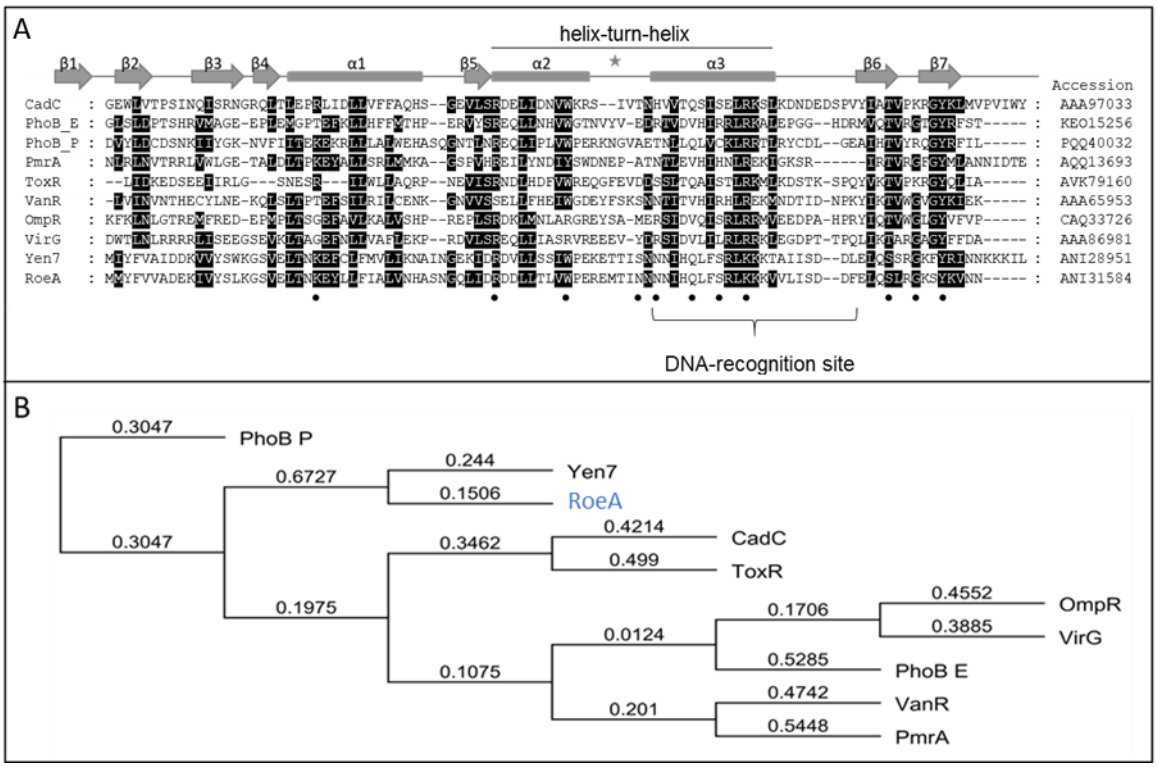

Figure 27: Amino acid alignment of the MH96 PhoB-like protein Roe (PL78_17385) with OmpR/PhoB-family transcriptional regulators from selected bacterial species. A) Eight DNA-binding domains of *Escherichia coli* CadC, PhoB (PhoB_E), *Photorhabdus luminescens* (PhoB_P), *Klebsiella pneumoniae* PmrA, *Vibrio cholerae* ToxR, *Enterococcus faecium* VanR E. coli OmpR, and *Agrobacterium tumefaciens* VirG aligned with *Y. entomophaga* Yen7 and RoeA. Accession numbers of the protein sequences are indicated. The alpha-helices of the helix-turn-helix motifs (α2 and α3) and its connecting loop (*) indicates the RNA-polymerase interaction region (Schlundt *et al.*, 2017). # denotes truncation point of KTMS12. • denotes residues necessary for DNA-binding (Schlundt *et al.*, 2017). B) Phylogenetic tree with Neighbour-Joining building method of the RoeA-homologous DNA-binding domains as used in A. Distances indicated at each branch.

While PhoB, and OmpR are typically found as part of a phosphate regulated two-component system, orphan proteins of this family have been classified as functional transcriptional regulators e.g. the *Chlamydia trachomatis* OmpR-like protein ChxR, the *Synechoccus elonatus* NblR, and the *Helicobacter pylori* HP1043 (Hong *et al.*, 2007; Kato *et al.*, 2008; Hickey *et al.*, 2011). Furthermore, CovR, an orphan response regulator, globally regulates virulence in *Streptococcus suis* serotype 2 and regulates hemolysis and pigmentation (Pan *et al.*, 2009). In the following Chapter (Chapter 6.3.2), DNA-binding proteins with homology to RoeA in other bacteria and their role in regulation will be discussed enabling the potential role of RoeA in virulence. The transcription of PhoB and OmpR-like protein is often auto-regulated and regulation of adjacent genes can often be observed (Olekhnovich *et al.*, 2013). Therefore, the genetic content of YeRER and *roeA* in other bacteria is of interest to predict the functionalities of these genes. The genetic content can help to understand the acquisition of the phage-like element and might give clues on the functionality in other bacteria.

Repeats and motifs prediction of the intergenic region (INT) of YeRER

With the motif search function in FIMO, five regions were identified which are possible DNA-binding sites by transcriptional regulators PhoP (1, 3, 4,5), Fur (1), or OmpR (2) – like regulators (Table S4, Fig. 28A). Manual assessment of the nucleotide sequence (Fig. S5) identified two long (31 bp) degenerate repeats with an identical core sequence (5' TTGCTGCTTTTATC 3') of 14 bp (Fig. 28B). BlastN of the core repeat showed that the repeat is unique to the INT in the MH96 genome.

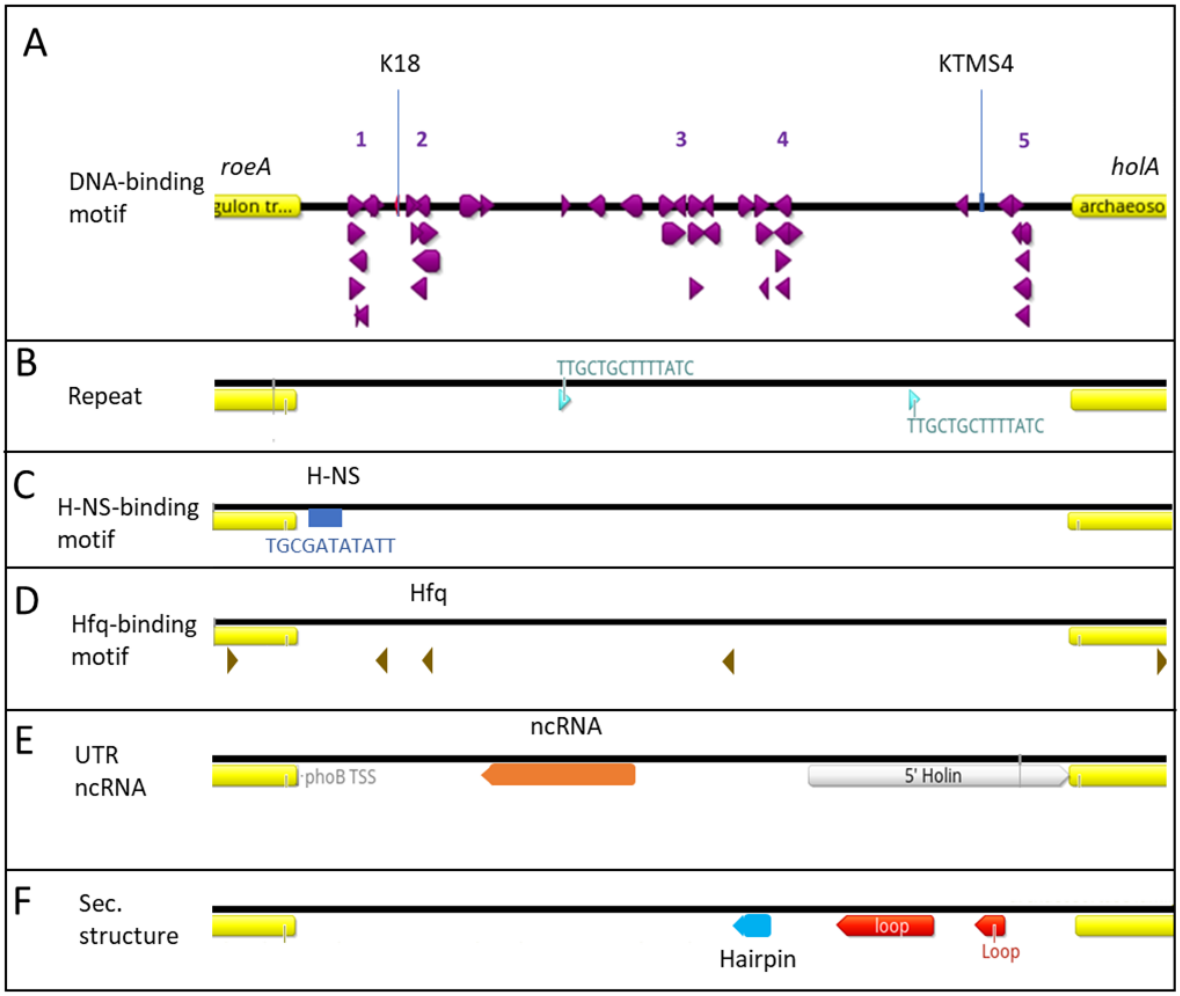

Figure 28: Structural and motif analysis of INT. *A)* Motifs of common DNA-binding motifs from Enterobactericeae. *B)* Location of two long degenerate repeats with perfect repeat core indicated *C)* H-NS binding motif derived from Lang *et al.* (2007) *D)* Hfq binding motif according to Lorenz *et al.* (2010) *E)* Transcriptome data of MH96 revealed 5'UTR (grey) of *roeA* and *holA,* and non-coding RNA (orange)with low transcript level could be identified. *FE)* Analysis of possible secondary structure identified 3 possible loop region with two within *holA* promoter (red) and one hairpin-like structure (blue) adjacent to Hfq binding motif.

Additionally, posttranscriptional regulation by RNA-binding proteins can occur. AgResearch in-house assessment identified Hfq-dependent protein secretion. Mutation of Hfq led to abolished protein secretion as observed for K18 (M. Hurst, pers. comm.). Due to exoproteome similarity between K18 and Hfq mutant, it was of interest to determine if potential Hfq binding sites can be found within the INT. Lorenz *et al.* (2010) identified three Hfq-binding motifs, which were used to search for Hfq binding sites in INT. Sequence analysis identified potential Hfq binding sites TT(A/G)TT(A/G)T located at position 129-135, 132-138, 187-193, and 591-597 in the intergenic region(Fig. 28C). Hfq acts as a global regulator, facilitating small RNA-mRNA interactions that control mRNA expression. Another binding motif of the transcriptional regulator H-NS was identified 35 bp 5' of *roeA* (Table S5), with the sequence TGCGATATATT derived from Lang *et al.* (2007) (Fig. 28D). The same H-NS binding consensus sequence was found once in the genome, 32 bp 5' of *yen7*, encoding for a RoeA paralogue.

The transcriptome data of MH96 and derivatives KTMS12, which has strongly reduced transcript levels of the YLC genes (Chapter 6.2), revealed reads covering 220 bp within the intergenic region of the YeRER, indicating a possible ncRNA (Fig. 29A, Fig. 28E).

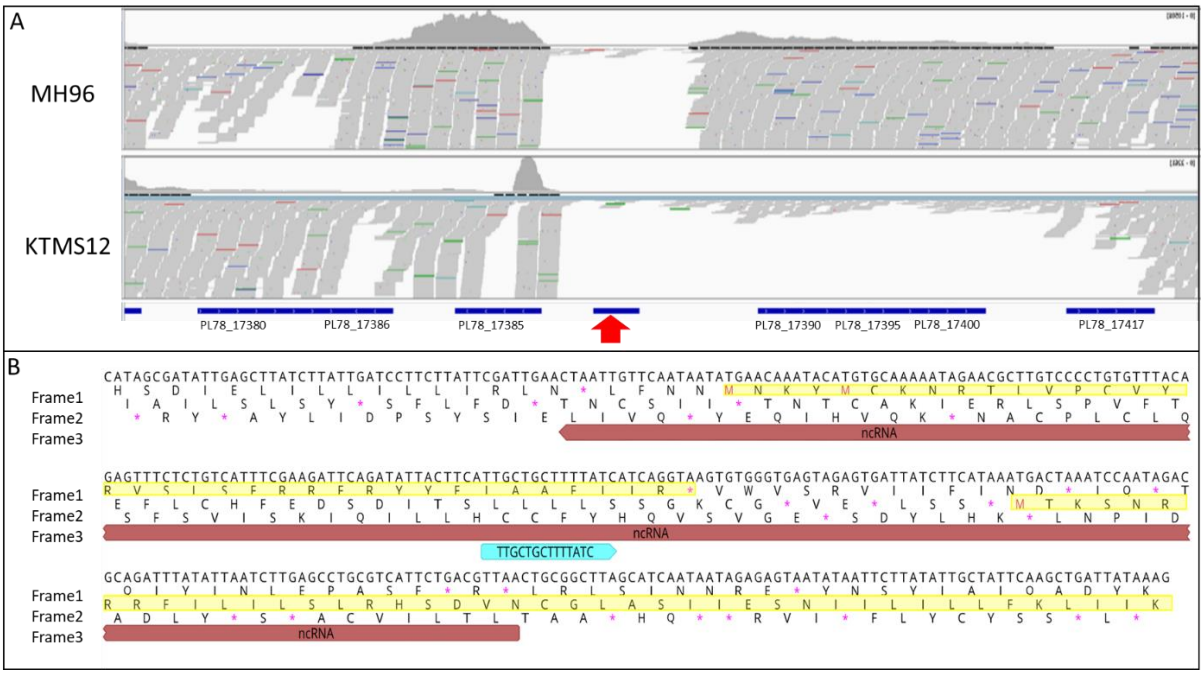

Figure 29: Identification of possible ncRNA of the YeRER cluster. *A)* RNAseq reads covering the Roe-region of wildtype MH96 and the *roeA*-transposon mutant KTMS12. Strongly decreased reads in over genes encoding the lysis cassette in *roeA*$^{-}$ mutant (KTMS12) alluding to down-regulation of the YLC cluster. A potential ncRNA (red arrow) with very low reads is located between *roeA* and *holA*. *B)* Nucleotide sequence and translation of forward reading frames encoding for a potential small protein (yellow highlight) of the ncRNA (red). Indicated is core region of the degenerate repeats (light blue).

The ncRNA contains two possible reading frames (ORF1 and ORF2) (Fig. 29B). BlastX and BlastP search of these regions did not identify any significant alignments with known proteins, nor could a ribosomal binding site, 4-13 bp upstream of the initiation codon, be allocated to these ORFs. Based on this it is unlikely that the 220 bp sequence encodes a protein and is therefore likely to be a ncRNA, which has been termed ncYLC220.

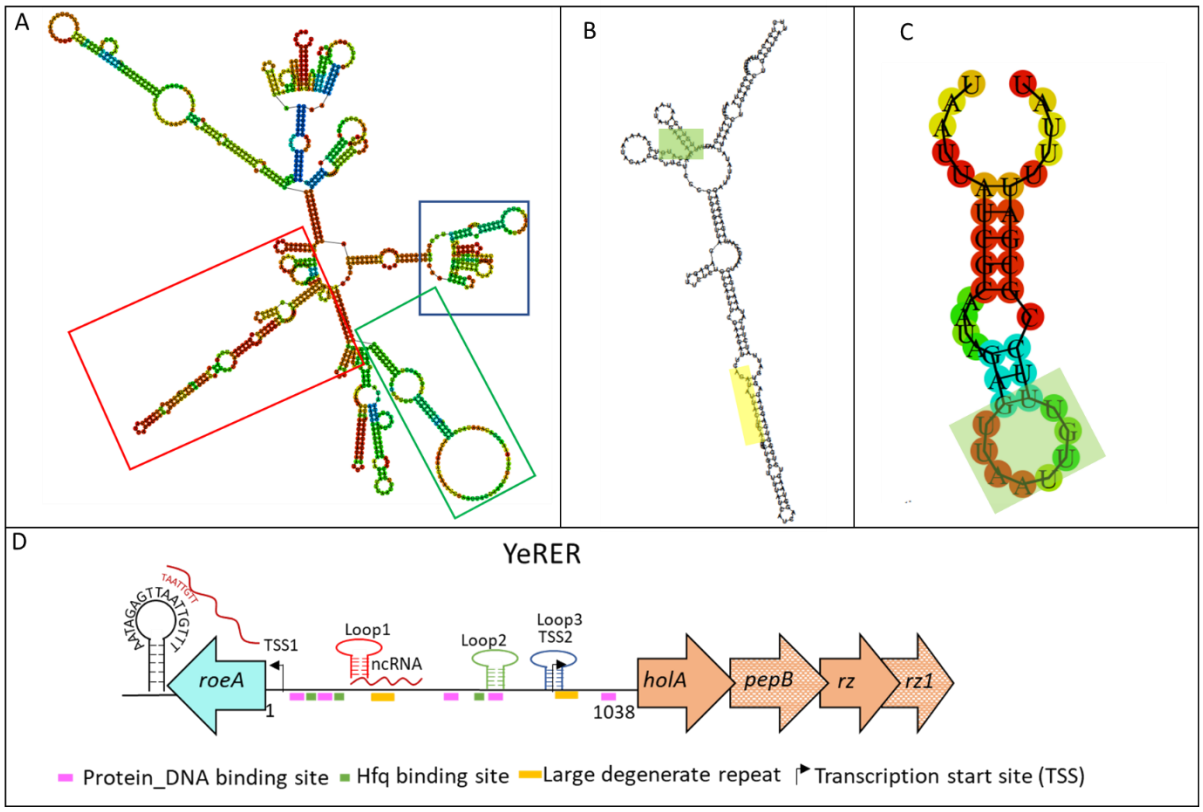

Figure 30: RNA structure analysis. *A)* RNA structure of the YeRER intergenic region (INT) with marked hairpins covering regions ncYLC220 (red loop) and hairpin(blue loop) over the degenerate repeat (yellow box) 5' *holA,* and a third hairpin (green loop) structure covering Protein/Hfq binding motifs (pink and green box, respectively). *B)* RNA structure of ncYLC220 harboring one degenerate repeat (yellow highlight) and a complementary nucleotide sequence (green highlight) to *roeA* terminator loop. *C)* Potential terminator of *roeA* with marked complementary nucleotide sequence (green highlight) to ncYLC220. *D)* Schematic of YeRER including secondary structures from ABC. TSS1 indicates predicted transcriptional start site (TSS) of *roeA,* and TSS2 indicates predicted TSS of *holA*, derived from transcriptome data.

Comparison of ncYLC220 nucleotide sequence to the RNA database (RNA central) using the RNA central interface with default settings revealed no hits. The ncYLC220 of the YeRER is located 249 bp 5’ of *roeA* and 569 bp 5’ of *holA* and has a low GC content of 34.5%. Analysis of folding structures, the minimum free energy (MFE) prediction model from online tool RNAfold, identified two possible structures of the region (Fig.30B). The ncYLC220 harbours a large degenerate repeat in a possible stem of a hairpin structure. Furthermore, a small inverse repeat of ncYLC220 (Fig. 30B) to that of a potential terminator structure 3’ *roeA* (Fig. 30C) was identified. Secondary structures of the transcribed RNA are likely involved in the regulation of gene transcription. The entire INT sequence was analysed for secondary

structure. Noteworthy are three hairpin/ loop structures located within INT (Fig 30D), of which one (Loop3) is located at the *holA* transcriptional start site, one at the Hfq binding motif (Loop2), and one within ncYLC220 (Loop1) (Fig. 30D). Loop1 confirms the analysed secondary structure of ncYLC220 in Fig. 30B.

To investigate a possible function of ncYLC220 and INT in protein secretion, the region and truncations of the region were *trans* complemented using the mid-copy vector pACYC184 (Fig.25D), as described in Chapter 6.4.2.

Synteny of the YeRER in Enterobacterales

Within the order Enterobacterales, the genera *Serratia, Chania, Vibrio,* and *Yersinia* were selected for synteny analysis of the RoeA protein (Fig. 31).

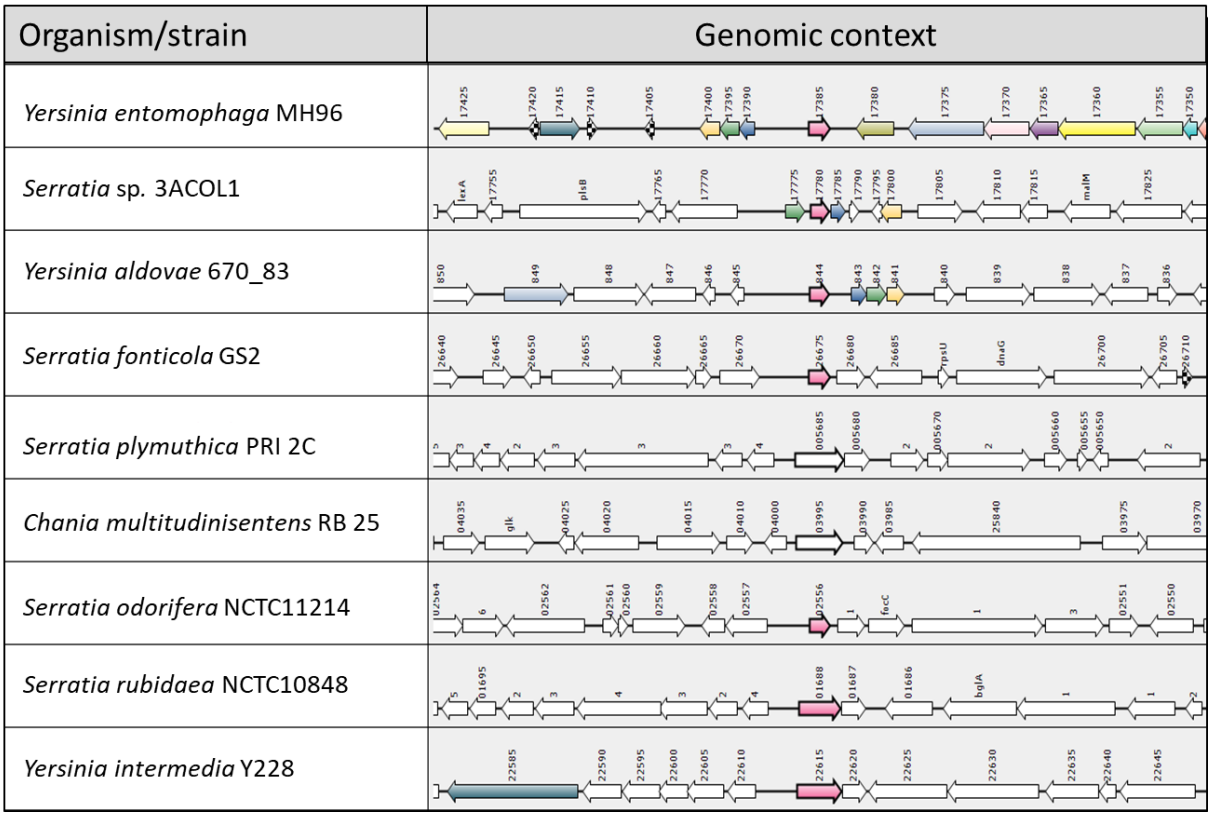

Figure 31: Interspecies synteny of *Y. entomophaga* MH96 transcriptional regulator RoeA. Comparison of the genetic context by Blast alignments of RoeA using the webserver SyntTax. Pink arrow indicating RoeA and RoeA-homologues. Numbers indicate the locus number of the individual strain.

The protein RoeA could be found in strains of the four genera and a RoeA-like protein was found in *Chania multitudinisentes*. The RoeA-homolog in *Serratia* sp. 3ACOL1 has high homology of 56% amino acid (aa) similarity and is associated with a lysis cassette as described for *Y. entomophaga* MH96. Interestingly *Serratia* sp. 3ACOL1 was isolated from the intestines of larvae of wood-boring beetles

(*Cerambycidae* sp.) in the Norwegian Boreal forest (BioSample: SAMN10216109). In *Yersinia, roeA* was found in *Y. aldovae* strain 670_83 and is co-located with a lysis cassette. The strain *Y. aldovae* 670-83 was isolated from a fish also in Norway (BioSample: SAMN03144720). The *Y. aldovae* RoeA homolog of locus 844 (128 aa) shares 51% amino acid similarity to RoeA from MH96 (136 aa) (Fig. 31). The synteny of the neighbouring genes to RoeA-homologs identified an ortholog MH96 lysis cassette in *Y. aldovae* (Fig. 31). The shared amino acid identity (74%) of MH95 HolA and *Y. aldovae* AT01_842 in the shared gene synteny indicates that *Y. aldovae* and *Y. entomophaga* might have shared a common ancestor before the acquisition of the YeRER. A RoeA-like protein was also found in *Y. intermedia* with 59% similarity to 76 aa of the 223 aa residues of the putative DNA binding protein of *Y. intermedia.* The synteny of DNA-binding protein in *Y. intermedia* (locus 2447) differs from MH96, where the gene is located adjacent to operons encoding a pore-forming efflux system (TolC) and type 1 fimbria protein.

Previously BLASTP (Chapter 3) identified a homologous RoeA-like protein in *Y. nurmii*. The SyntTax analysis was not available for the *Y. nurmii* species. Therefore, an additional analysis of the YeRER was performed on the *Y. nurmii* genome. The hypothetical protein encoded by *Y. nurmii* AD970_RS04640 is identical (99%) to RoeA. Furthermore, the genetic contents are highly similar to each other and will be discussed further in Chapter 6. 3. *Y. nurmii* genome encodes for a lysis cassette formed by a holin, M15-family endopeptidase and at least one spanin, as it can be found in *Y. entomophaga*. Interestingly, additional BLASTP analysis of RoeA within the Gamma-proteobacteria showed the highest homology, outside of the *Yersinia* genus, to RoeA-like proteins of *Cedecea neteri* CopR (58% similarity), *Salmonella enterica* hypothetical protein (58% similarity) and hypotheticals of several *Photorhabdus* strains (55-65% similarity). However, those RoeA homologs are not in co-location with a lysis cluster. To note, the program SyntTax only allows protein comparison to a pre-selection of genomes, a reason why RoeA homologs in *Y. nurmii* and *Photorhabdus* were not detected.

Synteny of HolA located in the MH96 lysis cassette shows a wide distribution of such lysis cassettes within several *Yersinia* species. (Fig. 32). Only in *Y. intermedia* and *Y. aldovae* could co-location of the DNA-binding protein (RoeA-like) with the lysis cassette be identified. Nucleotide alignment of the intergenic region of *Y. entomophaga*, *Y. aldovae,* and *Y. intermedia* showed no identity.

The homologous lysis cluster was found in the human pathogenic strains *Y. pestis* (75% similarity)*, Y. pseudotuberculosis* (75%), and *Y. enterocolitica* (80%) and the mammalian pathogen *Y. similis* (75 %). The lysis cassettes of those strains are located within the insecticidal-like toxin complex (TC) region, contrary to the MH96 YLC. A strain of *Y. frederiksinii* also had a homolog of a holin (65% similarity), an endopeptidase (65% similarity), and an additional gene with no amino acid similarity to the MH96 spanin. The HolA amino acid sequence was also compared to other genera of the Enterobacterales from *Escherichia, Erwinia, Citrobacter, Legionella, Pseudomonas, Salmonella, Serratia,* and *Vibrio* (Fig. S6).

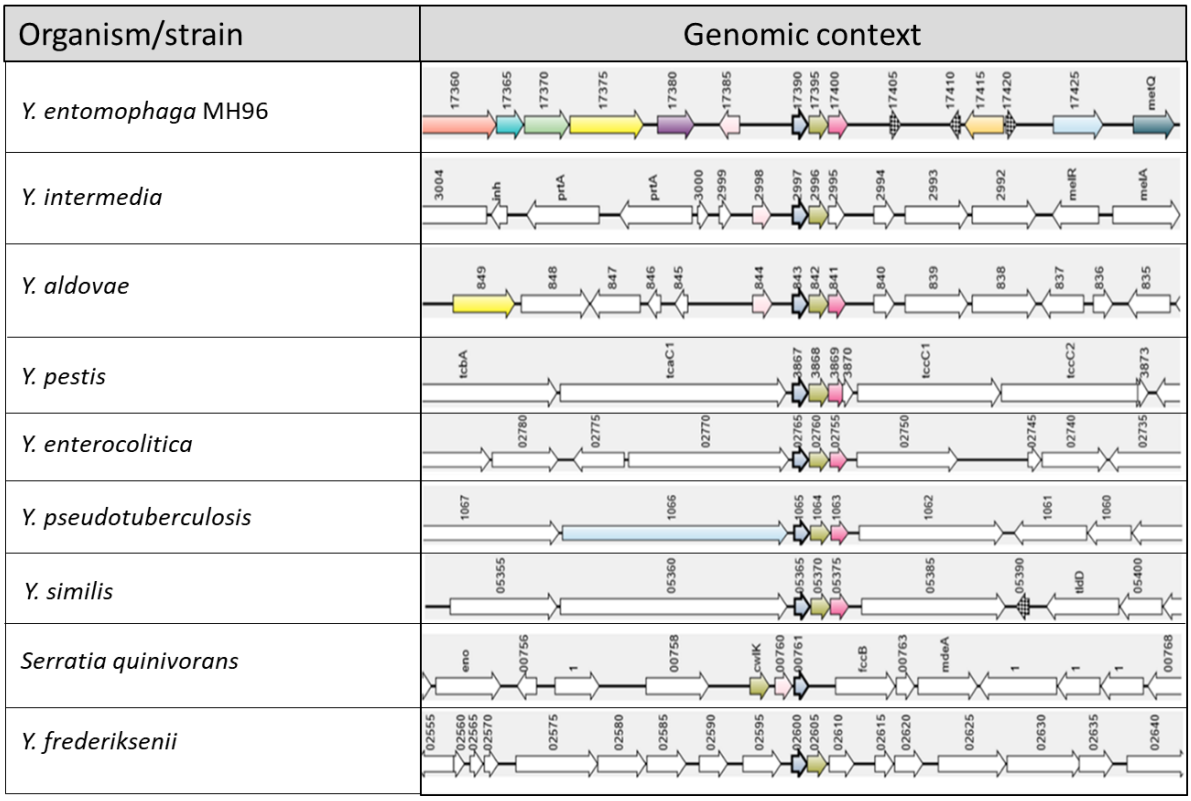

Figure 32: Synteny of holin HolA from the MH96 YLC within the genus *Yersinia*. The genomic region of MH96 holin-based lysis cassette encoding for a holin (blue), endolysin (green), and an i-spanin (pink) is co-located to the DNA-binding protein RoeA (pink) in four *Yersinia* species.

Outside of the genus *Yersinia*, only *S. quinivorans* (Fig. 32) encoded a similar lysis cassette with shared similarity to YLC. *S. quinivorans* encodes a holin (63% similarity), a predicted transcriptional regulator (RcsA) with no homology to RoeA, and an endopeptidase (73% similarity) as the third gene in the cassette. The previously described *Serratia* sp. 3ACOLI lysis cassette was not depicted in Fig. 32 because the aa similarity was not as high as many other lysis cassettes within the Enterobacteriaceae. In *Serratia marcescens*, an active lysis cassette of ChiW, ChiX forming holin and endolysin has been studied by Hamilton *et al.* (2014) and shared 50% and 59 % identity to HolA and PepB, respectively.

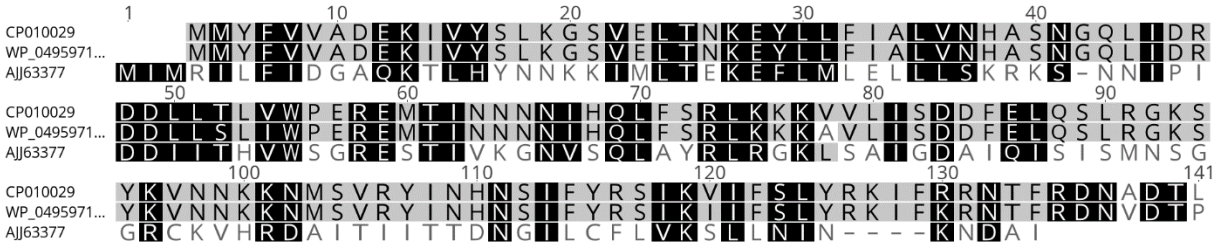

Figure 33: Amino acid alignments of RoeA (CP010029) and Roe-A homologs from *Y. nurmii* (WP_049567149) and *Y. aldovae* (AJJ63377). The residual similarity is indicated by black box (100%), grey box (80-100%), and white box less than 60%.

The synteny analysis revealed that *Y. nurmii* (AD970_RS04640) and *Y. aldovae* (AT01_884) (Fig. 33) have the same conserved region, whereas the gene orthologs in other organisms were not co-located with similar elements.

Summary of bioinformatic analysis of the YeRER

In summary, the YeRER is a region unique to *Y. entomophaga* and the closely related strain *Y. nurmii*. The YeRER encodes for the putative transcriptional regulator RoeA, with high similarity to DNA-binding sites of PhoB-like proteins. *Y. entomophaga* MH96 encodes for a RoeA paralog, termed Yen7, which is directly located 5' of the Yen-TC operon. Furthermore, encoded in the YeRER are genes encoding a phage-like lysis cassette comprising of a holin (HolA), a M15-family endopeptidase (PepB), and a spanin complex formed by IM-bound i-spanin (Rz) and the OM-bound o-spanin (Rz1). In contrast to RoeA, homologous lysis cassette can be found in other Gram-negative bacteria, especially within the genus *Yersinia.* The lysis cassettes of *Y. pestis*, *Y. pseudotuberculosis,* and *Y. enterocolitica* are located within the respective TC-operon. In contrast, the YLC in *Y. entomophaga* MH96 is located at a distance to the Yen-TC. The intergenic region of RoeA and YLC is unique to *Y. entomophaga* and *Y. nurmii* and contains multiple putative protein-binding sites to PhoB-like protein, H-NS, and Hfq. Furthermore, secondary structures such as 5' hairpins of YLC and a ncRNA within the intergenic region, as well as a putative RoeA terminator were identified during the bioinformatic assessment.

6.3.2 Characterisation of RoeA function in *Y. entomophaga* MH96

Phenotypic analysis of *roeA* mutants MH96Δ*roeA*, KTMS12 and K18

The *roeA* targeted mutagenesis resultant strain MH96Δ*roeA* was cultured as described in Chapter 6.1 and the exoproteome was analysed. In duplicate experiments, the mutant strain MH96Δ*roeA* released exoproteome with a similar concentration to MH96, which was observed by SDS-PAGE (data not shown). The *roeA* mutation in MH96Δ*roeA*, disrupted the *roeA* gene (by insertion of a spectinomycin cassette) at 23 nt past the Tn5 insertion site in KTMS12. KTMS12 in turn showed a decreased exoproteome release compared to MH96 and MH96Δ*roeA*. Within the 23 nt, the structure of the amino acids forms the first helix of the HTH-motif in PhoB homologs (Fig. 34). Due to the anomaly in exoproteome release between KTMS12 and MH96Δ*roeA*, the genome of KTMS12 was sequenced, validating the presence of a single transposon insertion within *roeA*, allowing the use of KTMS12 in further assessments. Due to the absence of a different exoproteome phenotype in MH96ΔroeA, this strain was not used further in the study. Instead, KTMS12 and K18 were used for phenotypical analysis.

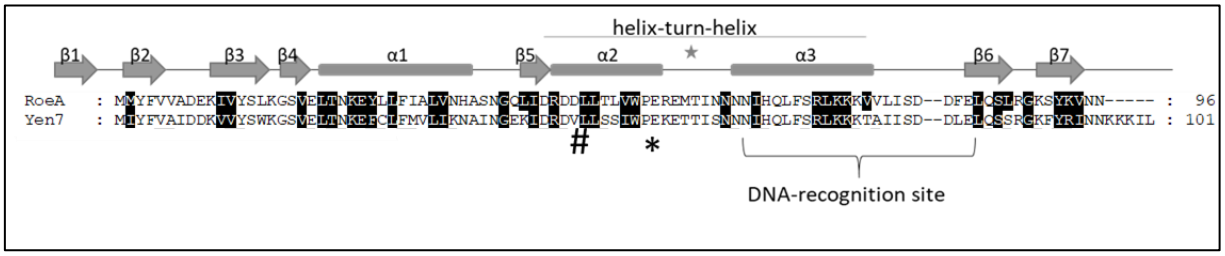

Figure 34: Amino acid sequences and secondary structures of RoeA and Yen7 paralog. Black boxes denote conserved amino acids in PhoB-like proteins (Chapter 6.1), * denotes KTMS12 Tn5 insertion point, # denotes MH96Δ*roeA* spectinomycin insertion point, star denotes HTH-motif.

As previously outlined in Chapter 3, KTMS12 was initially identified by HESA as showing reduced exoproteome. Further assessment of the protein content of the supernatant and cell pellets confirmed the observations from the HESA (Chapter 3), that the strain KTMS12 shows significant reductions in exoproteome, which was also observed in Y. *entomophaga* K18. Furthermore, expected protein bands of the Yen-TC complex were absent in cell pellets of the *roeA* mutant strains KTMS12 and K18 (Fig. 35A).

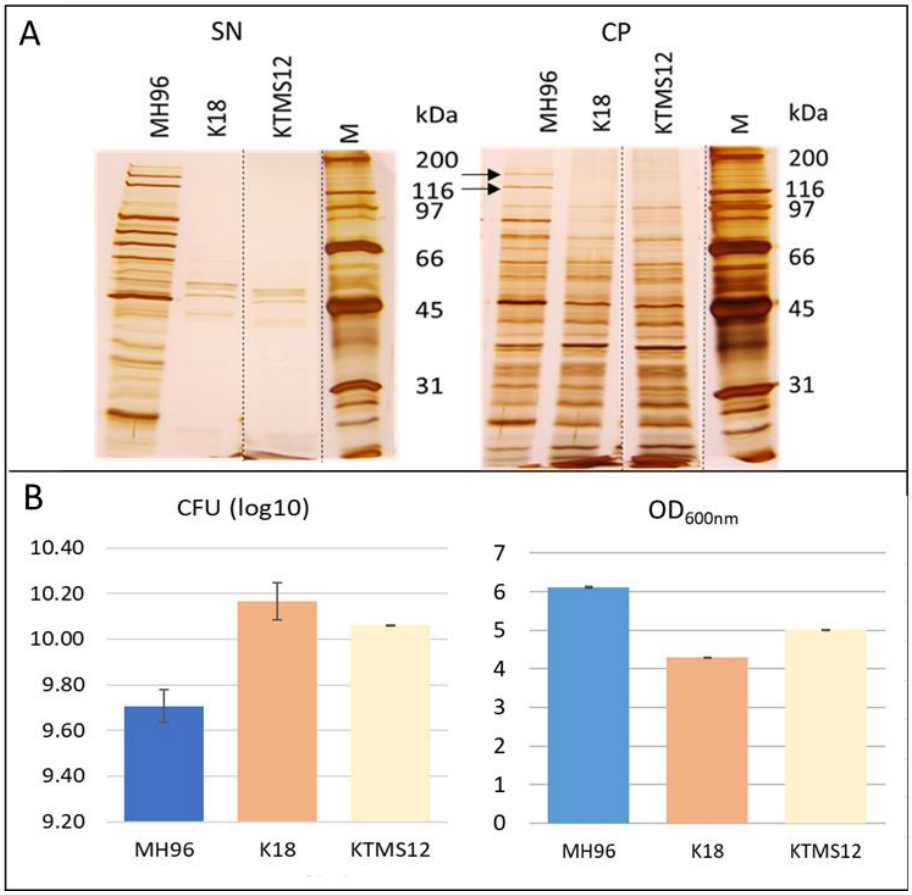

Figure 35: Comparison of MH96, K18 and KTMS12 cell culture at 16 h. *A)* Silver stained SDS-PAGE of 25 µl supernatant (SN) and cell pellets (CP) from cell cultures MH96, K18 and KTMS12 at 16 hpi in 50-ml LB-broth, and 1 µl of Marker (M). Black arrow denotes YenA1/2. Dotted lines indicate digital cropped gel for better visualization. *B)* CFUs and ODs of the cell culture at 16 hpi. Depicted are mean values with SD.

Cell cultures of KTMS12 and K18 reached an average OD 5 and 4.3 and cell density of 1.14×10^{10} and 1.18×10^{10} CFU/ml, respectively. In comparison to wild type strain MH96, the *roeA*-mutants showed a slightly, non-significant, reduced OD compared to wildtype strain MH96, while increased cell densities were measured (Fig. 35B). The KTMS12 cells were then assessed using light microscopy and TEM (Fig. 36) as outlined in Chapter 2.8.

Y. entomophaga MH96 are rod-shaped bacteria with an average length of 1.5 ± 0.39 µm and width of 0.8 ± 0.09 µm (Fig. 36ACEF). Mutation of *roeA* in KTMS12 led to a significant shortening of the cells with a length of 0.9 ± 0.30 µm and a similar width of 0.8 ± 0.13 µm (Fig. 36BDGH; Fig. 37). Furthermore, KTMS12 cells reached higher CFU/ml then MH96 after 16 hpi. Under the TEM, KTMS12 showed deformation of the outer membrane on the terminal corners (Fig. 36GH). Flagella-like structures were observed attached to the MH96 cells, but not attached to K18 cells. However, in both K18 and MH96 cell cultures, similar flagellar-like structures were found in the medium (Fig. S7).

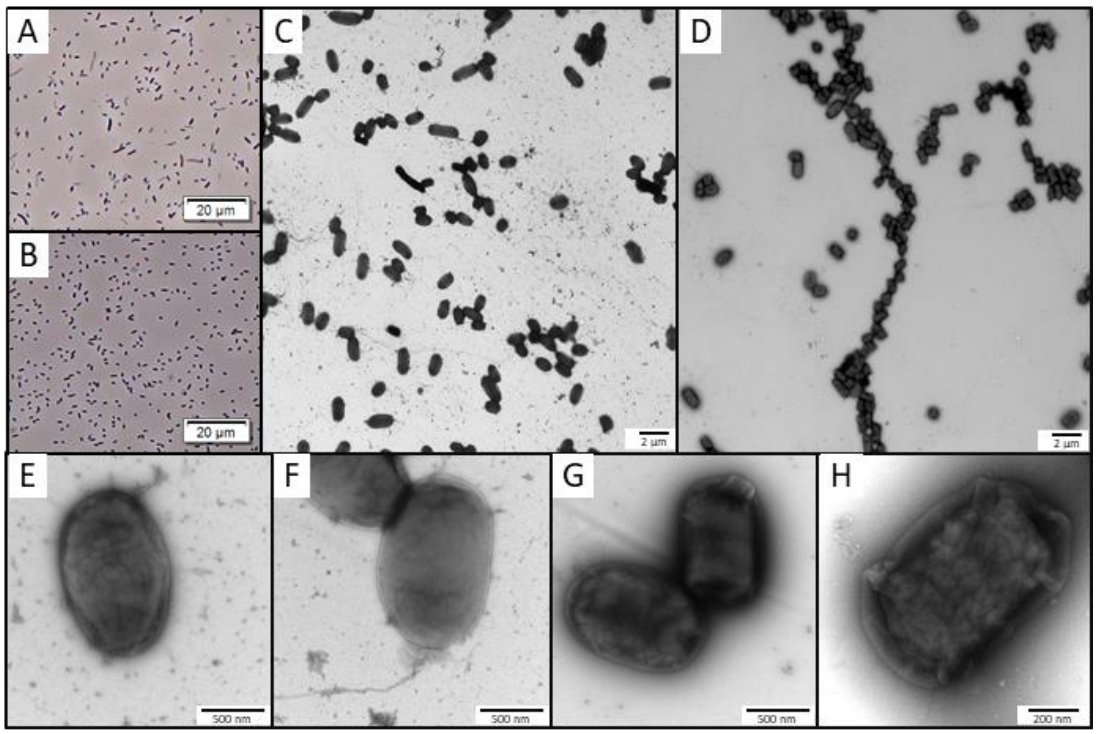

Figure 36: Cell morphology of MH96 and its *roeA* mutant KTMS12 derivative. *A)* Phase contrast- light microscopy of MH96 culture. Scale bar of 20 µm *B)* Phase contrast- light microscopy of KTMS12 culture. Scale bar of 20 µm *C, E, F*) Electron micrograph of MH96 cell. *D, G, H)* Electron micrograph of KTMS12 cells. All samples were taken from 16 h cultures incubated at 25°C. Scale bars of C and D is 2 µm and of EFGH is 500 nm.

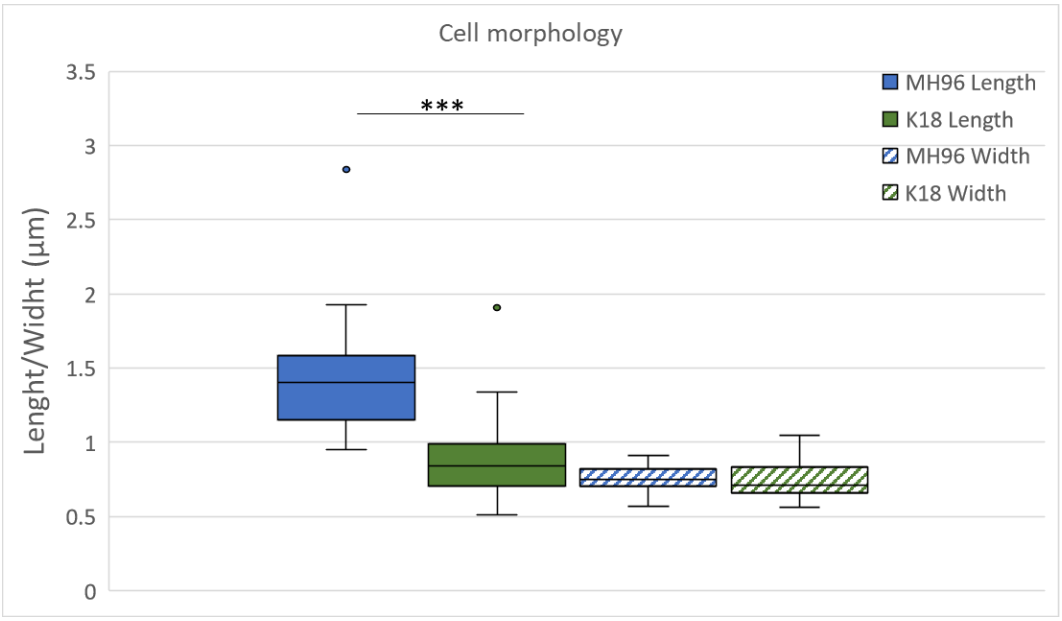

Figure 37: Cell size of MH96 and KTMS12 measured in Length and Width. *** indicates p<0.0005, calculated by unpaired, two-sided t-test.

LC-MS analysis of K18 secretome

In the exoproteome of the *roeA* mutant strain K18, only a few proteins are secreted in measurable abundance. Isolation of the SDS-PAGE bands of K18 and additional LC-MS analysis identified 11 proteins (Fig. 38. Table 13). These proteins function in lipid metabolism, cell motility, carbohydrate metabolism and transport, and secondary metabolite biosynthesis, transport, and catabolism.

Table 13: LC-MS results of K18 exoproteome

Description	Locus	Accession	-10 lgP	Coverage (%)	#Pept	#Uni	Avg. Mass (kDa)	Signal. Seq.
Serine 3-dehydrogenase	PL78_03960	A0A3S6EY30	444	93	66	63	51.18	-
Serine 3-dehydrogenase	PL78_03965	A0A3S6EX06	192	23	7	7	52.11	-
Fructose-bisphosphate aldolase	PL78_09345	A0A3S6F000	227	45	13	13	39.06	-
Phosphoglycerate kinase	PL78_09350	A0A3S6F0Z9	169	30	7	7	41.03	-
Thermolabile hemolysin	PL78_09600	A0A3S6F052	257	39	14	14	47.86	Sec
Chitinase	PL78_11910	A0A3S6F1Q8	326	70	32	32	38.47	Sec
Flagellar hook protein, FlgK	PL78_17660	A0A3S6F4R4	120	22	11	11	58.70	Sec
Flagellar cap protein, FliD	PL78_17770	A0A3S6F4M2	307	58	19	19	49.03	Sec
Flagellin	PL78_17775	A0A3S6F517	291	46	11	11	41.35	-
Flagellin	PL78_17780	A0A3S6F699	303	46	14	14	37.44	-
T3SS needle tip protein	PL78_18185	A0A3S6F562	313	61	25	25	44.67	-

#Pept: number of peptides
#Uni: number of unique peptides

Out of 11 proteins subjected to LC-MS/MS, four proteins are part of the flagellar apparatus (Table 13). The flagellum is a membrane-bound structure with a flagellar hook, flagellin, and the flagellar cap forming the extracellular part, which leads to cell motility, adhesion, or secretion and can be involved in virulence (Erhardt *et al.*, 2015; Dongre *et al.*, 2018; Schniederberend *et al.*, 2019). Further secreted proteins are Serine 3-hydrogenases, of the Serralysin 3-hydrogenase associated region (Hurst *et al.*, 2016), which are known to be secreted by HlyD of the T1SS, the thermolabile hemolysin (T1SS), fructose-biphosphate aldolase, and a chitinase (Table 13).

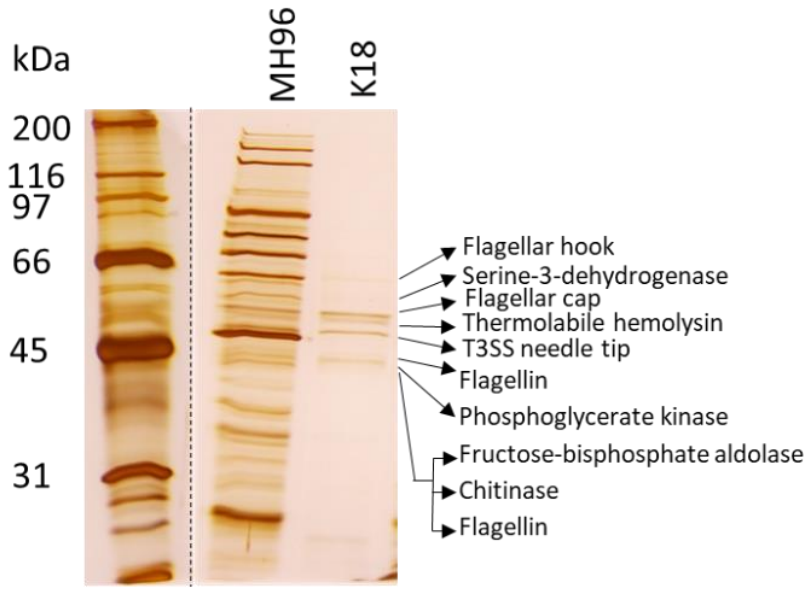

Figure 38: SDS-PAGE as a representative protein gel of bands in K18 supernatant, which were assessed by LC-MSMS.

Trans complementation of *roeA* mutants

The ability to restore exoproteome production through complementation of the *roeA* mutants KTMS12 and K18 was assessed by *trans* complementation pGEM-YeRER and pGEM-INT (Fig. 39).

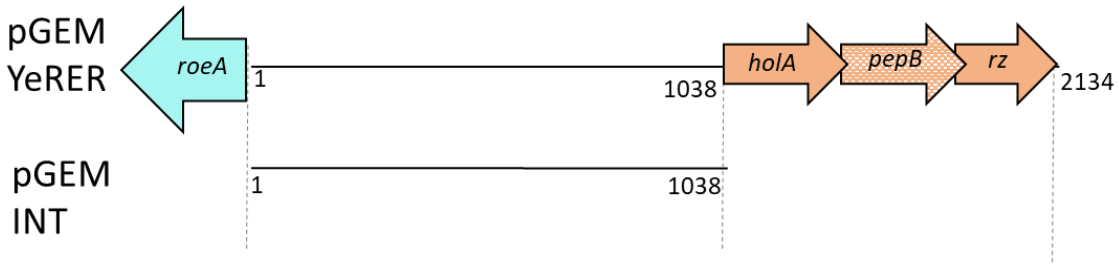

Figure 39: Schematic of YeRER and INT for *trans* complementation using pGEM-YeRER and pGEM-INT, respectively in MH96 and K18.

Overexpression of YeRER and INT using pGEM-YeRER and pGEM-INT, respectively, decreases protein secretion in MH96 at 16 hpi, while *trans* complementation with pGEM-INT almost completely abolished secretion. At 16 h the high copy plasmid pGEM-YeRER, harbouring *roeA*, intergenic region, and the lysis cassette, reduced exoproteome and abolished release of Yen-TC proteins (Fig. 40A). The intergenic region (INT) plasmid pGEM-INT did not affect exoproteome release of the K18 strain, however, *trans* complementation of K18 with pGEM-YeRER and pGEM-INT resulted in slightly elevated exoproteome release. In contrast, at 24 hpi both constructs led to increased exoproteome

concentration in MH96 (Fig. 40B). In the *roeA* mutant strain K18, complementation with pGEM-YeRER, which included a copy of *roeA,* partially restored the phenotype.

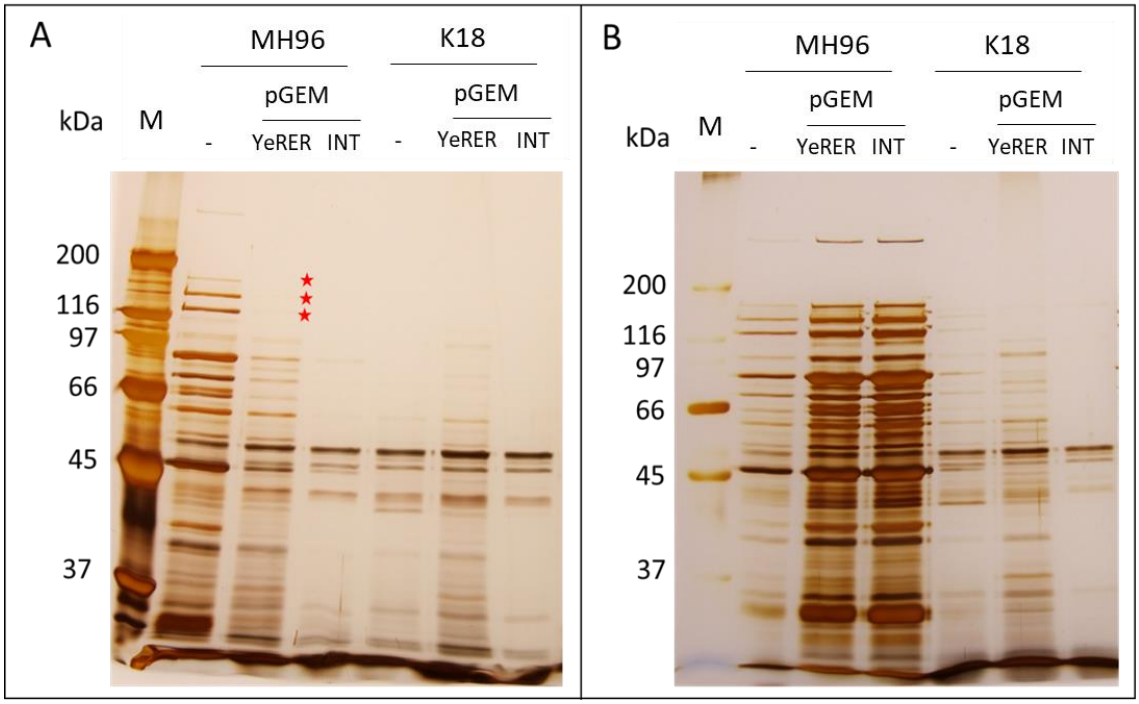

Figure 40: Exoproteome of MH96 and K18 after overexpression of pGEM YeRER and pGEM-INT. *A)* SDS-PAGE of exoproteome of MH96 and K18 constructs at 16 hpi. Stars denote Yen-TC proteins *B)* SDS-PAGE of exoproteome of MH96 and K18 constructs at 24 hpi.

The results of the *trans* complementation experiment (Fig. 40) showed that *roeA* mutation was partially restored with pGEM-YeRER, only at 24 h. At 16 hpi, the *trans* complementation of pGEM-INT and pGEM-YeRER caused decreased exoproteome release compared to MH96. While at 24 hpi the *trans* complementation showed increased exoproteome release compared to MH96. Hereby, differences in exoproteome release, observed in band-intensities by SDS-PAGE, in *trans* complementation of pGEM-INT and pGEM-YeRER in MH96 in a growth phase-dependent manner.

Trans- complementation of YeRER derivates in pACYC184 in K18

The K18 mutation is 5' of *roeA*, encoding for protein RoeA containing HTH-motif, which allows binding to DNA. A mutation in the 5' region causes inactivation of RoeA expression as seen in the *roeA* mutant KTMS12. To understand how *roeA* transcription is regulated, the YeRER, INT, and truncations of INT were cloned into the medium copy vector pACYC184 and the vectors p184INT, p184INT(K18), p184-5'*roeA*, p184-5'*holA*, p184ncYLC220, pACYC184NCYLC637, and p184-INT_YLC used to *trans* complement K18 (Fig. 41A).

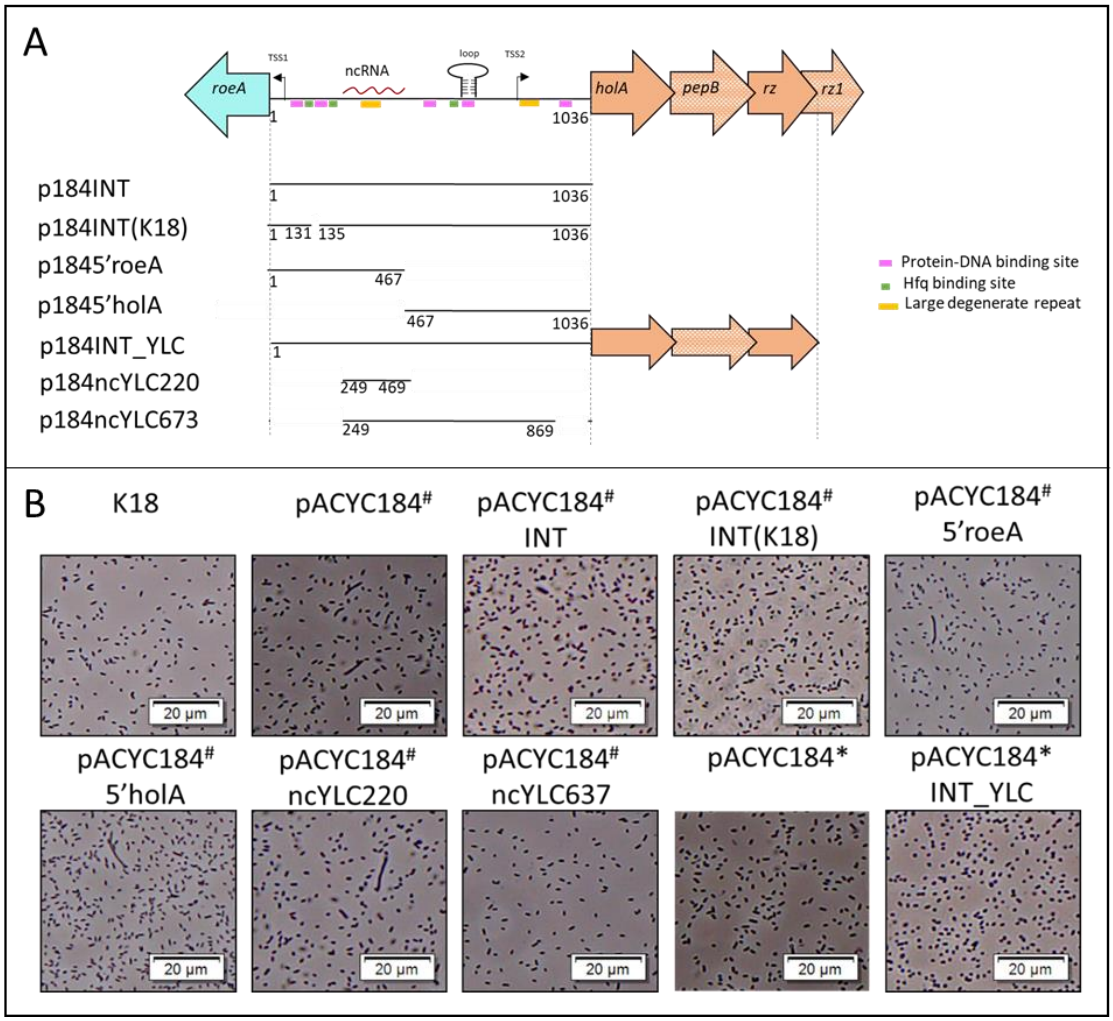

Figure 41: *Trans* complementation of YeRER construct in *Y. entomophaga* K18. *A)* Schematic of constructs in pACYC184. *B)* Light microscopy of K18 strain harboring pACYC184 constructs of INT and INT derivates. # denotes cells grown on tetracycline, * denotes cells grown on chloramphenicol.

Trans complementation of pACYC184 with inserts INT, INT(K18), 5'*roeA,* and 5' *holA* did not affect K18 and K18 pACYC184 phenotype. In p184-5'*roeA*, p184-5'*holA*, and p184ncYLC220, single elongated cells were observed but were also found in pACYC184 control. The *trans* complementation of the pACYC184 constructs did not restore exoproteome release in K18 (data not shown). Therefore, K18 phenotype could not be restored, which indicates that RoeA is tightly controlled by its promoter region and respective transcription factors binding to it.

Transcriptomics of the *roeA* mutant KTMS12

The identification of RoeA as a potential regulator of exoproteome release raises the questions as to which pathways or functions the regulator acts upon. To define possible target genes regulated by RoeA, the transposon mutant KTM12, which has an insertion 139 bp within *roeA,* was assessed using RNAseq. The transcriptome data was compared to that of the wild type strain MH96. Because KTMS12 showed increased CFUs compared to MH96, the transcriptome samples in duplicates were taken from cultures of similar CFU (KTMS12: 3.55×10^9 CFU/ml; MH96: 4.35×10^9 CFU/ml), rather than the same time of incubation.

The transcriptome analysis identified 1615 genes differentially expressed in the KTMS12 compared to wild type MH96; 2454 genes of the 4068 genes of the genome were not differentially expressed. The transcriptome data defined 287 genes that were significantly up-regulated (log2fold >1 and $p<0.05$) and 365 genes that were significantly down-regulated in KTMS12 (Table S6). Of the 190 up-regulated genes, COG functions could be assigned to: cell motility (22.6%), signal transduction (9.5%), cell wall/ membrane biogenesis (8.4%), carbohydrate metabolism and transport (8.4%), and phage assembly (7.9%) (Fig. 42). Of the down-regulated genes, 288 COG functions could be assigned in: translation (22.2%), amino acid metabolism and transport (16.7%), post-translational modification (protein turnover and chaperone functions) (8%), transcription (7.3%), energy production and conservation (6.6%) (Fig. 42).

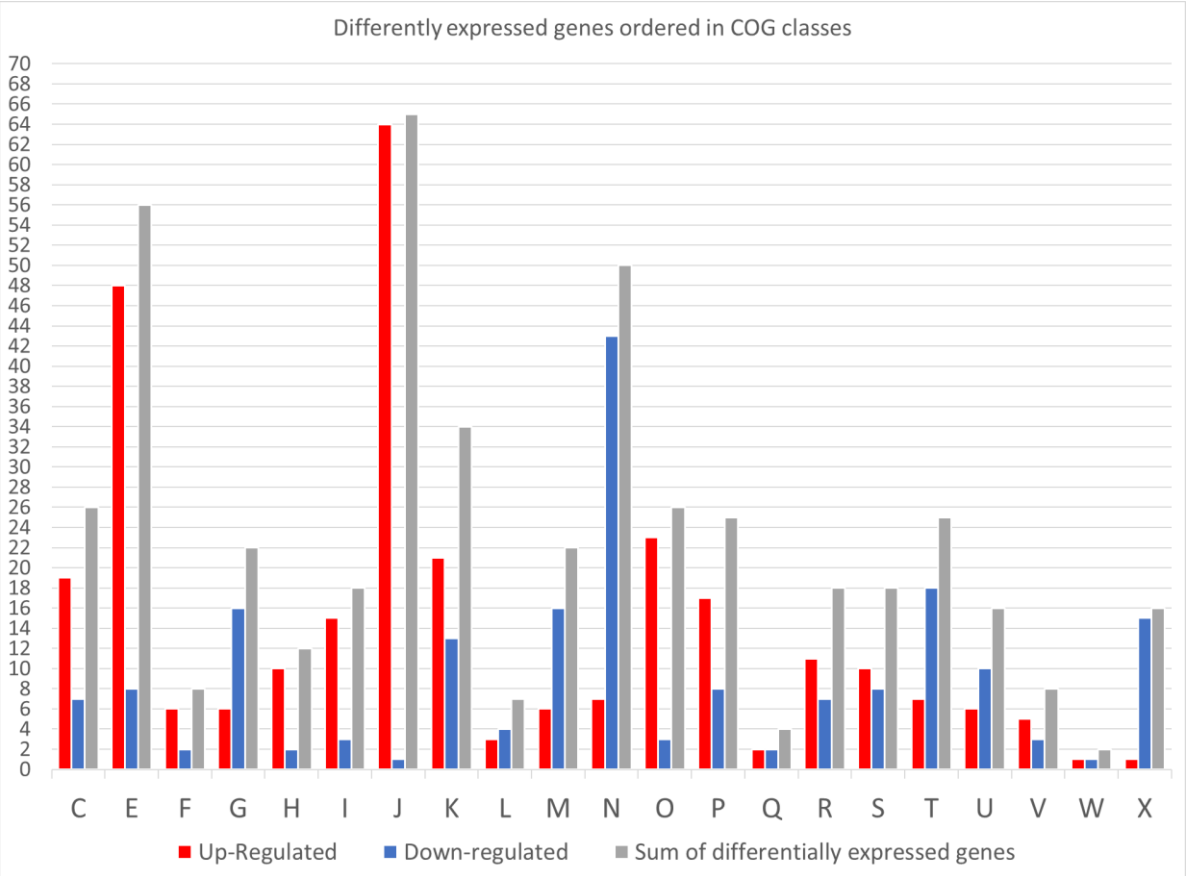

Figure 42: Number of genes with altered transcription levels in KTMS12 listed in classification COG function. C, Energy production and conversion; E Amino acid metabolites and transport; F Nucleotide metabolism and transport; G, Carbohydrate metabolism and transport; H, Coenzyme metabolites; I, Lipid metabolism; J, Translation; K, Transcription; L, Replication and repair; M, Cell wall/membrane/envelop biogenesis; N, Cell motility; O, Post-translational modification, protein turnover, chaperone functions; P, Inorganic ion transport and metabolism; Q, Secondary Structure; T, Signal Transduction; U, Intracellular trafficking and secretion; V, Defense mechanisms, W, Extracellular structures; X, Mobilome: Prophages, Transposons, R, General Functional Prediction only; S, Function Unknown.

The top 60 down-regulated and up-regulated genes of the *roeA* mutant KTMS12 are listed in Table 14. Down-regulated genes can be roughly clustered into functions of the transporter (tricarboxylate, amino acids, iron), stress response (chaperons GroELS, DnaJK, heat- cold shock proteins), ribosomal proteins, the Yen-TC cluster, and pertinent to this study's components of the YLC cluster, a finding which validates that RoeA is an activator of YLC expression. The top up-regulated genes of KTMS12 can be divided into the two major clusters of phage assembly and flagella biosynthesis (Table 14). Down-regulated genes play a part in fatty acid biosynthesis and T2SS mediated protein secretion (Table 14).

Table 14: Top 60 genes that are significantly, differently expressed in *roeA* mutant (KTMS12). Left: down-regulated genes, right: upregulated genes. List sorted by decreasing |log2| value.

Down-regulated					Up-regulated				
Locus	**log2**	**Description**	**COG**	**protein**	**Locus**	**log2**	**description**	**COG**	**protein**
PL78_05310	-11.88	chitin-binding protein	R	ANI29258	PL78_09335	12.09	Xre, transcriptional regulator	K	ANI30021
PL78_05495	-11.7	peptidase M66		ANI29294	PL78_09211	10.45	T6SS protein	U	NA
PL78_03745	-10.75	YenA1, toxin complex component		ANI28953	PL78_09150	9.88	late control protein D	X	ANI29984
PL78_03750	-10.59	YenA2, toxin complex component	V	ANI28954	PL78_09340	9.70	XerD, integrase	L	ANI30022
PL78_03760	-10.59	YenB, toxin complex component	R	ANI28956	PL78_09160	9.46	phage tail tape measure protein	X	ANI29986
PL78_11910	-10.58	glycosyl hydrolase family protein	G	ANI30527	PL78_09175	9.15	phage tail protein	X	ANI29989
PL78_03755	-10.39	Chi2, toxin complex component	G	ANI28955	PL78_09255	8.94	phage capsid protein		ANI30005
PL78_03740	-10.24	Chi1, toxin complex component	G	ANI28952	PL78_09185	8.92	Phage-related tail fibre protein	X	ANI29991
PL78_17395	-8.85	PepB, peptidase M15 of YLC	S	ANI31586	PL78_09280	8.81	bacteriophage protein		ANI30010
PL78_00655	-8.83	YbaB, Conserved DNA-binding protein	R	ANI28352	PL78_06005	8.66	thioesterase	Q	ANI29393
PL78_03765	-8.79	YenC1, toxin complex component	R	ANI28957	PL78_09218	8.57	virion morphogeneis protein	X	NA
PL78_17740	-8.53	DNA/RNA non-specific endonuclease	F	ANI31652	PL78_09145	8.52	Phage transcriptional activator		ANI29983
PL78_17390	-8.37	HolA, holin of YLC		ANI31585	PL78_09260	8.03	capsid scaffolding protein		ANI30006
PL78_03770	-7.97	YenC2, toxin complex component	R	ANI28958	PL78_09265	8.01	Terminase, Terminase-like family	X	ANI30007
PL78_12380	-7.29	IbpA, heat-shock protein of HSP20 family	O	ANI30619	PL78_01465	7.95	SucC, succinyl-CoA synthetase subunit beta	C	ANI28507
PL78_08970	-5.29	GspC, Type II secretory pathway		ANI29949	PL78_09290	7.91	Phage GPA, Bacteriophage replication gene A		ANI30012
PL78_04135	-5.06	porin	M	ANI29028	PL78_09155	7.86	tail assembly protein	X	ANI29985
PL78_12620	-4.68	AsnA, asparagine synthetase	E	ANI30667	PL78_09231	7.72	Rz, lysis protein- i-spanin		NA
PL78_01180	-4.64	amino acid transporter	E	ANI28456	PL78_09220	7.51	tail fiber protein		ANI29998
PL78_18780	-4.48	YenC3, toxin complex protein	R	ANI31857	PL78_09195	7.48	baseplate assembly protein	X	ANI29993
PL78_00635	-4.45	tricarboxylic transport membrane protein	C	ANI28348	PL78_09330	7.28	phage regulatory protein		ANI30020

Down-regulated					Up-regulated				
PL78_00630	-4.44	membrane protein Tripartite tricarboxylate transporter TctB family		ANI28347	PL78_09170	7.19	major tail tube protein	X	ANI29988
PL78_04115	-4.39	AstA, Arginine N-succinyltransferase beta subunit	E	ANI29024	PL78_09295	7.12	Dam, adenine methylase	L	ANI30013
PL78_17385	-4.36	RoeA, transcriptional regulator	(K)	ANI31584	PL78_09270	6.80	capsid portal protein	X	ANI30008
PL78_09586	-4.35	holin	(X)	NA	PL78_09230	6.69	lysozyme	M	ANI30000
PL78_00625	-4.23	TctA, tripartite tricarboxylate transporter	R	ANI28346	PL78_09300	6.41	DdnaQ, 3'-5' exonuclease	L	ANI30014
PL78_04110	-4.22	acetylornithine/succinyldiamopimelate /putrescine aminotransferase	E	ANI29023	PL78_09190	6.13	phage tail protein I	X	ANI29992
PL78_00665	-4.18	heat shock protein 90	O	ANI28354	PL78_09235	5.46	alpha/beta hydrolase		ANI30001
PL78_04120	-4.14	AstD, Aldehyde dehydrogenase family	C	ANI29025	PL78_09240	4.89	tail protein X	X	ANI30002
PL78_08960	-4.12	GspE, Type II secretory pathway	N	ANI29947	PL78_12010	4.83	BcsF, cellulose biosynthesis protein		ANI30547
PL78_13720	-4.11	DnaK, molecular chaperone	O	ANI30874	PL78_09205	4.81	baseplate assembly protein V	X	ANI29995
PL78_04125	-3.81	AstB, Succinylarginine dihydrolase	E	ANI29026	PL78_14590	4.78	SpaR, surface presentation of antigens protein	U	ANI31048
PL78_03780	-3.73	YenV	S	ANI28960	PL78_13180	4.61	SpeF, ornithine decarboxylase	E	ANI30770
PL78_01175	-3.7	EhuC, amino acid ABC transporter permease	E	ANI28455	PL78_14800	4.28	CueO. Cu-oxidase 4	P	ANI31086
PL78_07825	-3.59	HslU, ATP-dependent protease ATP binding subunit	O	ANI29729	PL78_17820	3.75	putative delta-1-pyrroline- 5-carboxylate dehydrogenase	E	ANI31668
PL78_17417	-3.58	AraC, family transcriptional regulator	K	NA	PL78_13175	3.74	PotE, putrescine transporter	E	ANI30769
PL78_10260	-3.53	SstT, serine/threonine transporter	E	ANI30204	PL78_17790	3.35	FliA, flagellar biosynthesis protein (sigma factor)	K	ANI31662
PL78_11440	-3.52	TauB. taurine transporter ATP-binding subunit	P	ANI30433	PL78_02115	3.25	XylG, sugar ABC transporter ATP-binding protein	G	ANI28632
PL78_07820	-3.4	HslV, ATP-dependent protease subunit	O	ANI29728	PL78_02110	2.94	XylF, sugar ABC transporter substrate-binding protein	G	ANI28631
PL78_02970	-3.32	amino acid transporter	E	ANI28802	PL78_02120	2.94	MglC, beta-methylgalactoside transporter permease	G	ANI28633

Down-regulated					Up-regulated				
PL78_13725	-3.3	DnaJ, molecular chaperone	O	ANI30875	PL78_17710	2.86	FliJ, flagellar type 3 export apparatus protein	N	ANI31646
PL78_16540	-3.27	HisJ, histidine ABC transporter substrate-binding protein	E	ANI31420	PL78_11000	2.85	LamB, maltoporin	G	ANI30352
PL78_11325	-3.12	RplD, ribosomal protein L4	J	ANI30410	PL78_17795	2.82	FliZ, flagellar biosynthesis protein		ANI31663
PL78_08445	-3.08	Acs, acetyl-CoA synthetase	I	ANI29851	PL78_01595	2.71	GalM, galactose-1-epimerase	G	ANI28529
PL78_11315	-3.08	RplB, ribosomal protein L2	J	ANI30408	PL78_01605	2.66	GalT, galactose-1-phosphate uridylyltransferase	G	ANI28531
PL78_11305	-3.07	RplV, ribosomal protein L22	J	ANI30406	PL78_16930	2.60	OmpC, porin	M	ANI31498
PL78_11335	-3.06	RpsJ, ribosomal protein S10	J	ANI30412	PL78_17620	2.58	FlgC, flagellar basal body rod protein	N	ANI31628
PL78_02090	-3.05	MFS transporter	G	ANI28627	PL78_17625	2.57	FlgD, flagellar basal body rod protein	N	ANI31629
PL78_11320	-3.03	RplW, ribosomal protein L23	J	ANI30409	PL78_15940	2.57	NanA, N-acetylneuraminate lyase	E	ANI31308
PL78_11330	-3.01	RplC, ribosomal protein L3	J	ANI30411	PL78_11945	2.54	cyclic-guanylate-specific phosphodiesterase	T	ANI30534
PL78_11310	-2.99	RpsS, ribosomal protein S19	J	ANI30407	PL78_17635	2.54	FlgF, flagellar basal body rod protein	N	ANI31631
PL78_11300	-2.97	RpsC, ribosomal protein S3	J	ANI30405	PL78_00115	2.48	lysozyme	M	ANI28245
PL78_06675	-2.95	FadE, acyl-CoA dehydrogenase	I	ANI29524	PL78_01610	2.43	GalE, UDP-galactose-4-epimerase	M	ANI28532
PL78_08450	-2.91	membrane protein	S	ANI29852	PL78_01845	2.42	ABC-type phosphate/phosphonate transport system, permease component	P	ANI28579
PL78_11895	-2.9	oligopeptidase A	E	ANI30524	PL78_17615	2.36	FlgB, flagellar basal body rod protein	N	ANI31627
PL78_08965	-2.88	GspD, Type II secretory pathway	U	ANI29948	PL78_02105	2.35	ccpA DNA-binding transcriptional regulator, LacI/PurR family	K	ANI28630
PL78_11295	-2.83	RplP, ribosomal protein L16	J	ANI30404	PL78_03470	2.30	SppA, signal peptide peptidase A	O	ANI28901
PL78_08325	-2.77	FxsA, exclusion suppressor	R	ANI29828	PL78_09225	2.30	lipoprotein Rz1 precursor		ANI29999
PL78_01165	-2.74	ArtP, arginine transporter ATP-binding subunit	E	ANI28453	PL78_17705	2.28	FliK, flagellar hook-length control protein	N	ANI31645
PL78_03735	-2.73	Yen7, transcriptional regulator	(K)	ANI28951	PL78_17640	2.28	FlgG, flagellar basal body rod protein	N	ANI31632

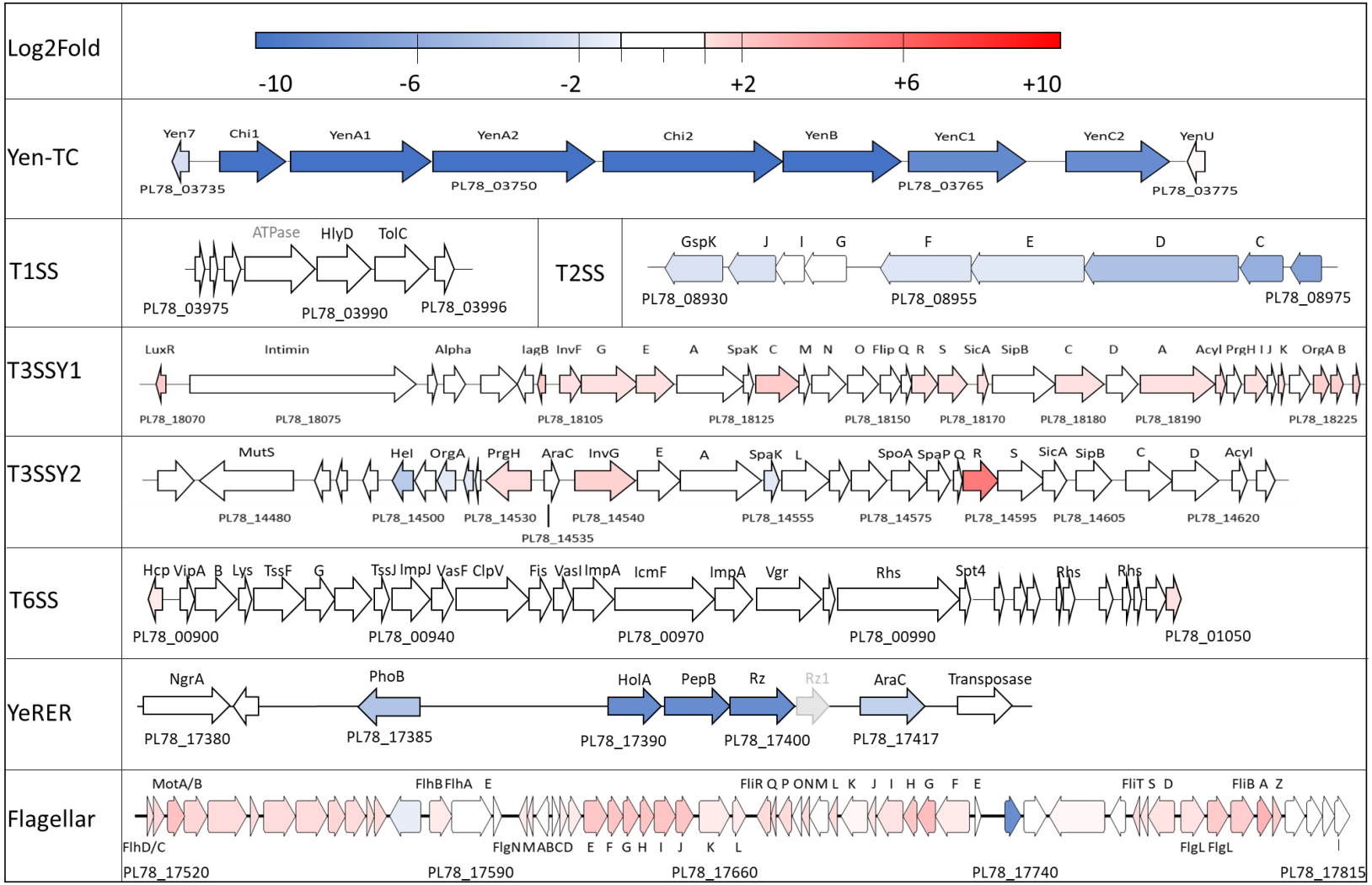

Figure 43: Schematic log2fold change of transcription levels of genes encoding for Yen-TC and secretion systems in the *roeA*-mutant, KTMS12, derived from transcriptome data. Downregulated genes in blue gradient, upregulated genes in red gradient. All non-significantly expressed genes or log2<1 are indicated in white. Grey arrow denotes gene not annotated in the library used for transcriptome data.

Inactivation of RoeA leads to downregulation of the Yen-TC cluster with up to 1000 fold change (Chi1,2; YenA1,2; YenB) (Fig. 43). The second most down-regulated gene in the *roeA* mutant is the gene on locus PL78_05495 encoding for the peptidase M66. Peptidases of the class M66 are metalloprotease often with zinc as a co-factor. The M66 homolog StcE in *E. coli* (EHEC) O0157:H7 is a virulence factor contributing to cell adhesion to the host cell (Hews *et al.*, 2017).

Furthermore, in *Y. entomophaga* KTMS12, the cluster encoding for the prophage genes (PL78_09145 – PL78_ 09335) are strongly up-regulated compared to wild type MH96. Within the cluster, its own transcriptional regulator XerD (PL78_09335) is up-regulated 4096 fold, being one of the strongest up-regulated genes in the KTMS12 genome. Interestingly, the *roeA* mutant shows down-regulation of stress-related proteins such as cold and heat-shock proteins and ribosomal proteins. The *roeA* mutant also showed a decrease in transcript levels of the genes encoding the chaperons DnaKJ, ClbP, GroEL, and GroES. The GroEL/GroES complex forms a molecular machinery that assists in the proper folding of proteins and therefore prevents aggregation of non-functional proteins within the cell (Hayer-Hartl *et al.*, 2016). Guisbert *et al.* (2004) described how a GroEL/S mutant increased sigma23 activity, which is also known to be controlled by the DnaK chaperon. Both GroEL/S and DNaJ/K were down-regulated in KTMS12, but none of the known sigma factors were differently expressed in KTMS12.

The *roeA* mutant KTMS12 and K18 showed strong abolition of protein secretion. Furthermore, cell pellets in SDS-PAGE lacked Yen-TC bands. This indicates the regulatory effect of RoeA on the Yen-TC complex, protein folding, or transcription of secretion systems. An additional focus of transcriptome analysis is the documented *Y. entomophaga* secretion systems (Fig. 43). The transcriptome data of the *roeA* mutant showed no significant differential expression of the secretion systems T1SS, T3SS, and T6SS (Fig. 43). However, the genes *gspCDEFJK* of the T2SS were down-regulated. Pertinent to this study, a mutation in *roeA*, KTMS12 down-regulated the expression of the YLC components and the YeRER genes (Fig. 43).

Swarming motility assay

In Chapters 6.2.2 and 6.2.3, the results of transcriptome analysis of KTMS12 revealed an increase in flagellar protein transcription and the presence of flagellar proteins in the supernatant as observed by SDS-PAGE (Fig. 35; Chapter 6.2.6). Contradictory to these results is the absence of visible flagella in TEM analysis (Fig. 36; Chapter 6.2.6). Cell motility benefits *Y. enterocolitica* cell invasion into host cells (Young *et al.*, 2000). To investigate motility in MH96 and the *roeA* mutant strains KTMS12 and K18, both swarming and swimming motility plate assays were performed in triplicate (Fig. S8).

Swimming motility, which was assessed by water agar plate assay where the plate was stabbed with a cell colony, did not reveal any motility. The swarming motility plates, where the cell culture was applied on top of the agar plate, showed differences in cell migration between the wild type strain MH96 and the *roeA* mutant strain KTMS12 (Fig. 44).

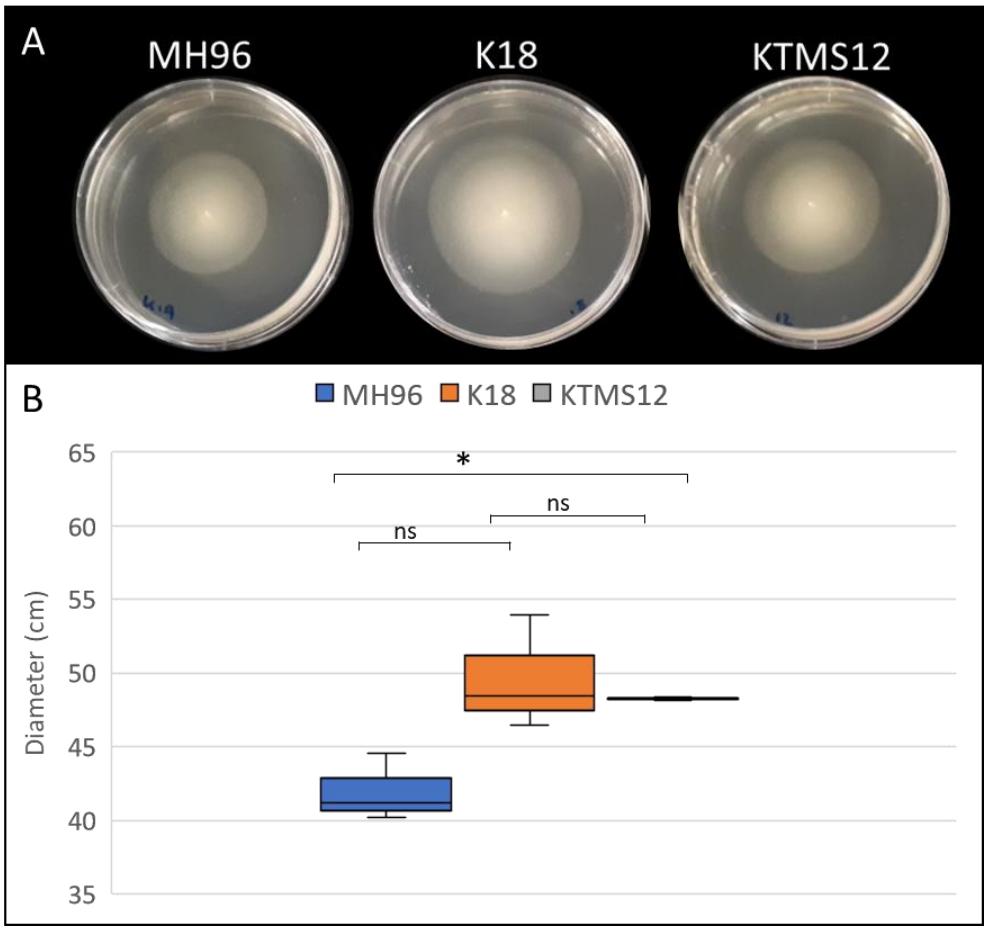

Figure 44: Swarming motility plate assay of the wild type strain M96 and the *roeA* mutant strains K18 and KTMS12. *A)* Photographs of swarming motility assay on 0.4% LB-agar plate using 2 µl per sample aliquoted onto the agar and incubation for 24 h at 25°C. Representative plates are shown, each assay was performed in triplicate. B) Bar plot of the measured diameter of the spreader cells. Indicated are mean, and distribution. Asterisk denotes $p<0.05$, ns denotes not significant. Significance calculated by 2-tailed, unpaired t-test.

The plate assay shows increased bacterial movement in K18 and KTMS12, which could be explained by the increased transcription of flagellar protein and the detached flagellar-like structures observed in the K18 cell culture. The strong shaking of the cell cultures can cause membrane-bound proteins such as flagella or fimbriae to break off and accumulate in the supernatant. Given the observations that the *roeA* mutant strain KTMS12 showed increased CFUs at 16 h compared to wild-type strain MH96 and the flagellar-like structures in the supernatant observed by TEM in both KTMS12 and MH96, it is likely that the increased colony diameter in the plate assay could be a result of increased bacterial motility in KTMS12 or a result of spreading by growth.

Summary on the potential role of the secretion regulator RoeA

The *roeA* mutant KTMS12, identified using the HESA shows decreased exoproteome release (Chapter 4.3). A complete deletion of *roeA* was not cloneable and gene-disruption in MH96Δ*roeA* encoding a 53 aa RoeA-truncation did not alter the exoproteome release. In KTMS12, RoeA is truncated to 46 aa residues lacking the α2 helix, part of the HTX-motif similar, which shows homology to HTX-motifs of PhoB-like proteins. The absence of the α2 leads to a severe decrease of the RoeA-dependent exoproteome release, indicating the role of α2 of RoeA in DNA-binding. Inactivity of RoeA, as seen in KTMS12 leads to a global effect on transcription and results in decreases exoproteome release. Exoproteome release could only partially be restored by *trans* complementation of the entire YeRER. In contrast, the *trans* complementation of YeRER in MH96 nearly abolished exoproteome release at 16 hpi, but not at 24 hpi, indicating a growth phase-dependent regulation of the YeRER derived exoproteome release.

LC-MS data of K18 identified the release of flagellar proteins indicating increased motility, which was confirmed by elevated transcript levels of flagellar genes and a significant increase of motility assessed by motility plate assay. Based on the same exoproteome profile in SDS-PAGE of the other *roeA* mutant KTMS12, it is to assume that KTMS12 exoproteins are the same as in K18.

Transcriptome data of KTMS12 indicate that the PL78_17385 encoding protein RoeA acts as a transcriptional regulator affecting a wide range of genes involved in translation and likely post-translational processes, metabolic pathways, cell motility, and defence mechanisms. Because of its broad gene regulation within the genome, RoeA can be classified as a global regulator in *Y. entomophaga*.

Bioinformatic analysis indicated regulation of *roeA* by other global regulators, H-NS and Hfq. Interestingly, many differently expressed genes in the *roeA* mutant could also be observed in the QS mutant KTMS23. RoeA does not directly regulate either AHL synthetase or the QS sensing protein

PL78_03845. Yet, QS and *roeA* mutants share regulatory pathways, such as upregulation of flagellar proteins and the MH96 prophage and downregulation of stress response gene, ribosomal proteins, the Yen-TC complex, and the YLC. Differential gene expression of stress response genes and motility genes in both KTMS12 and KTMS45 (QS mutant) indicate a role of RoeA in cell response to environmental changes, similar to that of QS.

It is noteworthy that RoeA regulates many other transcriptional regulators (Table S6 and S5) suggesting a complex pathway involved in protein secretion. It is therefore difficult to assess the direct effect of RoeA. Additionally, of the 49 identified genes (excluding *roeA*) in the HESA that are involved in protein secretion, only the YLC *holA* gene was significantly differentially expressed within the *roeA* mutant (Table S7). Further studies are required to assess genes, specifically involved in protein translocation and secretion, that are under direct regulation by RoeA or its MH96 Yen7 orthologue. The absence of Yen-TC toxin secretion in the *roeA* mutant also occurs in wild-type strain MH96 at higher temperatures such as 37°C (Hurst *et al.*, 2016). RoeA regulates other genes such as DNAJ/K and GroEL, known to be temperature-dependent. It is therefore likely that temperature is a modulating factor of RoeA response.

6.3.3 Characterisation of the *Y. entomophaga* lysis cassette

To characterise the YLC of *Y. entomophaga* MH96, the lysis cassette was overexpressed in the arabinose inducing vector (pARA) to test for lysis capability of the YLC encoded proteins as described below. Subsequently, the YCL was mutated and its role in exoproteome release was further investigated. Therefore, *trans* complementation of the YeRER were used to test if exoproteome release can be restored.

Overexpression of the *Y. entomophaga* MH96 native lysis cassette YLC

The overexpression of the native MH96 lysis cassette YLC, encoding for *holA*, *pepB,* and *rz*, using the vector pARA-HML (Fig. 45B), was tested in *E. coli* DH10β by observing the culture for culture clearing post-induction of pARA-HML with arabinose (0.2%). No culture clearance in *E. coli* DH10b was observed (data not shown). To remove the possibility of a MH96 specific system, pARA-HML was transferred into *Y. entomophaga* MH96 to assess lysis is the native strain.

Overexpression of the pARA-HML did not cause cell lysis of MH96 (Fig. 45). After inducing MH96 pARA-HML at an OD of 1 the OD remained at 1 until 30 min post-induction (with water only control), from where it increased over time and reached a final OD of 4.5 after 16 h. The uninduced sample of pARA-HML, slightly increased over time with a final OD of 3 at 16 h post-induction. This experiment was only performed once in 50-ml as an initial assessment of lysis and therefor needs to be repeated.

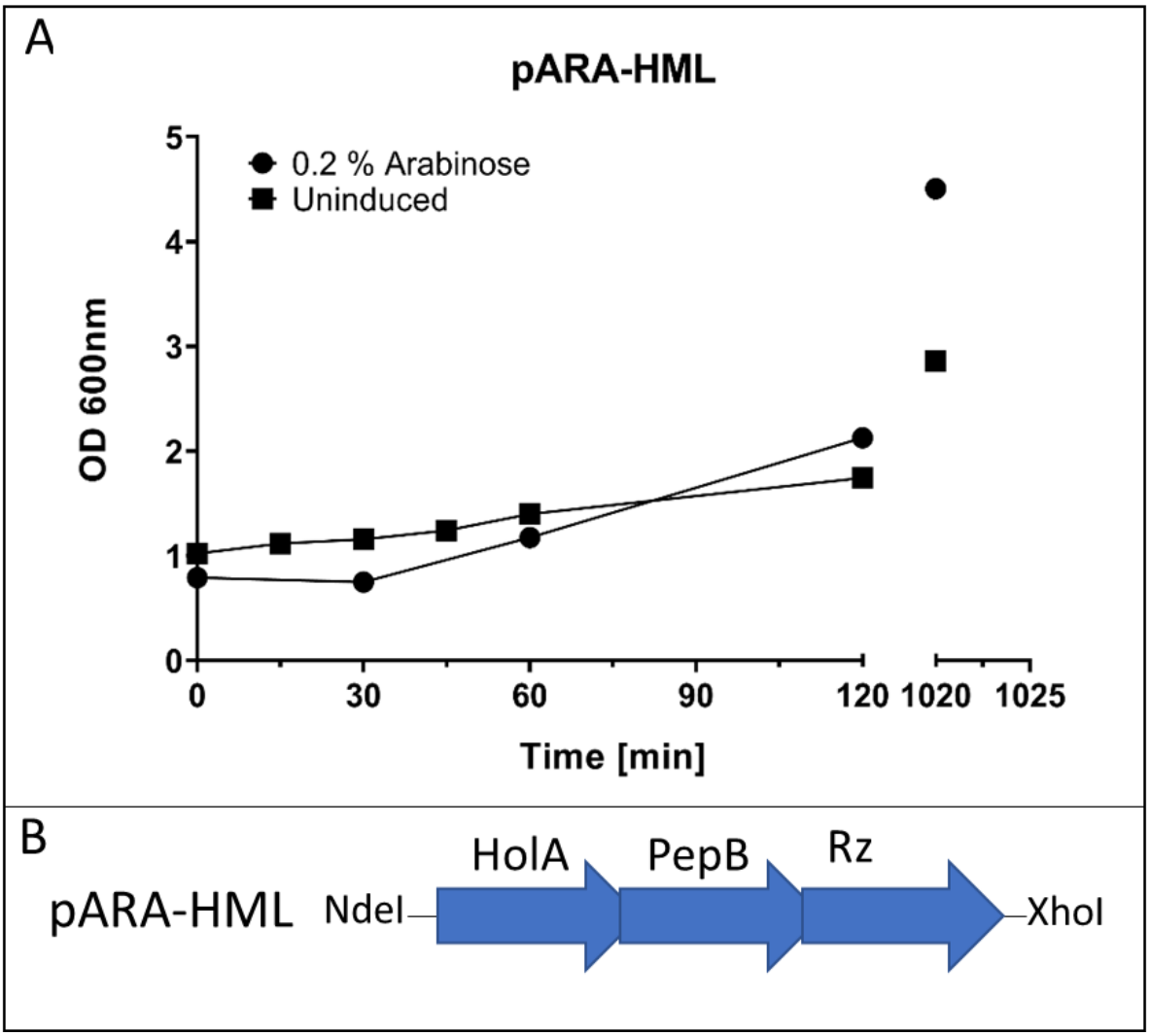

Figure 45: Overexpression of pARA-HML. *A)* Cell growth measured in OD, of MH96 pARA-HML induced (0.2% arabinose) and uninduced (0% arabinose) show no significant difference between the samples. Cell culture were grown in 50-ml broth until OD_{600} of 1 was reached, before induced with arabinose. *B)* Schematic of the native YLC as used in pARA-HML.

Overexpression of optimised lysis cassette constructs

Based on the absence of cell lysis through the expression of pARA-HML a synthetic variant (pARA-LK) was constructed (Chapter 6.2.8) wherein the ORFs, and their associated ribosomal binding sites, were separated from each other (Fig. 46F), allowing the successive expression of the YLC associated ORFs. As an initial test of the functionality of the induction plasmid pARA-LK, *E. coli* DH10β cells harbouring pARA-LK were induced with arabinose (0.2%) and observed for culture clearance. Culture clearance was visible 30min post-induction in *E. coli* DH10b (data not shown). As control DH10β pARA-LK was not induced and did not show visible culture clearance (data now shown). The vector pARA-LK was then assessed in *Y. entomophaga* MH96. Furthermore, to define the function of the potential fourth gene, *rz1*, the construct pARA-LK-Rz1 was also used in MH96.

In. *Y. entomophaga* MH96 pARA-LK, 15 min after the arabinose induction (0.2%), the cell density decreased sharply from OD 1 to OD 0.1, which was also visible in the clearance of the cell culture (Fig. 51B), resulting in almost complete cell lysis within less than 30 min of induction (Fig. 46). After 24 h the culture growth recovered to an OD = 2, after which none of the cells grew on LB agar plates with ampicillin but cells were recovered on LB agar without antibiotics. The absence of plasmid-bearing cells at 24 hpi (indicated by loss of ability to grow on ampicillin) suggests the expression of the lysis cassette is detrimental and results in plasmid loss. This would be compounded by the cleavage of ampicillin in the medium by the initially present plasmid-bearing strains allowing cells with no plasmid to survive at 24 hpi. Through the addition of the arabinose araC suppressor glucose, the glucose-treated cells grew until OD = 2 after 30 min and did not reach OD >3 after 24 h, due to lowered nutrients in 40% LB broth.

To define the function of the potential fourth gene, *rz1*, the construct pARA-LKRz1 was induced in MH96. Culturing of this construct in uninduced media (0% arabinose) strongly inhibited the growth. To decrease leakiness of pARA, and to inhibit the plasmid-derived gene expression for improved growth of the starter cell, 100% LB with 0.2% glucose was used in this experiment. Once grown to OD=1 the culture was induced with an arabinose concentration of 0.2%. Similar, to pARA-LK, cell lysis of MH96 pARA-LKRz1 occurred rapidly within 15 min (Fig. 46) post-induction, which was visible by in culture clearance 2 h post-induction (Fig. 46 DE). In contrast to pARA-LK, induction of the lysis cassette harbouring Rz1 showed no increase of OD of MH96 after 16 h. In these experiments, the control MH96 harbouring the empty pARA vector induced under the same conditions did not decrease in OD (data not shown).

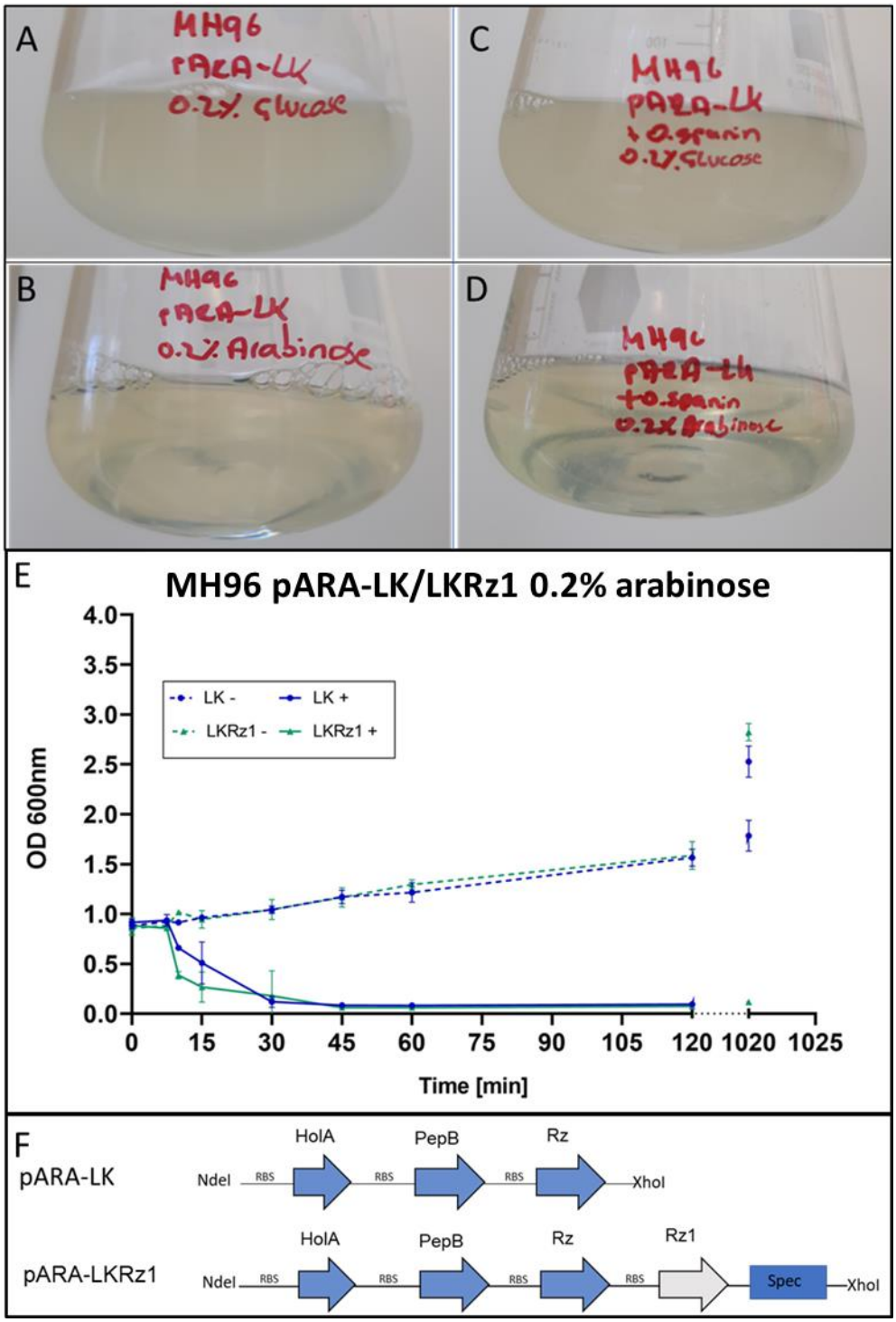

Figure 46: Induction of lysis cassette variations in MH96. Two different variants of the YLC were cloned into pARA and induced with 0.2% (+) or with 0.2% glucose (-) as transcription activation and inhibition, respectively. Culture flask of pARA-LK and pARA-LKRz1 at 4 h post-induction with 0.2% arabinose and 0.2% glucose in MH96. A) Culture flask of repressed pARA-LK with 0.2% glucose. *B)* Culture flask of induced pARA-LK with 0.2% arabinose. *C*) Culture flask of repressed pARA-LKRz1 with 0.2% glucose. *D)* Culture flask of induced pARA-LKRz1 with 0.2% arabinose. *E)* Optical density of MH96 with pARA-LK and pARA-LKRz1 upon induction (0.2% arabinose) and repression (0.2% glucose) of the plasmids, measured over time. *F)* Schematic of gene arrangement in pARA-LK and pARA-LKRz1: LK – optimized frame of *holA, pepB, rz,* and LKRz1 – optimized frame encoding *holA, pepB, rz, rz1*.

In summary, induction of the native lysis cassette potentially causes mild lysis activity resulting in an initial lag of cell growth. The gene arrangement of *holA* and *pepB* leads to an overlapping stop (*holA*) and start (*pepB*) codon, which likely leads to a translational coupling, termed termination-reinitiation (TeRE) (Huber *et al.*, 2019). Hereby, the expression and translation of *holA* results in the integration of holins within the inner membrane and multimerization of the holins forming holin-rafts, a process which decreases the proton motor force (White *et al.*, 2011). Eventually, the holins form a hole in the IM. Due to frameshift of the *pepB*, it is possible that its translation does not occur in pARA-HML, therefore the absent endopeptidase does not lyse the cells. It is possible that activation of the lysis genes requires an activator binding to 5' of YLC, which in return also needs to be overexpressed. Yet, severe cell lysis results in overexpression of optimized lysis cassette with and without the entire spanin complex (RzRz1). The induction of the entire lysis cassette including i- and o-spanins results in rapid cell lysis.

Morphological changes caused by overexpression of the lysis cassette

To understand the mechanistic effect of cell lysis, cell cultures MH96 with pARA empty, pARA-LK, and pARA-LKRz1 were assessed using Live-cell imaging in collaboration with Miki Feldmüller from the Pilhofer Laboratory at the ETH Zurich.

Live-cell imaging of pARA-LK and pARA-LKRz1 revealed a heteromorphic cell culture with cells of MH96-like rods, elongated rods, and filamented cells in all samples in different proportions within cultures. As expected, induction of the empty pARA caused no visible changes within cells during 20 min of imaging (Fig. 47A). To exclude the potential for late lysis, cells harbouring pARA only were also assessed 40 min post-induction with no visible change observed (Fig. S9). Induction of pARA-LK led to both cell elongation and bulging (15 min) before cells lysed (20 min) (Fig. 47B). In pARA-LKRz1 morphological changes in induced cells were already visible after 1 min. Many elongated cells were visible, and one to three "holes" were observed, most often but not only in elongated cells (Fig. 48). Within less than 5 min these "holes" were filled and cells started to elongate at the poles (10 min), which appeared brighter than the rest of the cells. After cell elongation, the bacterial cells started to lyse/ fade away (12 min). In some instances, budding of vesicles was observed.

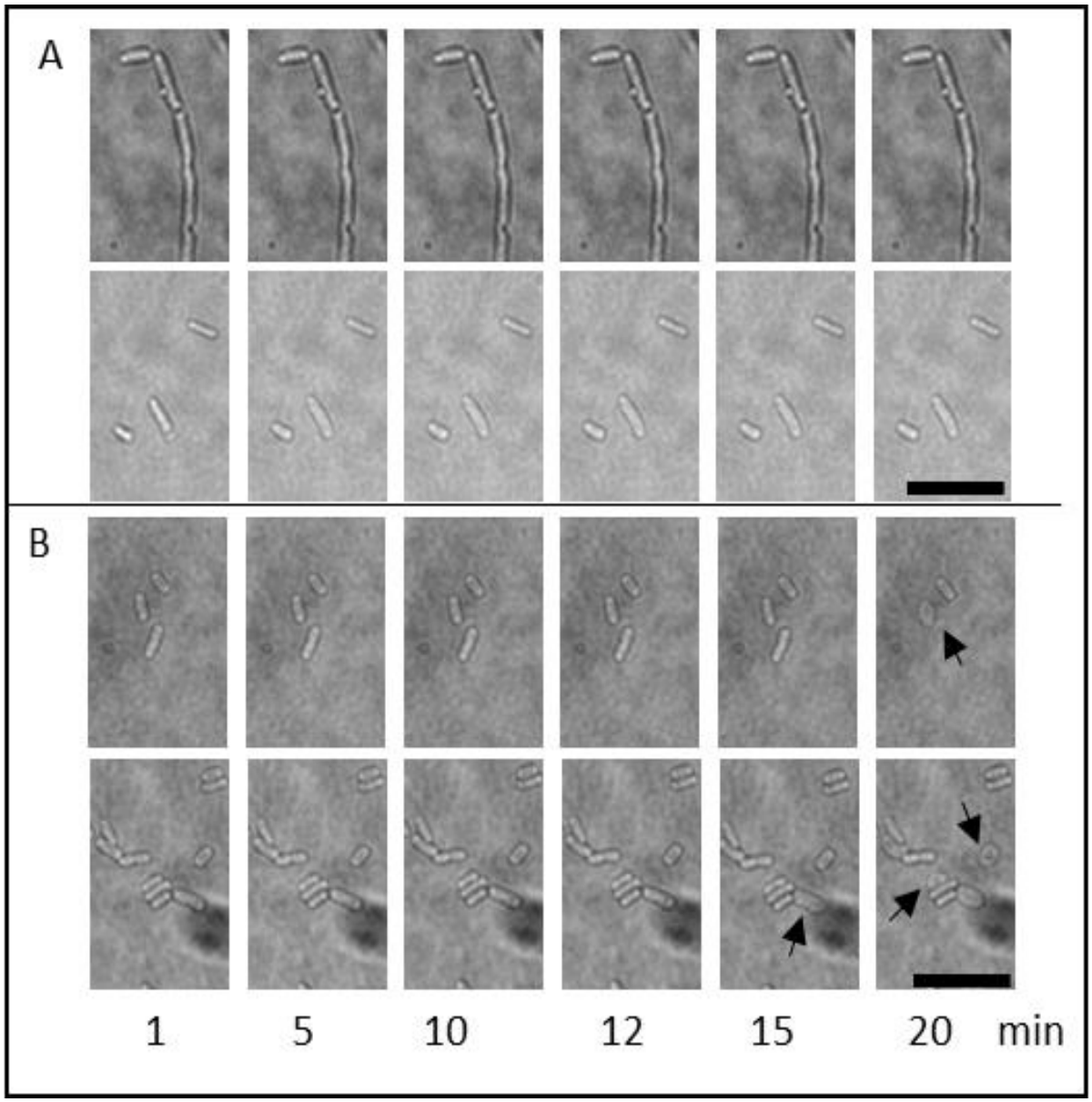

Figure 47: Live-cell imaging of induced lysis in MH96. All cells were grown with OD= 1 and the arabinose inducing vector pARA with different inserts was induced with 0.6% agarose and immediately pipetted on agarose patch and place for Live-cell imaging within 1 min. A) Induction of the empty pARA vector in MH96 as a negative control. B) Induction of pARA with insert LK containing encoding region *holA, pepB, rz*. AB) Black bar denotes scale of 10 µm. Live-cell imaging was undertaken in collaboration with Miki Feldmüller of the Pilhofer laboratory at the ETH Zurich. Black arrows indicate bulging cells.

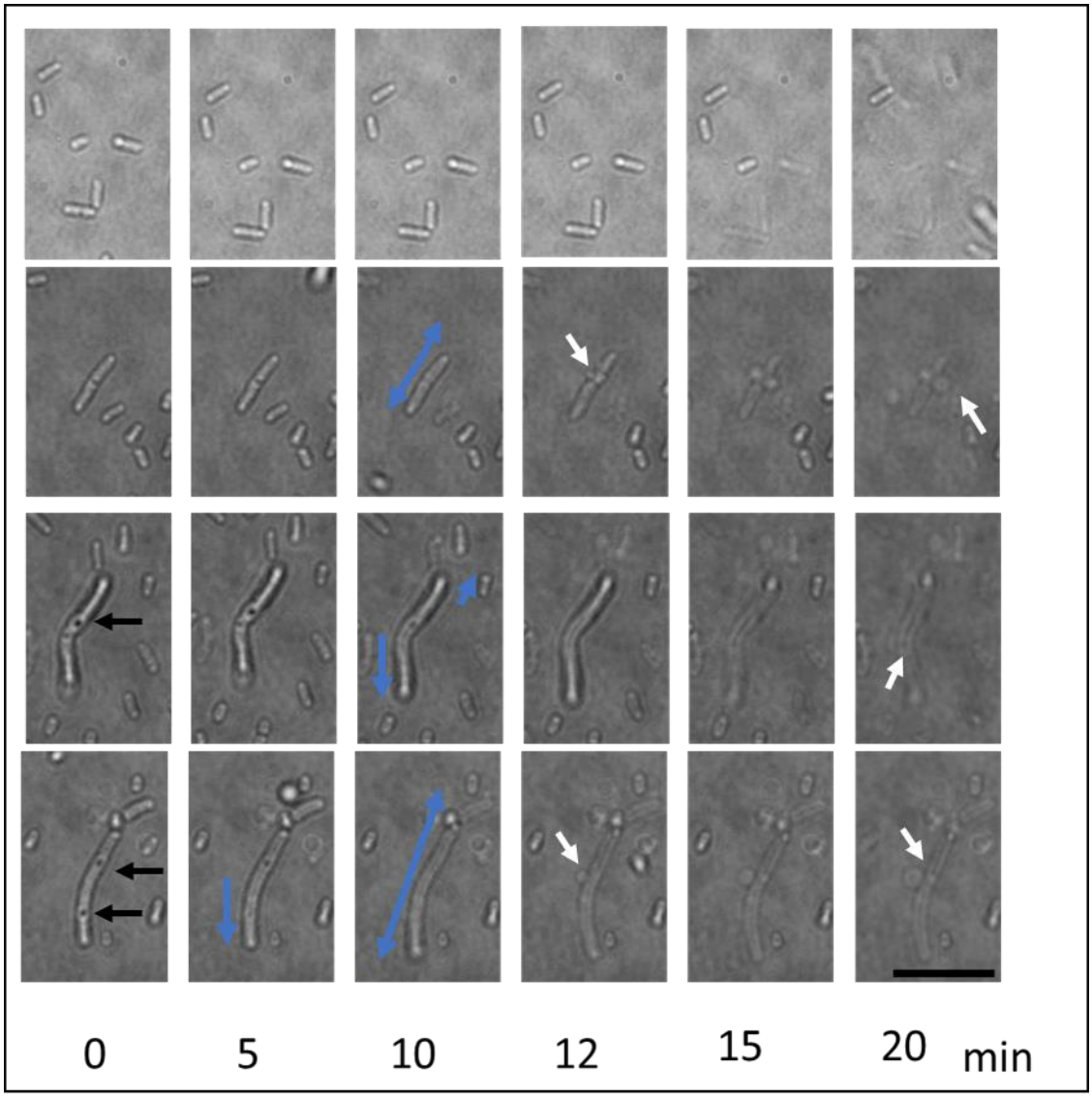

Figure 48: Live-cell imaging of pARA-LKRz1 induction in MH96. Induction of pARA with insert Lk-Rz1, encoding region *holA, pepB, rz, rz1*. The experiment was done twice and representative areas are depicted. Black arrows denote pore formation in MH96 cell wall. Blue arrows denote directed elongation of the cell. White arrows denote vesicle blebbing Live-cell imaging undertaken in collaboration with Miki Feldmüller of the Pilhofer laboratory at the ETH Zurich. Black bar denotes scale of 10 µm.

Characterisation of the YLC mutant

To understand the role of the lysis cassette in protein secretion, YLC was mutated and the gene cluster *holA-pepB-rz* was replaced with a kanamycin cassette from MH96ΔYLC as outlined in Chapter 2.2.12 (Construction of deletion mutants).

To determine if the YLC mutant differs in cell growth and cell shape compared to MH96, MH96ΔYLC and MH96 were independently grown in 50-ml LB broth for 16 h at 25°C and 200 rpm shaking. Cell culture of the MH96ΔYLC was compared to MH96 in cell density, cell numbers, and cell morphology,

and protein secretion using light microscopy and SDS-PAGE. SDS-PAGE showed that deletion of MH96 YLC resulted in the abolition of protein secretion and a change in cell morphology. Under light microscopy it was noted that in *Y. entomophaga* wild type MH96 cells were highly motile whereas MH96ΔYLC was non-motile. Despite the morphological changes in MH96ΔYLC, observed by light-microscopy (Fig. 49A), cell numbers and cell density were similar to MH96 between 1×10^9 and 1×10^{10} CFU/ml. Additional analysis through collaboration with Miki Feldmüller (ETH Zurich) in the final stages of the research using electron cryo-tomography (Titan Krios; FEI), revealed that the MH96ΔYLC produced filamentous elongated cells up to 10-fold longer (10 µm) than average-sized MH96 cells. Voids visible in the MH96 outer membrane and membrane blebbing were not observed in MH96ΔYLC, revealing YLC-likely underpins this process (Fig. 49B and C). The observation of elongated MH96ΔYLC cells by Cryo-ET, showed an intact cell wall, which indicates that the cell elongation did not cause cells to lyse.

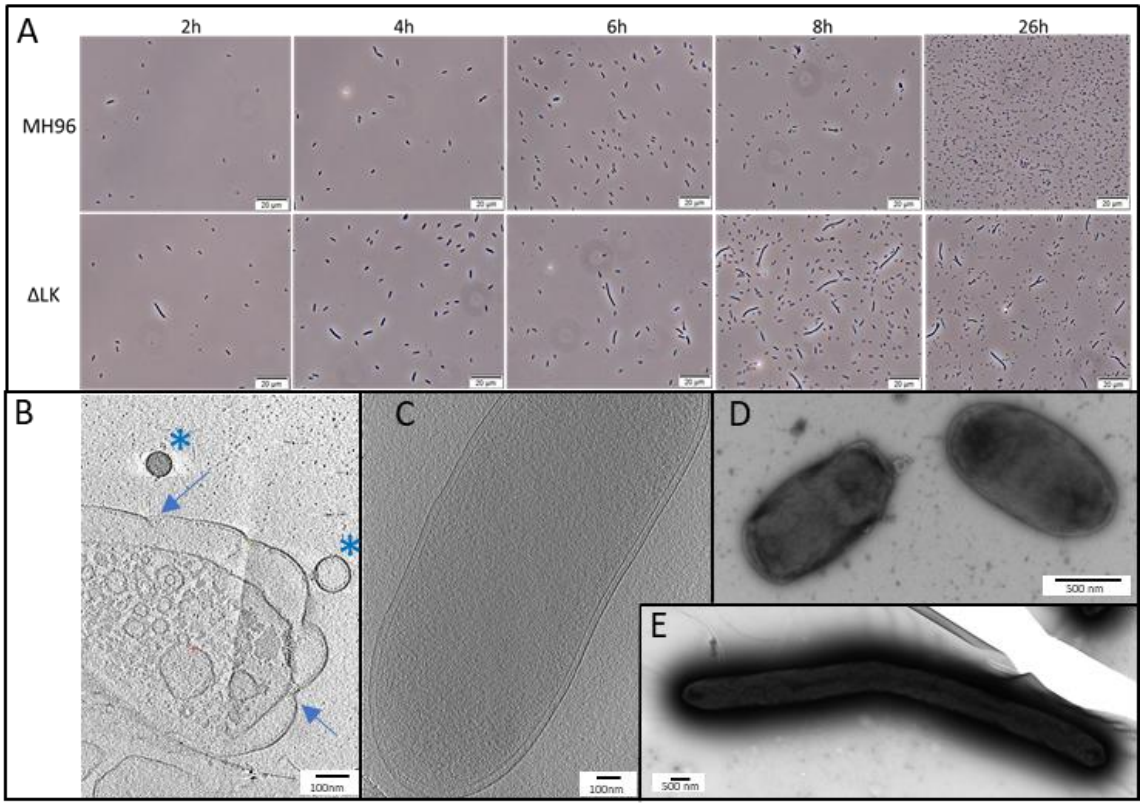

Figure 49: Morphology of *Y. entomophaga* MH96 and MH96ΔYLC. *A)* Light microscopy of MH96 and MH96ΔYLC. Scale bar indicates 20 µm. *B, D)* Electron micrographs of MH96 after 16 h incubation of 50-ml cell culture. Arrow indicating voids in the outer membrane, asterisks indicating membrane vesicles. *C, E)* Electron micrographs of MH96ΔYLC from 50-ml cell culture at 16 hpi. Scale bars are indicated.

In addition, using LIVE/DEAD staining of MH96 and MH96ΔYLC cells, showed a decreased ratio between intact and lysed cells in MH96ΔYLC with ca. 1% dead cells compared to 18 % in MH96 (Fig.

50). For this experiment, 90-100% of cells were stained by LIVE/DEAD stain. It is of note that with MH96 background fluorescence under phyco red filter was very strong in the 16 hpi sample, compared to MH96ΔYLC. Propidium iodide (PI), a component of the LIVE/DEAD stain, binds double-stranded DNA and can only diffuse through damaged cells, where it emits red light. One dye molecule of PI binds four to five base pairs enhancing DNA fluorescence. Externalized DNA, eDNA, which is either secreted or externalized by cell lysis, can lead to high background fluorescence using PI as seen for MH96 in Fig. 50 (Okshevsky and Meyer, 2015; Stiefel *et al.*, 2015; Feng *et al.*, 2018). It is therefore likely, that MH96 background fluorescence results in DNA accumulation in the culture, caused by MH96 cell lysis or leakage.

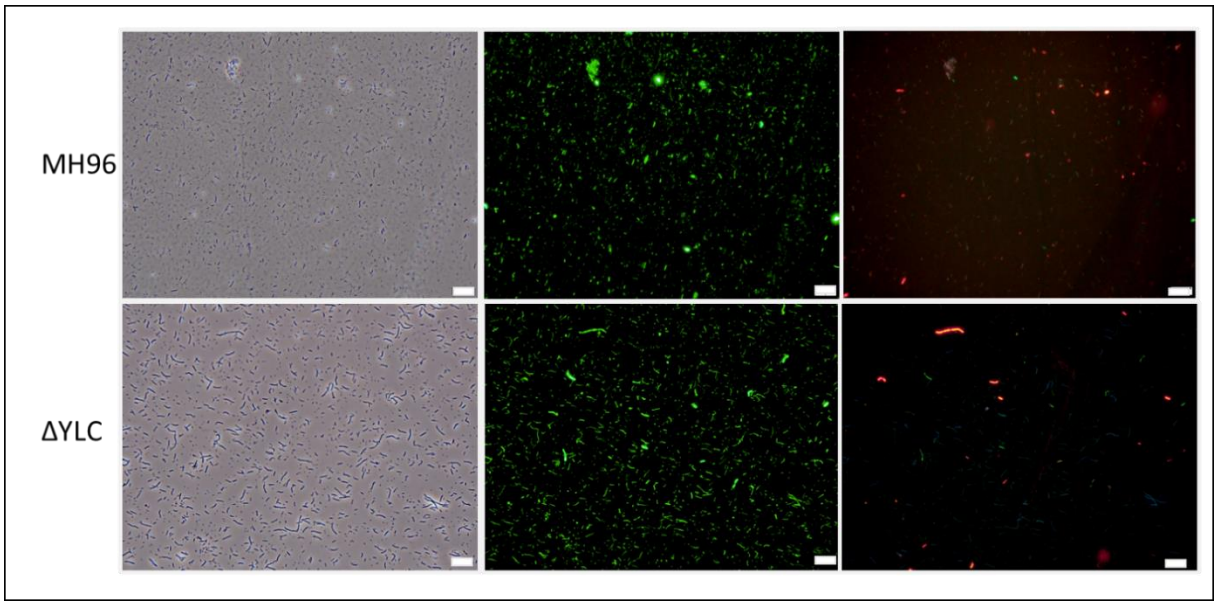

Figure 50: LIVE/DEAD staining of MH96 and MH96ΔYLC at 16 hpi using light (phase contrast) and fluorescent microscopy. Light microscopy of *Y. entomophaga* MH96 cells compared to MH96ΔYLC (left panels). MH96 cells seen as single rod-shaped bacteria, while elongated cells visible in MH96ΔYLC. LIVE/DEAD stained MH96 and MH96ΔYLC under GFP-UV filter (middle panel) and under DAPI filter (right) panel. White scale bar = 20 µm.

In the following Chapter, complementation of the MH96ΔYLC will be discussed. In this context, previous results indicated that the native lysis cassette, comprising a series of overlapping ORFs does not cause cell lysis, likely because of incorrect expression of components of the lysis cassette due to overlapping ORFs. However, the deletion of YLC leads to dramatic phenotypical changes in cell morphology and exoproteome production.

In a complementation experiment, the YLC including the entire intergenic region (5' of YLC) was cloned into the mid copy vector pACYC184 as outlined in Chapter 2.4.4.

Trans complementation of MH96ΔYLC with p184INT_YLC restored cell shape and protein secretion (Fig 51A-C) with significant differences in cell morphology, optical density, and cell counts between MH96ΔYLC p184 and MH96ΔYLC p184-INT_YLC (Fig. 51D). The observed increase in cell counts of 1.96 × 10^9 CFU/ml in the *trans* complemented strain (MH96ΔYLC p184INT_YLC) compared to 8.56 × 10^8 CFU/ml in MH96ΔYLC p184 (Fig. 51D) may relate to the restoration of exoproteome release while the accumulation of protein in MH96ΔYLC p184 and production of elongated cells (Fig. 51A-C) is likely detrimental to cell growth. Nevertheless, complementation with p184INT-YLC restores MH96-like cell shape in MH96ΔYLC and restores the exoproteome (Fig. 51A-C).

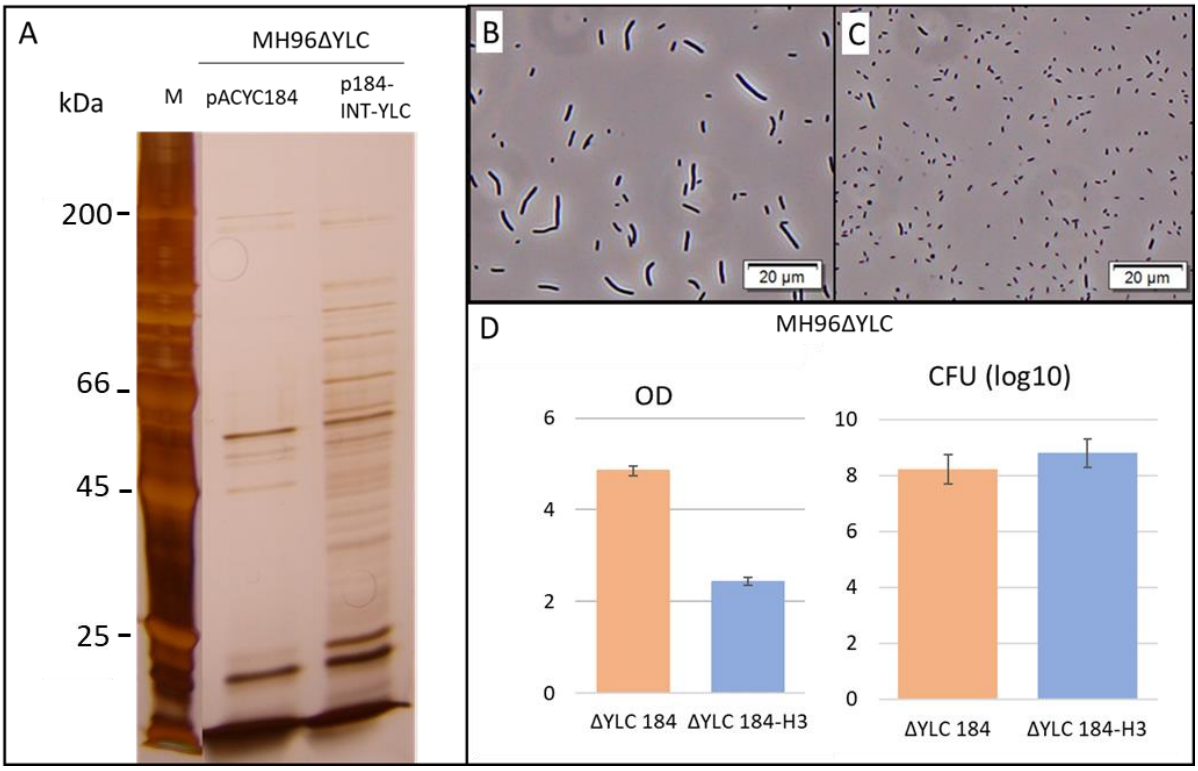

Figure 51: Complementation of YLC and intergenic (INT-YLC) region in MH96ΔYLC using vector pACYC184 of 50-ml cultures at 16 hpi. *A)* SDS-PAGE of culture supernatant of MH96ΔYLC harboring empty pACYC184 and MH96ΔYLC 184-YeRER. M denoted protein marker. *B)* Light microscopy of MH96ΔYLC pACYAC184 at 16 hpi. Scale bar indicated *C)* Light microscopy of MH96ΔYLC 184-H3 at 16 hpi. *D)* Optical density and cell density in CFU/ml measured from 50-ml cultures at 16 hpi in duplicate. Indicate is mean value and SD.

***Trans*- complementation in YLC mutants KTMS4 and MH96ΔYLC**

In the initial HESA experiment, three transposon mutants (KTMS4, KTMS31, and KTMS46) were identified in the *holA* promotor region of the YLC (Chapter 4.3.2). Cells of these transposon mutant strains nearly abolished exoproteome release, and also showed elongated cells (Fig. S10) as it was observed for MH96ΔYLC. As an exemplary sample of the *holA* transposon mutants, KTMS4 was chosen for *trans* complementation of the YeRER, the intergenic region (INT), and its derivates, which was also assessed in MH96ΔYLC. Previous transcriptome data of MH96 and KTMS12 (Chapter 6.2) identified a long *holA* promoter region with indications of binding sites for transcription factors such as PhoB, and through RNAfold analysis, the formation of a regulatory secondary structure. The *trans* complementation was used to test if the YeRER elements, such as ncRNA, and secondary structures, can restore exoproteome release despite the absence of the YLC, indicating an additional secretion mechanism controlled by the YeRER.

The effect of *trans* complementation of the intergenic region in MH96ΔYLC, as constructed previously in Chapter 6.1, was assessed for exoproteome, cell counts, and cell shape (Fig. 52). The MH96ΔYLC pACYC18-Tet and pACYC184-Cm were used as controls for the respective construct. The controls showed low exoproteome concentrations at ~10^9 CFU/ml. Complementation of INT and truncation of INT did not show reduced exoproteome release compared to control pACYC184-Tet (Fig. 52). In contrast, *trans* complementation of MH96ΔYLC with the intergenic region and the YLC genes in p184INT_YLC partially restored wild type phenotype with restored protein secretion (Fig. 52A) The *trans* complementation of pACYC184 constructs showed a non-significant increase in cell counts compared to their respective controls (Fig. 52B). The secretion phenotype of MH96ΔYLC -pACYC184 harbouring INT and INT truncations (but not in INT_YLC) slightly decreased the exoproteome concentration observed by SDS-PAGE (Fig. 52A), and a change in cell morphology, from elongated cells to MH96- like small rods, was observed (Fig. 52C).

Cells of MH96ΔYLC were elongated under standard culturing conditions (Chapter 2.2). *Trans* complementing the intergenic region (p184INT) in MH96ΔYLC restored cell shape to that of wild type strain MH96 with small rod-shaped cells observed. This result was also achieved through *trans* complementation of MH96ΔYLC with p1845'hol, p184ncYLC220, and p184ncYLC637, as well as p184INT_YLC. T*rans* complementation with the intergenic region derived from K18, which harbours a 3 bp deletion 5' of *roeA,* using p184-INT(K18) with MH96ΔYLC, resulted in cell shortening with similar cell length to that of uncomplemented MH96 cells (Fig. 49A). *Trans* complementation of MH96ΔYLC with 5'*roeA* showed no effect in cell size or exoproteome release compared to MH96ΔYLC pACYC184 control.

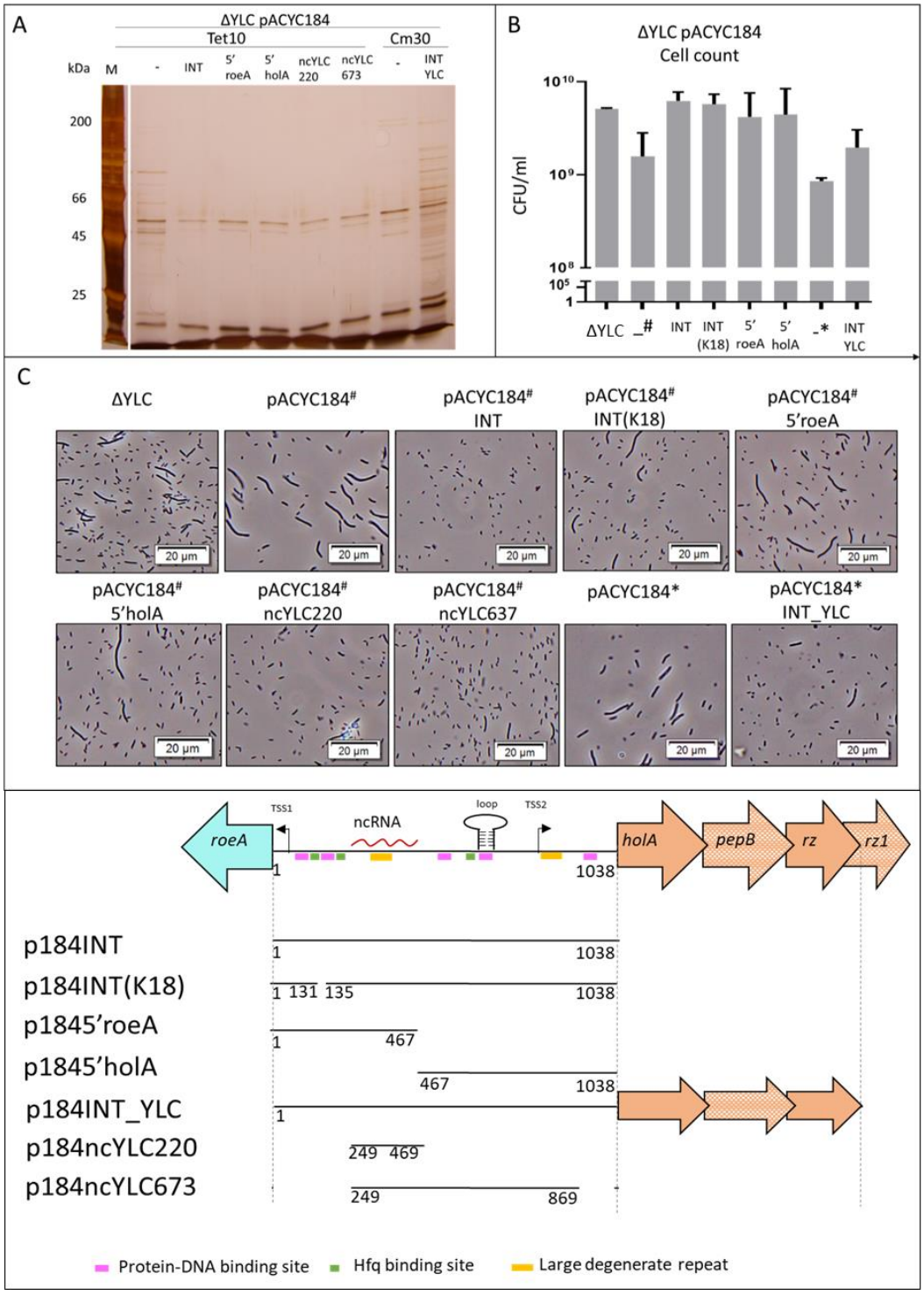

Figure 52: *Trans* complementation of MH96ΔYLC with MH96 intergenic region construct using pACYC184 expression vector. Samples were taken from 50-ml cultures at 16 hpi and incubation at 25°C, 200 rpm shaking. *A)* SDS-PAGE of exoproteome in the supernatant of MH96 YeRER constructs in pACYC184. *B)* Cell density measured in CFU/ml of the construct. Bar denotes the mean of triplicates and error bar denotes standard division. *C)* Representative Light microscopy images in phase contrast of MH96ΔYLC cells *trans* complementation. Of each sample, a representative of triplicates is depicted. – denotes empty control vector. # denotes cells grown in tetracycline (10 µg/ml) and * denotes cells grown in chloramphenicol (30 µg/ml). *D)* Schematic of pACYC184 constructs.

The *trans* complementation of KTMS4 with p184-INT, INT(K18), and INT_YLC decreased cell length of the majority of cells, compared to KTMS4 pACYC184(Fig. 53C). Although cell growth of all strains reached between 10^9-10^{10} CFU/ml (Fig. 53B), similar to MH96ΔYLC, in KTMS4 *trans* complementation with either p184INT, p184-INT(K18), p184-5'*roeA*, p184-5'*holA*, p184-ncYLC220, and p184-ncYLC637 did not alter protein secretion (Fig. 53A), which indicates the relevance of the promoter region YLC, in which the KTMS4 transposon insertion is located.

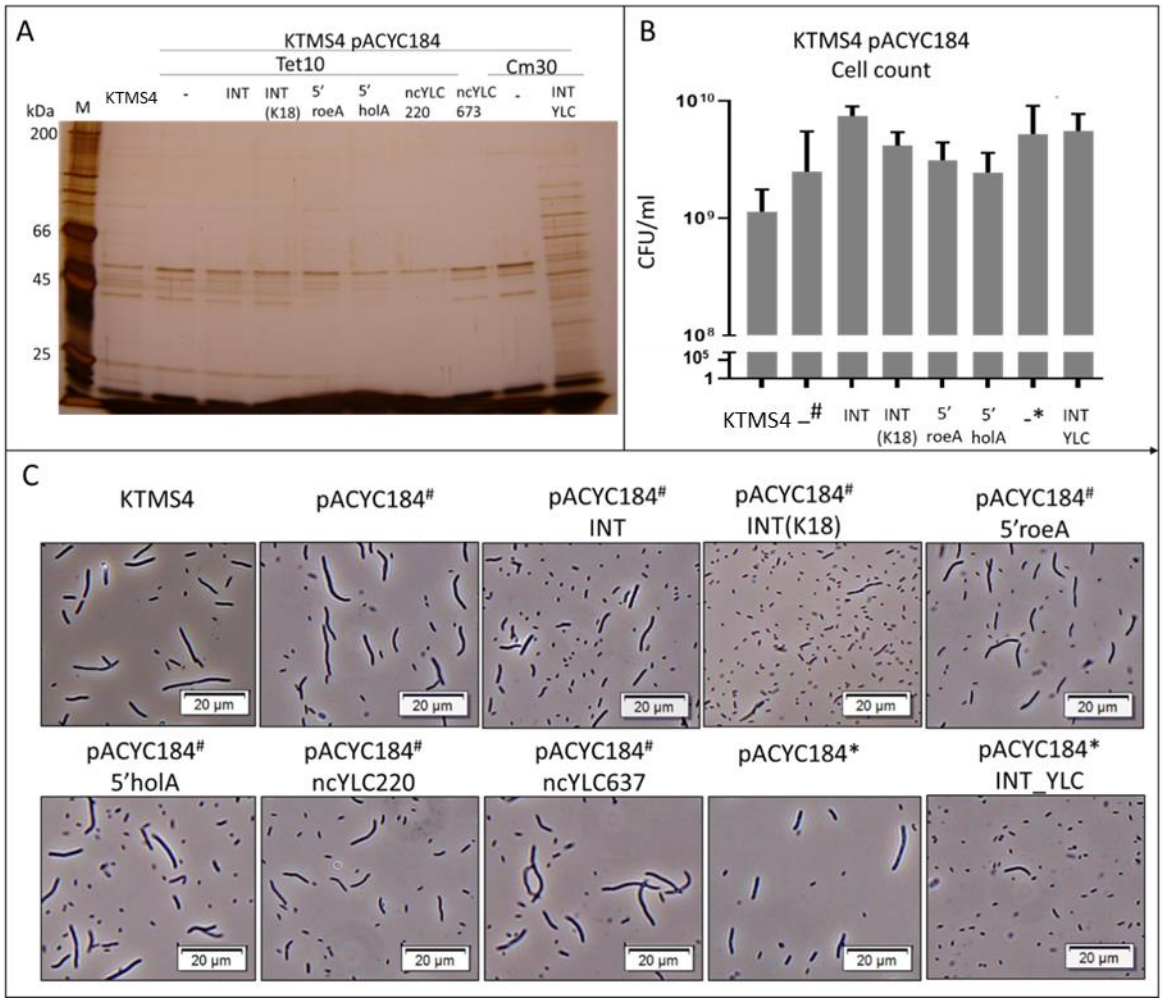

Figure 53: *Trans* complementation of YLC mutant KTMS4 intergenic region with pACYC184 expression vector. Sample were taken from 50-ml cultures at 16 hpi and incubation at 25°C, 200 rpm shaking. *A)* SDS_PAGE of exoproteome in supernatant of MH96 YeRER constructs in pACYC184. *B)* Cell density measured in CFU/ml of the construct. Bar denotes average of three experiments and error bar denotes standard division. *C)* Light microscopy in phase contrast of KTMS4 cells. Each sample is a representative of triplicate experiments. – denotes empty control vector. # denotes cells grown in tetracycline (10 µg/ml) and * denotes cells grown in chloramphenicol (30 µg/ml).

Summary role of YLC in the YeRER

The YLC, which is encoding for holin, endolysin, and a spanin complex is crucial for exoproteome release in MH96. The absence of the YLC results in: i) elongated, smooth cells; ii) a lack of OMV formation; iii) decreased exoproteome. The absence of OMV production in MH96ΔYLC implicates YeRER dependent OMV production, caused by YLC activity. In contrast, the cells of the wild type strain MH96 have an outer cell membrane with voids and abundant vesicle formation. Based on transcriptome data (Chapter 6.2), the MH96 lysis cassette components holin, endolysin, and the spanin complex are moderately-transcribed compared to Yen-TC (<10 fold). It is plausible that the holin-translocated M15 peptidase contributes to peptidoglycan structure and OM bulging as seen in MH96. In addition, the spanin complex could contribute as anchor points between OM and IM on the non-bulging areas, which are seen as voids in the OM. Deletion of the YLC resulted in the loss of membrane bulging and exoproteome release, which reveals that the YLC is integral to the bulging and release of OMVs. The deletion of the YLC does not affect the viability of the cell culture, which was confirmed by LIVE/DEAD stain and cell density, which were similar to MH96. The MH96ΔYLC phenotype of cell elongation and decreased exoproteome release could be restored by *trans* complementation of p184-INT_YLC. *Trans* complementation of p184-INT(K18) partially restored cell morphology with the major subpopulation showing MH96-like cell shape. This study also identified that the lysis cassette components induce lysis when expressed in an optimised frame (pARA-LK). Additionally, inducing to the putative o-spanin Rz1 (Chapter 6.3.1) in pARA-LKRz1 resulted in faster cell lysis, validating the existence and functionality of Rz1 in MH96. The induction of the optimised lysis cassette also caused clearance of the cell culture in *E. coli* DH10β, indicating that the observed cell lysis in MH96 was caused by YLC in a strain-unspecific manner. Upon induction of YLC, cell elongation and pore formation were visible during Live-cell imaging. Additionally, the expression of pARA-LKRz1 caused membrane blebbing before cell lysis. When the native *Y. entomophaga* MH96-encoded YLC was induced in pARA-HML no cell lysis (as observed by OD) occurred, which is likely prevented by the overlapping genes resulting in frameshift, and back translational coupling of the YLC.

6.3.4 Complementation of YeRER constructs in MH96

Previously, *trans* complementation of YeRER constructs using pACYC184 derivatives was undertaken for K18, KTMS4, and MH96ΔYLC. The results show a hierarchical regulation of protein secretion between the lysis cassette and RoeA, of which the latter plays a global regulatory role. The transposon insertions of KTMS4, KTMS31, and KTMS35 and the K18 mutation within the intergenic region (INT) are positioned at distance 5' *roeA* and 5' *holA,* suggesting the existence of transcription factors that bind to the intergenic region. Further evidence for this was provided through the *trans* complementation of pGEM-INT in MH96, which resulted in a decreased exoproteome release after 16 h (Chapter 6.2). Furthermore, sequence analyses of the INT region identified possible binding sites of Hfq and PhoB-like proteins, and transcriptome data identified a possible ncRNA within the region, with sequence identity to a possible transcription terminator loop of *roeA*. Due to the importance of the INT intergenic region in exoproteome release, complementation experiments defined the role of the intergenic region on the wild type strain MH96.

Trans complementation of the MH96 intergenic region including the YLC (INT_YLC), the intergenic region (INT), and the K18 intergenic region (INT(K18)) using p184INT-YLC, p184INT, and p184INT(K18), respectively, resulted in decreased protein secretion relative to the wild type control harbouring the empty pACYC184 vector (Fig. 54A). SDS-PAGE assessment of the *trans* complementation of ncYLC220 and ncYLC637(in p184ncYLC220 and p184ncYLC637) with MH96 showed that protein secretion was abolished, as was also seen in *roeA* and YLC mutants. An increase in protein secretion was observed through the *trans* complementation of 5'*roeA* and 5' *holA* with p5'*roeA* and p5' *holA.* At 16 hpi, all samples had cell counts within the same log-range (10^9-10^{10}) (Fig. 54B), therefore, effects of cell growth on secretion within this sample set were removed as a variable. To understand morphological changes upon overexpression of p184INT derivates it is important to note that wild-type strain MH96 comprises subpopulations of rod-shaped and spherical cells (Chapter 3.3). Subtle effects on cell morphology were only observed through the *trans* complementation of p184ncYLC220 and p184ncYLC637 with MH96 where an abundance of smaller, spherical cells was observed (Fig. 54C). Conversely, the *trans* complementation of 5'*holA* with MH96 revealed an increase in elongated, where likely dead cells appearing as faded cells by phase-contrast microscopy (Fig. 54C).

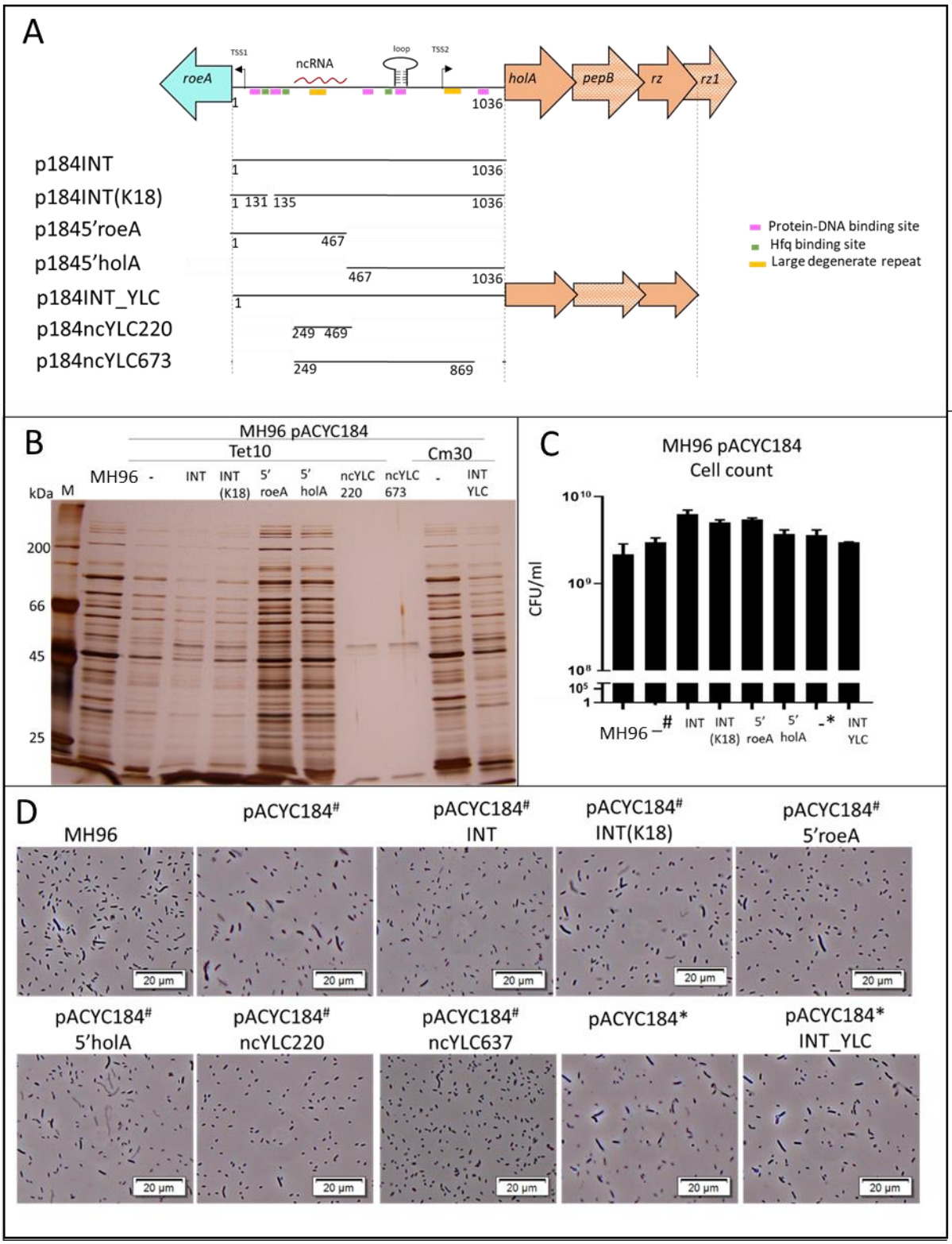

Figure 54: *Trans* complementation of MH96 intergenic region with pACYC184 expression vector. *A)* A schematic of the used vectors in relation to the YeRER. *B)* SDS-PAGE of exoproteome in the supernatant of MH96 YeRER constructs in pACYC184. Samples were taken from 50-ml cultures at 16 hpi and incubation at 25°C, 200 rpm shaking. *C)* Cell density measured in CFU/ml of the construct. Bar denotes the average of three experiments and error bar denotes standard division. *D)* Representative photographs of light microscopy in phase contrast of MH96 cells containing the listed vectors in A. – denotes empty control vector. # denotes cells grown in tetracycline (10 µg/ml) and * denotes cells grown in chloramphenicol (30 µg/ml).

Complementation of the ncYLC220 in *Y. entomophaga* MH96 and derivates

Transcriptome data identified a 220 bp long ncRNA within the intergenic region of YeRER. The expression vector p184ncYLC220 was assessed in strains MH96, K18, KTMS4, and MH96ΔYLC (Fig. 55).

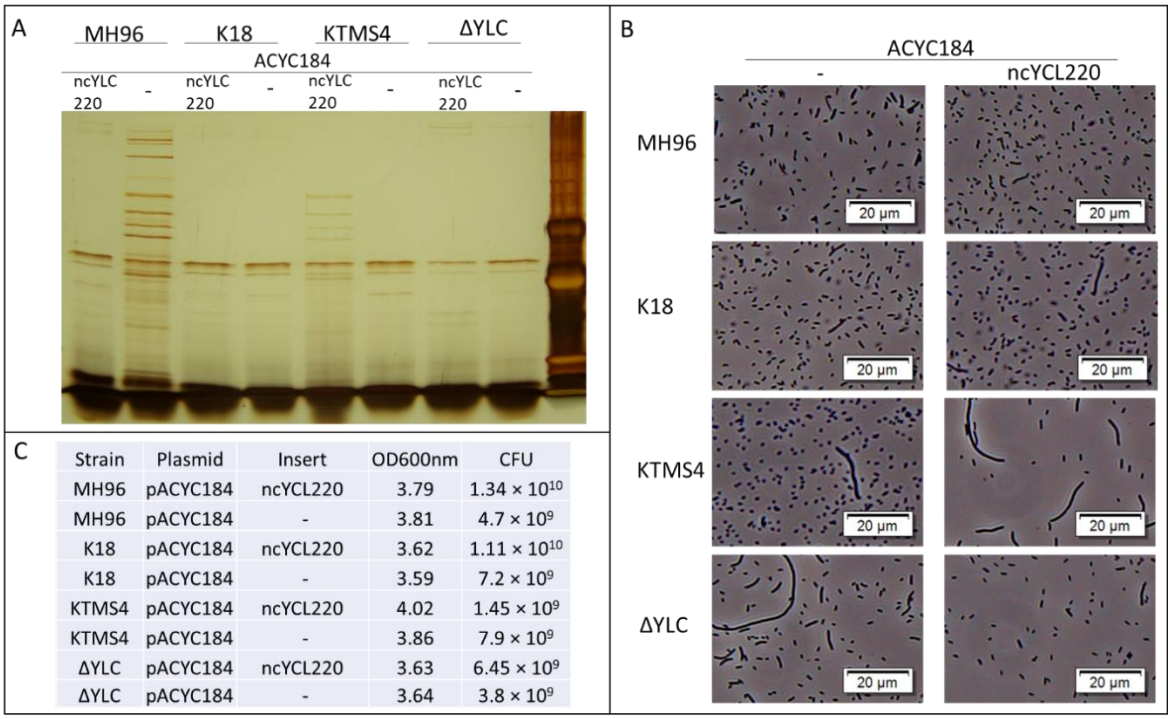

C

Strain	Plasmid	Insert	OD600nm	CFU
MH96	pACYC184	ncYCL220	3.79	1.34×10^{10}
MH96	pACYC184	-	3.81	4.7×10^{9}
K18	pACYC184	ncYCL220	3.62	1.11×10^{10}
K18	pACYC184	-	3.59	7.2×10^{9}
KTMS4	pACYC184	ncYCL220	4.02	1.45×10^{9}
KTMS4	pACYC184	-	3.86	7.9×10^{9}
ΔYLC	pACYC184	ncYCL220	3.63	6.45×10^{9}
ΔYLC	pACYC184	-	3.64	3.8×10^{9}

Figure 55: Overexpression of the ncYLC (ncHol) in mid-copy plasmid pACYC184 (ACYC184) in MH96, intergenic mutant strains K18 and KTMS4 , and the YLC mutant strain MH96ΔYLC and control strain with pACYC184 empty vector (-). *A)* SDS-PAGE of cell cultures at 16 hpi, 25°C. Samples of empty vector and pACYC184 harboring ncYLC grown in LB broth with Tet10. *B)* Light microscopy of cell cultures in A. Scale bar indicates 20 µm. *C)* Cell density and cell count of cultures used in A and B, showing similar growth of analyzed cell cultures.

Overexpression using p184ncYLC220 abolished exoproteome production in MH96 and did not affect exoproteome production in K18 and MH96ΔYLC (Fig. 55A). The exoproteome in KTMS4 was slightly increased by pNcYLC220 overexpression. The elongated cells in MH96ΔYLC, were shorter in the *trans* complementation of ncYLC220 with p184ncYLC220 in MH96ΔYLC, whereas a subpopulation of KTMS4 elongates. *Trans* complementation of ncYLC220 with p184ncYLC220 in KTMS4 leads to partial exoproteome release, partially restored wild type (MH96) exoproteome (Fig. 55A). In contrast, *trans* complementation of ncYLC220 in MH96 causes decreased exoproteome release, with a similar exoproteome profile as seen in YeRER mutants (Fig. 55A). The results strongly indicate that the identified ncRNA of 220 bp length, ncYLC220, plays an important role in protein release. Truncation of ncYLC (ncYLC80 and ncYLC110) (Fig. 56A) did not alter secretion nor cell morphology. Furthermore, as previously described, *trans* complementation of INT led to decreased exoproteome in the supernatant

in MH96 (Fig. 54), and the same intergenic region missing the ncRNA (INTΔncYLC220) did not cause such an effect (Fig. 56B) in MH96. Within the ncYLC220, a degenerate repeats sequence is similar to one lying 5' of *holA* (Fig.56A). The two repeats are located 438 bp apart. Within this region, a secondary loop structure was identified.

Further validation for the importance of the ncYLC220 in MH96 was confirmed through the *trans* complementation of the INT excluding the region forming a loop (INTΔLoop) where exoproteome production was observed (Fig. 56). Interestingly, both p184ncYLC and p184INTΔLoop *trans* complementation in MH96 showed reduced exoproteome as seen in *roeA* and MH96ΔYLC mutant strains.

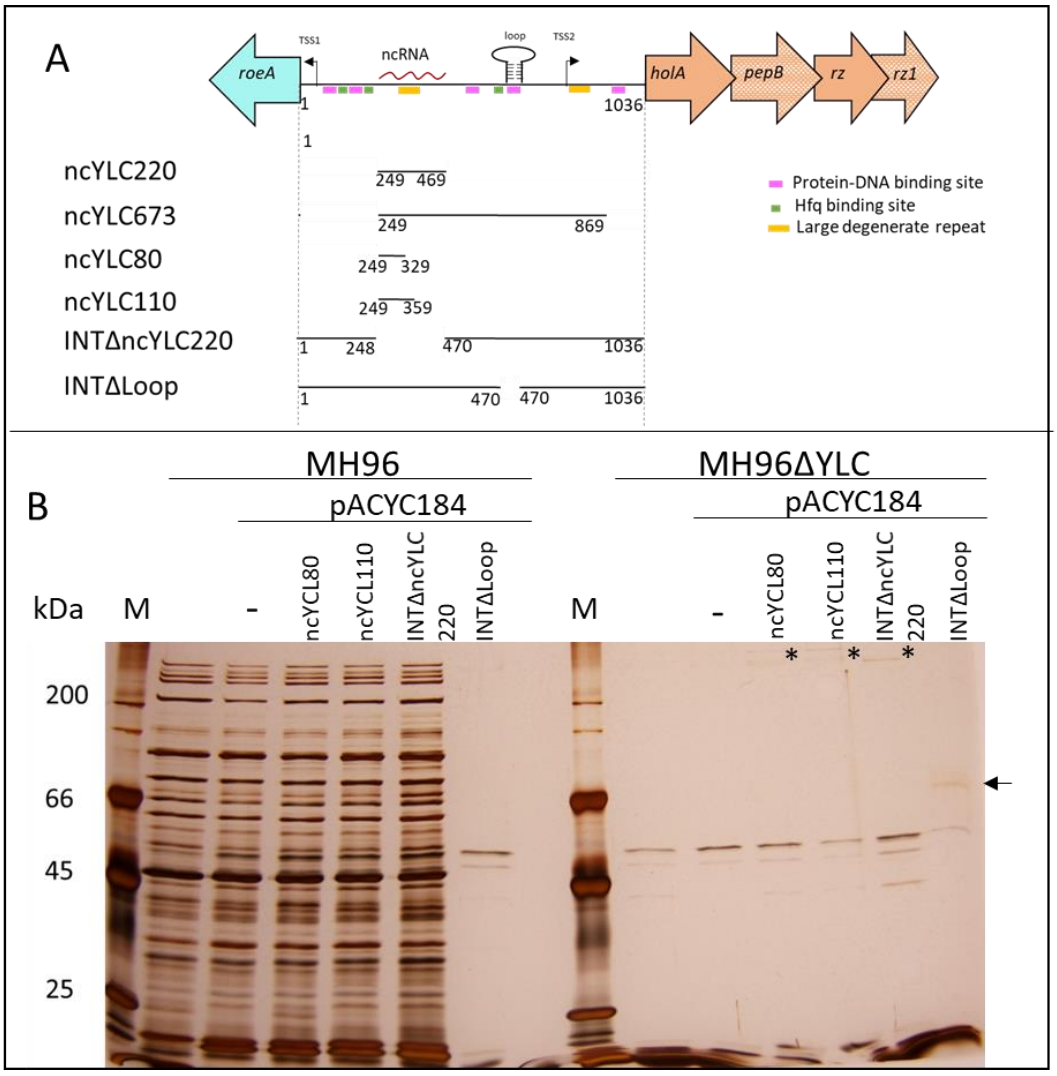

Figure 56: *Trans* complementation of YeRER and ncYLC constructs in MH96 and MH96ΔYLC. A) Schematic of pACYC184 constructs for *trans* complementation if INTand ncYLC derivates (also found in Table 12). *B)* Exoproteome analysis of trans complementation of constructed shown in A. Arrow indicates unique 66 kDa exoprotein in MH96ΔYLC p184INTtΔLoop. Asterisks denote high molecular weight bands in MH96ΔYLC *trans* complements.

Overexpression of p184ncYLC80 and p184ncYLC110, as well as p184INTΔncYLC in MH96ΔYLC did not alter the intensity of exoproteome release, observed by SDS-PAGE (Fig. 56B). However, high molecular weight bands >200 kDa, can be observed in MH96ΔYLC p184ncYLC80, p184ncYLC110, and p184INTΔncYLC, respectively, which are absent in MH96ΔYLC and MH96ΔYLC pACYC184The *trans* complementation of p184INTΔLoop construct produced a higher molecular weight (MW) band of 66 kDa (Fig. 56), and absence of several lower MW bands, which indicates altered expression of exoproteins and their release by INTΔLoop. These results indicate, that even in absence of YLC the YeRER intergenic region is likely to act in *trans* and regulates other secretion mechanisms.

6.3.5 Summary on the role of the YeRER intergenic region in exoproteome release and cell morphology

The YeRER comprises of a 1,083 bp intergenic region, with multiple protein-binding motifs, which form secondary structures, and INT encodes for a 220 nt ncRNA (Chapter 6.3.1). This study identified that *trans* complementation of the INT, using p184-INT, reduces exoproteome release in *Y. entomophaga* MH96. A shortened version of the INT identified the importance of the ncYLC220 in exoproteome release, which was strongly reduced upon *trans* complementation of p184-ncYLC220. The ncYLC220 harbours a complementary nucleotide sequence to the putative terminator loop of RoeA identified in Chapter 6.3.1. As discussed in Chapter 6.3.2, the inactivation of RoeA (as seen in K18) results in decreased exoproteome release. NcYLC220 likely binds to the putative terminator loop 3' of *roeA*, which leads to stabilization of the termination loop and stalling of the ribosome during translation, and inhibition of RoeA activity results in decreased exoproteome release. In MH96, reduced exoproteome release was observed when the intergenic region, depleted of a region forming a secondary structure within Hfq-binding motif, was *trans* complemented in MH96 using p184-INTΔLoop, indicating a potential role of Hfq in the regulation of the YLC. In contrast to RoeA and the YLC, the intergenic only has a subtle effect on cell morphology as it was observed in MH96 p184-ncYLC220.

6.4 Discussion

Initial screening of MH96 transposon mutants for deficient protein secretion revealed the YeRER, encoding for a DNA-binding protein and a phage-like lysis cassette. The components of YeRER were therefore investigated and reported on in this Chapter. Bioinformatic analysis revealed the novelty of the YeRER, which can only be found in *Y. entomophaga, Y. nurmii*, and *Y. aldovae*. Taxonomically, *Y. entomophaga,* and *Y. nurmii* are closely related (Reuter *et al.*, 2014). Interestingly, *Y. nurmii* was isolated from broiler meat and not shown to be pathogenic (Murros-Kontiainen *et al.*, 2011a). A common ancestral strain *Y. aldovae* shows low homology in the RoeA-like protein and the next neighbouring ancestors of *Y. nurmii* and *Y. entomophaga*, which are *Y. pseudotuberculosis, Y. pestis,* and *Y. similis,* do not encode a RoeA-like gene (Reuter *et al.*, 2014). It is therefore likely that *roeA* was acquired in Y*. aldovae* and is the ancestral gene of *Y. entomophaga* and *Y. nurmii*. The human pathogens *Y. pseudotuberculosis* and *Y. pestis* but also *Y. similis* might have lost the gene locus. If RoeA plays a pivotal role in virulence, it is plausible that after the acquisition of the main virulence plasmid pYV of *Y. pseudotuberculosis* and *Y. pestis*, the possession of *roeA* was non-beneficial. *Y. similis* does not harbour such a plasmid and therefore is not pathogenic in its mammalian host (Sprague *et al.*, 2005). It is likely that *Y. similis* does not require the potential virulence-associated regulator RoeA. This study identified the role of RoeA as a global regulator activator, identified by mutation of *roeA* in KTMS12 which resulted in the repression of gene expression of 365 genes including genes of the Yen-TC and the YeRER genes, which are required for the release of exoproteins.

Interestingly, the most repressed gene in KTMS12 encodes for the peptidases M66. The metallo-endopeptidase StcE in *E. coli* (EHEC) O0157:H7 is secreted by T2SS and acts as a mucinase allowing the bacterium to adhere to its host cell (Lathem *et al.*, 2002; Grys *et al.*, 2005). The peptidase cleaves glycoprotein 340 and human mucin 7, which are found in mucosal tissues such as the intestinal epithelial surface (Strous and Dekker, 1992; Osei *et al.*, 2018). In contrast, the M66-like protein TagA of *Areominosa salmonicida* (44% identity to M66 of *Y. entomophaga* MH96) secretes in a T3SS-independent manner (Vanden Bergh *et al.*, 2013). TagA and StcE are both regulated by global transcriptional regulators: the LEE-encoded regulator (Ler) in *E. coli;* and ToxR in *A. salmonicidia*. Based on the literature and the co-repression of M66 with other exoproteins such as the Yen-TC, it is likely that the peptidase M66 also acts as a T2SS effector protein in MH96. M66 released into the supernatant could not be observed by SDS-PAGE and LC-MS/MS of KTMS12. However, the peptidase M66 was not the focus of this study and will need to be validated in further studies.

The mutation of *roeA*, also decreases transcription of genes encoding for stress-related proteins such as cold and heat-shock proteins, ribosomal proteins, and chaperons DnaKJ, ClbP, GroEL, and GroES. In *E. coli,* the DnaJ/K complex binds and degrades sigma32 in a heat-dependent manner (Suzuki *et al.*, 2012).The regulation of heat-shock proteins by RoeA leads to the assumption that *roeA* is under the regulation of a sensory protein or mechanism such as ncRNA (riboswitch), which in turn regulates pathways of protein folding and finally leads to degradation of unfolded proteins by proteases. Such unfolded proteins are likely exoproteins and/or proteins of secretion pathways which could explain the non-secreting phenotype in the *roeA* mutant strain KTMS12. RoeA plays an essential role in the exoproteome release, which is correlated with YLC expression. Mutation of *roeA* in *Y. entomophaga* MH96 decreased T2SS but did not affect other secretion systems (T1,3-6SS) nor the translocation pathways Sec or Tat. T3,4,6SSs, in particular, are used by the cell to secrete effector molecules or toxins to attack eukaryotic or interspecies-bacterial cells (Green *et al.*, 2016). The *in vitro* conditions used in the current study do not mimic the host environment, which results in overall low expression of the T3-6SS in MH96. Hence, a mutation of *roeA* as a secretion activator would not cause a significant change in the gene expression of T3,4,6SS genes. While no effect can be detected on secretion systems, RoeA strongly regulates several translational genes such as genes encoding for ribosomal proteins. Additionally, RoeA strongly affects Yen-TC and YeRER expression where >1000 fold and >400 fold, respective down-regulation was observed, respectively. It is also to note that the 3-bp deletion upstream of *roeA* in the K18 strain, likely leads to the repression of *roeA* transcription, resulting in a similar phenotype as observed in KTMS12. This indicates, together with bioinformatic analysis of potential DNA-binding sites, the inhibition of an activator, such as OmpR- or PhoB-like regulators, that bind either at or upstream of the 3-bp deletion.

Orthologues of the MH96 lysis cassette was found in many Enterobacteriaceae. It is plausible that elements in the YeRER have a shared functionality based on standard genome reduction and recombination principles (Feldman *et al.*, 1996; Sloan and Moran, 2012). The functionality of lysis cassettes in *S. marcescens* and *Y. enterocolitica* W22703 have been shown, which leads to the assumption that YLC of MH96 is also functional. In *Y. enterocolitica* W22703, the lysis cassette can be found within the insecticidal toxin complex (TC) operon (Starke *et al.*, 2013). Toxin complexes (TCs) are composed of three subunits: TcA, TcB and TcC. TCs were firstly described in *P. luminescens,* with oral insecticidal activity and can be found in many other species such as *Y. pestis*, *Y. pseudotuberculosis*, *Morganella morganii,* and the strains *B. thuringiensis* and *Y. entomophaga* (Waterfield *et al.*, 2001; Blackburn *et al.*, 2011). TCs are very large complexes and due to their large size are unlikely to be secreted by typical secretion systems, such as T1-6SS. The *Y. pestis* TC components YitA and YipA are not secreted by T3SS, even under conditions optimal for effector

secretion by the T3SS (Spinner *et al.*, 2013). The TCs of *P. luminescens*, *Xenorhabdu*s, and several *Yersinia* strains are located in the insecticidal island. Within the genus *Yersinia*, TCs are located in the Tc-PAI$_{Ye}$ pathogenicity island. Also encoded in the Tc-PAI$_{Ye}$ are phage-like genes encoding for a lysis cassette. The entomopathogens *S. entomophila* produces another large toxin complex, the antifeeding prophage (Afp), for which the secretion mechanism is yet to be determined. Interestingly, the Afp is co-located with a similar lysis cassette to that found in Tc-PAI$_{Ye}$ (Hurst *et al.*, 2004). In MH96, such lysis genes are not found within the TC operon. Yet, this study identified an orphan lysis cassette, YLC, with an important role in protein secretion. Mutation of the YLC abolished exoproteome release, which could be partially restored upon *trans* complementation of the INT_YLC. It was demonstrated that the YLC HolA, PepB, and the spanin complex are functional proteins, but arrangements of the genes in the MH96 genome is such that they do not cause lysis when overexpressed. In contrast, overexpression of the *Y. enterocolitica* W22703 lysis cassette in several *Yersinia* strains, such as *Y. enterocolitica*, *Y. pseudotuberculosis,* and *Y. kristensenii* did cause cell lysis (Springer *et al.*, 2018).

It is important to note that YLC encodes overlapping reading frames, requiring a back movement of the RNA polymerase for their correct translation. Such overlapping reading frames are often found in phage-like lysis cassettes such as in the *P. aeruginosa* phage φKMV or the λ phage-like lysis cassettes (Briers *et al.*, 2011; Rajaure *et al.*, 2015). Induced cell lysis in MH96 could only be observed in an optimised frame of MH96 YLC (pARA-YLC-Rz1). Expression, IM integration, and pore formation of holins are the rate-limiting step for cell lysis, as they allow the endolysin to access the peptidoglycan (Saier and Reddy, 2015). Endolysins, such as muramidase or amidase, then degrade the PG and cause membrane instability, leading to cell lysis.

Holins of phage-like lysis cassettes encode for dual start motifs as seen for lambda S105/S107 encoding for a holin/anti-holin complex (Graschopf and Blasi, 1999). HolA of *Y. entomophaga* MH96 does not contain such dual start motif which leads to the suggestion that holin activation is coupled with *holA* expression. This study identified QS-dependent expression of the YLC genes and a QS dependency of secretome production. As previously outlined, the TC-PAI$_{Ye}$ of other *Yersinia* strains also encodes a lysis cassette similar to YLC. The Yen-TC cluster of Y. *enterocolitica* is regulated by the DNA-binding protein TcaR2 located 5' of *tcaA (Starke et al., 2013)*. In MH96, a RoeA-paralogue called Yen7 is located 5'of *chi1* of the Yen-TC. Aligned studies of *Y. entomophaga* (Amber Paulson pers. comm.) found that mutation of Yen7 did not alter exoproteome production at 25°C. However, the same study identified restored exoproteome release upon induction of pBAD-Yen7 at 37°C, which also correlates with recovered plasmid stability relative to its instability at 25°C. The data suggest that RoeA and Yen7 can both regulate exoproteome release, but the drivers of their respective expression are

unknown. This study identified global regulation of the exoproteome by RoeA, similar to that of Hfq (M. Hurst, unpublished data) which cannot be restored by *trans* complementation of the YeRER. In fact, the deletion of the post-transcriptional regulator Hfq decreased YeRER gene expression in Hfq mutant and increased in YmoA (M. Hurst, unpublished). In *Y. enterocolitica*, Hfq is a post-transcriptional regulator that mediates sRNA-mRNA interactions (Schiano *et al.*, 2014). In *Y. enterocolitica,* Hfq is one of the main regulators of virulence genes such as *rovA*, *yadA*, *invA,* and genes of the T3SS (Kakoschke *et al.*, 2016; Bancerz-Kisiel *et al.*, 2018). Sequence analyses identified possible binding sites of Hfq within the YeRER intergenic region. *Trans* complementation of the intergenic region (INT) and derivates of INT did not alter K18 phenotype but decreased MH96 exoproteome. In particular, *trans* complementation of ncYLC220 abolished protein secretion in MH96. Reduced exoproteome by overexpression of INT in MH96 is either an effect of the comprised ncYLC220 or by titering out transcription factors binding to DNA-motifs located 5' of YLC and *roeA*, respectively. Only *trans* complementation by INT_YLC restored MH96ΔYLC secretome without causing cell lysis.

Besides the effects on the exoproteome of K18 and MH96ΔYLC, morphological changes were observed. While K18 cells are small, homogeneous cells, MH96ΔYLC shows heterogeneous cell shapes with many elongated cells. This study suggests that HolA proteins form an unspecific pore through which most MH96 exoproteins translocate. It is plausible that the absence of the pores, formed by holins, leads to protein accumulation within the cell plasma causing lateral cell elongation, as observed in MH96ΔYLC. Based on the absence of dead cells (confirmed through the use of LIVE/DEAD stain), this process must be accompanied by the insertion of new cell wall material to maintain viable cells as described in *E. coli* and *B. subtilis* (Turner et al., 2013). For example, the peptidoglycan layer, which is proposed to give bacterial shape, prevents cell lysis caused by high internal osmotic pressure. Lateral cell elongation is a complicated process of PG polymerisation and integration (Cava *et al.*, 2013). Such cell elongation is common in *E. coli* and *B. subtilis,* but the extent of elongation in MH96ΔYLC is very atypical. Cell elongation of Gram-negative bacteria is linked to the FtsZ, mutations of which cause morphological changes to spherical mini-cells, twisted cells, or elongated filamentous cells in *B. subtilis* (Jensen *et al.*, 2005). In *S. aureus,* the deletion of the cell wall anchored protein GspB results in cell lysis, whereas overexpression of GspB inhibits cell divisions and causes cell elongation (Eswara *et al.*, 2018). Turner *et al.* (2018) showed the importance of glycan chains for cell morphology in *E. coli*, where long-chain glycans are predominantly found in rod-shaped bacteria, while the cell wall of spherical cells is comprised mainly of short glycan chains. However, the protein MreB, a component of the so-called elongasome, also plays a vital role in the rod-shaped morphology (Ranjit *et al.*, 2020). Another component of the elongasome is the Penicillin Binding Protein 1a (PBP1a) protein Pbp1. In *B. subtillis* and *P. aeruginosa* it was shown that mutation of MreB and Pbp1 changes cell morphology to

mini-spheric cells with increased cell fitness (Dion *et al.*, 2019). Based on transcriptome data of KTMS12, which resulted in shortened cells, no RoeA-associated transcriptional regulation of either an FtsZ, GspB or the MreB were observed.

Based on the presence of elongated cells in *Y. entomophaga* MH96ΔYLC, the current study proposes that as opposed to the FtsZ/MreB model discussed above, cell elongation reflects protein accumulation within the cell. It is likely that the non-integration of the Holin-protein HolA in MH96ΔYLC, interferes with the formation of the cell wall. Furthermore, HolA likely forms a pore with low protein specificity, allowing exo-cytoplasmatic proteins to enter the periplasm. The absence of HolA-pores could lead to the accumulation of these proteins within the cell, increasing the cell turgor and forcing cell elongation upon its weakest cell-wall structure, the poles. The absence of the lysis cassette and high turgor prevent OMV formation, which was observed in MH96ΔYLC by Cryo-ET. The OMV biogenesis model described the accumulation of peptidoglycan fragments, caused by peptidoglycan degradation during peptidoglycan turnover, and increases the periplasmic turgor. An increased turgor then leads to bulging of the OM and OMV formation. It is likely that OMV formation constitutes the major secretory mechanism of MH96 (Haurat *et al.*, 2015). The *Y. entomophaga* MH96 cell wall differs from cell walls observed in other Gram-negative bacteria (Matias and Beveridge, 2006). It is plausible that the cell wall structure of MH96 hinders the successful integration of secretion systems into the cell wall. Summarising, the native YLC is necessary for OMV formation and protein secretion in *Y. entomophaga.* Lysis cassettes such as YLC are commonly found in other Gram-negative bacteria and associated with large toxin complex such as TcdA/B (Govind *et al.*, 2015; Mehner-Breitfeld *et al.*, 2018). This data suggests that the MH96 YLC does not cause cell lysis, but under certain conditions is involved in the release of toxin complexes that are too large for the common secretion systems as mentioned above.

MH96 cells are highly vesiculated and produce abundant OMVs. MH96ΔYLC cells do not produce OMVs and have smooth OMs. OMVs are export mechanisms of several toxins, such as Shiga toxin or heat-labile toxin in *E. coli*, TcdAB in *C. difficile,* or VacA in *H. pylori* (Horstman and Kuehn, 2000; Yokoyama *et al.*, 2000; Chitcholtan *et al.*, 2008; Govind and Dupuy, 2012). This study linked morphological effects, in terms of cell shape and OMV formation, to the YeRER, a region which is necessary for the release of exoproteins including the Ten-TC. In conclusion, this study validated the direct role of YLC in exoproteome release and links this to OMV formation.

Chapter 7

Transcriptional regulation during fermentation of *Y. entomophaga* MH96

7.1 Introduction

In LB broth the entomopathogen *Y. entomophaga* releases large amounts of exoproteins. The main *Y. entomophaga* MH96 virulence factor, the Yen-TC, is increasingly released over time, in a QS--dependent manner. Up-scaled fermentation of *Y. entomophaga* MH96 is used in the production of a biopesticide, as a precursor to its incorporation into a formulated product. Using *Y. entomophaga* formulated as bait to target porina larvae of the genus *Wiseana* (Lepidoptera: Hepialidae), the bacterium showed similar effectiveness as the chemical insecticide diflubenzuron (Hurst *et al.*, 2020). However, the authors suggested that further work was required to improve shelf stability. In the assessment of exoproteome release by SDS-PAGE during fermentation, S. Jones *et al.* (AgResearch) observed a drop of pH correlating with the initiation of exoproteome release (pers. comm). A temporary drop in pH occurs in a wide range of bacteria grown in LB media (Sánchez-Clemente *et al.*, 2018). LB media is nutrient-rich, containing high amounts of peptides from tryptone and yeast extract with limited carbon sources. Sanchez-Clemente *et al.* (2018) demonstrated the changes in culture pH depend on the selected media carbon sources, while pH below 6 negatively affects *E. coli* cell growth. In *Y. pseudotuberculosis*, secretion of exoproteins by the T6SS4 is OmpR-regulated in a pH-dependent manner (Zhang *et al.*, 2013). Furthermore, the global regulator RovM regulates, in a network with CsrABC and RovA, the T6SS and the arginine-dependent acid resistance system (AR3) (Dai *et al.*, 2018). Bacterial pH homeostasis is maintained by the control of a proton transporter, which is coupled to sodium ion cycling (Minato *et al.*, 2013). In *Y. pestis* the Na+/H+ antiporter is pH-dependent and is inactive at a pH less than 7 (Ganoth *et al.*, 2011). This chapter focuses on transcriptional factors contributing to secretion during the fermentation process of *Y. entomophaga* MH96, specifically changes in gene expression around the observed pH shift during the fermentation process. The use of a fermenter enables real-time monitoring of variables such as pH and oxygen during the fermentation and allows the targeted collection of samples for transcriptomic assessment. The resultant data can then be linked to correlate the expression of genes identified through HESA such as *roeA* and its associated YLC, as well as genes encoding exoproteins including the Yen-TC.

7.2 Method:

7.2.1 Bacterial strains and culture conditions

Y. entomophaga MH96 was cultured in Luria Bertani (Miller base) broth or on LB agar. Starter cultures for the fermentation were inoculated from agar plates into 3-ml LB broth and cultured for 7 h at 25°C, 200 rpm. Of the 3 ml culture, 500 µl was used to seed a 50-ml culture flask and the flask was incubated for another 16h at 25°C, 200 rpm. An aliquot (1% v/v) was then used to inoculate 1 L LB broth in a 1-l L Multifors2 bioreactor. The fermentation was set to the following parameters:

Table 15: Adjusted parameter during the fermentation of *Y. entomophaga* MH96

Paramter	Settings
Temperature	25
Stirring	100 rpm
Gas Mix	21
Air Flow	0.5
Anti-foam	None
pH	Not adjusted
pO2	Not adjusted

7.2.2 Assessment of bacterial growth and changes in pH during fermentation

For assessment of bacterial growth during fermentation, three 1-L fermenters were inoculated from the same pre-culture and run with the same conditions (Table 15) and media (LB broth). During the 24 h fermentation, the Fermenter software (Infors) records the parameters at 10 min intervals. Before the RNA collection, a preassessment of the fermentation was done under the same conditions as described above, to estimate the time point when a temporary drop in pH occurs. The preassessment trials showed a decrease in pH from 6.8 to 6.3-6.4 between 7 and 7.5 hpi. For the current study, at selected time-points: prior, during and post pH shift, culture samples (T1-T5) were collected to determine CFU and OD, to analyse the secretome as described in Chapter 7.3.1 (Table 16), and to collect RNA.

7.2.3 Transcriptomics

Experimental set-up

To understand the underlying mechanism in protein secretion and pH shift linked to fermentation, samples with different pH were chosen to be analysed by RNAseq. The main interest in the transcriptome studies was at the time of the drop in pH. With reference to Figure 59 and Table 16, samples were taken at T1 before the pH drop at 4 hpi, during pH drop at T2 (7.3 hpi) and after the pH

dropped at T3 (8.3 hpi) and T4 (9.3 hpi), sampling points which spanned 5.3 h. As this is a narrow window, a fifth outlier sample (T5) was taken at 24 hpi. This helped identify genes that were constitutively expressed or transcribed in the late stationary growth phase.

Sample preparations for transcriptomics

RNA isolation was performed as outlined in Chapter 2.6.2 using the RNA Mini Kit (QIAGEN) and the corresponding RNA protect bacteria (QIAGEN) and RNase-Free DNase Set Kits (QIAGEN).

From each fermenter, 1 ml of culture samples were immediately transferred into 2 ml of RNA protect bacteria (QIAGEN) and vortexed. After 5 min incubation time, at 25°C, the samples were spun down at 5,000 × *g* for 10 min. The supernatant was decanted, and pellets were placed at -80°C.

As described in Chapter 2.6.3, the RNA was isolated using the RNA Mini Kit according to the manufacturer's instructions. The RNAseq data were further analysed by Charles Hefer (AgResearch) with the protocols outlined in Chapter 2.8.

The DeSeq2 workflow was used for quality control of the collected RNA samples. To assess the similarity between the samples, the principal component analysis (PCA) and hierarchical clustering methods were used. The PCA and hierarchical clustering identified sample outliers and how well samples of the triplicates clustered together. As a quality control of transcript levels, all genes with zero counts in all samples were removed, as were genes with extreme count outliers as well as genes with low mean normalised counts (<150). In the hierarchical cluster methods, a heatmap was constructed based on the distances between rows/columns of the distance matrix generated by DeSeq2.

For the visualisation of gene expression during the fermenter time-points T1-T5 a co-expression analysis of the RNAseq data was performed using the *coseq* package (Rau *et al.*, 2015). This package uses a slope heuristic approach with an integrated complemented likelihood criterion. In this study, the "kmeans approach & logCLR (LOG centred log-ratio transformation)" algorithm with default settings and k=2: 20 and was used for the co-expression analysis (Godichon-Baggioni *et al.*, 2018). The algorithm sorts genes into Clusters of gene expression, which were then plotted and an expression trendline in the respective Cluster could be observed. Genes of the Clusters were then plotted on the respective heat map.

7.3 Results

7.3.1 Assessment of cell count and pH of collected samples

To understand cell growth during fermentation, and to correlate those with cell grown in a flask, the CFU and OD were assessed. Furthermore, pH was measured during the fermentation to collect samples correlating to the temporary pH drop.

The pH of the starter LB (Miller) broth was 6.8 and decreased within 7 hpi to pH 6.4 (Table 16). Within 2.33 h the pH increased back to pH 6.8 and kept increasing during the remaining fermentation to pH 8 at 24 hpi. The assessment of the culture supernatant of the samples T1-T5, revealed exoproteome release at 7 hpi at a pH of 6.5, with increasing band intensities over time observed in SDS-PAGE, indicating increasing exoproteome concentration (Fig. 57). The initial exoproteome release was observed 20 min before the minimum pH of 6.46 at 7.33 hpi (T2) was reached. To note, in the fermenter the CFU at this time-point (T2), when the pH drop occurred, was 1.44×10^9 CFU/ml (Table 16). Previously, using 50 mL shake flask, initiation of exoproteome release in *Y. entomophaga* MH96 was seen at 3×10^9 CFU/ml (Chapter 3), a cell number that was only reached at 24 h hpi of the fermentation (Fig. 57B).

Table 16: Assessment of the cell culture during fermentation in OD, CFU and pH.

Time [hpi]	pH			OD600nm			CFU			ØpH	ØOD	ØCFU
4:20 (T1)	6.81	6.86	6.91	0.54	0.53	0.59	2.73×10^8	3.24×10^8	3.44×10^8	6.86	0.55	3.14×10^8
7:00*	6.42	6.49	6.58	2.14	2.07	2.02	1.39×10^9	1.95×10^9	9.9×10^8	6.50	2.07	1.44×10^9
7:20†(T2)	6.40	6.45	6.53	2.23	2.16	2.04	2.18×10^9	1.69×10^9	9.33×10^8	6.46	2.14	1.60×10^9
8:20 (T3)	6.64	6.68	6.69	2.57	2.59	2.69	1.66×10^9	1.20×10^9	2.41×10^9	6.67	2.61	1.76×10^9
9:20 (T4)	6.80	6.85	6.86	3.27	3.03	2.68	1.84×10^9	1.92×10^9	2.48×10^9	6.84	2.99	2.08×10^9
24:00(T5)	8.03	8.05	8.01	2.72	2.47	2.74	5.17×10^9	3.31×10^9	2.79×10^9	8.03	2.64	3.76×10^9

* indicates time-point that was sampled but not used in transcriptomics
†time of pH drop
Ø indicates average

The assessment of fermentation data reveals the initiation of secretion lies between T1 and T2 when the pH dropped to its minimum at cell number between 3.14×10^8 and 1.4×10^9 CFU/ml (Table 16).

7.3.2 Assessment of the exoproteome profile during fermentation

To determine the initiation of exoproteome release during fermentation, the exoproteome was assessed by SDS-PAGE, which showed an increase of exoproteome release into the supernatant over time (Fig. 57). The exoproteome concentration of samples collected from 7 hpi onwards were

sufficient for visualization. The initial exoproteome release correlates with lowered pH. However, the cell density reached during the fermenter time-point T2-T4, when the exoproteome release was detected, was lower than observed during the 50-ml shaking culture (Chapter 3.3.1) (Fig. 57B). Nevertheless, the cell population had entered the stationary growth phase in both cultures at the measured cell densities.

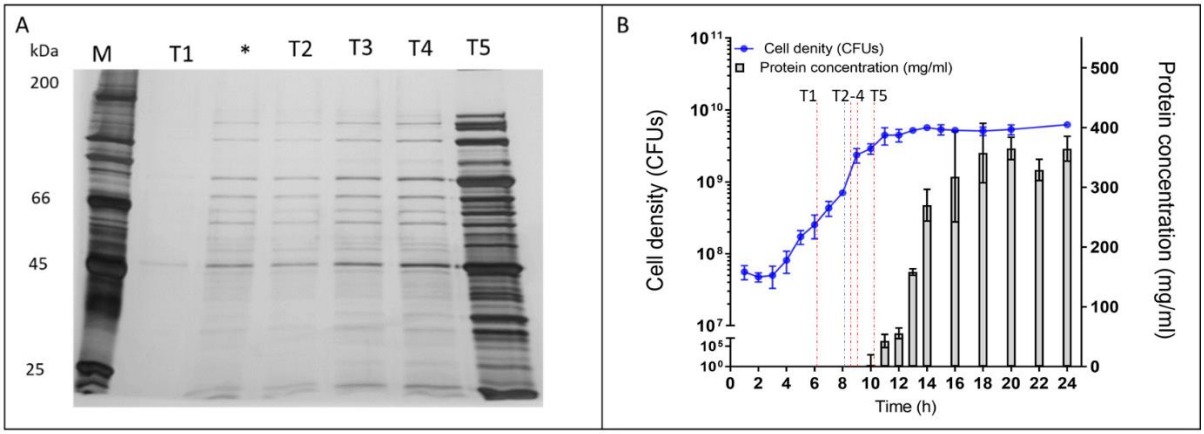

Figure 57: Exoproteome assessment of the fermenter, correlating with exoproteome in 50-ml flask of *Y. entomophaga* MH96. *A)* SDS-PAGE of exoproteome of MH96 culture during fermentation. At time-points T1-T5, when T2 indicates the time-point of minimum pH in the culture. * denotes additional sample 20 min prior to T2, when exoproteome visible. *B) Y. entomophaga* MH96 growth curve related to exoproteome from Chapter 3, with indicated lines (blue and red, dashed lines), correlating the CFU in the fermenter of T1-T5 samples to CFU in 50-ml flask cultures. Blue line indicates T2, when pH reached a minimum in the fermenter, red lines denote T1, T3-5 samples of the fermenter.

7.3.3 Transcriptome analysis of *Y. entomophaga* MH96 during fermentation

INTRO

Quality control of the transcriptome analysis

For quality control of the samples, principal component analysis (PCA) was used. The PCA showed samples in triplicate clustered together and a close relationship between samples of T3 and T4 (Fig. 58). The clustering of the respective sample sets allowed further usage of the transcriptome data to assess differently expressed genes during fermentation.

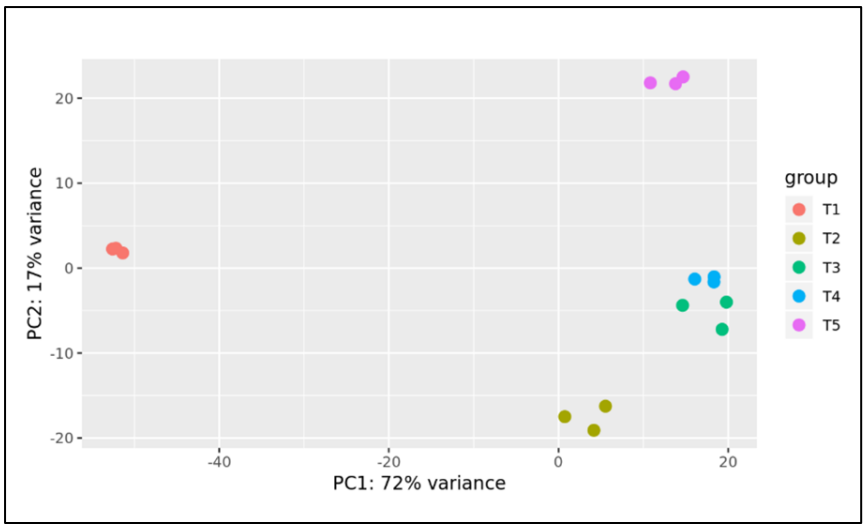

Figure 58: Principal component analysis of the triplicate fermenter samples of T1-T5, using plotPCA with default settings of the DESeq2 package.

Using the hierarchical clustering method (HCM) (Chapter 7.2), 3,213 genes were identified that are differentially expressed with p< 0.05 between the time-points T1-T5 (Fig. 59). There were 3092 differentially expressed genes between T1/T2, 1748 between T2/T3, only 232 between T3/T4, and 2053 between T4/T5 (Fig. 59).

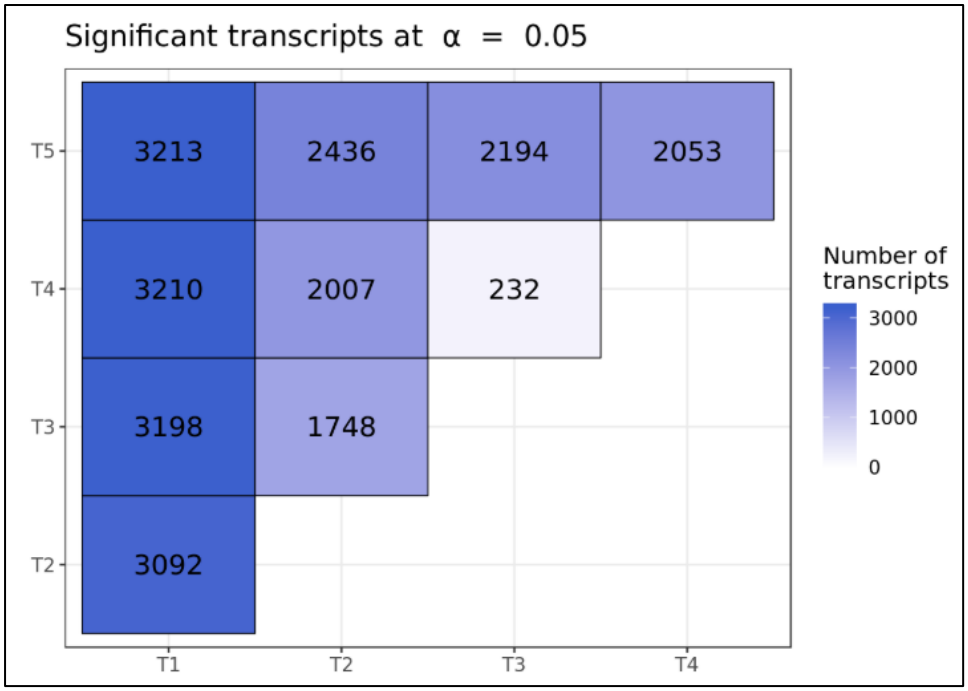

Figure 59: Differential gene expression analysis between each sample T1-T5 of fermentation, with significant gene expression differentials.

Co-expression analysis and clustering of expression profiles

The HCM identifies genes that were differently expressed between time-points, for example, T1vsT2, T1vsT3, T1vsT4 and so on. The HCM does not inform on the changes in the expression profile of specific genes. Therefore, a clustering approach was used to understand the change in transcription level over time T1-T5 of each gene. Using the *coseq* co-expression analysis, the algorithm identified seven clusters according to their gene expression trendline (Fig. 60).

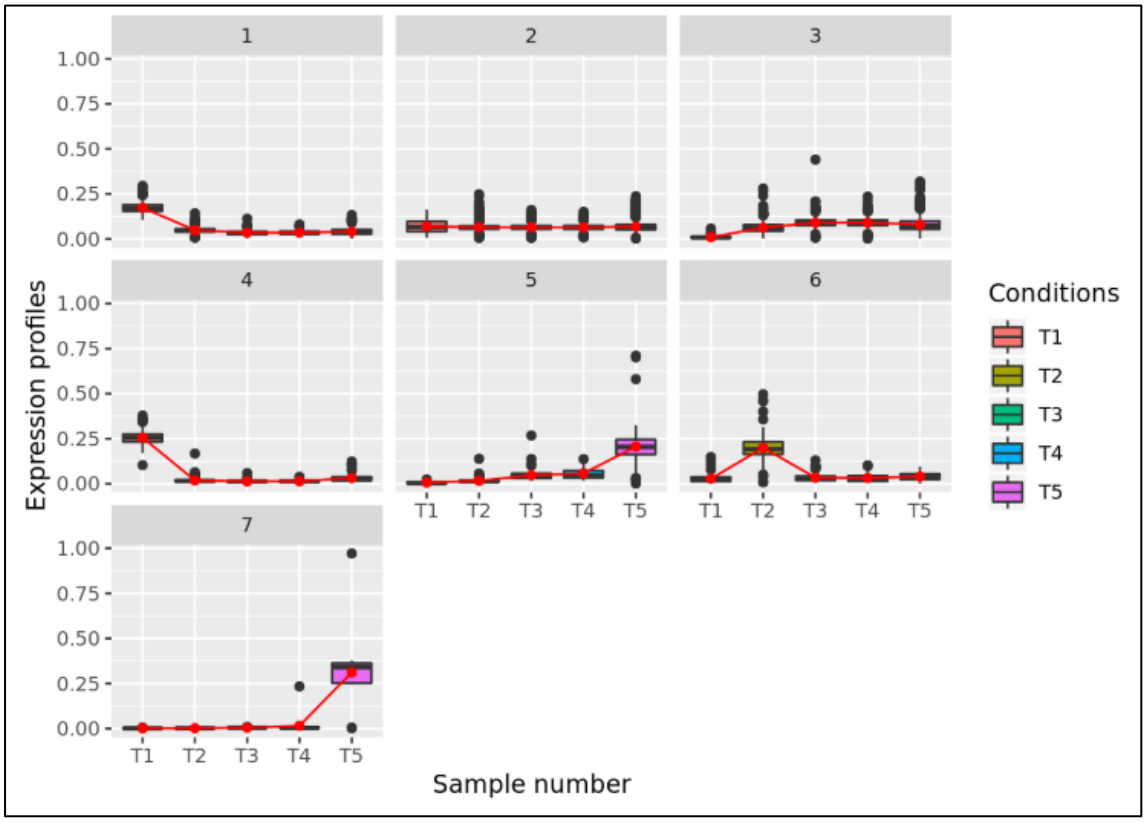

Figure 60: Co-expression analysis of gene expression during fermentation at time-points T1-T5. Black dots denote respective gene, coloured box denotes gene variance with a mean expression value of respective time-point T1-T5 (LogCLR), red line denotes trendline of gene expression. Cluster 1 denotes genes that are upregulated in T1 but remain similar in T2-T5. Cluster 2 denotes genes that are similarly expressed from T1-T5. Cluster 3 denotes genes that increase in expression levels from T1-T4. Cluster 4 denotes genes that are only highly expressed in T1, with higher expression value compared to genes in Cluster 1. Cluster 5 denotes genes with increasing gene expression from T1-T5 and high expression in T5. Cluster 6 denotes genes that are highly expressed at the T2 time-point which coincides with a drop in pH. Cluster 7 denotes genes that are highly expressed in T5.

Genes within these clusters were sorted by associated COG function when possible (Fig. 61). Cluster 1 and 4 represent genes that were highly expressed in the early fermentation stage (4 hpi at 3.14×10^8

CFU/ml). Of the significantly differentially expressed genes, 428 genes were in Cluster 1, and 57 genes in Cluster 4, of which 340 and 48 genes could be assigned a COG function, respectively.

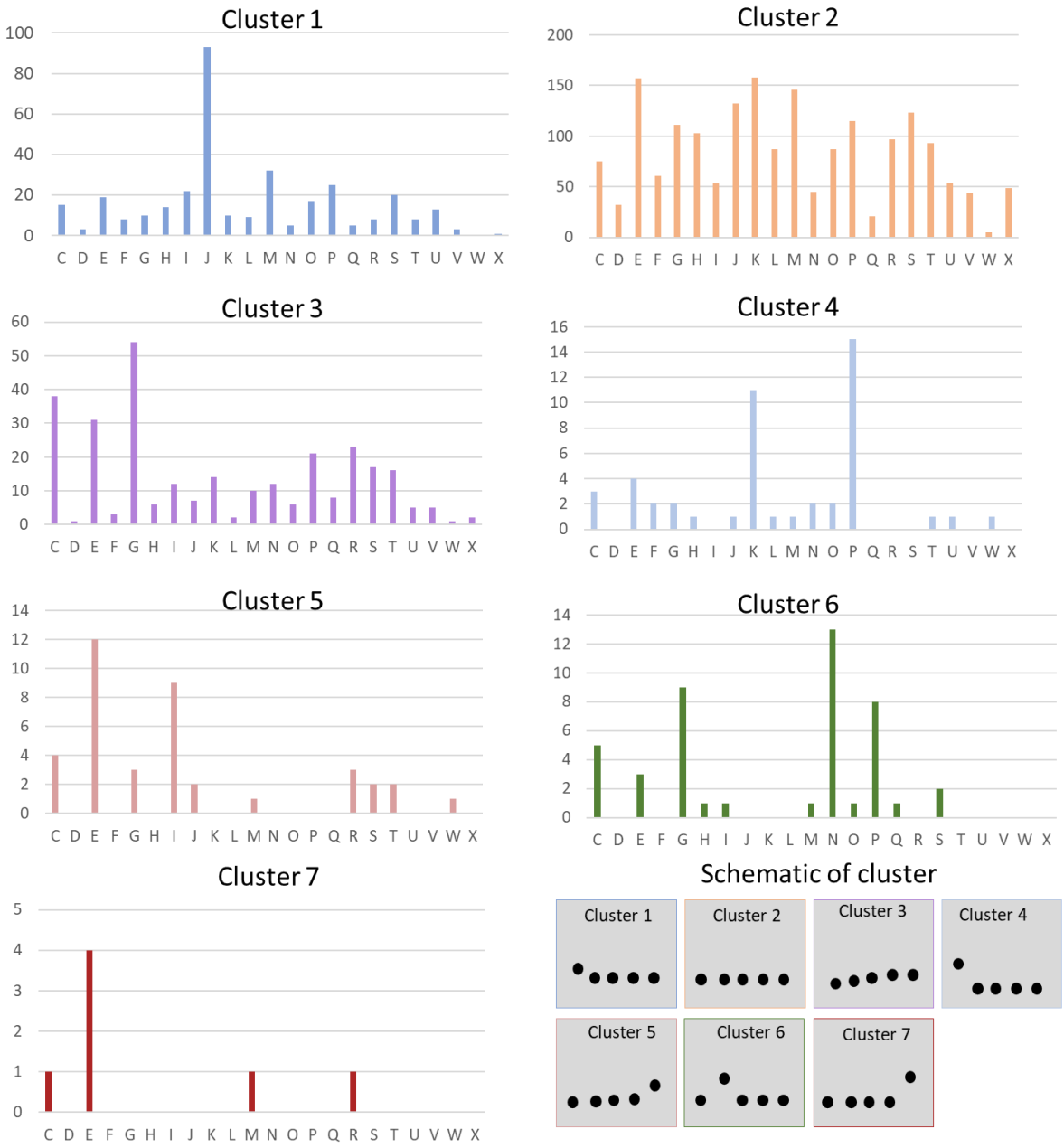

Figure 61: Number of genes of differentially expressed genes ($p<0.005$) during fermentation at time-points 1-4 per COG functions, which are grouped in 7 clusters of gene expression profile. Clusters are derived from cluster analysis and gene expression of genes over time of the respective cluster are indicated in Schematic of the clusters. Indicated are COG: C, Energy production and conversion; D, Cell division; E Amino acid metabolites and transport; F Nucleotide metabolism and transport; G, Carbohydrate metabolism and transport; H Coenzyme transport and metabolism; I, Lipid metabolism; J, Translational processes; K, Transcription; L, Replication and repair; M, Cell wall/membrane/envelop biogenesis; N, Cell motility; O, post-translational modification; P, Inorganic ion transport and metabolism; Q, Secondary structure; T, signal transduction mechanism; U, Intracellular trafficking and secretion; V, Defense mechanisms; W, extracellular structures; X, Mobilome: Prophages, Transposons; R, General functional prediction only; S, Function unknown.

In Cluster 1, the largest group of genes comprise COG functions of translation, ribosomal structure and biogenesis (94 genes), cell wall biogenesis (33 genes), inorganic ion transport and metabolism (25 genes), and 22 genes involved in lipid transport and metabolism. In Cluster 4 which represents genes that are only highly expressed in T1, 15 genes were assigned COG functions of inorganic ion transport and metabolism and 11 genes functioned in transcriptional processes. Interestingly, the cluster analysis did not identify clusters in which a strong downregulation of genes occurred only during the pH drop at T2 occurs, but consistent repression of genes in Cluster 1 and 4.

Cluster 2, reflecting genes that are similarly expressed between T1-T5, was comprised of the largest number of expressed genes (2252), 1848 encompassing all COG classifications (Fig. 62). Cluster 3 related to genes that were increasingly expressed over time during the fermentation process from T1 to T5. Of 368 genes, 294 were assigned with a COG function, with 54 involved in carbohydrate transport and metabolism, 38 in energy production and conservation, and 31 in amino acid transport and metabolism. Clusters 5 and 7 included genes, which were highly expressed only in T5 at 24 hpi. Of the 50 genes in Cluster 5, 39 genes were assigned with a COG function and all 7 genes in Cluster 7 were also assigned with COG functions. COG functions in Cluster 5 were mainly in amino acid transport and metabolism (12 genes), and 9 genes were involved in lipid transport and metabolism. In Cluster 7, 4 genes function in amino acid transport and metabolism. Cluster 6 included genes that were highly up-regulated only in time-point T2 (at 7.3 hpi), when pH minimum was reached. The cluster comprised 49 genes of which 45 were assigned with a COG classification, with genes involved in cell motility (13), carbohydrate transport and metabolism (9 genes), and 8 genes in inorganic ion transport and metabolism.

Gene expression profile analysis according to cluster analysis

To define genes that are linked to exoproteome release and pH shift in the fermentation process, highly up- or down-regulated genes during the pH drop are of interest. Highly upregulated genes during the pH drop in T2 were found in Cluster 6. Furthermore, this study is interested in the gene expression profile of genes involved in exoproteome release, which were identified by the HESA in Chapter 4, including genes of the YeRER (Chapter 6). In this Chapter, all identified clusters were assessed using gene expression profiles visualised by heatmaps of each gene of a cluster. Due to the high number of genes in Cluster 1 and 2, the focus was only on relevant genes for regulation of exoproteome release in relation to a changing pH, such as transcriptional and translational regulators,

genes of function in amino acid transport and metabolism, as these could contribute to changes in pH, and genes associated with HESA and the YeRER.

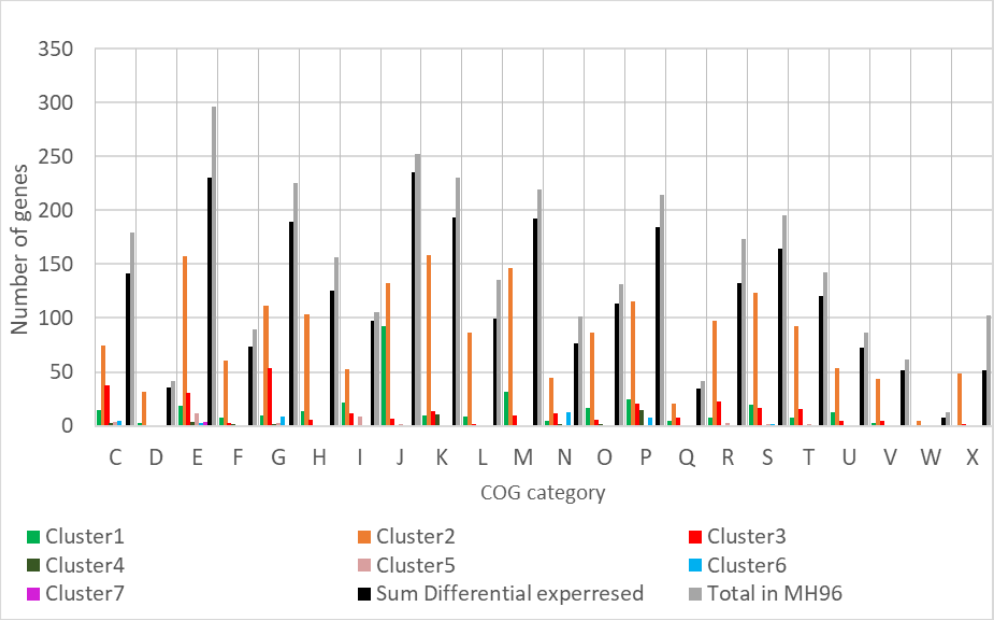

Figure 62: COG function of genes during the fermentation of *Y. entomophaga* in LB broth at 25°C. COG functions are sorted by Cluster 1-7 derived from cluster analysis. Indicated is the sum of differently expressed genes in the respective COG category (black bar) and COG classification of all gene products of the entire genome (grey bars). C, Energy production and conversion; D, Cell division; E Amino acid metabolites and transport; F Nucleotide metabolism and transport; G, Carbohydrate metabolism and transport; H Coenzyme transport and metabolism; I, Lipid metabolism; J, Translational processes; K, Transcription; L, Replication and repair; M, Cell wall/membrane/envelop biogenesis; N, Cell motility; O, post-translational modification; P, Inorganic ion transport and metabolism; Q, Secondary structure; T, signal transduction mechanism; U, Intracellular trafficking and secretion; V, Defense mechanisms; W, extracellular structures; X, Mobilome: Prophages, Transposons; R, General functional prediction only; S, Function unknown.

Down-regulation of genes upon pH shift in Cluster 1 and Cluster 4

Clusters 1 and 4 describe genes that are down-regulated from the pH drop onwards compared to T1. As previously mentioned, Cluster 1 comprised of 428 genes, 93 of which function in translational processes (Table S8). Most genes (57 genes) function in translational processes as ribosomal proteins or sigma factors (File S3), which indicates a reduction in post-transcriptional processes at this growth stage, when a cell density of 1.44×10^9 CFU/ml was reached. It is likely, that down-regulation of genes involved in translation is a cell density- or growth phase-dependent effect, rather than caused by a changing pH. Genes of Cluster 1 with the highest fold change between averaged reads of T2 compared to T1 are listed in Table 17 and denote significantly repressed genes in T2, correlating with a decreased pH in the medium. Fourteen of these genes are associated with TonB-dependent iron transport. Also found in Cluster 1 was the protein NhaA, which forms the sodium/proton antiporter. To note, the paralog NhaB, was not differentially expressed between time-points T1-5.

Table 17: Genes of Cluster 1 that are highly repressed in T2 compared to T1, measured by the ratio of the average reads.

Locus	Description	COG	T2/T1	Av T1	Av T2	Av T3	Av T4	Av T5
PL78_02925	membrane protein	S	7.21	226	31	20	34	28
PL78_02940	OpgC, glucans biosynthesis protein	M	5.02	460	92	91	74	68
PL78_03030	sulfurtransferase	R	6.67	5929	889	805	639	681
PL78_03185	NADH dehydrogenase	C	8.09	10900	1347	1034	969	1023
PL78_03910	decarboxylase	E	11.60	1353	117	115	129	335
PL78_03915	L-lysine 6-monooxygenase	Q	6.55	1085	166	176	143	333
PL78_03930	iron-siderophore transport system	P	5.30	694	131	100	110	92
PL78_03935	iron ABC transporter permease	P	7.13	490	69	70	79	66
PL78_03940	iron ABC transporter permease	P	9.24	428	46	49	68	50
PL78_03950	TonB-dependent receptor	P	11.05	3278	297	299	329	548
PL78_04080	ChaA, proton exchanger	P	6.35	3334	525	513	590	410
PL78_05040	predicted membrane protein		6.43	568	88	58	56	104
PL78_05515	FecI, RNA polymerase sigma factor	K	11.93	171	14	18	23	17
PL78_06545	hydroxamate-type ferrisiderophore receptor	P	10.82	3080	285	331	303	484
PL78_07705	glutathione peroxidase	O	7.02	1480	211	242	218	155
PL78_08295	chitin-binding protein	R	6.09	187	31	41	27	43
PL78_08425	TonB, periplasmic protein	M	6.81	540	79	74	59	87
PL78_09360	hypothetical protein		5.17	712	138	95	99	70
PL78_09390	MetK, S-adenosylmethionine synthetase	H	6.55	34113	5206	3690	4512	4149
PL78_09415	deoxyribonuclease I	L	5.10	809	159	112	102	54
PL78_09615	FecC, iron-dicitrate transporter permease subunit	P	8.46	569	67	57	78	60
PL78_09630	FecR, iron dicitrate transport regulator	P	8.60	734	85	78	76	94
PL78_09675	peptide synthetase	Q	5.09	807	159	156	166	164
PL78_09680	oxidoreductase	I	5.26	696	132	150	116	213
PL78_09690	EntE, enterobactin synthase subunit E	Q	8.38	1670	199	220	179	437
PL78_09735	hypothetical protein	S	10.62	467	44	47	41	113
PL78_09740	enterochelin esterase	P	11.22	2812	251	246	227	736
PL78_09780	ExbD, biopolymer transporter	U	16.19	2731	169	212	160	824
PL78_10235	PrmC, 23S rRNA methyltransferase	J	5.42	7639	1409	1119	1000	755
PL78_10775	PanF, sodium/panthothenate symporter	H	5.06	2578	509	356	290	324
PL78_11550	TsgA, MFS transporter	G	7.57	7687	1015	843	717	469
PL78_12235	superoxide dismutase	P	5.53	34017	6152	2862	1604	9438
PL78_12335	membrane protein	M	5.35	5972	1117	1043	666	256
PL78_12465	Pilin	N	5.05	1221	242	200	211	238
PL78_13130	RecQ	L	6.13	51761	8448	7370	9135	5853
PL78_13500	hypothetical protein		5.23	150	29	29	44	54
PL78_14155	SpeD, S-adenosylmethionine decarboxylase	E	5.20	16981	3268	1825	1399	2454
PL78_14175	hpt hypoxanthine phosphoribosyltransferase	F	5.68	6028	1061	621	625	621
PL78_14290	hypothetical protein		5.30	196	37	26	34	22
PL78_15445	IscR, transcriptional regulator	K	6.03	6297	1044	820	733	1463
PL78_15450	IscS, cysteine desulfurase	E	5.55	17171	3093	2221	2044	3926
PL78_15460	IscA, iron-sulfur cluster assembly protein	O	5.58	3645	653	418	406	807
PL78_15895	hypothetical protein	M	13.02	286	22	52	53	41
PL78_16190	phosphoglycerol transferase	M	6.25	12230	1958	1186	940	973
PL78_16735	hypothetical protein		8.13	423	52	41	46	32
PL78_17195	lysine transporter	E	6.30	8121	1290	1079	994	877
PL78_17451	CspD, cold-shock protein	K	8.69	1008	116	123	153	148
PL78_17500	membrane protein involved in acid resistance	S	5.82	398	68	60	55	20
PL78_17830	iron permease	P	17.64	1258	71	101	85	406
PL78_17840	peroxidase	P	14.63	3369	230	254	266	1340
PL78_18280	AcpP, acyl carrier protein	I	5.45	836	153	73	68	66
PL78_18290	DNA gyrase subunit B	S	5.46	1504	275	158	121	98
PL78_18550	phospholipid:lipid A palmitoyltransferase		8.46	3458	409	380	373	291
PL78_18580	Ferric iron reductase FhuF-like transporter	P	13.88	504	36	37	52	82
PL78_19025	iron transporter	P	5.43	1130	208	196	194	242

Av denotes the average read of the triplicates in the respective time-point. COG classification: C, Energy production and conversion; E Amino acid metabolites and transport; F, Nucleotide transport and metabolism; G, Carbohydrate metabolism and transport; H Coenzyme transport and metabolism; I, Lipid metabolism; J, translational processes; K, Transcription; L, Replication and repair; M, Cell wall/membrane/envelop biogenesis; N, Cell motility; O, post-translational modification; P, Inorganic ion transport and metabolism; Q, Secondary structure; U, Intracellular trafficking and secretion; R, General functional prediction only; S, Function unknown.

In Cluster 4, genes encoding for transcriptional regulators (12 genes), predominantly cold-shock proteins (7 genes), were identified (Table S9). The down-regulation of the cold-shock proteins CspA1,2,3,4; CspC and CspF1,2 indicated a response to the pH changes in the medium. Other transcriptional regulators are Fis, AraC-like regulator, and RNA polymerase sigma factor and sigma subunit (Fig. 63).

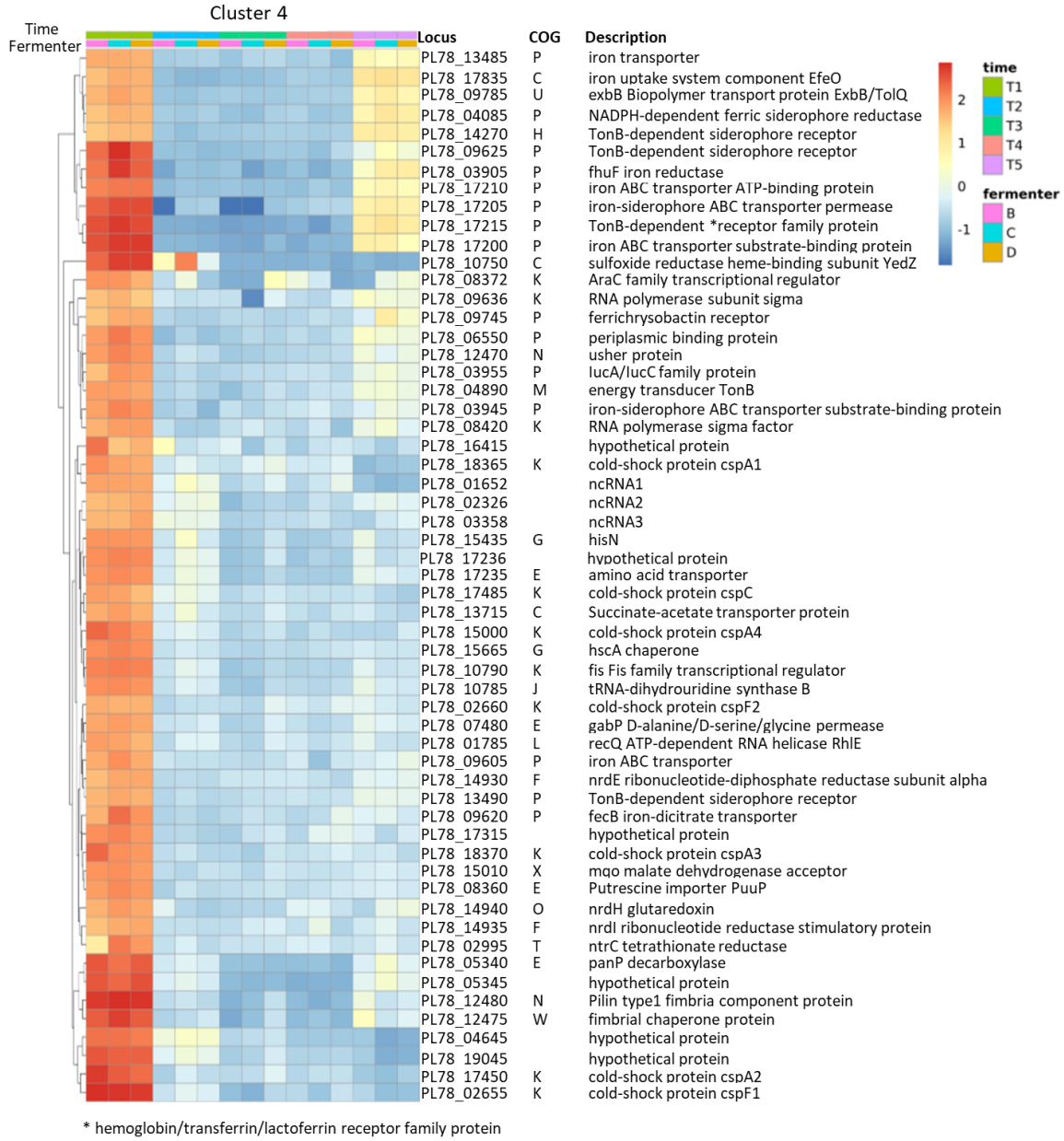

Figure 63: Heatmap of differential expressed genes in Cluster 4, with highly upregulated genes at T5 (24 hpi). C, Energy production and conversion; E Amino acid metabolites and transport; F Nucleotide metabolism and transport; G, Carbohydrate metabolism and transport; H Coenzyme transport and metabolism; J, Translational processes; K, Transcription; L, Replication and repair; M, Cell wall/membrane/envelop biogenesis; N, Cell motility; O, post-translational modification; P, Inorganic ion transport and metabolism; T, signal transduction mechanism; U, Intracellular trafficking and secretion; W, extracellular structures.

Other genes in Cluster 4 encoded for TonB-dependent siderophore receptors, OM-bound proteins, which form an ABC-transporter with TonB- to pump siderophores into the periplasm. Many of these siderophores bind iron ions. Interestingly, 14 other genes involved in iron transport are also down-regulated from T2 onwards and found in Cluster 1, indicating the strong relevance of iron homeostasis during the fermentation process with decreasing pH of the cell culture.

Up-regulation of genes during pH shift in Cluster 6

Cluster 6 described genes that are strongly up-regulated at time-point T2, when the pH drop occurred. Co-expression analysis of the RNAseq transcriptome identified 14 genes of the flagellum that are highly up-regulated in T2, when the pH drop occurs. These proteins are Flg- and Fli- proteins encoding the T3SS-like basal body of the flagellar (Fig. 64). Regarding flagella formation and activation, the motor proteins MotAB were continuously expressed (Cluster 2) and chemotaxis proteins were not significantly expressed under the fermentation conditions. Of note are genes of sugar transport/import such as maltose and trehalose, and genes of the sulfate transport in Cluster 6. The import of sugar occurs by an ABC transporter, which utilises in-flowing protons to import sugar molecules. A similar process is used by the flagellar motor, to generate the movement of the flagellum. Furthermore, the sulfate regulated Cys operon is highly expressed at T2, including protein CysW and CysT of the ABC transporter.

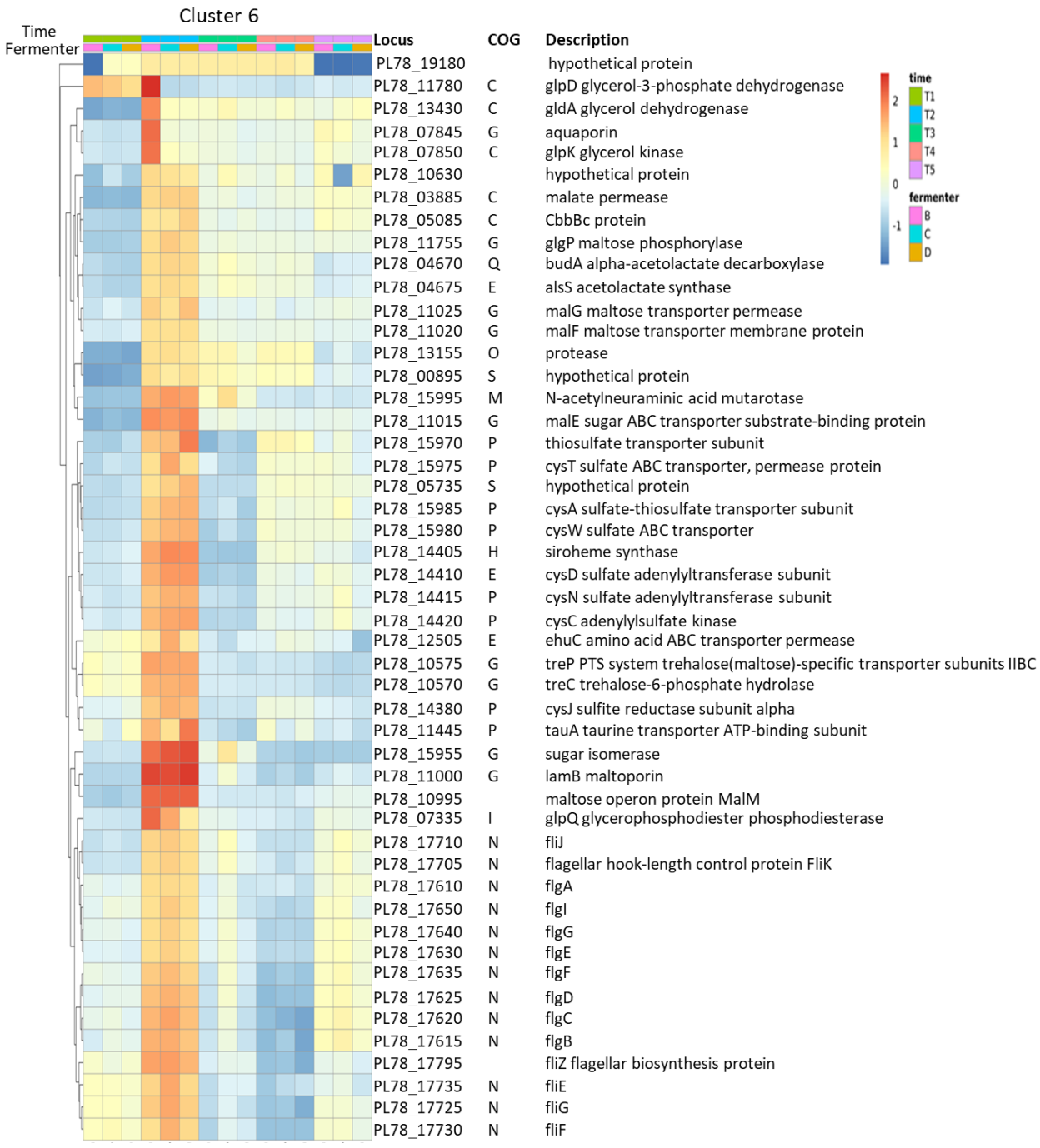

Figure 64: Heatmap of differentially expressed genes from Cluster 6. C, Energy production and conversion; E Amino acid metabolites and transport; G, Carbohydrate metabolism and transport; H Coenzyme transport and metabolism; I, Lipid metabolism; J, Translational processes; M, Cell wall/membrane/envelop biogenesis; N, Cell motility; O, Post-translational modification; P, Inorganic ion transport and metabolism; Q, Secondary structure; S, Function unknown.

.

Up-regulation of genes in time-point T5 (24 hpi) in Cluster 7 and Cluster 5

Clusters 5 and 7 comprise genes that are only highly expressed in T5 (24 hpi) compared to T1-T4. Over time, during the fermentation, the pH increased and reached pH8 at 24 hpi (T5).

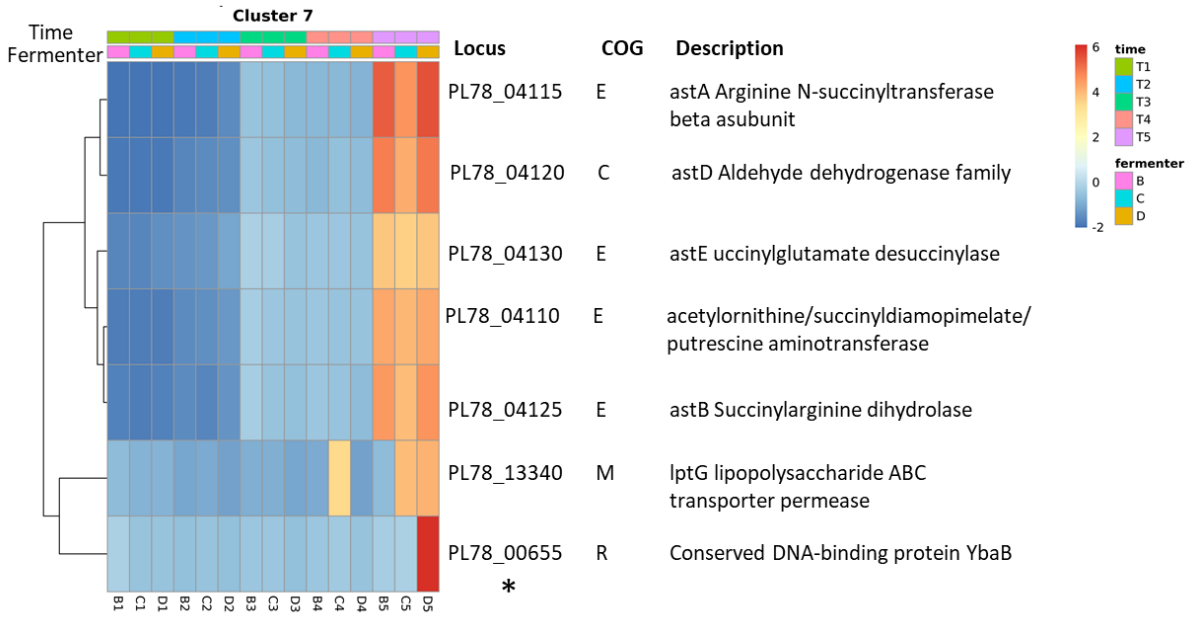

Figure 65: Heatmap of differential expressed genes in Cluster 7, with highly upregulated genes at T5 (24 hpi). * denotes outlier. C, Energy production and conversion; E Amino acid metabolites and transport; M, Cell wall/membrane/envelop biogenesis; Transposons; R, General functional prediction only.

Based on assessments of COGs in Cluster 7 (Fig. 65) and Cluster 5 (Fig. 66), genes were involved in amino acid transport and metabolism, specifically, arginine and histidine, two negatively charged amino acids, which were up-regulated in T5 (Table S10). The genes of the fatty acid degradation *fadA*, *fadB*, *fadE,* and *fadI*, in Cluster 5 were highly expressed at T5 (Fig. 66). The fatty acid degradation pathway metabolises acyl-coenzyme A to acetyl-coenzyme A (Acetyl-CoA) and gains energy in form of FADH2 and NADH. Furthermore, acetyl-coenzyme A can then be utilised in further pathways, such as the citric acid cycle, to obtain energy (Jansen and Steinbuchel, 2014).

Interestingly, of the 50 highly expressed genes from Cluster 5, 38 were down-regulated in QS mutant KTMS23 and the *roeA* mutant KTMS12 and another seven genes of the 50 genes only in KTMS23 (Table S11).

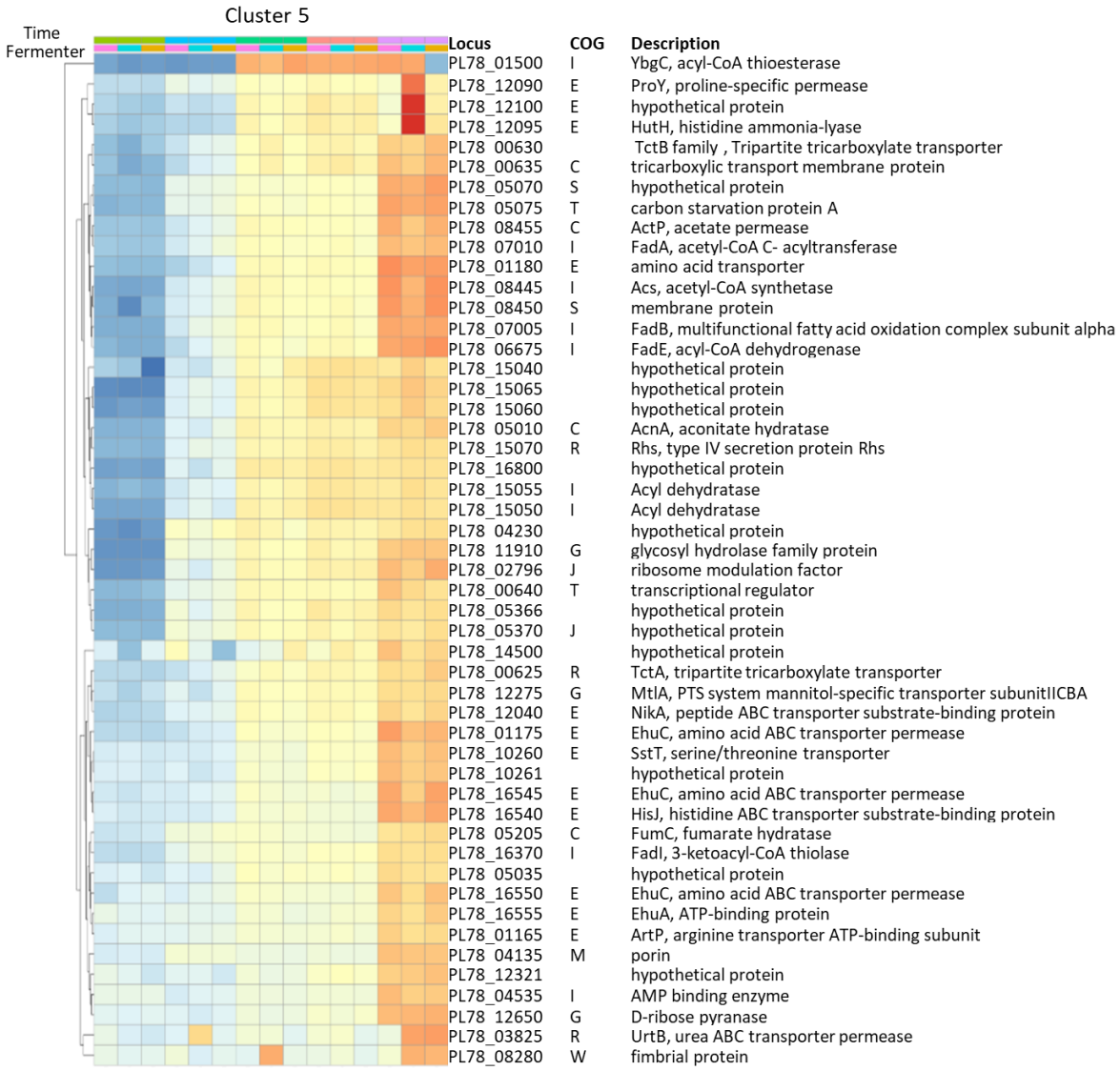

Figure 66: Heatmap of differential expressed genes in Cluster 7, with highly upregulated genes at T5 (24 hpi). C, Energy production and conversion; E Amino acid metabolites and transport; G, Carbohydrate metabolism and transport; I, Lipid metabolism; J, Translational processes; M, Cell wall/membrane/envelop biogenesis; W, extracellular structures; S, Function unknown; R, General functional prediction only.

Of these seven genes, three are located in the Rhs5 effector island (Hurst *et al.*, 2016). Of the seven genes in Cluster 7, all but one (encoding for IptG) were found to be down-regulated in the KTMS23 and KTMS12 (Table S11). The main COG classification of genes in Cluster 7 and 5, which are also under the control of RoeA and QS, function in amino acid transport and metabolism as well as the lipid transport and metabolism. Both are important when bacteria are grown in carbon-depleted media, to utilise amino acids and lipids such as fatty acids as alternative carbon sources (Clark and Cronan, 2005; Bren *et al.*, 2016). One of the amino acid transporters is encoded by *ehu* operon including *hisJ*, found in Cluster 5 and down-regulated in KTMS12 and KTMS23. The Ehu transporter is an ABC-type transporter for ectoine, which served as an osmotic protectant (Jebbar *et al.*, 2005).

Assessments of genes expressed in Cluster 2 with consistent gene-expression profile

Genes that were constitutively expressed were found in Cluster 2. Genes that were not differentially expressed between T1-T5 were not assessed in detail as they are unlikely to contribute to transcriptional regulation upon a trigger such as pH. However, referring to the heatmap of Cluster 2 (Fig. 67), some genes were strongly altered in T2 compared to T1, which might indicate a response to the lowered pH at T2.

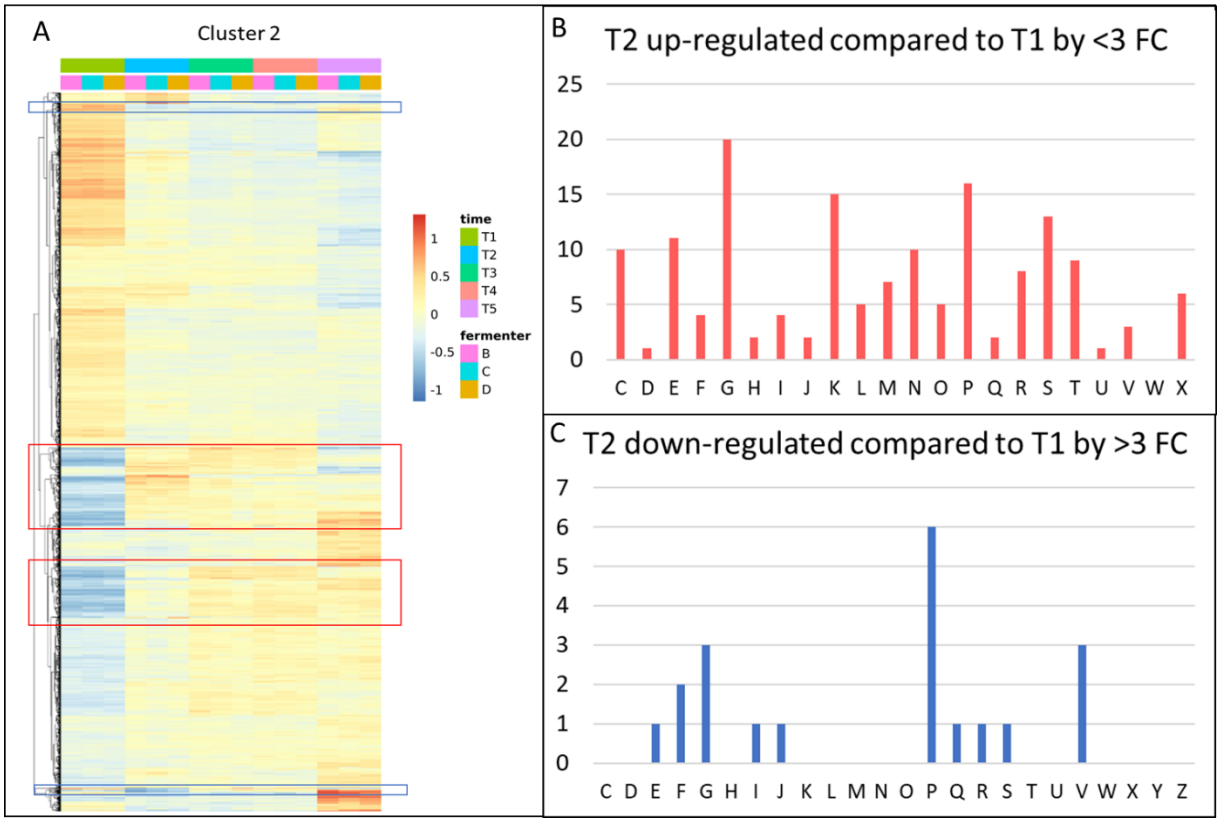

Figure 67: Differentially expressed gene sin Cluster 2. A) Heatmap of differential expressed genes in Cluster 4, constitutively expressed between T1-T5. Outliers are boxed: - black box denotes genes that are downregulated inT1 compared to T2, and red box denotes genes that are up-regulated in T1 compared to T2. *B)* Genes that are up-regulated in T2 compared to T1 with fold change (FC) > 3. *C)* Genes that are down-regulated in T2 compared to T1 with FC >3. COGs: C, Energy production and conversion; D, Cell division; E Amino acid metabolites and transport; F Nucleotide metabolism and transport; G, Carbohydrate metabolism and transport; H Coenzyme transport and metabolism; I, Lipid metabolism; J, Translational processes; K, Transcription; L, Replication and repair; M, Cell wall/membrane/envelop biogenesis; N, Cell motility; O, post-translational modification; P, Inorganic ion transport and metabolism; Q, Secondary structure; T, signal transduction mechanism; U, Intracellular trafficking and secretion; V, Defence mechanisms; W, extracellular structures; X, Mobilome: Prophages, Transposons; R, General functional prediction only; S, Function unknown.

In T2, 24 genes were down-regulated in comparison to T1 by >3 fold change (FC), of which 20 could be assigned with COG classification, which are in inorganic ion transport mechanisms (6), defence mechanisms (4), carbohydrate – (3), nucleotide- (2), amino acid – (1), lipid (1) transport and metabolism, as well as translational genes and a secondary metabolite biosynthesis gene (Table S12). In contrast, 191 genes were up-regulated in T2 compared to T1 by > 3 FC (Table S12). A COG could be assigned to 154 genes. The main COG functions are carbohydrate- and inorganic ion transport and metabolism, as well as genes involved in transcriptional processes, which were removed from further analysis as these genes, are unlikely to be affected by the pH drop.

The transcriptional activator FlhCD of the flagellum operon and the flagellar motor proteins MotAB are within the genes that were expressed >3 FC in T2 compared to T1. Furthermore, the YeRER genes encoding for the holin HolA, the endopeptidase PepB and the i-spanin Rz were also found to be 3.5 FC and 3.3 FC up-regulated in T2 compared to T1. As previously mentioned, RoeA – the putative transcriptional activator of YLC - had a 9.9 FC increase in T2 compared to T1 (Table 18).

The up-regulation of *roeA* and the YLC genes at time-point T2 correlates with the detectable exoproteome in the culture supernatant via SDS-PAGE (Fig. 57A) and validates the importance of the YeRER in exoproteome release. The YLC gene expression increased over time with the highest expression at 24 hpi (T5) (Table 18). In correlation to released exoproteins is the increased expression level of the released Yen-TC proteins, which already had high basal gene expression over time with up to 11.4 FC increase in T5 compared to T1 of YenC1 (Table 18). Of note, the genes encoding the Yen-TC, including *chi1* and *chi2,* were some of the highest expressed genes during fermentation (T2- T5), followed by porins including OmpA, and chaperons GroEL and DnaK. The highest expressed gene was the peptidase M66. Interestingly those chaperons, peptidase M66, as well as Yen-TC and YLC were down-regulated in the QS and *roeA* mutants (Chapter 4 and 6), indicating that QS/*roeA* regulation occurs during the fermentation process past T2 (7.3 hpi). In relation to the results of the previous Chapters 4, 5, and 6, Table 18 shows the genes identified in the HESA, their expression in the *roeA*- and QS mutants, and the cluster of gene expression in the fermentation. The comparison shows that 19 of the genes identified in the HESA (Chapter 4) were constitutively expressed during the fermentation, and therefore unlikely cause the initiation of exoproteome release. In Table 18 all HESA associated genes are listed, of which three genes were down-regulated upon pH shift (Cluster 1), which encoded SpeA arginine decarboxylase (PL78_09380) LPS synthase protein WaaC (PL78_07980) and LPS associated Prt paratose synthase (PL78_00700). The other HESA proteins (6) were found in Cluster 3 of the fermentation (Table S13).

Table 18: Expression profile of genes from YeRER and Yen-TC cluster as well as HESA associated genes.

Locus	Description	COG	FC T2/T1	Transcription level				
				Av T1	Av T2	Av T3	Av T4	Av T5
YeRER-associated genes								
PL78_1738	RoeA, PhoB-like regulator	K(X)	9.87	4577	45154	44641	45423	37612
PL78_1739	HolA, holin	(X)	3.48	2002	6974	8067	7838	10536
PL78_1739	PepB, peptidase M15	(X)	3.59	1563	5604	6568	6379	7613
PL78_1740	Rz1, i-spanin	(X)	3.39	1355	4594	5361	5178	5631
QS genes								
PL78_0384	GerE, LuxR family transcritional regulator	K	0.59	5704	3363	2504	2106	854
PL78_0385	acyl-homoserine-lactone synthase	T	0.83	4131	3424	2252	1934	1232
Yen-TC genes								
PL78_0372	Yen5, Posphate regulon sensor kinase PhoR	T	0.66	118	78	73	78	91
PL78_0373	Yen6, regulator		2.19	2650	5802	3490	2390	1113
PL78_0373	Yen7, regulator		2.03	2467	5003	3749	2597	1538
PL78_0374	Chi1, toxin complex component	G	3.47	109402	379254	520837	539353	530165
PL78_0374	YenA1, toxin complex component		3.25	137859	447718	711749	728313	861866
PL78_0375	YenA2, toxin complex component	V	3.18	105536	335656	564833	587655	750741
PL78_0375	Chi2, toxin complex component	G	3.50	22030	77169	136744	140088	196423
PL78_0376	YenB, toxin complex component	R	3.49	40966	142973	270967	311144	432280
PL78_0376	YenC1, toxin complex component	R	4.30	11668	50123	88707	100323	132922
PL78_0377	YenC2, toxin complex component	R	3.21	10632	34179	62354	67735	82413
PL78_0377	YenU	G	1.15	2635	3038	3351	3281	3740
PL78_0378	YenV	S	0.26	536	138	36	35	104
HESA-associated genes*								
PL78_0070	Prt, paratose synthase	M	0.49	7419	3628	2401	1859	1655
PL78_0071	WzX, O-antigen flippase	M	0.56	4688	2640	1818	1521	1280
PL78_0075	ManB, phosphomannomutase	G	0.75	11343	8543	6063	4888	4132
PL78_0143	GltA, type II citrate synthase	C	14.01	982	13755	32554	22665	18087
PL78_0347	SppA, signal peptide peptidase	O	1.83	2	4	3	4	3
PL78_0416	non-ribosomal peptide synthetase	Q	1.78	1006	1794	2607	2664	7342
PL78_0427	Regulator of sirC expression	T	0.66	3232	2126	1929	1888	1312
PL78_0480	DNA-binding protein H-NS	K	1.06	26186	27868	29286	25527	13173
PL78_0480	thymidine kinase	F	1.00	512	510	526	580	436
PL78_0750	O-antigen translocase	M	1.11	2023	2246	1466	1297	915
PL78_0750	WecE, TDP-4-oxo-6-deoxy-D-glucose aminotransferase	M	1.30	2982	3866	2276	1825	1729
PL78_0755	RecQ, ATP-dependent RNA helicase RhlB	L	0.64	19294	12419	11316	10075	8677
PL78_0756	PPx, guanosine polyphosphate pyrophosphohydrolase	F	0.58	8716	5078	4293	3799	3394
PL78_0798	WaaC, ADP-heptose LPS heptosyltransferase	M	0.46	2985	1370	957	803	614
PL78_0833	AspA, aspartate ammonia-lyase	E	93.97	1577	148224	79157	54501	41439
PL78_0938	SpeA, arginine decarboxylase	E	0.44	18968	8352	6055	5063	4526
PL78_0965	LpdA, pyridine nucleotide-disulfide oxidoreductase	C	2.30	161	370	453	361	247
PL78_1117	TrkA, potassium transporter	P	0.73	3173	2314	1940	1586	1071
PL78_1148	hypothetical protein	R	2.41	401	967	916	704	467
PL78_1148	NtcA, transcriptional regulator	T	2.39	6963	16627	14271	12249	10775
PL78_1165	intracellular growth attenuator protein igaA		0.70	3638	2564	2878	2739	2136
PL78_1298	Mdh, malate dehydrogenase	C	7.21	7025	50647	74899	58739	97488
PL78_1448	MutS, DNA mismatch repair protein	L	0.84	6207	5201	4548	3998	4384
PL78_1448	YscW, Type III secretion system lipoprotein chaperone		0.60	18	11	16	16	27
PL78_1540	DNA-binding transcriptional regulator, GntR family	K	0.99	4313	4269	4441	3830	1940
PL78_1557	GuaB,inosine-5-monophosphate dehydrogenase	T	0.67	13956	9302	6023	5606	2865
Highly expressed genes								
PL78_05495	peptidase M66		10.54	94831	999352	1740420.7	1899922	2024722
PL78_02825	porin OmpA	M	0.76	419370	317332	253224	250600	275347
PL78_13720	dnaK molecular chaperone	O	1.28	172455	220284.67	210400.67	187631.7	98796.3
PL78_08315	groEL molecular chaperone	O	1.28	198262	253614.67	205805.67	154397.3	122438
PL78_02730	porin	M	4.01	49281	197433	148220.67	166433	164445
PL78_01065	cold-shock protein cspE		5.36	5613	30062	51509	62248	29523

COGs: C, Energy production and conversion; E, Amino acid metabolites and transport; F Nucleotide metabolism and transport; G, Carbohydrate metabolism and transport; K, Transcription; L, Replication, and repair; M, Cell wall/membrane/envelop biogenesis; O, post-translational modification; P, Inorganic ion transport and metabolism; Q, Secondary structure; T, signal transduction mechanism; V, Defence mechanisms; R, General functional prediction only; S, Function unknown.

These genes encoded GltA type II citrate synthetase (PL78_01430), non-ribosomal peptide synthetase (PL78_04165), AspA aspartate ammonia-lyase (PLL78_08330), Mdh malate dehydrogenase (PL78_12985), and the YeRER proteins RoeA (PL78_17385) and HolA (PL17390) (Table 19). Cluster 3 described the gene expression which increased over time. Based on SDS-PAGE analysis it is not surprising that the Yen-TC genes were also expressed increasingly over time (Cluster 3).

Table 19: Comparison of gene expression in *roeA* mutant KTMS12 (Chapter 6), AHL synthetase-mutant KTMS23 (QS) compared to MH96 (Chapter 5) and expression cluster during fermentation.

Locus	Description	COG	KTMS12/ MH96 (FC)	KTMS23/ MH96 (FC)	Fermenter Cluster
HESA-associated genes					
PL78_00700	Prt, paratose synthase	M	1.64	1.84	1
PL78_00710	WzX, O-antigen flippase	M	1.39	1.49	2
PL78_00755	ManB, phosphomannomutase	G	1.65	1.69	2
PL78_01430	GltA, type II citrate synthase	C	3.66	2.20	3
PL78_03470	SppA, signal peptide peptidase	O	4.92	3.56	N.A.
PL78_04165	non-ribosomal peptide synthetase	Q	1.88	1.46	3
PL78_04270	Regulator of sirC expression	T	0.99	1.24	2
PL78_04800	H-NS, DNA-binding protein	K	1.14	1.17	2
PL78_04805	thymidine kinase	F	1.48	1.01	2
PL78_07500	O-antigen translocase	M	1.08	1.27	2
PL78_07505	WecE, TDP-4-oxo-6-deoxy-D-glucose aminotransferase	M	1.05	1.38	2
PL78_07555	recQ, ATP-dependent RNA helicase	L	1.34	1.15	2
PL78_07560	Ppx, guanosine polyphosphate pyrophosphohydrolase	F	1.33	1.02	2
PL78_07980	WaaC, ADP-heptose LPS heptosyltransferase	M	1.02	1.17	1
PL78_08330	AspA, aspartate ammonia-lyase	E	1.75	3.18	3
PL78_09380	SpeA, arginine decarboxylase	E	1.16	1.15	1
PL78_09650	LpdA, pyridine nucleotide-disulfide oxidoreductase	C	1.34	1.10	2
PL78_11175	TrkA, potassium transporter	P	1.65	1.41	2
PL78_11480	hypothetical protein	R	1.24	1.28	2
PL78_11485	NtcA, Crp/Fnr family transcriptional regulator	T	1.29	1.42	2
PL78_11650	IgaA, intracellular growth attenuator protein		1.83	1.07	2
PL78_12985	Mdh, malate dehydrogenase	C	2.35	1.47	3
PL78_14480	MutS, DNA mismatch repair protein	L	1.10	1.10	NA
PL78_14485	YscW, Type III secretion system lipoprotein chaperone		1.89	2.04	2
PL78_15400	DNA-binding transcriptional regulator, GntR family	K	1.21	1.04	2
PL78_15570	GuaB, inosine-5-monophosphate dehydrogenase	T	1.58	1.40	2

Locus	Description	COG	KTMS12/ MH96 (FC)	KTMS23/ MH96 (FC)	Fermenter Cluster
YeRER					
PL78_17385	RoeA, transcriptional regulator	(K/X)	20.53	5.35	3
PL78_17390	HolA, holin	(X)	330.84	3.78	3
PL78_17395	PepB, endopeptidase	(X)	461.44	4.79	2
PL78_17400	Rz, i-spanin	(X)	282.09	4.41	2
Yen-TC					
PL78_03725	Yen5 Posphate regulon sensor kinase PhoR	T	1.95	1.58	N.A.
PL78_03730	Yen6 regulator		1.02	1.22	2
PL78_03735	Yen7 regulator	(K)	6.63	1.13	2
PL78_03740	Chi1 toxin complex component	G	1209.34	5.31	3
PL78_03745	YenA1 toxin complex component		1722.16	6.82	3
PL78_03750	YenA2 toxin complex component	V	1541.37	7.52	3
PL78_03755	Chi2 toxin complex component	G	1341.84	7.52	3
PL78_03760	YenB toxin complex component	R	1541.37	8.06	3
PL78_03765	YenC1 toxin complex component	R	442.64	6.73	3
PL78_03770	YenC2 toxin complex component	R	250.73	3.84	3
PL78_03775	YenU	G	0.75	1.19	2
PL78_03780	YenV	S	13.27	9.78	1
PL78_03785	YenT heat stable endotoxin		2.58	1.37	N.A.
QS					
PL78_03845	GerE, LuxR family transcriptional regulator	K	1.75	1.45	2
PL78_03850	AHL, acyl-homoserine-lactone synthase	T	1.46	2.48	2

COGs: C, Energy production and conversion; E, Amino acid metabolites and transport; F Nucleotide metabolism and transport; G, Carbohydrate metabolism and transport; K, Transcription; L, Replication, and repair; M, Cell wall/membrane/envelop biogenesis; O, post-translational modification; P, Inorganic ion transport and metabolism; Q, Secondary structure; T, signal transduction mechanism; V, Defence mechanisms; R, General functional prediction only; S, Function unknown.

Cluster: 1 – high expression only in T1, 2 – continuously expressed, 3 – increasing gene expression over time from T1-T5.

FC: Fold change of transcript read counts

7.4 Discussion

The exoproteome release during the fermentation process in *Y. entomophaga* MH96 coincides with a decrease in pH of the culture medium. This Chapter reported transcriptome data of samples prior to, during, and post the pH drop. A temporary change of medium pH has been observed in other bacteria such as *E. coli*, *Serratia marcescens, Pseudomonas veronii, Corynebacterium ammoniagenes* and others (Ratzke and Gore, 2018; Sánchez-Clemente *et al.*, 2018). However, a release of exoproteins to the time of the pH drop has not been investigated to date. The transcriptome data of this study revealed ABC transporter for sugars such as trehalose and maltose, and for sulfate transport, which are highly elevated at T2 when the pH reached its minimum of 6.4.

The sulfate transporter CysZ in *E. coli* was shown to be pH-dependent and decreased sulfate transport with increasing pH from pH7-7.9 (Zhang *et al.*, 2014). ABC transporters, such as the Cys-transporter, utilise the proton gradient for the transport of the substrate. In Gram-negative bacteria, the proton gradient occurs between the cytoplasm and the periplasm. Another study showed the increased expression of the respiratory chain complex to pump protons out of the cell upon acidic challenge (Sousa *et al.*, 2012). However, the transcriptome data in this study did not identify differentially expressed genes of the respiratory complex.

In respect to exoproteome release, the transcriptome data identified increasing expression levels of the transcriptional regulator RoeA in T2 by ca. 10-fold change (FC) compared to T1. Correlating this with transcriptome data of the *roeA* mutant KTMS12 (Chapter 6), co-regulation of the YLC genes (~3.5 FC), and the Yen-TC genes (~3.5 FC) with *roeA* was observed. In this part of the study, the OMV formation was not investigated. It is expected that OMV formation occurs, which releases the Yen-TC proteins detected in SDS-PAGE, transcriptome data of OMV-associated genes such as GroEL/ES or OM proteins OmpA and OmpC showed they were not differentially expressed during the fermentation. Furthermore, gene expression of Yen7, the RoeA-paralog identified during the HESA, decreased over time in contrast to RoeA gene-expression which increased over time revealing, which indicates that these paralogues are likely to be regulated by alternate mechanisms. Other potential regulators of exoproteome release (identified by HESA in Chapter 4) have been identified as strongly up-regulated in T2 compared to T1. These comprise YeRER and Yen-TC genes, but also GltA, encoding for the type II citrate synthase (14 FC), and the aspartate ammonia-lyase AspA (94 FC). AspA genes were strongly expressed at T2 to then decreased over time reaching expression level 2 FC at T5 compared to T1, indicating a clear response to the changing conditions at T2. However, other aspartate associated genes were not differentially expressed. The serine protease AspA is auto-transported in *Neisseria meningitidis* and contains serine protease activity (Turner *et al.*, 2002). In the fungus *Penicillium*

roquerforti, the maturation of AspA occurs in acidic but not alkaline pH (Gente *et al.*, 2001). Hu *et al.* (2010) also described the role of ApsA in acid survival in *Y. pseudotuberculosis*, by producing ammonia from aspartate. The same study also identified increased expression of AspA at acidic pH (Hu *et al.*, 2010), which is consistent with AspA expression in *Y. entomophaga* MH96. In *Y. pseudotuberculosis*, pH-related regulation by OmpR and the T6SS has been observed (Zhang *et al.*, 2013). In the current study, no correlation between the expression of any secretion systems encoded by *Y. entomophaga* MH96, and pH-dependent exoproteome release could be observed. For example, genes of the T2SS, in Cluster 2, were continuously low expressed (max. 668 reads of *gspD* at T5), indicating that the T2SS is not the major mechanism of exoproteome release in MH96 (Table S12). In contrast, the T3SS and the T6SS are higher expressed compared to T2SS, but co-expression analysis showed no significant difference in gene expression between time-points T1-T5 (Table S12). The high expression of T3SS and T6SS, in addition to the high up-regulation of the genes important for iron transport, can be seen in *Y. pseudotuberculosis* and *Y. pestis in vivo,* indicating the relevance of pH shift for virulence in the host (Chen *et al.*, 2016).

It is important to note that during the fermentation process a constant air mix was applied. However, the oxygen level decreased from 97% to 2 % within 4 h of the fermentation run, from where it was held between 3-15%. While samples at T1 were collected when the low oxygen level was reached, it is possible that transcriptome levels adjusted at T2 towards the low oxygen level. Further studies are needed to investigate the influence of pH or oxygen on exoproteome release in MH96.

However, the increasing exoproteome release and the increased expression of the YeRER cluster, especially of holin, which is the rate-limiting step in classical cell lysis, and Yen-TCs indicates the relevance of YeRER to exoproteome release during fermentation.

Chapter 8

Final Discussion

To address the hypothesis, that a more stable and robust biopesticide product of *Y. entomophaga* can be developed by decreasing the metabolic burden to the cell, caused by the production and release of exoproteins over the secretion system, it was essential to develop a consistent sampling protocol, which allows exoproteome assessment. The exoproteome of MH96 *in vitro* comprises the main virulence factor, the Yen-TC, and other proteins such as outer membrane proteins (OmpA, OmpC), GroEL, and other proteins (Hurst *et al.*, 2011b). This study showed that exoproteome release is initiated at the late exponential phase when grown in LB broth. At a time when exoproteome release was observed (16 hpi), *Y. entomophaga* MH96 cells were viable and highly vesiculated.

The exoproteome or secretome are often identified by whole proteomic analysis using bioinformatic approaches, identifying secretion signal sequences or 2D-gel coupled with LC-MS/MS analysis (Pacheco *et al.*, 2011; Santos *et al.*, 2012; Gardiner *et al.*, 2017; Nirujogi *et al.*, 2017; Su *et al.*, 2017). In line with the aim of identifying genes that are involved in exoproteome release in *Y. entomophaga* MH96, a high-throughput exoproteome screening assay (HESA) was successfully developed in this study.

The HESA identified 35 mutants with insertions within 21 different genes, including 7 transcriptional regulators and four intergenic regions. Many of the identified genes are components of metabolic pathways, LPS synthesis, and transcriptional regulation. In relation to HESA, the identification of three transcriptional regulators, RoeA, RbsR (PL78_12675), and YhfX (PL78_15400) was important to this study as these regulators are likely to underpin a function in exoproteome regulation. Furthermore, the identification of four intergenic regions, where mutations lead to decreased exoproteome release, underpins a regulatory effect on the adjacent genes. For example, adjacent to the intergenic region PL78_04805/04800 are genes encoding for H-NS and RadA. H-NS is a global transcriptional repressor and RadA a DNA repair protein. The regulator H-NS binds to AT-rich double-strand DNA either down- or up/stream of the initiating RNA polymerase and forms a loop structure and therefore hinders transcription by the RNA polymerase (Lang *et al.*, 2007; Shin *et al.*, 2015; Boudreau *et al.*, 2018). H-NS represses many genes involved in virulence such as the T3SS and T6SS in *S. enterica* serovar Typhimurium, T3SS1 in *V. parahaemolyiticus* but also exoproteins such as the cholera toxin in *V. cholerae* or the invasion protein (*Inv*) in *Y. enterocolitica* (Ellsion and Miller, 2006; Kodama *et al*, 2010; Stonehouse *et al.*, 2011). Therefore, the identification of the H-NS locus, which is known to regulate

secretion, by the HESA underpins the effectiveness of the method to identify regulators in exoproteome release in *Y. entomophaga*. Furthermore, bioinformatic analysis of the intergenic region of YeRER, identified a possible H-NS binding site 5' of *roeA*. It is likely that *roeA* expression, and therefore exoprotein release, is under regulation of H-NS.

Using the HESA, the YeRER was identified and described. RoeA regulates the expression of Yen-TC, and secretion of other proteins including GroEL, DnaK, and OmpA.

In line with the aim to characterise the role of QS in exoproteome release, this study showed that *Y. entomophaga* exoproteome production and release is growth-dependent and linked to, but not exclusively regulated by, QS. Many studies have shown the regulation of secretion systems, such as T3SS in *P. aeruginosa*, T3SSs in *E. coli*, or the regulation of respective effector proteins such as T6SS effector Hcp in *Aeromonas hydrophila,* ExoS (T3SS) in *P. aeruginosa,* by QS (Hogardt *et al.*, 2004; Sircili *et al.*, 2004; Bleves *et al.*, 2005; Khajanchi *et al.*, 2009; Pena *et al.*, 2019; Turkina and Vikstrom, 2019) (Pena *et al.* 2019; Turkina and Vilkström, 2019; Bleves *et al.*, Sircili *et al.*, 2004; 2005; Khajanchi *et al.*, 2009; Hogardt *et al.*, 2004). However, most studies were targeted to specific effector proteins of a single secretion system and not at the overall exoproteome. This current study demonstrated that QS is implicated in the global regulation of MH96 exoproteome release. The reduction of the exoproteome in KTMS23 did not cause a loss in virulence for *G. mellonella* larvae when injected with the mutant. This study revealed that QS mutation releases exoproteome at 1×10^{10} CFU/ml compared to 3×10^{9} CFU/ml in MH96, validating QS- negatively regulated MH96 exoproteome release, which Is in line with the transcriptomics of KTMS23, where RoeA and YLC gene expression was down-regulated. The QS mutant reaches higher cell density after 24 h compared to MH96 and showed decreased exoproteome concentration, which likely reflects reduced metabolic load on the cell as a result of decreased exoproteome release. Interestingly, through transcriptome analysis, it was shown that the QS mutation led to repression of 195 genes and activation of 153 (by 2 fold and higher) that were also similarly repressed/ activated in the *roeA* mutant KTMS12 (Table S11), indicating that the QS and RoeA system are linked with each other. The KTMS12 gene *roeA* was also significantly down-regulated in the QS mutant by a 5 fold change, revealing that *roeA* transcription is cell-density and QS dependent, which in turn activates transcription of exoproteins including the Yen-TC and exoproteome release mechanisms such as the proposed YLC.

RNAseq of *roeA* mutant KTMS12 and QS mutant KTMS23 revealed that both activate gene expression of the PL78_09335-09270 genes encoding a putative prophage and the MH96 flagellum genes. Temperate prophages can be beneficial by encoding antibiotic resistances, drug efflux pumps, or cell division inhibiting factors (Ramisetty and Sudhakari, 2019). On the other hand, temperate phages can

cause cell lysis upon entry of the lytic cycle, which is correlated with stress factors, such as temperature, acidic- or oxygen stress, antimicrobials, or DNA stress as caused by mitomycin C (Choi *et al.*, 2010; Shan *et al.*, 2014; Veses-Garcia *et al.*, 2015; Kim *et al.*, 2018) (Shan *et al.*, 2014; Choi *et al.*, 2010; Veses-Garcia *et al.*, 2015; Kim *et al.*, 2018). Prophage genes in MH96 in exponential phase are not expressed, which indicates either the repression of these genes by transcriptional regulators, such as RoeA, QS or culture conditions do not cause stress to the cell and therefore do not initiate expression of the prophage genes. However, deletion of *roeA* caused a significant decrease in exoproteome release, despite activated expression of the prophage genes and its associated lysis cassette, indicating that expression of the prophage lysis cassette does not contribute to exoproteome release. In this respect, the YeRER encoded lysis cassette YLC was strongly down-regulated in the KTMS12 (*roeA* mutant), indicating a regulation of YLC- derived exoproteome release by RoeA. The exoproteome profile of KTMS12 was similar to the profile of KTMS4 (YLC mutant), with only 11 proteins present in the culture supernatant including flagella proteins and serralysin (Table 10).

Bioinformatic analysis identified binding motifs of PhoB-like proteins 5' of YLC, which likely regulate YLC gene expression in a RoeA-dependent manner. Correlating to *roeA* mutant transcriptome data, two other transcriptional regulators of the PhoB-like family were found to be differentially expressed in the *roeA* mutant. One of them is the RoeA paralog Yen7 (6.5 fold change, down-regulated). The other transcriptional regulator is YycF-like protein (PL78_09580) (5.2 fold change, down-regulated), which was identified in the initial HESA, but not further discussed as the exoproteome concentration of the 50-ml culture measured by Bradford assay did not validate a decreased exoproteome concentration. Interestingly, YycF is located 5' of the holin (PL78_09586), which is significantly down-regulated in KTMS12 as well, and the adjacent genes encoding the predicted PirAB insect toxin (PL78_09590/09595) are not differentially expressed compared to wild type MH96 (Table S6). YycF is part of the YycG/YycF two-component system in Gram-positive bacteria with low G+C content, such as *B. subtilis* and *Streptococcus pneumoniae,* where it represses genes involved in cell wall metabolism and fatty acid biosynthesis *(*Howell *et al.,* 2003; Mohedano *et al.,* 2016). The protein Yen7 is located 5' of the Yen-TC associated Chi1. Transcriptome data of the *roeA* mutant showed the down-regulation of Yen-TC and the YLC genes. The high amino acid similarity between Yen7 and RoeA, and the proximity of *yen7* to the Yen-TC operon and *roeA* to the YLC operon, are indicative of co-regulation of exoproteome/toxin production and release. It is likely that RoeA and Yen7, which are under the regulation of RoeA, bind to the YLC promoter region as transcriptional regulators. Of interest, a transposon insertion (in KTMS24) in the intergenic region of *yen7* and *chi1* increased exoproteome release (Table 9). The mutation of the intergenic region likely removes the binding site of a Yen-TC inhibitor, or inhibits *yen7* expression, which again acts as transcriptional repressor of the Yen-TC.

Studies by Amber Paulson (AgResearch) on the Yen6/Yen7 transcriptional regulation could not confirm Yen7 activity and this needs to be further investigated. However, SDS-PAGE assessments of K18 and KTMS12 (*roeA* mutants) supernatant and cell pellet, revealed the Yen-TC associate proteins were missing, confirming the results of KTMS12 transcriptome data showing down-regulation of Yen-TC genes by RoeA. As further evidence, the *trans* complementation of pGEM-YeRER (comprising of *roeA,* INT, *holA, pepB,* and *rz1*) in K18, partially restored exoproteome release, visible by SDS-PAGE, indicating the regulatory role of RoeA in co-location with YLC in protein release. Decreased exoproteome release of the transposon mutations (KTMS4, KTMS31, and KTMS46) in the 5' region of YLC, which through RNAseq was found to contain the *holA* 5' UTR, may indicate that transcription factors are binding to the 5'UTR. Alternately, secondary structures of the YLC 5' UTR control gene expression similar to the RNA-based-thermosensor of holin CidA in *S. aureus* (Hussein *et al.*, 2019). In *S. epidermidis* the antiholin LrgA gene expression is under the control of RsaE, a small regulatory RNA, binding to the 5' UTR (Schoenfelder *et al.*, 2019). Exoproteome release in MH96 was not altered by *trans* complementation with p184-5'hol (region 5' UTR of YLC) or p184-5'roeA (region 5' of *roeA*), indicating efficient binding of a putative transcription factor to the YLC and *roeA* promoter region. Critically, through *trans* complementation of p184INT and p184ncYLC220, a 200 bp ncRNA, ncYLC has been identified in the INT region of YeRER, which plays a significant role in the regulation of exoproteome in *Y. entomophaga* MH96. In *S. epidermidis* the ncRNA RsaE regulates biofilm formation, which is based on exoproteome release (Schoenfelder *et al.*, 2019). However, there is no sequence identity between ncYLC220 and RsaE or any other known ncRNA to date, indicating that ncYCL220 is a unique ncRNA.

Furthermore, several Hfq-binding motifs were identified within the intergenic region of YeRER, of which one is located in a potential RNA loop structure 5' of *holA* Hfq, which is a global post-transcriptional regulator facilitating the binding between small RNAs and target mRNAs. Hfq negatively regulates secretion systems such as T3SS in Gram-negative bacteria e.g. *E. coli* and *Y. pestis* (Sittka *et al.*, 2008; Lathem *et al.*, 2014). Despite several potential regulatory mechanisms -such as H-NS, Hfq, and PhoB-like binding motifs, secondary structures of *holA* and *roeA* 5' UTR, and ncYLC220, identified in the YeRER of MH96 that contribute to the release of the exoproteome, it is yet to be determined how it is regulated and under what conditions.

This study also showed that YLC is critical for exoproteome release in *Y. entomophaga* MH96, suggesting that the YLC pore-forming holin and the peptidoglycan degrading endolysin are required for protein translocation of exoproteins such as the Yen-TC, as it was shown for the toxin transport in *C. difficile* (Mehner-Breitfeld *et al.*, 2018). Furthermore, mutation of the holin/endolysin complex (YLC)

alters MH96 cell shape. Interestingly through the use of Live-cell imaging, cell elongation was observed when inducing the components of the YLC, using synthetic expression vector pARA-YLCRz1, prior to the lysis event. Expressing the native YLC of MH96, using pARA-HML where initiation codon of endolysin and the spanin genes overlap, resulting in a frameshift, did not cause such cell elongation. The transcriptome data of MH96 and K18 indicates that the YLC operon is transcribed into a polycistronic transcript from a common promoter, which is in agreement with the literature (Huber *et al.*, 2019). However, the overlapping genes can be translationally regulated by translational coupling, a mechanism that can adjust the expression ratios of the adjacent genes (Button and Galan, 2011; Tian and Salis, 2015). Phage-induced lysis is rate-limited by expression, integration, and multimerization of the holin, and the subsequent translocation of the respective endolysin by holin upon an unknown trigger (Saier *et al.*, 2015).The translational coupling of the YCL holin and endolysin in *Y. entomophaga* possibly adjusts the endolysin expression to inhibit cell lysis. This indicates a complex regulatory mechanism between holin and endolysin during and post transcription.

With respect to RNAseq data, *holA, pepB,* and *rz* are co-expressed. Cell elongation, such as seen after pARA-YLCRz1 induction, was also observed in *E. coli* upon induction of λ phage lysis cassette followed by sudden cell burst (Cahill *et al.*, 2019). Studies of induced λ phage showed that cell physiology, measured by proton motor force (pmf), is maintained until seconds before the bursting event (Grundling *et al.*, 2000). The same study suggested that integration and accumulation of holin in the IM does not change the pmf, or that changes in pmf can be compensated by proton efflux (Grundling *et al.*, 2000). Based on the results of the study by Grundling *et al.* (2011) and based on the finding of this study, the following model by which the lysis cassette releases exoproteins is proposed:

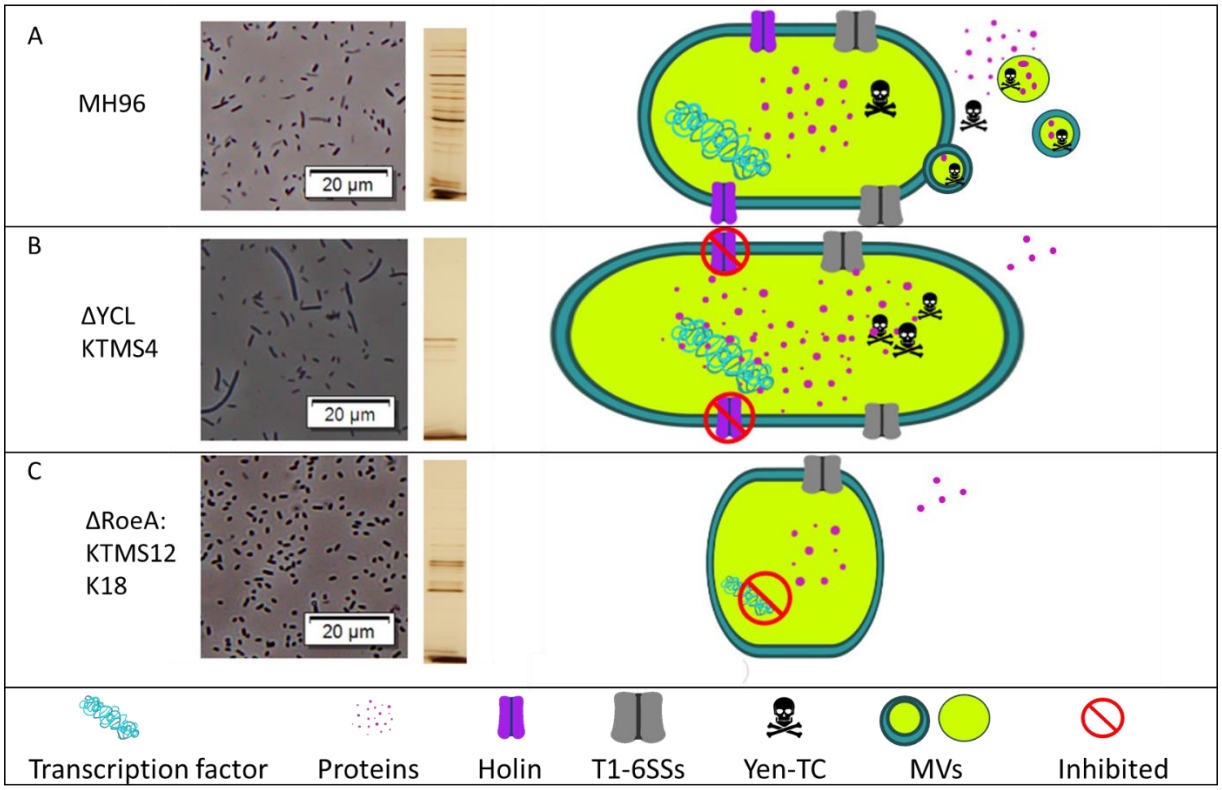

Figure 68: Schematic of cell shape formation based on exoproteome production and release. *A) Y. entomophaga* wild type strain MH96 as rod-shaped, and OMV forming cells with high exoproteome release when YLC genes and *roeA* were expressed. *B)* Deletion of YLC genes causing cell elongation and abolished exoproteome, caused by the absence of the holin hindering translocation of exoproteins such as Yen-TC, which accumulate in the cytoplasm and causing cell elongation. *C)* Deletion of *roeA* down-regulates YLC and expression of exoproteins, such as Yen-TC, which therefore do not accumulate in the cell. Down-regulation of LPS and cell wall synthesis proteins in the *roeA* mutant result in the shortening of the cell.

In *Y. entomophaga* MH96, the holin integration and formation of an unspecific pore in the IM leads to the translocation of endolysin (PepB), but also exoproteins such as Yen-TC (Fig. 68A) into the periplasm. The endolysin degrades the peptidoglycan, causing instability of the cell wall, which then causes exoproteome release, potentially by OMV formation (Fig. 68A). On the basis that holins form unspecific pores and the abolished exoproteome in the YLC mutant in this study, it can be assumed that holins such as HolA function as a general translocon of proteins that are not secreted by T1-6SSs. In the absence of such holins, it is assumed that these exoproteins cannot be released and therefore accumulate in the cytoplasm causing cell elongation (Fig 68B). The YLC is under the regulation of RoeA, which also regulates many other exoproteins such as Yen-TC. Despite the down-regulation of holin, cells do not elongate in the *roeA* mutant, possibly as a result of the decreased amount of exoproteins and ribosomal proteins expressed, as seen in KTMS12 (Fig. 68C).

However, in both, the *roeA* and the YLC mutants, through Cryo-ET (preliminary data) no OMV formation was observed as it was seen in MH96. In this study, Cryo-ET of *Y. entomophaga* MH96 identified membrane bulging and vesicle formation in high abundance. Many Gram-negative bacteria release OMVs with virulent cargo such Shiga toxin and Heat labile enterotoxin in *E. coli*, Pertussis toxin in *B. pertussis*, Rtx toxin in *V. cholera,* and adhesions in *Y. pestis* (Hozbor *et al.*, 1999; Kolling and Matthews, 1999; Horstman *et al.*, 2000; Altindis *et al.*, 2014; Eddy *et al.*, 2014). Proteomic assessments of *Y. pestis* OMVs, grown at 37°C, identified 270 proteins associated with the outer membrane, inner membrane, and periplasm, including the virulence factors: adhesion Ail, F1 outer fimbrial antigen, and protease Pla (Eddy *et al.*, 2014). The same authors also identified the sRNA -chaperon Hfq in OMVs (Eddy *et al.*, 2014). Furthermore, the OMV of *Y. pseudotuberculosis* YPIII harboured a high number of Yop proteins and the cytotoxic necrotizing factor (CNFγ), causing virulence (Monnappa *et al.*, 2018).

Based on the Cryo-ET images and exoproteome assessment by SDS-PAGE of *Y. entomophaga* MH96 and MH96ΔYLC, it is probable that the YLC in its natural state does not lyse but instead initiates the cellular blebbing in a precise orchestrated production of OMVs wherein the cells remain viable and therefore may present a new mechanism of bacteria secretion.

Preliminary proteomics of *Y. entomophaga* MH96 OMVs, investigated by Miki Feldmüller (ETH, Switzerland), identified Yen-TC components. For further studies, the final analysis of the OMV proteome is crucial. Furthermore, isolated OMVs should be assessed for virulence in a bioassay against *C. giveni*. If virulence still occurs by oral application of isolated OMVs, these membrane vesicles could be of great use in the development of a biopesticide. In fact, OMVs have already been applied in the field of pesticide development. A study by Su *et al.* (2017) used Gram-negative bacteria-derived membrane vesicles as a transport mechanism of degradative proteases for organophosphate pesticide degradation. Also, several studies by Alves and his co-workers demonstrated the suitability of and high tolerance against pH, temperature, and high salt concentration of OMVs when packed with phosphotriesterase (Alves *et al.*, 2016; Alves *et al.*, 2018).

While further studies are needed to define the regulation and underlying triggers of exoproteome release in Y. *entomophaga*, this study identified a unique rare mechanism based on a membrane vesicle inducing endolysin cassette, which is co-regulated with Yen-TC expression by the DNA-binding protein RoeA. Based on the finding of transcriptomics of the *roeA* mutant KTMS12, the QS mutant KTMS23, and the fermenter, the type 1-6 secretion systems are not the main mechanisms by which exoproteome release occurs in *Y. entomophaga*. The following exoproteome release model is proposed. The protein RoeA acts as a global regulator for gene transcription of genes implicated in virulence such as Yen-TC, YLC, flagella, T2SS, but also regulates phage genes (Fig. 69A), as identified

by RNAseq of KTMS12. In turn, *roeA* expression is under the control of QS, Hfq, RoeA itself, and H-NS, as identified by RNAseq of KTMS23, KTSM12, and ΔHfq (Hurst, unpublished) and by H-NS and PhoB-like binding motifs 5' of *roeA*. Additionally, the RoeA paralog Yen7 was identified which might interact with RoeA. RoeA activates the expression of exoproteins such as Yen-TC, Yen7, and the YLC, which is also under the control of a regulatory RNA (ncYLC220) and potentially by other transcriptional and post-transcriptional factors (Fig. 69B). The expressed and translated holin HolA of the YLC integrates into the IM and form a non-specific pore allowing translocation of endolysin and other proteins such as the Yen-TC (Fig. 69CD). Accumulation of exoproteins and endolysin activity cause cell wall instability. The detachment of the OM, caused by cell wall instability, leading to the formation of OMV carrying exoproteins as cargo (Fig. 69D).

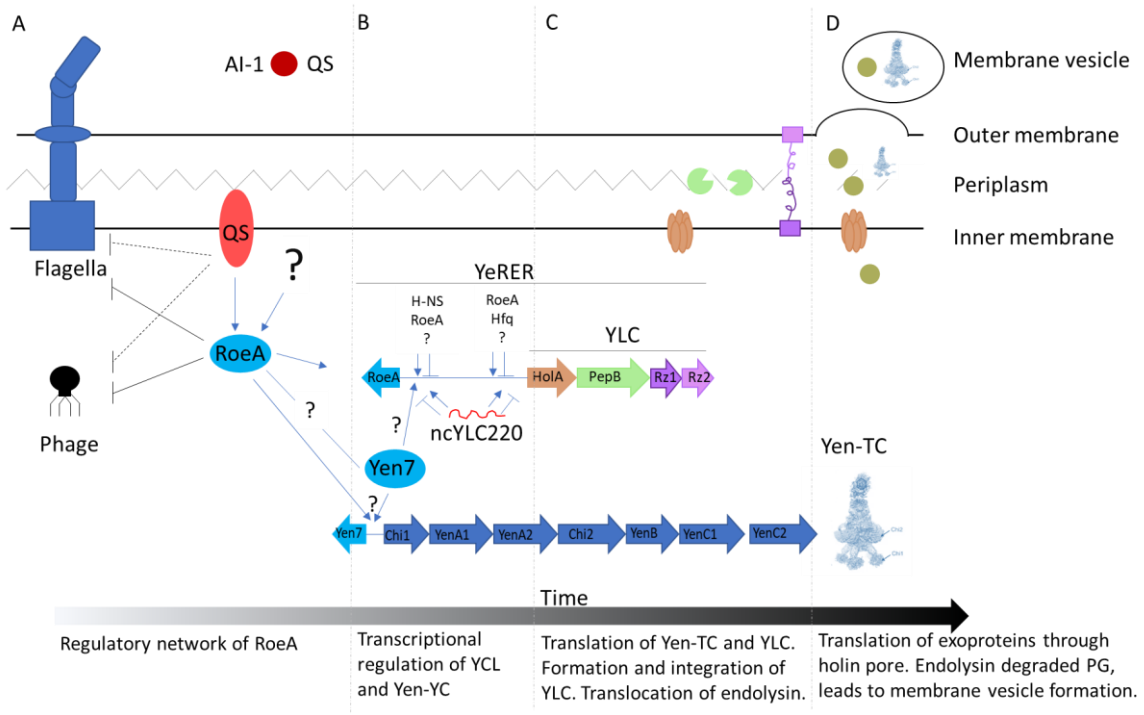

Figure 69: Model of exoproteome release by the YeRER. 1) RoeA is the global regulator of MH96 exoproteome production and release and can be induced by QS and potentially other, unknown mechanisms. RoeA regulates the transcription of many genes including flagellar prophage and the exoproteome associated Yen-TC proteins, Yen7, and YLC. B) YLC and Yen-TC are under the regulation of RoeA and potentially under the regulation of RoeA paralog Yen7. YLC is regulated by secondary structure, ncYLC220, and unknown binding proteins, such as PhoB-like and Hfq. C) Translation of YLC leads to the integration of Holin HolA, and the spanin complex RzRz1. Translocation of endolysin PepB leads to degradation of the peptidoglycan. D) Non-specific pore formed by HolA allows translocation of exoproteins (green circle), and Yen-TC into the periplasm. Additional disruption of the cell wall, by peptidoglycan degradation, initiates OMV formation, which carries exoproteins such as Yen-TC. ? indicates yet to be defined factors which likely are involved in the exoproteome release.

With the current knowledge, the hypothesis - a more stable, robust product can be developed by decreasing the metabolic burden of the cell, caused by the production of large toxins and the associated secretion system – cannot be disapproved. However, the results of this study indicate that the YLC induces exoproteome release by OMV formation. Furthermore, repression of the global regulator of exoproteome release leads to inactivation of YLC-depended exoproteome release, which correlates with increased cell density and formation of smaller, potentially more robust cells. This study indicates that the proposed hypothesis can be approved, but further studies to investigate the robustness and stability of a product are needed to confirm or deny the hypothesis with certainty.

Main conclusion

This thesis aimed to identify mechanisms of *Y. entomophaga* MH96 exoproteome release. Key findings of this study are the release of exoproteins in stationary phase, a growth phase often associated with QS. QS is involved in the regulation of the main virulence factor Yen-TC but also of the identified cluster, the YeRER, which is strongly linked with exoprotein release in MH96. The transcriptional regulator RoeA of the YeRER was shown to be a major activator of the Yen-TC cluster and of the YLC, which is indicative of the main release mechanism of the exoproteome. This study also linked YLC activity with OMV formation, which potentially is a release mechanism for large toxin complexes such as the Yen-TC in *Y. entomophaga*. The mutation of the AHL synthetase and *roeA* decreased the exoproteome release while increasing in CFU, which indicates a release burden on the cell when producing fewer exoproteins.

Chapter 9

Future perspectives

Chapter 3: Characterisation of the *Y. entomophaga* MH96 growth and secretion phenotype

Chapter 3 described the exoproteome release in MH96 cultures over time, correlating with membrane blebbing and OMV formation. In the ongoing collaboration with the ETH Zürich, we are aiming to quantify membrane blebbing in MH96 during different growth-phase to evaluate the relevance of OMV formation in the release of exoproteins. Further assessment of OMV content is relevant to understand which proteins are released by OMVs and if cytosolic proteins can also be transported.

Furthermore, and overlapping to Chapter 6, it is of interest to examine OMV formation in non-secreting strains MH96ΔYLC and K18 and compare to OMV formation and exoproteome release in MH96.

Chapter 4: Development of a high-throughput exoproteome screening assay (HESA) to identify regulators of Y. entomophaga exoproteome production

The successful HESA identified transcriptional regulator of exoproteome release in MH96. For further studies the HESA should be applied to other bacteria including the model bacterium *E. coli*. Furthermore, the HESA can be modified to test for mutations that increase exoproteome, which could further identify transcriptional regulators of exoprotein in MH96 and other bacteria.

Chapter 5: Quorum sensing controls protein secretion in *Y. entomophaga*

Exoproteome analysis of the QS mutant KTMS23 identified the QS-dependent release of exoproteins in the stationary phase. Using transcriptome data a decreased expression of YeRER genes and Yen-TC genes was observed. In the next step, the initiation of QS during the cell growth should be assessed using the QS-reporter plasmid pJBA132, which allows the detection of pJBA132-dependent GFP fluorescence proportional to AHL synthetase expression in MH96. This would allow to asses the CFU density at which QS is initiated. The information gained from the experiment may be relevant during fermentation and formulation processes of the biopesticide.

Chapter 6: Characterisation of the YLC

Using the HESA method, the RoeA transcriptional regulator was identified. Due to the high impact of the RoeA in exoproteome release further studies are needed. RoeA binding sites 5' of *roeA*, *holA* can be assessed. Additionally, the mutant KTMS24, carrying a transposon insertion in the intergenic region of *yen7-chi1*, showed an increase in exoproteome release, which indicates the binding of a transcriptional repressor of the Yen-TC operon. Using electromobility shift assays RoeA and its homolog Yen7 should be assessed in binding 5' of *roeA, holA,* and *chi1*. Eventually, binding affinities to those regions can be assessed to understand potential co-regulation between Yen7 and RoeA.

Furthermore, RoeA-reporter can be used to assess different culture conditions. Including temperature and pH, that may impact the *roeA* transcription.

The YLC was identified as the main mechanism for exoprotein release. Further studies are needed to assess the role in OMV formation, which is linked to the Yen-TC release in *Y. entomophaga.* Mutations of *holA, pepB,* and *rz,* respectively will help to understand the importance of each component of the YLC in the exoproteome release. Furthermore, GFP-reporters of the YLC proteins will be used for Cryo-ET-based protein localisation within the cell and within OMVs to assess their function during exoprotein release. Transcriptional and translational reporter will allow to determine if YLC expression and integration occurs within the entire population or in a sub-population of MH96.

A transcriptional reporter will be used to investigate YLC gene regulation by transcriptional regulators including QS, RoeA, and external factors including pH and temperature.

Further assessments:

The collected data from the above experiments will be needed to fully address the hypothesis: "A more stable, robust product can be developed by decreasing the metabolic burden of the cell, caused by the production of large toxins and the associated secretion system". In particular, studies to assess the metabolic burden on the bacterial population needs to be established. Such studies can include a detailed assessment of cell growth or Flux Balance Analysis of phosphate/oxygen ratios as an indicator for altered cell physiology or bioproduction/ metabolic pathways, respectively.

Once a decreased metabolic burden has been observed a product, like a bait, can be established using fermentation and formulation processes, which then allows testing for bioactivity and robustness of the product. This will be needed to answer the initial hypothesis, whether a decreased metabolic burden can increase the stability and shelf-life of the developed product/biopesticide.

References

Abbas-Ali, B. and Coleman, G. (1977). "The characteristics of extracellular protein secretion by *Staphylococcus aureus* (Wood 46) and their relationship to the regulation of alpha-toxin formation." J Gen Microbiol **99**(2): 277-282.

Abby, S. S., Cury, J., Guglielmini, J., et al. (2016). "Identification of protein secretion systems in bacterial genomes." Sci Rep **6**: 23080.

Abisado, R. G., Benomar, S., Klaus, J. R., et al. (2018). "Bacterial quorum sensing and microbial community interactions." MBio **9**(3).

Agrawal, T. and Kotasthane, A. S. (2012). "Chitinolytic assay of indigenous *Trichoderma* isolates collected from different geographical locations of Chhattisgarh in Central India." Springerplus **1**(1): 73.

Altindis, E., Fu, Y. and Mekalanos, J. J. (2014). "Proteomic analysis of *Vibrio cholerae* outer membrane vesicles." Proc Natl Acad Sci U S A **111**(15): E1548-1556.

Alves, N. J., Moore, M., Johnson, B. J., et al. (2018). "Environmental decontamination of a chemical warfare simulant utilizing a membrane vesicle-encapsulated phosphotriesterase." ACS Appl Mater Interfaces **10**(18): 15712-15719.

Alves, N. J., Turner, K. B. and Walper, S. A. (2016). "Directed protein packaging within outer membrane vesicles from *Escherichia coli*: Design, production and purification." J Vis Exp(117).

Andersen, J. B., Heydorn, A., Hentzer, M., et al. (2001). "Gfp-based N-acyl homoserine-lactone sensor systems for detection of bacterial communication." Appl Environ Microbiol **67**(2): 575-585.

Andreazza, F., Vacacela Ajila, H. E., Haddi, K., et al. (2018). "Toxicity to and egg-laying avoidance of *Drosophila suzukii* (Diptera: Drosophilidae) caused by an old alternative inorganic insecticide preparation." Pest Manag Sci **74**(4): 861-867.

Anisimov, A. P., Dentovskaya, S. V., Titareva, G. M., et al. (2005). "Intraspecies and temperature-dependent variations in susceptibility of *Yersinia pestis* to the bactericidal action of serum and to polymyxin B." Infect Immun **73**(11): 7324-7331.

Antunes, L. C. M., Ferreira, R. B. R., Buckner, M. M. C., et al. (2010). "Quorum sensing in bacterial virulence." Microbiology **156**(Pt 8): 2271-2282.

Armengaud, J., Christie-Oleza, J. A., Clair, G., et al. (2012). "Exoproteomics: exploring the world around biological systems." Expert Rev Proteomics **9**(5): 561-575.

Atkinson, S., Goldstone, R. J., Joshua, G. W., et al. (2011). "Biofilm development on *Caenorhabditis elegans* by *Yersinia* is facilitated by quorum sensing-dependent repression of type III secretion." PLoS Pathog **7**(1): e1001250.

Atkinson, S. and Williams, P. (2016). "*Yersinia* virulence factors - a sophisticated arsenal for combating host defences." F1000Res **5**.

Axler-DiPerte, G. L., Hinchliffe, S. J., Wren, B. W., et al. (2009). "YtxR acts as an overriding transcriptional off switch for the *Yersinia enterocolitica* Ysc-Yop type 3 secretion system." J Bacteriol **191**(2): 514-524.

Bailey, J. and Manoil, C. (2002). "Genome-wide internal tagging of bacterial exported proteins." Nat Biotechnol **20**(8): 839-842.

Baldi, D. L., Higginson, E. E., Hocking, D. M., et al. (2012). "The type II secretion system and its ubiquitous lipoprotein substrate, SslE, are required for biofilm formation and virulence of enteropathogenic *Escherichia coli*." Infect Immun **80**(6): 2042-2052.

Bancerz-Kisiel, A., Pieczywek, M., Lada, P., et al. (2018). "The most important virulence markers of *Yersinia enterocolitica* and their role during infection." Genes (Basel) **9**(5).

Bayles, K. W. (2007). "The biological role of death and lysis in biofilm development." Nat Rev Microbiol **5**(9): 721-726.

Bender, J. K., Wille, T., Blank, K., et al. (2013). "LPS structure and PhoQ activity are important for *Salmonella Typhimurium* virulence in the *Galleria mellonella* infection model [corrected]." PLoS One **8**(8): e73287.

Bengoechea, J. A., Najdenski, H. and Skurnik, M. (2004). "Lipopolysaccharide O antigen status of *Yersinia enterocolitica* O:8 is essential for virulence and absence of O antigen affects the expression of other *Yersinia* virulence factors." Mol Microbiol **52**(2): 451-469.

Bent, Z. W., Branda, S. S. and Young, G. M. (2013). "The *Yersinia enterocolitic*a Ysa type III secretion system is expressed during infections both *in vitro* and *in vivo*." Microbiologyopen **2**(6): 962-975.

Berc, A., Petrinec, Z., Matasin, Z., et al. (1999). "*Yersinia ruckeri* septicaemia in experimentally infected carp (*Cyprinus carpio* L.) fingerlings." Acta Vet Hung **47**(2): 161-172.

Berry, J., Rajaure, M., Pang, T., et al. (2012). "The spanin complex is essential for lambda lysis." J Bacteriol **194**(20): 5667-5674.

Berry, J., Summer, E. J., Struck, D. K., et al. (2008). "The final step in the phage infection cycle: the Rz and Rz1 lysis proteins link the inner and outer membranes." Mol Microbiol **70**(2): 341-351.

Beveridge, T. J. (1999). "Structures of gram-negative cell walls and their derived membrane vesicles." J Bacteriol **181**(16): 4725-4733.

Birnboim, H. C. and Doly, J. (1979). "A rapid alkaline extraction procedure for screening recombinant plasmid DNA." Nucleic Acids Res **7**(6): 1513-1523.

Blackburn, M. B., Martin, P. A., Kuhar, D., et al. (2011). "The occurrence of photorhabdus-like toxin complexes in *Bacillus thuringiensis*." PLoS One **6**(3): e18122.

Bleves, S., Soscia, C., Nogueira-Orlandi, P., et al. (2005). "Quorum sensing negatively controls type III secretion regulon expression in *Pseudomonas aeruginosa* PAO1." J Bacteriol **187**(11): 3898-3902.

Block, A. and Alfano, J. R. (2011). "Plant targets for *Pseudomonas syringae* type III effectors: virulence targets or guarded decoys?" Curr Opin Microbiol **14**(1): 39-46.

Blum, H., Beier, H. and Gross, H. J. (1987). "Improved silver staining of plant proteins, RNA and DNA in polyacrylamide gels." Electrophoresis **8**(2): 93-99.

Blummel, A. S., Drepper, F., Knapp, B., et al. (2017). "Structural features of the TatC membrane protein that determine docking and insertion of a twin-arginine signal peptide." J Biol Chem **292**(52): 21320-21329.

Bontemps-Gallo, S., Fernandez, M., Dewitte, A., et al. (2019). "Nutrient depletion may trigger the *Yersinia pestis* OmpR-EnvZ regulatory system to promote flea-borne plague transmission." Mol Microbiol **112**(5): 1471-1482.

Borlee, B. R., Goldman, A. D., Murakami, K., et al. (2010). "*Pseudomonas aeruginosa* uses a cyclic-di-GMP-regulated adhesin to reinforce the biofilm extracellular matrix." Mol Microbiol **75**(4): 827-842.

Boudreau, B. A., Kotlajich, M. V. and Landick, R. (2018). "*In Vitro* transcription assay to quantify effects of H-NS filaments on RNA chain elongation by RNA polymerase." Methods Mol Biol **1837**: 351-386.

Bouwman, H., Yohannes, Y. B., Nakayama, S. M. M., et al. (2019). "Evidence of impacts from DDT in pelican, cormorant, stork, and egret eggs from KwaZulu-Natal, South Africa." Chemosphere **225**: 647-658.

Boyer, F., Fichant, G., Berthod, J., et al. (2009a). "Dissecting the bacterial type VI secretion system by a genome wide *in silico* analysis: what can be learned from available microbial genomic resources?" BMC Genomics **10**: 104.

Boyer, M. and Wisniewski-Dye, F. (2009b). "Cell-cell signalling in bacteria: not simply a matter of quorum." FEMS Microbiol Ecol **70**(1): 1-19.

Bradfield, P. F., Johnson-Leger, C. A., Zimmerli, C., et al. (2008). "LPS differentially regulates adhesion and transendothelial migration of human monocytes under static and flow conditions." Int Immunol **20**(2): 247-257.

Bradford, M. M. (1976). "A rapid and sensitive method for the quantitation of microgram quantities of protein utilizing the principle of protein-dye binding." Anal Biochem **72**: 248-254.

Bren, A., Park, J. O., Towbin, B. D., et al. (2016). "Glucose becomes one of the worst carbon sources for *E.coli* on poor nitrogen sources due to suboptimal levels of cAMP." Sci Rep **6**: 24834.

Briegel, A., Li, X., Bilwes, A. M., et al. (2012). "Bacterial chemoreceptor arrays are hexagonally packed trimers of receptor dimers networked by rings of kinase and coupling proteins." Proc Natl Acad Sci U S A **109**(10): 3766-3771.

Briers, Y., Peeters, L. M., Volckaert, G., et al. (2011). "The lysis cassette of bacteriophage varphiKMV encodes a signal-arrest-release endolysin and a pinholin." Bacteriophage **1**(1): 25-30.

Brillard, J., Duchaud, E., Boemare, N., et al. (2002). "The PhlA hemolysin from the entomopathogenic bacterium *Photorhabdus luminescens* belongs to the two-partner secretion family of hemolysins." J Bacteriol **184**(14): 3871-3878.

Brzostkowska, M., Raczkowska, A. and Brzostek, K. (2012). "OmpR, a response regulator of the two-component signal transduction pathway, influences *inv* gene expression in *Yersinia enterocolitica* O9." Front Cell Infect Microbiol **2**: 153.

Burtnick, M. N., Brett, P. J. and DeShazer, D. (2014). "Proteomic analysis of the *Burkholderia pseudomallei* type II secretome reveals hydrolytic enzymes, novel proteins, and the deubiquitinase TssM." Infect Immun **82**(8): 3214-3226.

Buttner, D. and He, S. Y. (2009). "Type III protein secretion in plant pathogenic bacteria." Plant Physiol **150**(4): 1656-1664.

Button, J. E. and Galan, J. E. (2011). "Regulation of chaperone/effector complex synthesis in a bacterial type III secretion system." Mol Microbiol **81**(6): 1474-1483.

Caffrey, D. R., Dana, P. H., Mathur, V., et al. (2007). "PFAAT version 2.0: a tool for editing, annotating, and analyzing multiple sequence alignments." BMC Bioinformatics **8**: 381.

Cahill, J., Rajaure, M., O'Leary, C., et al. (2017). "Genetic analysis of the lambda spanins Rz and Rz1: identification of functional domains." G3 (Bethesda) **7**(2): 741-753.

Cahill, J. and Young, R. (2019). "Phage lysis: multiple genes for multiple barriers." Adv Virus Res **103**: 33-70.

Cascales, E. and Cambillau, C. (2012). "Structural biology of type VI secretion systems." Philos Trans R Soc Lond B Biol Sci **367**(1592): 1102-1111.

Catalao, M. J., Gil, F., Moniz-Pereira, J., et al. (2013). "Diversity in bacterial lysis systems: bacteriophages show the way." FEMS Microbiol Rev **37**(4): 554-571.

Cava, F., Kuru, E., Brun, Y. V., et al. (2013). "Modes of cell wall growth differentiation in rod-shaped bacteria." Curr Opin Microbiol **16**(6): 731-737.

Cezairliyan, B. and Ausubel, F. M. (2017). "Investment in secreted enzymes during nutrient-limited growth is utility dependent." Proc Natl Acad Sci U S A **114**(37): E7796-E7802.

Chakraborty, S. and Kenney, L. J. (2018). "A new role of OmpR in Acid and osmotic stress in *Salmonella* and *E. coli*." Front Microbiol **9**: 2656.

Chang, A. C. and Cohen, S. N. (1978). "Construction and characterization of amplifiable multicopy DNA cloning vehicles derived from the P15A cryptic miniplasmid." J Bacteriol **134**(3): 1141-1156.

Chen, P. E., Cook, C., Stewart, A. C., et al. (2010). "Genomic characterization of the *Yersinia* genus." Genome Biol **11**(1): R1.

Chen, S., Thompson, K. M. and Francis, M. S. (2016). "Environmental regulation of *Yersinia* pathophysiology." Front Cell Infect Microbiol **6**: 25.

Chitcholtan, K., Hampton, M. B. and Keenan, J. I. (2008). "Outer membrane vesicles enhance the carcinogenic potential of *Helicobacter pylori*." Carcinogenesis **29**(12): 2400-2405.

Choi, S., Dunams, D. and Jiang, S. C. (2010). "Transfer of cholera toxin genes from O1 to non-O1/O139 strains by vibriophages from California coastal waters." J Appl Microbiol **108**(3): 1015-1022.

Choudhary, A. and Sharma, D. C. (2008). "Dynamics of pesticide residues in nectar and pollen of mustard (*Brassica juncea* (L.) Czern.) grown in Himachal Pradesh (India)." Environ Monit Assess **144**(1-3): 143-150.

Christensen, J. E., Pacheco, S. A. and Konkel, M. E. (2009). "Identification of a *Campylobacter jejuni*-secreted protein required for maximal invasion of host cells." Mol Microbiol **73**(4): 650-662.

Christie, P. J., Whitaker, N. and Gonzalez-Rivera, C. (2014). "Mechanism and structure of the bacterial type IV secretion systems." Biochim Biophys Acta **1843**(8): 1578-1591.

Chung, L. K. and Bliska, J. B. (2016). "*Yersinia* versus host immunity: how a pathogen evades or triggers a protective response." Curr Opin Microbiol **29**: 56-62.

Clark, D. P. and Cronan, J. E. (2005). "Two-carbon compounds and fatty acids as carbon sources." EcoSal Plus **1**(2).

Coil, D., Jospin, G. and Darling, A. E. (2015). "A5-miseq: an updated pipeline to assemble microbial genomes from Illumina MiSeq data." Bioinformatics **31**(4): 587-589.

Coil, D. A. and Anne, J. (2009). "Twitching motility in *Legionella pneumophila*." FEMS Microbiol Lett **293**(2): 271-277.

Collyn, F., Lety, M. A., Nair, S., et al. (2002). "*Yersinia pseudotuberculosis* harbors a type IV pilus gene cluster that contributes to pathogenicity." Infect Immun **70**(11): 6196-6205.

Cope, L. D., Yogev, R., Muller-Eberhard, U., et al. (1995). "A gene cluster involved in the utilization of both free heme and heme:hemopexin by *Haemophilus influenzae* type b." J Bacteriol **177**(10): 2644-2653.

Cork, S. C., Collins-Emerson, J. M., Alley, M. R., et al. (1999). "Visceral lesions caused by *Yersinia pseudotuberculosis*, serotype II, in different species of bird." Avian Pathol **28**(4): 393-399.

Cornelis, G. R. (1998). "The *Yersinia* Yop virulon, a bacterial system to subvert cells of the primary host defense." Folia Microbiol (Praha) **43**(3): 253-261.

Cornelis, G. R. (2002). "*Yersinia* type III secretion: send in the effectors." J Cell Biol **158**(3): 401-408.

Costa, T. R., Felisberto-Rodrigues, C., Meir, A., et al. (2015). "Secretion systems in Gram-negative bacteria: structural and mechanistic insights." Nat Rev Microbiol **13**(6): 343-359.

Coulthurst, S. (2019). "The Type VI secretion system: a versatile bacterial weapon." Microbiology **165**(5): 503-515.

Cournac, A. and Plumbridge, J. (2013). "DNA looping in prokaryotes: experimental and theoretical approaches." J Bacteriol **195**(6): 1109-1119.

Crane, J. M. and Randall, L. L. (2017). "The sec system: Protein export in *Escherichia coli*." EcoSal Plus **7**(2).

Crhanova, M., Malcova, M., Mazgajova, M., et al. (2011). "LPS structure influences protein secretion in *Salmonella enterica*." Vet Microbiol **152**(1-2): 131-137.

Dahlawi, S. M. and Siddiqui, S. (2017). "Calcium polysulphide, its applications and emerging risk of environmental pollution-a review article." Environ Sci Pollut Res Int **24**(1): 92-102.

Dai, Q., Xu, L., Xiao, L., et al. (2018). "RovM and CsrA negatively regulate urease expression in *Yersinia pseudotuberculosis*." Front Microbiol **9**: 348.

Dame, R. T., Noom, M. C. and Wuite, G. J. (2006). "Bacterial chromatin organization by H-NS protein unravelled using dual DNA manipulation." Nature **444**(7117): 387-390.

Das, A. and Xie, Y. H. (1998). "Construction of transposon Tn3phoA: its application in defining the membrane topology of the *Agrobacterium tumefaciens* DNA transfer proteins." Mol Microbiol **27**(2): 405-414.

Das, C., Mokashi, C., Mande, S. S., et al. (2018). "Dynamics and control of flagella assembly in *Salmonella typhimurium*." Front Cell Infect Microbiol **8**: 36.

Datsenko, K. A. and Wanner, B. L. (2000). "One-step inactivation of chromosomal genes in *Escherichia coli* K-12 using PCR products." Proc Natl Acad Sci U S A **97**(12): 6640-6645.

Dave, M. N., Silva, J. E., Elicabe, R. J., et al. (2016). "*Yersinia enterocolitica* YopH-deficient strain activates neutrophil recruitment to Peyer's patches and promotes clearance of the virulent strain." Infect Immun **84**(11): 3172-3181.

Davis, K. M. (2018). "All *Yersinia* are not created equal: Phenotypic adaptation to distinct niches within mammalian tissues." Front Cell Infect Microbiol **8**: 261.

Dean, P. (2011). "Functional domains and motifs of bacterial type III effector proteins and their roles in infection." FEMS Microbiol Rev **35**(6): 1100-1125.

Deatherage, B. L. and Cookson, B. T. (2012). "Membrane vesicle release in bacteria, eukaryotes, and archaea: a conserved yet underappreciated aspect of microbial life." Infect Immun **80**(6): 1948-1957.

Deatherage, D. E. and Barrick, J. E. (2014). "Identification of mutations in laboratory-evolved microbes from next-generation sequencing data using breseq." Methods Mol Biol **1151**: 165-188.

Deep, A., Chaudhary, U. and Gupta, V. (2011). "Quorum sensing and bacterial pathogenicity: From molecules to disease." J Lab Physicians **3**(1): 4-11.

Denks, K., Vogt, A., Sachelaru, I., et al. (2014). "The Sec translocon mediated protein transport in prokaryotes and eukaryotes." Mol Membr Biol **31**(2-3): 58-84.

Depluverez, S., Devos, S. and Devreese, B. (2016). "The role of bacterial secretion systems in the virulence of Gram-negative airway pathogens associated with cystic fibrosis." Front Microbiol **7**: 1336.

Desvaux, M., Khan, A., Beatson, S. A., et al. (2005). "Protein secretion systems in *Fusobacterium nucleatum*: genomic identification of Type 4 piliation and complete Type V pathways brings new insight into mechanisms of pathogenesis." Biochim Biophys Acta **1713**(2): 92-112.

Deutsch, C. A., Tewksbury, J. J., Tigchelaar, M., et al. (2018). "Increase in crop losses to insect pests in a warming climate." Science **361**(6405): 916-919.

Dewey, J. S., Savva, C. G., White, R. L., et al. (2010). "Micron-scale holes terminate the phage infection cycle." Proc Natl Acad Sci U S A **107**(5): 2219-2223.

Diepold, A. and Wagner, S. (2014). "Assembly of the bacterial type III secretion machinery." FEMS Microbiol Rev **38**(4): 802-822.

Dillon, S. C. and Dorman, C. J. (2010). "Bacterial nucleoid-associated proteins, nucleoid structure and gene expression." Nat Rev Microbiol **8**(3): 185-195.

Dion, M. F., Kapoor, M., Sun, Y., et al. (2019). "*Bacillus subtilis* cell diameter is determined by the opposing actions of two distinct cell wall synthetic systems." Nat Microbiol **4**(8): 1294-1305.

Dongre, M., Singh, B., Aung, K. M., et al. (2018). "Flagella-mediated secretion of a novel *Vibrio cholerae* cytotoxin affecting both vertebrate and invertebrate hosts." Commun Biol **1**: 59.

Drebes Dorr, N. C. and Blokesch, M. (2018). "Bacterial type VI secretion system facilitates niche domination." Proc Natl Acad Sci U S A **115**(36): 8855-8857.

Durand, S., Braun, F., Helfer, A. C., et al. (2017). "sRNA-mediated activation of gene expression by inhibition of 5'-3' exonucleolytic mRNA degradation." Elife **6**.

Eberhard, A., Burlingame, A. L., Eberhard, C., et al. (1981). "Structural identification of autoinducer of *Photobacterium fischeri* luciferase." Biochemistry **20**(9): 2444-2449.

Eddy, J. L., Gielda, L. M., Caulfield, A. J., et al. (2014). "Production of outer membrane vesicles by the plague pathogen Yersinia pestis." PLoS One **9**(9): e107002.

El Qaidi, S., Scott, N. E., Hays, M. P., et al. (2020). "An intra-bacterial activity for a T3SS effector." Sci Rep **10**(1): 1073.

El Tahir, Y. and Skurnik, M. (2001). "YadA, the multifaceted *Yersinia* adhesin." Int J Med Microbiol **291**(3): 209-218.

Ellison, D. W. and Miller, V. L. (2006). "H-NS represses inv transcription in *Yersinia enterocolitica* through competition with RovA and interaction with YmoA." J Bacteriol **188**(14): 5101-5112.

Engvall, E. and Perlmann, P. (1971). "Enzyme-linked immunosorbent assay (ELISA). Quantitative assay of immunoglobulin G." Immunochemistry **8**(9): 871-874.

Erhardt, M. and Dersch, P. (2015). "Regulatory principles governing *Salmonella* and *Yersinia* virulence." Front Microbiol **6**: 949.

Erridge, C., Bennett-Guerrero, E. and Poxton, I. R. (2002). "Structure and function of lipopolysaccharides." Microbes Infect **4**(8): 837-851.

Eswara, P. J., Brzozowski, R. S., Viola, M. G., et al. (2018). "An essential S*taphylococcus aureus* cell division protein directly regulates FtsZ dynamics." Elife **7**.

Ewing, W. H., Ross, A. J., J., B. D., et al. (1978). "*Yersinia ruckeri* sp. nov. te Redmouth (RM) Bacterium." International Journal of Systematic Bacteriology **28**(1): 37-44.

Faden, F., Eschen-Lippold, L. and Dissmeyer, N. (2016). "Normalized quantitative western blotting based on standardized fluorescent labeling." Methods Mol Biol **1450**: 247-258.

Feldman, M. W., Otto, S. P. and Christiansen, F. B. (1996). "Population genetic perspectives on the evolution of recombination." Annu Rev Genet **30**: 261-295.

Feng, J., Ma, L., Nie, J., et al. (2018). "Environmental stress-induced bacterial lysis and extracellular dna release contribute to *Campylobacter jejuni* biofilm formation." Appl Environ Microbiol **84**(5).

Fernandez-Ruiz, I., Coutinho, F. H. and Rodriguez-Valera, F. (2018). "Thousands of novel endolysins discovered in uncultured phage genomes." Front Microbiol **9**: 1033.

Fink, D. L., Buscher, A. Z., Green, B., et al. (2003). "The *Haemophilus influenzae* Hap autotransporter mediates microcolony formation and adherence to epithelial cells and extracellular matrix via binding regions in the C-terminal end of the passenger domain." Cell Microbiol **5**(3): 175-186.

Fiocca, R., Necchi, V., Sommi, P., et al. (1999). "Release of *Helicobacter pylori* vacuolating cytotoxin by both a specific secretion pathway and budding of outer membrane vesicles. Uptake of released toxin and vesicles by gastric epithelium." J Pathol **188**(2): 220-226.

Folichon, M., Arluison, V., Pellegrini, O., et al. (2003). "The poly(A) binding protein Hfq protects RNA from RNase E and exoribonucleolytic degradation." Nucleic Acids Res **31**(24): 7302-7310.

Frohlich, K. S. and Vogel, J. (2009). "Activation of gene expression by small RNA." Curr Opin Microbiol **12**(6): 674-682.

Fu, X., Himes, B. A., Ke, D., et al. (2014). "Controlled bacterial lysis for electron tomography of native cell membranes." Structure **22**(12): 1875-1882.

Gagic, D., Ciric, M., Wen, W. X., et al. (2016). "Exploring the secretomes of microbes and microbial communities using filamentous phage display." Front Microbiol **7**: 429.

Gallique, M., Bouteiller, M. and Merieau, A. (2017). "The type vi secretion system: a dynamic system for bacterial communication?" Front Microbiol **8**: 1454.

Ganoth, A., Alhadeff, R., Kohen, D., et al. (2011). "Characterization of the Na(+)/H(+) antiporter from *Yersinia pestis*." PLoS One **6**(11): e26115.

Gardiner, M., Bournazos, A. M., Maturana-Martinez, C., et al. (2017). "Exoproteome analysis of the seaweed pathogen *Nautella italica* R11 reveals temperature-dependent regulation of RTX-Like proteins." Front Microbiol **8**: 1203.

Garg, G. and Ranganathan, S. (2011). "*In silico* secretome analysis approach for next generation sequencing transcriptomic data." BMC Genomics **12 Suppl 3**: S14.

Garst, A. D., Edwards, A. L. and Batey, R. T. (2011). "Riboswitches: structures and mechanisms." Cold Spring Harb Perspect Biol **3**(6).

Gente, S., Billon-Grand, G., Poussereau, N., et al. (2001). "Ambient alkaline pH prevents maturation but not synthesis of ASPA, the aspartyl protease from *Penicillium roqueforti.*" Curr Genet **38**(6): 323-328.

Ghosal, D., Kim, K. W., Zheng, H., et al. (2019). "*In vivo* structure of the *Legionella* type II secretion system by electron cryotomography." Nat Microbiol **4**(12): 2101-2108.

Gigante, A. M., Hampton, C. M., Dillard, R. S., et al. (2017). "The Ms6 mycolyl-arabinogalactan esterase LysB is essential for an efficient mycobacteriophage-induced lysis." Viruses **9**(11).

Gilbert, K. B., Kim, T. H., Gupta, R., et al. (2009). "Global position analysis of the *Pseudomonas aeruginosa* quorum-sensing transcription factor LasR." Mol Microbiol **73**(6): 1072-1085.

Gill, J. J., Berry, J. D., Russell, W. K., et al. (2012). "The *Caulobacter crescentus* phage phiCbK: genomics of a canonical phage." BMC Genomics **13**: 542.

Glare, T. R., Gwynn, R. L. and Moran-Diez, M. E. (2016). "Development of biopesticides and future opportunities." Methods Mol Biol **1477**: 211-221.

Glare, T. R. and O'Callaghan, M. (2019). "Microbial biopesticides for control of invertebrates: Progress from New Zealand." J Invertebr Pathol **165**: 82-88.

Godichon-Baggioni, A., Maugis-Rabusseau, C. and Rau, A. (2018). "Clustering transformed compositional data using K-means, with applications in gene expression and bicycle sharing system data." Journal of Applied Statistics.

Gonzales, L., Ali, Z. B., Nygren, E., et al. (2013). "Alkaline pH Is a signal for optimal production and secretion of the heat labile toxin, LT in enterotoxigenic *Escherichia coli* (ETEC)." PLoS One **8**(9): e74069.

Govind, R. and Dupuy, B. (2012). "Secretion of *Clostridium difficile* toxins A and B requires the holin-like protein TcdE." PLoS Pathog **8**(6): e1002727.

Govind, R., Fitzwater, L. and Nichols, R. (2015). "Observations on the Role of TcdE isoforms in *Clostridium difficile* toxin secretion." J Bacteriol **197**(15): 2600-2609.

Grant, C. E., Bailey, T. L. and Noble, W. S. (2011). "FIMO: scanning for occurrences of a given motif." Bioinformatics **27**(7): 1017-1018.

Graschopf, A. and Blasi, U. (1999). "Molecular function of the dual-start motif in the lambda S holin." Mol Microbiol **33**(3): 569-582.

Gray, K. M. and Garey, J. R. (2001). "The evolution of bacterial LuxI and LuxR quorum sensing regulators." Microbiology **147**(Pt 8): 2379-2387.

Green, E. R. and Mecsas, J. (2016). "Bacterial secretion systems: An overview." Microbiol Spectr **4**(1).

Groisman, E. A. (2016). "Feedback control of two-component regulatory systems." Annu Rev Microbiol **70**: 103-124.

Grote, J., Krysciak, D. and Streit, W. R. (2015). "Phenotypic heterogeneity, a phenomenon that may explain why quorum sensing does not always result in truly homogenous cell behavior." Appl Environ Microbiol **81**(16): 5280-5289.

Grundling, A., Blasi, U. and Young, R. (2000). "Biochemical and genetic evidence for three transmembrane domains in the class I holin, lambda S." J Biol Chem **275**(2): 769-776.

Grys, T. E., Siegel, M. B., Lathem, W. W., et al. (2005). "The StcE protease contributes to intimate adherence of enterohemorrhagic *Escherichia coli* O157:H7 to host cells." Infect Immun **73**(3): 1295-1303.

Guerin, J., Bigot, S., Schneider, R., et al. (2017). "Two-partner secretion: Combining efficiency and simplicity in the secretion of large proteins for bacteria-host and bacteria-bacteria interactions." Front Cell Infect Microbiol **7**: 148.

Guijarro, J. A., Garcia-Torrico, A. I., Cascales, D., et al. (2018). "The infection process of *Yersinia ruckeri*: Reviewing the pieces of the jigsaw puzzle." Front Cell Infect Microbiol **8**: 218.

Guisbert, E., Herman, C., Lu, C. Z., et al. (2004). "A chaperone network controls the heat shock response in *E. coli*." Genes Dev **18**(22): 2812-2821.

Gunn, J. S. (2001). "Bacterial modification of LPS and resistance to antimicrobial peptides." J Endotoxin Res **7**(1): 57-62.

Hamilton, J. J., Marlow, V. L., Owen, R. A., et al. (2014). "A holin and an endopeptidase are essential for chitinolytic protein secretion in *Serratia marcescens*." J Cell Biol **207**(5): 615-626.

Hammann, C. and Westhof, E. (2007). "Searching genomes for ribozymes and riboswitches." Genome Biol **8**(4): 210.

Hampton, C. M., Guerrero-Ferreira, R. C., Storms, R. E., et al. (2017). "The opportunistic pathogen *Vibrio vulnificus* produces outer membrane vesicles in a spatially distinct manner related to capsular polysaccharide." Front Microbiol **8**: 2177.

Hartland, E. L., Green, S. P., Phillips, W. A., et al. (1994). "Essential role of YopD in inhibition of the respiratory burst of macrophages by *Yersinia enterocolitica*." Infect Immun **62**(10): 4445-4453.

Haurat, M. F., Aduse-Opoku, J., Rangarajan, M., et al. (2011). "Selective sorting of cargo proteins into bacterial membrane vesicles." J Biol Chem **286**(2): 1269-1276.

Haurat, M. F., Elhenawy, W. and Feldman, M. F. (2015). "Prokaryotic membrane vesicles: new insights on biogenesis and biological roles." Biol Chem **396**(2): 95-109.

Hawgood, B. J. (2008). "Alexandre Yersin (1863-1943): Discoverer of the plague *Bacillus*, explorer and agronomist." J Med Biogr **16**(3): 167-172.

Hayer-Hartl, M., Bracher, A. and Hartl, F. U. (2016). "The GroEL-GroES chaperonin machine: A nano-cage for protein folding." Trends Biochem Sci **41**(1): 62-76.

Heiniger, R. W., Winther-Larsen, H. C., Pickles, R. J., et al. (2010). "Infection of human mucosal tissue by *Pseudomonas aeruginosa* requires sequential and mutually dependent virulence factors and a novel pilus-associated adhesin." Cell Microbiol **12**(8): 1158-1173.

Henderson, I. R., Cappello, R. and Nataro, J. P. (2000). "Autotransporter proteins, evolution and redefining protein secretion." Trends Microbiol **8**(12): 529-532.

Heroven, A. K., Nagel, G., Tran, H. J., et al. (2004). "RovA is autoregulated and antagonizes H-NS-mediated silencing of invasin and *rovA* expression in *Yersinia pseudotuberculosis*." Mol Microbiol **53**(3): 871-888.

Hertwig, S., Klein, I., Lurz, R., et al. (2003). "PY54, a linear plasmid prophage of *Yersinia enterocolitica* with covalently closed ends." Mol Microbiol **48**(4): 989-1003.

Hews, C. L., Tran, S. L., Wegmann, U., et al. (2017). "The StcE metalloprotease of enterohaemorrhagic *Escherichia coli* reduces the inner mucus layer and promotes adherence to human colonic epithelium *ex vivo*." Cell Microbiol **19**(6).

Hickey, J. M., Weldon, L. and Hefty, P. S. (2011). "The atypical OmpR/PhoB response regulator ChxR from *Chlamydia trachomatis* forms homodimers *in vivo* and binds a direct repeat of nucleotide sequences." J Bacteriol **193**(2): 389-398.

Hinnebusch, B. J. and Erickson, D. L. (2008). "*Yersinia pestis* biofilm in the flea vector and its role in the transmission of plague." Curr Top Microbiol Immunol **322**: 229-248.

Hoang, T. T., Sullivan, S. A., Cusick, J. K., et al. (2002). "Beta-ketoacyl acyl carrier protein reductase (FabG) activity of the fatty acid biosynthetic pathway is a determining factor of 3-oxo-homoserine lactone acyl chain lengths." Microbiology **148**(Pt 12): 3849-3856.

Hoch, J. A. (2000). "Two-component and phosphorelay signal transduction." Curr Opin Microbiol **3**(2): 165-170.

Hoekstra, D., van der Laan, J. W., de Leij, L., et al. (1976). "Release of outer membrane fragments from normally growing *Escherichia coli*." Biochim Biophys Acta **455**(3): 889-899.

Hogardt, M., Roeder, M., Schreff, A. M., et al. (2004). "Expression of *Pseudomonas aeruginosa exoS* is controlled by quorum sensing and RpoS." Microbiology **150**(Pt 4): 843-851.

Hong, E., Lee, H. M., Ko, H., et al. (2007). "Structure of an atypical orphan response regulator protein supports a new phosphorylation-independent regulatory mechanism." J Biol Chem **282**(28): 20667-20675.

Hooker-Romero, D., Mettert, E., Schwiesow, L., et al. (2019). "Iron availability and oxygen tension regulate the *Yersinia* Ysc type III secretion system to enable disseminated infection." PLoS Pathog **15**(12): e1008001.

Horstman, A. L. and Kuehn, M. J. (2000). "Enterotoxigenic *Escherichia coli* secretes active heat-labile enterotoxin via outer membrane vesicles." J Biol Chem **275**(17): 12489-12496.

Howell, A., Dubrac, S., Andersen, K. K., et al. (2003). "Genes controlled by the essential YycG/YycF two-component system of *Bacillus subtilis* revealed through a novel hybrid regulator approach." Mol Microbiol **49**(6): 1639-1655.

Hozbor, D., Rodriguez, M. E., Fernandez, J., et al. (1999). "Release of outer membrane vesicles from *Bordetella pertussis*." Curr Microbiol **38**(5): 273-278.

Hu, Y., Lu, P., Zhang, Y., et al. (2010). "Characterization of an aspartate-dependent acid survival system in *Yersinia pseudotuberculosis*." FEBS Lett **584**(11): 2311-2314.

Huber, M., Faure, G., Laass, S., et al. (2019). "Translational coupling via termination-reinitiation in archaea and bacteria." Nat Commun **10**(1): 4006.

Hueck, C. J. (1998). "Type III protein secretion systems in bacterial pathogens of animals and plants." Microbiol Mol Biol Rev **62**(2): 379-433.

Hurst, M. R., Beattie, A., Altermann, E., et al. (2016). "The draft genome sequence of the *Yersinia entomophaga* entomopathogenic type strain MH96T." Toxins (Basel) **8**(5).

Hurst, M. R., Beattie, A. K., Jones, S. A., et al. (2015). "Temperature-dependent *Galleria mellonella* mortality as a result of *Yersinia entomophaga* infection." Appl Environ Microbiol **81**(18): 6404-6414.

Hurst, M. R., Becher, S. A., Young, S. D., et al. (2011a). "*Yersinia entomophaga* sp. nov., isolated from the New Zealand grass grub *Costelytra zealandica*." Int J Syst Evol Microbiol **61**(Pt 4): 844-849.

Hurst, M. R., Glare, T. R. and Jackson, T. A. (2004). "Cloning *Serratia entomophila* antifeeding genes--a putative defective prophage active against the grass grub *Costelytra zealandica*." J Bacteriol **186**(15): 5116-5128.

Hurst, M. R., Jones, S. A., Binglin, T., et al. (2011b). "The main virulence determinant of *Yersinia entomophaga* MH96 is a broad-host-range toxin complex active against insects." J Bacteriol **193**(8): 1966-1980.

Hurst, M. R., Swaminathan, J., Wright, D. A., et al. (2020). "Development of a *Yersinia entomophaga* bait for control of larvae of the porina moth (*Wiseana* spp.), a pest of New Zealand improved grassland systems." Pest Manag Sci **76**(1): 350-359.

Hurst, M. R., van Koten, C. and Jackson, T. A. (2014). "Pathology of *Yersinia entomophaga* MH96 towards *Costelytra zealandica* (Coleoptera; Scarabaeidae) larvae." J Invertebr Pathol **115**: 102-107.

Hussein, H., Fris, M. E., Salem, A. H., et al. (2019). "An unconventional RNA-based thermosensor within the 5' UTR of *Staphylococcus aureus cidA*." PLoS One **14**(4): e0214521.

Indrelid, S., Mathiesen, G., Jacobsen, M., et al. (2014). "Computational and experimental analysis of the secretome of *Methylococcus capsulatus* (Bath)." PLoS One **9**(12): e114476.

Jan, M. R., Shah, J., Khawaja, M. A., et al. (2009). "DDT residue in soil and water in and around abandoned DDT manufacturing factory." Environ Monit Assess **155**(1-4): 31-38.

Jarchau, T., Chakraborty, T., Garcia, F., et al. (1994). "Selection for transport competence of C-terminal polypeptides derived from *Escherichia coli* hemolysin: the shortest peptide capable of autonomous HlyB/HlyD-dependent secretion comprises the C-terminal 62 amino acids of HlyA." Mol Gen Genet **245**(1): 53-60.

Jayakumar, S., Muralidharan, S. and Dhananjayan, V. (2020). "Organochlorine pesticide residues among colonial nesting birds in Tamil Nadu, India: A maiden assessment from their breeding grounds." Arch Environ Contam Toxicol **78**(4): 555-567.

Jebbar, M., Sohn-Bosser, L., Bremer, E., et al. (2005). "Ectoine-induced proteins in *Sinorhizobium meliloti* include an Ectoine ABC-type transporter involved in osmoprotection and ectoine catabolism." J Bacteriol **187**(4): 1293-1304.

Jensen, S. O., Thompson, L. S. and Harry, E. J. (2005). "Cell division in *Bacillus subtilis*: FtsZ and FtsA association is Z-ring independent, and FtsA is required for efficient midcell Z-Ring assembly." J Bacteriol **187**(18): 6536-6544.

Kadurugamuwa, J. L. and Beveridge, T. J. (1999). "Membrane vesicles derived from *Pseudomonas aeruginosa* and *Shigella flexneri* can be integrated into the surfaces of other Gram-negative bacteria." Microbiology **145 (Pt 8)**: 2051-2060.

Kakoschke, T. K., Kakoschke, S. C., Zeuzem, C., et al. (2016). "The RNA chaperone Hfq is essential for virulence and modulates the expression of four adhesins in *Yersinia enterocolitica*." Sci Rep **6**: 29275.

Kanonenberg, K., Schwarz, C. K. and Schmitt, L. (2013). "Type I secretion systems - a story of appendices." Res Microbiol **164**(6): 596-604.

Kaplan, H. B. and Greenberg, E. P. (1985). "Diffusion of autoinducer is involved in regulation of the *Vibrio fischeri* luminescence system." J Bacteriol **163**(3): 1210-1214.

Kasai, N., Arata, S., Mashimo, J., et al. (1986). "Synthetic *Salmonella*-type lipid A antigen with high serological specificity." Infect Immun **51**(1): 43-48.

Kato, H., Chibazakura, T. and Yoshikawa, H. (2008). "NblR is a novel one-component response regulator in the cyanobacterium *Synechococcus elongatus* PCC 7942." Biosci Biotechnol Biochem **72**(4): 1072-1079.

Kearse, M., Moir, R., Wilson, A., et al. (2012). "Geneious Basic: an integrated and extendable desktop software platform for the organization and analysis of sequence data." Bioinformatics **28**(12): 1647-1649.

Khajanchi, B. K., Sha, J., Kozlova, E. V., et al. (2009). "N-acylhomoserine lactones involved in quorum sensing control the type VI secretion system, biofilm formation, protease production, and *in vivo* virulence in a clinical isolate of *Aeromonas hydrophila*." Microbiology **155**(Pt 11): 3518-3531.

Kida, Y., Shimizu, T. and Kuwano, K. (2011). "Cooperation between LepA and PlcH contributes to the *in vivo* virulence and growth of *Pseudomonas aeruginosa* in mice." Infect Immun **79**(1): 211-219.

Kilic, S., White, E. R., Sagitova, D. M., et al. (2014). "CollecTF: a database of experimentally validated transcription factor-binding sites in Bacteria." Nucleic Acids Res **42**(Database issue): D156-160.

Kim, S., Kim, S. H., Rahman, M., et al. (2018). "Characterization of a *Salmonella enteritidis* bacteriophage showing broad lytic activity against Gram-negative enteric bacteria." J Microbiol **56**(12): 917-925.

Kim, T. J., Young, B. M. and Young, G. M. (2008). "Effect of flagellar mutations on *Yersinia enterocolitica* biofilm formation." Appl Environ Microbiol **74**(17): 5466-5474.

Kirn, T. J., Bose, N. and Taylor, R. K. (2003). "Secretion of a soluble colonization factor by the TCP type 4 pilus biogenesis pathway in *Vibrio cholerae*." Mol Microbiol **49**(1): 81-92.

Kolling, G. L. and Matthews, K. R. (1999). "Export of virulence genes and Shiga toxin by membrane vesicles of *Escherichia coli* O157:H7." Appl Environ Microbiol **65**(5): 1843-1848.

Kongari, R., Rajaure, M., Cahill, J., et al. (2018). "Phage spanins: diversity, topological dynamics and gene convergence." BMC Bioinformatics **19**(1): 326.

Konninger, U. W., Hobbie, S., Benz, R., et al. (1999). "The haemolysin-secreting ShlB protein of the outer membrane of *Serratia marcescens*: Determination of surface-exposed residues and formation of ion-permeable pores by ShlB mutants in artificial lipid bilayer membranes." Mol Microbiol **32**(6): 1212-1225.

Koraimann, G. (2003). "Lytic transglycosylases in macromolecular transport systems of Gram-negative bacteria." Cell Mol Life Sci **60**(11): 2371-2388.

Korotkov, K. V., Sandkvist, M. and Hol, W. G. (2012). "The type II secretion system: biogenesis, molecular architecture and mechanism." Nat Rev Microbiol **10**(5): 336-351.

Krupovic, M. and Bamford, D. H. (2008). "Holin of bacteriophage lambda: structural insights into a membrane lesion." Mol Microbiol **69**(4): 781-783.

Kuehn, M. J. and Kesty, N. C. (2005). "Bacterial outer membrane vesicles and the host-pathogen interaction." Genes Dev **19**(22): 2645-2655.

Kuhn, M. J., Schmidt, F. K., Farthing, N. E., et al. (2018). "Spatial arrangement of several flagellins within bacterial flagella improves motility in different environments." Nat Commun **9**(1): 5369.

Kulp, A. and Kuehn, M. J. (2010). "Biological functions and biogenesis of secreted bacterial outer membrane vesicles." Annu Rev Microbiol **64**: 163-184.

Kulp, A. J., Sun, B., Ai, T., et al. (2015). "Genome-wide assessment of outer membrane vesicle production in *Escherichia coli*." PLoS One **10**(9): e0139200.

Kumar, G., Menanteau-Ledouble, S., Saleh, M., et al. (2015). "*Yersinia ruckeri,* the causative agent of enteric redmouth disease in fish." Vet Res **46**: 103.

Kumar, S., Chandra, A. and Pandey, K. C. (2008). "*Bacillus thuringiensis* (Bt) transgenic crop: an environment friendly insect-pest management strategy." J Environ Biol **29**(5): 641-653.

Kummerli, R. and Brown, S. P. (2010). "Molecular and regulatory properties of a public good shape the evolution of cooperation." Proc Natl Acad Sci U S A **107**(44): 18921-18926.

Laarmann, S., Cutter, D., Juehne, T., et al. (2002). "The *Haemophilus influenzae* Hia autotransporter harbours two adhesive pockets that reside in the passenger domain and recognize the same host cell receptor." Mol Microbiol **46**(3): 731-743.

Laemmli, U. K. (1970). "Cleavage of structural proteins during the assembly of the head of bacteriophage T4." Nature **227**(5259): 680-685.

Laganenka, L., Sander, T., Lagonenko, A., et al. (2019). "Quorum sensing and metabolic state of the host control lysogeny-lysis switch of bacteriophage T1." MBio **10**(5).

Lahteenmaki, K., Kukkonen, M. and Korhonen, T. K. (2001). "The Pla surface protease/adhesin of *Yersinia pestis* mediates bacterial invasion into human endothelial cells." FEBS Lett **504**(1-2): 69-72.

Lang, B., Blot, N., Bouffartigues, E., et al. (2007). "High-affinity DNA binding sites for H-NS provide a molecular basis for selective silencing within proteobacterial genomes." Nucleic Acids Res **35**(18): 6330-6337.

LaRock, C. N., Yu, J., Horswill, A. R., et al. (2013). "Transcriptome analysis of acyl-homoserine lactone-based quorum sensing regulation in *Yersinia pestis* [corrected]." PLoS One **8**(4): e62337.

Lathem, W. W., Grys, T. E., Witowski, S. E., et al. (2002). "StcE, a metalloprotease secreted by *Escherichia coli* O157:H7, specifically cleaves C1 esterase inhibitor." Mol Microbiol **45**(2): 277-288.

Lathem, W. W., Schroeder, J. A., Bellows, L. E., et al. (2014). "Posttranscriptional regulation of the *Yersinia pestis* cyclic AMP receptor protein Crp and impact on virulence." MBio **5**(1): e01038-01013.

Le Baut, G., O'Brien, C., Pavli, P., et al. (2018). "Prevalence of *Yersinia* species in the ileum of Crohn's disease patients and controls." Front Cell Infect Microbiol **8**: 336.

Le Guern, A. S., Martin, L., Savin, C., et al. (2016). "Yersiniosis in France: overview and potential sources of infection." Int J Infect Dis **46**: 1-7.

Le Guern, A. S., Savin, C., Bremont, S., et al. (2018). "First isolation of *Yersinia entomophaga* in human urinary tract." New Microbes New Infect **26**: 3-7.

Lee, H. J. and Gottesman, S. (2016). "sRNA roles in regulating transcriptional regulators: Lrp and SoxS regulation by sRNAs." Nucleic Acids Res **44**(14): 6907-6923.

Lee, P. A., Tullman-Ercek, D. and Georgiou, G. (2006). "The bacterial twin-arginine translocation pathway." Annu Rev Microbiol **60**: 373-395.

Lenders, M. H., Weidtkamp-Peters, S., Kleinschrodt, D., et al. (2015). "Directionality of substrate translocation of the hemolysin A Type I secretion system." Sci Rep **5**: 12470.

Leo, J. C., Grin, I. and Linke, D. (2012). "Type V secretion: mechanism(s) of autotransport through the bacterial outer membrane." Philos Trans R Soc Lond B Biol Sci **367**(1592): 1088-1101.

Lertsethtakarn, P., Ottemann, K. M. and Hendrixson, D. R. (2011). "Motility and chemotaxis in *Campylobacter* and *Helicobacter*." Annu Rev Microbiol **65**: 389-410.

Lesic, B., Starkey, M., He, J., et al. (2009). "Quorum sensing differentially regulates *Pseudomonas aeruginosa* type VI secretion locus I and homologous loci II and III, which are required for pathogenesis." Microbiology **155**(Pt 9): 2845-2855.

Li, N., Zhu, Y., LaFrentz, B. R., et al. (2017). "The Type IX secretion system is required for virulence of the fish pathogen *Flavobacterium columnare*." Appl Environ Microbiol **83**(23).

Li, W., Ancona, V. and Zhao, Y. (2014). "Co-regulation of polysaccharide production, motility, and expression of type III secretion genes by EnvZ/OmpR and GrrS/GrrA systems in *Erwinia amylovora*." Mol Genet Genomics **289**(1): 63-75.

Li, Z. and Nair, S. K. (2012). "Quorum sensing: how bacteria can coordinate activity and synchronize their response to external signals?" Protein Sci **21**(10): 1403-1417.

Liang, H., Deng, X., Li, X., et al. (2014). "Molecular mechanisms of master regulator VqsM mediating quorum-sensing and antibiotic resistance in *Pseudomonas aeruginosa*." Nucleic Acids Res **42**(16): 10307-10320.

Lin, Z., Puchalla, J., Shoup, D., et al. (2013). "Repetitive protein unfolding by the trans ring of the GroEL-GroES chaperonin complex stimulates folding." J Biol Chem **288**(43): 30944-30955.

Lindhout, T., Lau, P. C. Y., Brewer, D., et al. (2009). "Truncation in the core oligosaccharide of lipopolysaccharide affects flagella-mediated motility in *Pseudomonas aeruginosa* PAO1 via modulation of cell surface attachment." Microbiology **155**(Pt 10): 3449-3460.

Lindmark, B., Rompikuntal, P. K., Vaitkevicius, K., et al. (2009). "Outer membrane vesicle-mediated release of cytolethal distending toxin (CDT) from *Campylobacter jejuni.*" BMC Microbiol **9**: 220.

Linhartova, I., Bumba, L., Masin, J., et al. (2010). "RTX proteins: a highly diverse family secreted by a common mechanism." FEMS Microbiol Rev **34**(6): 1076-1112.

Liu, J. M. and Camilli, A. (2010). "A broadening world of bacterial small RNAs." Curr Opin Microbiol **13**(1): 18-23.

Lorenz, C., Gesell, T., Zimmermann, B., et al. (2010). "Genomic SELEX for Hfq-binding RNAs identifies genomic aptamers predominantly in antisense transcripts." Nucleic Acids Res **38**(11): 3794-3808.

Lorow, D. and Jessee, J. (1990). "Max efficiency DH10B: a host for cloning methylated DNA." Focus 12:19.

Loveless, B. J. and Saier, M. H., Jr. (1997). "A novel family of channel-forming, autotransporting, bacterial virulence factors." Mol Membr Biol **14**(3): 113-123.

Lubin, E. A., Henry, J. T., Fiebig, A., et al. (2016). "Identification of the PhoB Regulon and role of PhoU in the phosphate starvation response of *Caulobacter crescentus*." J Bacteriol **198**(1): 187-200.

Maffei, B., Francetic, O. and Subtil, A. (2017). "Tracking proteins secreted by bacteria: What's in the toolbox?" Front Cell Infect Microbiol **7**: 221.

Mariappan, V., Vellasamy, K. M., Thimma, J. S., et al. (2010). "Identification of immunogenic proteins from *Burkholderia cepacia* secretome using proteomic analysis." Vaccine **28**(5): 1318-1324.

Marinus, M. G., Carraway, M., Frey, A. Z., et al. (1983). "Insertion mutations in the *dam* gene of *Escherichia coli* K-12." Mol. Gen. Genet. **192**: 288-289.

Marlovits, T. C., Kubori, T., Sukhan, A., et al. (2004). "Structural insights into the assembly of the type III secretion needle complex." Science **306**(5698): 1040-1042.

Mashburn, L. M. and Whiteley, M. (2005). "Membrane vesicles traffic signals and facilitate group activities in a prokaryote." Nature **437**(7057): 422-425.

Matias, V. R. and Beveridge, T. J. (2006). "Native cell wall organization shown by cryo-electron microscopy confirms the existence of a periplasmic space in *Staphylococcus aureus*." J Bacteriol **188**(3): 1011-1021.

McBroom, A. J. and Kuehn, M. J. (2007). "Release of outer membrane vesicles by Gram-negative bacteria is a novel envelope stress response." Mol Microbiol **63**(2): 545-558.

McClean, K. H., Winson, M. K., Fish, L., et al. (1997). "Quorum sensing and *Chromobacterium violaceum*: exploitation of violacein production and inhibition for the detection of N-acylhomoserine lactones." Microbiology **143 (Pt 12)**: 3703-3711.

Mehner-Breitfeld, D., Rathmann, C., Riedel, T., et al. (2018). "Evidence for an adaptation of a phage-derived holin/endolysin system to toxin transport in *Clostridioides difficile*." Front Microbiol **9**: 2446.

Melkani, G. C., Zardeneta, G. and Mendoza, J. A. (2005). "On the chaperonin activity of GroEL at heat-shock temperature." Int J Biochem Cell Biol **37**(7): 1375-1385.

Mesarich, C. H., Griffiths, S. A., van der Burgt, A., et al. (2014). "Transcriptome sequencing uncovers the Avr5 avirulence gene of the tomato leaf mold pathogen *Cladosporium fulvum*." Mol Plant Microbe Interact **27**(8): 846-857.

Mesarich, C. H., Rees-George, J., Gardner, P. P., et al. (2017). "Transposon insertion libraries for the characterization of mutants from the kiwifruit pathogen *Pseudomonas syringae* pv. actinidiae." PLoS One **12**(3): e0172790.

Metcalf, W. W., Jiang, W. and Wanner, B. L. (1994). "Use of the rep technique for allele replacement to construct new *Escherichia coli* hosts for maintenance of R6K gamma origin plasmids at different copy numbers." Gene **138**(1-2): 1-7.

Meuskens, I., Saragliadis, A., Leo, J. C., et al. (2019). "Type V secretion systems: An overview of passenger domain functions." Front Microbiol **10**: 1163.

Mezei, L. M. and Storts, D. R. (1994). Purification of PCR products. PCR Technology: Current Innovations. H. G. Griffin and A. M. Griffin. Boca Raton, Florida, USA., CRC Press**:** 21.

Michel, G. P., Durand, E. and Filloux, A. (2007). "XphA/XqhA, a novel GspCD subunit for type II secretion in *Pseudomonas aeruginosa*." J Bacteriol **189**(10): 3776-3783.

Mikula, K. M., Kolodziejczyk, R. and Goldman, A. (2012). "*Yersinia* infection tools-characterization of structure and function of adhesins." Front Cell Infect Microbiol **2**: 169.

Miller, M. B. and Bassler, B. L. (2001). "Quorum sensing in bacteria." Annu Rev Microbiol **55**: 165-199.

Minamino, T. (2014). "Protein export through the bacterial flagellar type III export pathway." Biochim Biophys Acta **1843**(8): 1642-1648.

Minato, Y., Ghosh, A., Faulkner, W. J., et al. (2013). "Na+/H+ antiport is essential for *Yersinia pestis* virulence." Infect Immun **81**(9): 3163-3172.

Mizobata, T. and Kawata, Y. (2018). "The versatile mutational "repertoire" of *Escherichia coli* GroEL, a multidomain chaperonin nanomachine." Biophys Rev **10**(2): 631-640.

Mohedano, M. L., Amblar, M., de la Fuente, A., et al. (2016). "The response regulator YycF inhibits expression of the fatty acid biosynthesis repressor Fabt in *Streptococcus pneumoniae*." Front Microbiol **7**: 1326.

Monnappa, A. K., Bari, W., Seo, J. K., et al. (2018). "The Cytotoxic Necrotizing Factor of *Yersinia pseudotuberculosis* (CNFy) is carried on extracellular membrane vesicles to host cells." Sci Rep **8**(1): 14186.

Morimoto, Y. V. and Minamino, T. (2014). "Structure and function of the bi-directional bacterial flagellar motor." Biomolecules **4**(1): 217-234.

Morita, Y., Kodama, K., Shiota, S., et al. (1998). "NorM, a putative multidrug efflux protein, of *Vibrio parahaemolyticus* and its homolog in *Escherichia coli.*" Antimicrob Agents Chemother **42**(7): 1778-1782.

Morris, C., Yip, C. M., Tsui, I. S., et al. (2003). "The shufflon of *Salmonella enterica* serovar Typhi regulates type IVB pilus-mediated bacterial self-association." Infect Immun **71**(3): 1141-1146.

Motohira, K., Ikenaka, Y., Yohannes, Y. B., et al. (2019). "Dichlorodiphenyltrichloroethane (DDT) levels in rat livers collected from a malaria vector control region." J Vet Med Sci **81**(11): 1575-1579.

Mukherjee, S. and Bassler, B. L. (2019). "Bacterial quorum sensing in complex and dynamically changing environments." Nat Rev Microbiol **17**(6): 371-382.

Murros-Kontiainen, A., Fredriksson-Ahomaa, M., Korkeala, H., et al. (2011a). "*Yersinia nurmii* sp. nov." Int J Syst Evol Microbiol **61**(Pt 10): 2368-2372.

Murros-Kontiainen, A., Johansson, P., Niskanen, T., et al. (2011b). "*Yersinia pekkanenii* sp. nov." Int J Syst Evol Microbiol **61**(Pt 10): 2363-2367.

Natale, P., Bruser, T. and Driessen, A. J. (2008). "Sec- and Tat-mediated protein secretion across the bacterial cytoplasmic membrane--distinct translocases and mechanisms." Biochim Biophys Acta **1778**(9): 1735-1756.

Ng, Y. K., Grasso, M., Wright, V., et al. (2018). "The quorum sensing system of *Yersinia enterocolitica* 8081 regulates swimming motility, host cell attachment, and virulence plasmid maintenance." Genes (Basel) **9**(6).

Nirody, J. A., Berry, R. M. and Oster, G. (2016). "The limiting speed of the bacterial flagellar motor." Biophys J **111**(3): 557-564.

Nirujogi, R. S., Muthusamy, B., Kim, M. S., et al. (2017). "Secretome analysis of diarrhea-inducing strains of *Escherichia coli*." Proteomics **17**(6).

Notti, R. Q. and Stebbins, C. E. (2016). "The structure and function of type III secretion systems." Microbiol Spectr **4**(1).

O'Farrell, P. H. (1975). "High resolution two-dimensional electrophoresis of proteins." J Biol Chem **250**(10): 4007-4021.

Oberto, J. (2013). "SyntTax: a web server linking synteny to prokaryotic taxonomy." BMC Bioinformatics **14**: 4.

Ochsner, U. A., Snyder, A., Vasil, A. I., et al. (2002). "Effects of the twin-arginine translocase on secretion of virulence factors, stress response, and pathogenesis." Proc Natl Acad Sci U S A **99**(12): 8312-8317.

Okshevsky, M. and Meyer, R. L. (2015). "The role of extracellular DNA in the establishment, maintenance and perpetuation of bacterial biofilms." Crit Rev Microbiol **41**(3): 341-352.

Olekhnovich, I. N., Vitko, S., Chertihin, O., et al. (2013). "Mutations to essential orphan response regulator HP1043 of *Helicobacter pylori* result in growth-stage regulatory defects." Infect Immun **81**(5): 1439-1449.

Olsen, J. E., Hoegh-Andersen, K. H., Casadesus, J., et al. (2013). "The role of flagella and chemotaxis genes in host pathogen interaction of the host adapted *Salmonella enterica* serovar Dublin compared to the broad host range serovar S. Typhimurium." BMC Microbiol **13**: 67.

Omasits, U., Ahrens, C. H., Muller, S., et al. (2014). "Protter: interactive protein feature visualization and integration with experimental proteomic data." Bioinformatics **30**(6): 884-886.

Orench-Rivera, N. and Kuehn, M. J. (2016). "Environmentally controlled bacterial vesicle-mediated export." Cell Microbiol **18**(11): 1525-1536.

Osei, K. A., Deivanayagam, C. and Nichols, J. J. (2018). "Glycoprotein 340 in mucosal immunity and ocular surface." Ocul Surf **16**(3): 282-288.

Ozdemir, F. and Arslan, S. (2015). "Genotypic and phenotypic virulence characteristics and antimicrobial resistance of *Yersinia* spp. isolated from meat and milk products." J Food Sci **80**(6): M1306-1313.

Pacheco, L. G., Slade, S. E., Seyffert, N., et al. (2011). "A combined approach for comparative exoproteome analysis of *Corynebacterium pseudotuberculosis.*" BMC Microbiol **11**(1): 12.

Palmer, L. E., Hobbie, S., Galan, J. E., et al. (1998). "YopJ of *Yersinia pseudotuberculosis* is required for the inhibition of macrophage TNF-alpha production and downregulation of the MAP kinases p38 and JNK." Mol Microbiol **27**(5): 953-965.

Pan, X., Ge, J., Li, M., et al. (2009). "The orphan response regulator CovR: a globally negative modulator of virulence in *Streptococcus suis* serotype 2." J Bacteriol **191**(8): 2601-2612.

Pang, T., Savva, C. G., Fleming, K. G., et al. (2009). "Structure of the lethal phage pinhole." Proc Natl Acad Sci U S A **106**(45): 18966-18971.

Papenfort, K. and Bassler, B. L. (2016). "Quorum sensing signal-response systems in Gram-negative bacteria." Nat Rev Microbiol **14**(9): 576-588.

Paulander, W., Varming, A. N., Bojer, M. S., et al. (2018). "The *agr* quorum sensing system in *Staphylococcus aureus* cells mediates death of sub-population." BMC Res Notes **11**(1): 503.

Pearson, J. P., Van Delden, C. and Iglewski, B. H. (1999). "Active efflux and diffusion are involved in transport of *Pseudomonas aeruginosa* cell-to-cell signals." J Bacteriol **181**(4): 1203-1210.

Pena, R. T., Blasco, L., Ambroa, A., et al. (2019). "Relationship between quorum sensing and secretion systems." Front Microbiol **10**: 1100.

Penfold, R. J. and Pemberton, J. M. (1992). "An improved suicide vector for construction of chromosomal insertion mutations in bacteria." Gene **118**(1): 145-146.

Perez-Rodriguez, R., Fisher, A. C., Perlmutter, J. D., et al. (2007). "An essential role for the DnaK molecular chaperone in stabilizing over-expressed substrate proteins of the bacterial twin-arginine translocation pathway." J Mol Biol **367**(3): 715-730.

Picard, F., Dressaire, C., Girbal, L., et al. (2009). "Examination of post-transcriptional regulations in prokaryotes by integrative biology." C R Biol **332**(11): 958-973.

Pieper, R., Huang, S. T., Clark, D. J., et al. (2008). "Characterizing the dynamic nature of the *Yersinia pestis* periplasmic proteome in response to nutrient exhaustion and temperature change." Proteomics **8**(7): 1442-1458.

Pieper, R., Huang, S. T., Robinson, J. M., et al. (2009). "Temperature and growth phase influence the outer-membrane proteome and the expression of a type VI secretion system in *Yersinia pestis*." Microbiology **155**(Pt 2): 498-512.

Pier, G. B. (2007). "*Pseudomonas aeruginosa* lipopolysaccharide: a major virulence factor, initiator of inflammation and target for effective immunity." Int J Med Microbiol **297**(5): 277-295.

Pierson, D. E. (1994). "Mutations affecting lipopolysaccharide enhance ail-mediated entry of *Yersinia enterocolitica* into mammalian cells." J Bacteriol **176**(13): 4043-4051.

Pignati, M. T., Pezzuti, J. C. B., Souza, L. C., et al. (2018). "Assessment of mercury concentration in turtles (*Podocnemis unifilis*) in the Xingu River Basin, Brazil." Int J Environ Res Public Health **15**(6).

Pimenta, A. L., Young, J., Holland, I. B., et al. (1999). "Antibody analysis of the localisation, expression and stability of HlyD, the MFP component of the *E. coli* haemolysin translocator." Mol Gen Genet **261**(1): 122-132.

Pugsley, A. P. (1993). "The complete general secretory pathway in gram-negative bacteria." Microbiol Rev **57**(1): 50-108.

Raetz, C. R., Garrett, T. A., Reynolds, C. M., et al. (2006). "Kdo2-Lipid A of *Escherichia coli,* a defined endotoxin that activates macrophages via TLR-4." J Lipid Res **47**(5): 1097-1111.

Raetz, C. R. and Whitfield, C. (2002). "Lipopolysaccharide endotoxins." Annu Rev Biochem **71**: 635-700.

Rahmati, S., Yang, S., Davidson, A. L., et al. (2002). "Control of the AcrAB multidrug efflux pump by quorum-sensing regulator SdiA." Mol Microbiol **43**(3): 677-685.

Rajaure, M., Berry, J., Kongari, R., et al. (2015). "Membrane fusion during phage lysis." Proc Natl Acad Sci U S A **112**(17): 5497-5502.

Ramisetty, B. C. M. and Sudhakari, P. A. (2019). "Bacterial 'grounded' prophages: Hotspots for genetic renovation and innovation." Front Genet **10**: 65.

Ramnath, L., Sithole, B. and Govinden, R. (2017). "Identification of lipolytic enzymes isolated from bacteria indigenous to Eucalyptus wood species for application in the pulping industry." Biotechnol Rep (Amst) **15**: 114-124.

Ranjit, D. K., Liechti, G. W. and Maurelli, A. T. (2020). "Chlamydial MreB directs cell division and peptidoglycan synthesis in *Escherichia coli* in the absence of FtsZ activity." MBio **11**(1).

Rapisarda, C., Cherrak, Y., Kooger, R., et al. (2019). "*In situ* and high-resolution cryo-EM structure of a bacterial type VI secretion system membrane complex." EMBO J **38**(10).

Ratzke, C. and Gore, J. (2018). "Modifying and reacting to the environmental pH can drive bacterial interactions." PLoS Biol **16**(3): e2004248.

Rau, A., Maugis-Rabusseau, C., Martin-Magniette, M. L., et al. (2015). "Co-expression analysis of high-throughput transcriptome sequencing data with Poisson mixture models." Bioinformatics **31**(9): 1420-1427.

Reboul, A., Lemaitre, N., Titecat, M., et al. (2014). "*Yersinia pestis* requires the 2-component regulatory system OmpR-EnvZ to resist innate immunity during the early and late stages of plague." J Infect Dis **210**(9): 1367-1375.

Reuter, S., Connor, T. R., Barquist, L., et al. (2014). "Parallel independent evolution of pathogenicity within the genus *Yersinia*." Proc Natl Acad Sci U S A **111**(18): 6768-6773.

Rice, K. C. and Bayles, K. W. (2008). "Molecular control of bacterial death and lysis." Microbiol Mol Biol Rev **72**(1): 85-109, table of contents.

Robinson, C., Matos, C. F., Beck, D., et al. (2011). "Transport and proofreading of proteins by the twin-arginine translocation (Tat) system in bacteria." Biochim Biophys Acta **1808**(3): 876-884.

Roggenkamp, A., Ackermann, N., Jacobi, C. A., et al. (2003). "Molecular analysis of transport and oligomerization of the *Yersinia enterocolitica* adhesin YadA." J Bacteriol **185**(13): 3735-3744.

Roh, J. Y., Choi, J. Y., Li, M. S., et al. (2007). "*Bacillus thuringiensis* as a specific, safe, and effective tool for insect pest control." J Microbiol Biotechnol **17**(4): 547-559.

Rohde, J. R., Luan, X. S., Rohde, H., et al. (1999). "The *Yersinia enterocolitica* pYV virulence plasmid contains multiple intrinsic DNA bends which melt at 37 degrees C." J Bacteriol **181**(14): 4198-4204.

Roier, S., Zingl, F. G., Cakar, F., et al. (2016). "A novel mechanism for the biogenesis of outer membrane vesicles in Gram-negative bacteria." Nat Commun **7**: 10515.

Rose, R. W., Bruser, T., Kissinger, J. C., et al. (2002). "Adaptation of protein secretion to extremely high-salt conditions by extensive use of the twin-arginine translocation pathway." Mol Microbiol **45**(4): 943-950.

Rossmanith, J. and Narberhaus, F. (2016). "Exploring the modular nature of riboswitches and RNA thermometers." Nucleic Acids Res **44**(11): 5410-5423.

Roy, K., Hilliard, G. M., Hamilton, D. J., et al. (2009). "Enterotoxigenic *Escherichia coli* EtpA mediates adhesion between flagella and host cells." Nature **457**(7229): 594-598.

Ruhal, R., Antti, H., Rzhepishevska, O., et al. (2015). "A multivariate approach to correlate bacterial surface properties to biofilm formation by lipopolysaccharide mutants of *Pseudomonas aeruginosa*." Colloids Surf B Biointerfaces **127**: 182-191.

Rutherford, S. T. and Bassler, B. L. (2012). "Bacterial quorum sensing: its role in virulence and possibilities for its control." Cold Spring Harb Perspect Med **2**(11).

Sachelaru, I., Winter, L., Knyazev, D. G., et al. (2017). "YidC and SecYEG form a heterotetrameric protein translocation channel." Sci Rep **7**(1): 101.

Saier, M. H., Jr. and Reddy, B. L. (2015). "Holins in bacteria, eukaryotes, and archaea: multifunctional xenologues with potential biotechnological and biomedical applications." J Bacteriol **197**(1): 7-17.

Salacha, R., Kovacic, F., Brochier-Armanet, C., et al. (2010). "The P*seudomonas aeruginosa* patatin-like protein PlpD is the archetype of a novel Type V secretion system." Environ Microbiol **12**(6): 1498-1512.

Salmond, G. P. and Fineran, P. C. (2015). "A century of the phage: past, present and future." Nat Rev Microbiol **13**(12): 777-786.

Sánchez-Clemente, R., Igeño, M. I., Población, A. G., et al. (2018). "Study of pH changes in media during bacterialgrowth of several environmental strains " Proceedings **2**(1297).

Sandkvist, M. (2001a). "Biology of type II secretion." Mol Microbiol **40**(2): 271-283.

Sandkvist, M. (2001b). "Type II secretion and pathogenesis." Infect Immun **69**(6): 3523-3535.

Santos, S. G., Diniz, C. G., Silva, V. L., et al. (2012). "Differentially regulated proteins in *Prevotella intermedia* after oxidative stress analyzed by 2D electrophoresis and mass spectrometry." Anaerobe **18**(1): 76-82.

Savin, C., Martin, L., Bouchier, C., et al. (2014). "The *Yersinia pseudotuberculosis* complex: characterization and delineation of a new species, *Yersinia wautersii*." Int J Med Microbiol **304**(3-4): 452-463.

Savva, C. G., Dewey, J. S., Moussa, S. H., et al. (2014). "Stable micron-scale holes are a general feature of canonical holins." Mol Microbiol **91**(1): 57-65.

Schertzer, J. W. and Whiteley, M. (2012). "A bilayer-couple model of bacterial outer membrane vesicle biogenesis." MBio **3**(2).

Schiano, C. A., Koo, J. T., Schipma, M. J., et al. (2014). "Genome-wide analysis of small RNAs expressed by *Yersinia pestis* identifies a regulator of the Yop-Ysc type III secretion system." J Bacteriol **196**(9): 1659-1670.

Schlundt, A., Buchner, S., Janowski, R., et al. (2017). "Structure-function analysis of the DNA-binding domain of a transmembrane transcriptional activator." Sci Rep **7**(1): 1051.

Schmelcher, M., Donovan, D. M. and Loessner, M. J. (2012). "Bacteriophage endolysins as novel antimicrobials." Future Microbiol **7**(10): 1147-1171.

Schneider, C. A., Rasband, W. S. and Eliceiri, K. W. (2012). "NIH Image to ImageJ: 25 years of image analysis." Nat Methods **9**(7): 671-675.

Schniederberend, M., Williams, J. F., Shine, E., et al. (2019). "Modulation of flagellar rotation in surface-attached bacteria: A pathway for rapid surface-sensing after flagellar attachment." PLoS Pathog **15**(11): e1008149.

Schoenfelder, S. M. K., Lange, C., Prakash, S. A., et al. (2019). "The small non-coding RNA RsaE influences extracellular matrix composition in *Staphylococcus epidermidis* biofilm communities." PLoS Pathog **15**(3): e1007618.

Schuster, M., Sexton, D. J., Diggle, S. P., et al. (2013). "Acyl-homoserine lactone quorum sensing: from evolution to application." Annu Rev Microbiol **67**: 43-63.

Schwechheimer, C. and Kuehn, M. J. (2015). "Outer-membrane vesicles from Gram-negative bacteria: biogenesis and functions." Nat Rev Microbiol **13**(10): 605-619.

Schwiesow, L., Lam, H., Dersch, P., et al. (2015). "*Yersinia* type III secretion system master regulator LcrF." J Bacteriol **198**(4): 604-614.

Senf, F., Tommassen, J. and Koster, M. (2008). "Polar secretion of proteins via the Xcp type II secretion system in *Pseudomonas aeruginosa*." Microbiology **154**(Pt 10): 3025-3032.

Shan, J., Korbsrisate, S., Withatanung, P., et al. (2014). "Temperature dependent bacteriophages of a tropical bacterial pathogen." Front Microbiol **5**: 599.

Shan, S. O., Schmid, S. L. and Zhang, X. (2009). "Signal recognition particle (SRP) and SRP receptor: a new paradigm for multistate regulatory GTPases." Biochemistry **48**(29): 6696-6704.

Shao, Y. and Bassler, B. L. (2014). "Quorum regulatory small RNAs repress type VI secretion in *Vibrio cholerae*." Mol Microbiol **92**(5): 921-930.

Shaw, R. J., McNeill, M. M., Maass, D. R., et al. (2003). "Identification and characterisation of an aspartyl protease inhibitor homologue as a major allergen of *Trichostrongylus colubriformis*." Int J Parasitol **33**(11): 1233-1243.

Shin, J., Lee, O. C. and Sung, W. (2015). "How a short double-stranded DNA bends." J Chem Phys **142**(15): 155101.

Silverman, J. M., Brunet, Y. R., Cascales, E., et al. (2012). "Structure and regulation of the type VI secretion system." Annu Rev Microbiol **66**: 453-472.

Simon, S., Schell, U., Heuer, N., et al. (2015). "Inter-kingdom signaling by the *Legionella* quorum sensing molecule LAI-1 modulates cell migration through an IQGAP1-Cdc42-ARHGEF9-dependent pathway." PLoS Pathog **11**(12): e1005307.

Sircili, M. P., Walters, M., Trabulsi, L. R., et al. (2004). "Modulation of enteropathogenic *Escherichia coli* virulence by quorum sensing." Infect Immun **72**(4): 2329-2337.

Sittka, A., Lucchini, S., Papenfort, K., et al. (2008). "Deep sequencing analysis of small noncoding RNA and mRNA targets of the global post-transcriptional regulator, Hfq." PLoS Genet **4**(8): e1000163.

Sizova, O. V., Kondakova, A. N., Shashkov, A. S., et al. (2017). "Structure and gene cluster of a tyvelose-containing O-polysaccharide of an entomopathogenic bacterium *Yersinia entomophaga* MH96(T) related to *Yersinia pseudotuberculosis*." Carbohydr Res **445**: 93-97.

Sloan, D. B. and Moran, N. A. (2012). "Genome reduction and co-evolution between the primary and secondary bacterial symbionts of psyllids." Mol Biol Evol **29**(12): 3781-3792.

Smith, K. D., Shanahan, C. A., Moore, E. L., et al. (2011). "Structural basis of differential ligand recognition by two classes of bis-(3'-5')-cyclic dimeric guanosine monophosphate-binding riboswitches." Proc Natl Acad Sci U S A **108**(19): 7757-7762.

Smith, T. J., Sondermann, H. and O'Toole, G. A. (2018). "Type 1 does the two-step: Type 1 secretion substrates with a functional periplasmic intermediate." J Bacteriol **200**(18).

Sousa, P. M. F., Videira, M. A. M., Bohn, A., et al. (2012). "The aerobic respiratory chain of *Escherichia coli*: from genes to supercomplexes." Microbiology **158**(Pt 9): 2408-2418.

Sperandio, V., Mellies, J. L., Nguyen, W., et al. (1999). "Quorum sensing controls expression of the type III secretion gene transcription and protein secretion in enterohemorrhagic and enteropathogenic *Escherichia coli*." Proc Natl Acad Sci U S A **96**(26): 15196-15201.

Spinner, J. L., Carmody, A. B., Jarrett, C. O., et al. (2013). "Role of *Yersinia pestis* toxin complex family proteins in resistance to phagocytosis by polymorphonuclear leukocytes." Infect Immun **81**(11): 4041-4052.

Sprague, L. D. and Neubauer, H. (2005). "*Yersinia aleksiciae* sp. nov." Int J Syst Evol Microbiol **55**(Pt 2): 831-835.

Springer, K., Reuter, S., Knupfer, M., et al. (2018). "Activity of a holin-endolysin system in the insecticidal pathogenicity island of *Yersinia enterocolitica.*" J Bacteriol **200**(16).

Starke, M., Richter, M. and Fuchs, T. M. (2013). "The insecticidal toxin genes of *Yersinia enterocolitica* are activated by the thermolabile LTTR-like regulator TcaR2 at low temperatures." Mol Microbiol **89**(4): 596-611.

Stauber, J. L., Loginicheva, E. and Schechter, L. M. (2012). "Carbon source and cell density-dependent regulation of type III secretion system gene expression in *Pseudomonas syringae* pathovar tomato DC3000." Res Microbiol **163**(8): 531-539.

Stiefel, P., Schmidt-Emrich, S., Maniura-Weber, K., et al. (2015). "Critical aspects of using bacterial cell viability assays with the fluorophores SYTO9 and propidium iodide." BMC Microbiol **15**: 36.

Strous, G. J. and Dekker, J. (1992). "Mucin-type glycoproteins." Crit Rev Biochem Mol Biol **27**(1-2): 57-92.

Sturm, A., Heinemann, M., Arnoldini, M., et al. (2011). "The cost of virulence: retarded growth of *Salmonella typhimurium* cells expressing type III secretion system 1." PLoS Pathog **7**(7): e1002143.

Su, F.-H., Tabañag, I. D. F., Wu, C.-Y., et al. (2017). "Decorating outer membrane vesicles with organophosphorus hydrolase and cellulose binding domain for organophosphate pesticide degradationtsai." Chemical Engineering Journal **308**: 1 - 7.

Summer, E. J., Berry, J., Tran, T. A., et al. (2007). "Rz/Rz1 lysis gene equivalents in phages of Gram-negative hosts." J Mol Biol **373**(5): 1098-1112.

Suzuki, H., Ikeda, A., Tsuchimoto, S., et al. (2012). "Synergistic binding of DnaJ and DnaK chaperones to heat shock transcription factor sigma32 ensures its characteristic high metabolic instability:

implications for heat shock protein 70 (Hsp70)-Hsp40 mode of function." J Biol Chem **287**(23): 19275-19283.

Terashima, H. and Imada, K. (2018). "Novel insight into an energy transduction mechanism of the bacterial flagellar type III protein export." Biophys Physicobiol **15**: 173-178.

Thoma, S. and Schobert, M. (2009). "An improved *Escherichia coli* donor strain for diparental mating." FEMS Microbiol Lett **294**(2): 127-132.

Thomas, S., Holland, I. B. and Schmitt, L. (2014). "The Type 1 secretion pathway - the hemolysin system and beyond." Biochim Biophys Acta **1843**(8): 1629-1641.

Tian, T. and Salis, H. M. (2015). "A predictive biophysical model of translational coupling to coordinate and control protein expression in bacterial operons." Nucleic Acids Res **43**(14): 7137-7151.

Tjalsma, H., Bolhuis, A., Jongbloed, J. D., et al. (2000). "Signal peptide-dependent protein transport in *Bacillus subtilis*: a genome-based survey of the secretome." Microbiol Mol Biol Rev **64**(3): 515-547.

To, K. H., Dewey, J., Weaver, J., et al. (2013). "Functional analysis of a class I holin, P2 Y." J Bacteriol **195**(6): 1346-1355.

Toyofuku, M. (2019). "Bacterial communication through membrane vesicles." Biosci Biotechnol Biochem **83**(9): 1599-1605.

Toyofuku, M., Carcamo-Oyarce, G., Yamamoto, T., et al. (2017). "Prophage-triggered membrane vesicle formation through peptidoglycan damage in *Bacillus subtilis*." Nat Commun **8**(1): 481.

Toyofuku, M., Nomura, N. and Eberl, L. (2019). "Types and origins of bacterial membrane vesicles." Nat Rev Microbiol **17**(1): 13-24.

Trovato, A., Seno, F., Zanardo, M., et al. (2014). "Quorum vs. diffusion sensing: a quantitative analysis of the relevance of absorbing or reflecting boundaries." FEMS Microbiol Lett **352**(2): 198-203.

Tsai, C. S. and Winans, S. C. (2010). "LuxR-type quorum-sensing regulators that are detached from common scents." Mol Microbiol **77**(5): 1072-1082.

Turkina, M. V. and Vikstrom, E. (2019). "Bacteria-Host Crosstalk: Sensing of the quorum in the context of *Pseudomonas aeruginosa* infections." J Innate Immun **11**(3): 263-279.

Turnbull, L., Toyofuku, M., Hynen, A. L., et al. (2016). "Explosive cell lysis as a mechanism for the biogenesis of bacterial membrane vesicles and biofilms." Nat Commun **7**: 11220.

Turner, D. P., Wooldridge, K. G. and Ala'Aldeen, D. A. (2002). "Autotransported serine protease A of *Neisseria meningitidis*: an immunogenic, surface-exposed outer membrane, and secreted protein." Infect Immun **70**(8): 4447-4461.

Turner, R. D., Hurd, A. F., Cadby, A., et al. (2013). "Cell wall elongation mode in Gram-negative bacteria is determined by peptidoglycan architecture." Nat Commun **4**: 1496.

Turner, R. D., Mesnage, S., Hobbs, J. K., et al. (2018). "Molecular imaging of glycan chains couples cell-wall polysaccharide architecture to bacterial cell morphology." Nat Commun **9**(1): 1263.

Turovskiy, Y., Kashtanov, D., Paskhover, B., et al. (2007). "Quorum sensing: fact, fiction, and everything in between." Adv Appl Microbiol **62**: 191-234.

Twittenhoff, C., Heroven, A. K., Muhlen, S., et al. (2020). "An RNA thermometer dictates production of a secreted bacterial toxin." PLoS Pathog **16**(1): e1008184.

Vanden Bergh, P., Heller, M., Braga-Lagache, S., et al. (2013). "The *Aeromonas salmonicida* subsp. salmonicida exoproteome: determination of the complete repertoire of type-three secretion system effectors and identification of other virulence factors." Proteome Sci **11**(1): 42.

Verbeke, F., De Craemer, S., Debunne, N., et al. (2017). "Peptides as quorum sensing molecules: measurement techniques and obtained levels *in vitro* and *in vivo*." Front Neurosci **11**: 183.

Vermassen, A., Leroy, S., Talon, R., et al. (2019). "Cell wall hydrolases in bacteria: Insight on the diversity of cell wall amidases, glycosidases and peptidases toward peptidoglycan." Front Microbiol **10**: 331.

Veses-Garcia, M., Liu, X., Rigden, D. J., et al. (2015). "Transcriptomic analysis of Shiga-toxigenic bacteriophage carriage reveals a profound regulatory effect on acid resistance in *Escherichia coli*." Appl Environ Microbiol **81**(23): 8118-8125.

Vijayaraghavan, P. and Vincent, S. G. (2012). "Purification and characterization of carboxymethyl cellulase from *Bacillus* sp. isolated from a paddy field." Pol J Microbiol **61**(1): 51-55.

Vivek-Ananth, R. P., Mohanraj, K., Vandanashree, M., et al. (2018). "Comparative systems analysis of the secretome of the opportunistic pathogen *Aspergillus fumigatus* and other *Aspergillus* species." Sci Rep **8**(1): 6617.

von Tils, D., Bladel, I., Schmidt, M. A., et al. (2012). "Type II secretion in *Yersinia*-a secretion system for pathogenicity and environmental fitness." Front Cell Infect Microbiol **2**: 160.

Voulhoux, R., Ball, G., Ize, B., et al. (2001). "Involvement of the twin-arginine translocation system in protein secretion via the type II pathway." EMBO J **20**(23): 6735-6741.

Wagner-Dobler, I., Thiel, V., Eberl, L., et al. (2005). "Discovery of complex mixtures of novel long-chain quorum sensing signals in free-living and host-associated marine alphaproteobacteria." Chembiochem **6**(12): 2195-2206.

Wagner, S., Grin, I., Malmsheimer, S., et al. (2018). "Bacterial type III secretion systems: a complex device for the delivery of bacterial effector proteins into eukaryotic host cells." FEMS Microbiol Lett **365**(19).

Wagner, V. E., Bushnell, D., Passador, L., et al. (2003). "Microarray analysis of *Pseudomonas aeruginosa* quorum-sensing regulons: effects of growth phase and environment." J Bacteriol **185**(7): 2080-2095.

Wagner, V. E., Gillis, R. J. and Iglewski, B. H. (2004). "Transcriptome analysis of quorum-sensing regulation and virulence factor expression in *Pseudomonas aeruginosa*." Vaccine **22 Suppl 1**: S15-20.

Wandersman, C. and Delepelaire, P. (1990). "TolC, an *Escherichia coli* outer membrane protein required for hemolysin secretion." Proc Natl Acad Sci U S A **87**(12): 4776-4780.

Wang, I. N., Deaton, J. and Young, R. (2003). "Sizing the holin lesion with an endolysin-beta-galactosidase fusion." J Bacteriol **185**(3): 779-787.

Want, M. Y., Islamuddin, M., Chouhan, G., et al. (2015). "Therapeutic efficacy of artemisinin-loaded nanoparticles in experimental visceral leishmaniasis." Colloids Surf B Biointerfaces **130**: 215-221.

Waterfield, N. R., Bowen, D. J., Fetherston, J. D., et al. (2001). "The tc genes of *Photorhabdus*: a growing family." Trends Microbiol **9**(4): 185-191.

Waters, C. M. and Bassler, B. L. (2005). "Quorum sensing: cell-to-cell communication in bacteria." Annu Rev Cell Dev Biol **21**: 319-346.

Weber, B. S., Ly, P. M. and Feldman, M. F. (2017). "Screening for secretion of the type VI secretion system protein Hcp by enzyme-linked immunosorbent assay and colony blot." Methods Mol Biol **1615**: 465-472.

Weiss, A. A., Johnson, F. D. and Burns, D. L. (1993). "Molecular characterization of an operon required for pertussis toxin secretion." Proc Natl Acad Sci U S A **90**(7): 2970-2974.

Wellington, S. and Greenberg, E. P. (2019). "Quorum sensing signal selectivity and the potential for interspecies cross talk." MBio **10**(2).

West, S. A., Winzer, K., Gardner, A., et al. (2012). "Quorum sensing and the confusion about diffusion." Trends Microbiol **20**(12): 586-594.

White, R., Chiba, S., Pang, T., et al. (2011). "Holin triggering in real time." Proc Natl Acad Sci U S A **108**(2): 798-803.

Winans, S. C. (2011). "A new family of quorum sensing pheromones synthesized using S-adenosylmethionine and Acyl-CoAs." Mol Microbiol **79**(6): 1403-1406.

Winans, S. C. and Bassler, B. L. (2002). "Mob psychology." J Bacteriol **184**(4): 873-883.

Xavier, K. B. (2018). "Bacterial interspecies quorum sensing in the mammalian gut microbiota [C. R. Biologies 341 (2018) https://doi.org/10.1016/j.crvi.2018.03.006]." C R Biol **341**(5): 300.

Xavier, K. B. and Bassler, B. L. (2005). "Regulation of uptake and processing of the quorum-sensing autoinducer AI-2 in *Escherichia coli*." J Bacteriol **187**(1): 238-248.

Xu, M., Struck, D. K., Deaton, J., et al. (2004). "A signal-arrest-release sequence mediates export and control of the phage P1 endolysin." Proc Natl Acad Sci U S A **101**(17): 6415-6420.

Yan, Z., Yin, M., Xu, D., et al. (2017). "Structural insights into the secretin translocation channel in the type II secretion system." Nat Struct Mol Biol **24**(2): 177-183.

Yang, S., Lopez, C. R. and Zechiedrich, E. L. (2006). "Quorum sensing and multidrug transporters in *Escherichia coli*." Proc Natl Acad Sci U S A **103**(7): 2386-2391.

Yang, X., Thornburg, T., Suo, Z., et al. (2012). "Flagella overexpression attenuates *Salmonella* pathogenesis." PLoS One **7**(10): e46828.

Yokoyama, K., Horii, T., Yamashino, T., et al. (2000). "Production of shiga toxin by *Escherichia coli* measured with reference to the membrane vesicle-associated toxins." FEMS Microbiol Lett **192**(1): 139-144.

Young, G. M., Badger, J. L. and Miller, V. L. (2000). "Motility is required to initiate host cell invasion by *Yersinia enterocolitica.*" Infect Immun **68**(7): 4323-4326.

Young, R. (2014). "Phage lysis: three steps, three choices, one outcome." J Microbiol **52**(3): 243-258.

Yu, Y. J., Wang, X. H. and Fan, G. C. (2018). "Versatile effects of bacterium-released membrane vesicles on mammalian cells and infectious/inflammatory diseases." Acta Pharmacol Sin **39**(4): 514-533.

Zgurskaya, H. I., Lopez, C. A. and Gnanakaran, S. (2015). "Permeability barrier of Gram-negative cell envelopes and approaches to bypass it." ACS Infect Dis **1**(11): 512-522.

Zhang, L., Jiang, W., Nan, J., et al. (2014). "The *Escherichia coli* CysZ is a pH dependent sulfate transporter that can be inhibited by sulfite." Biochim Biophys Acta **1838**(7): 1809-1816.

Zhang, W., Wang, Y., Song, Y., et al. (2013). "A type VI secretion system regulated by OmpR in *Yersinia pseudotuberculosis* functions to maintain intracellular pH homeostasis." Environ Microbiol **15**(2): 557-569.

Zhang, W., Xu, S., Li, J., et al. (2011). "Modulation of a thermoregulated type VI secretion system by AHL-dependent quorum sensing in *Yersinia pseudotuberculosis*." Arch Microbiol **193**(5): 351-363.

Zheng, J., Ho, B. and Mekalanos, J. J. (2011). "Genetic analysis of anti-amoebae and anti-bacterial activities of the type VI secretion system in *Vibrio cholerae*." PLoS One **6**(8): e23876.